EXPOSING THE POTENTIAL OF WDR5 WIN SITE INHIBITORS FOR THE

TREATMENT OF RHABDOID TUMORS

By

Andrea C. Florian

Dissertation

Submitted to the Faculty of the

Graduate School of Vanderbilt University

in partial fulfillment of the requirements

for the degree of

DOCTOR OF PHILOSOPHY

in

Cell and Developmental Biology

May 13, 2022

Nashville, TN

Approved:

Stephen W. Fesik, Ph.D.

Maureen Gannon, Ph.D.

Ethan Lee, M.D., Ph.D.

William P. Tansey, Ph.D.

Marija Zanic, Ph.D.

ACKNOWLEDGMENTS

TABLE OF CONTENTS

LIST OF TABLES

Page

LIST OF FIGURES

Page

LIST OF ABBREVIATIONS

RT: Rhabdoid Tumors

AT/RT: Atypical Teratoid Rhabdoid Tumors

MRT: Malignant Rhabdoid Tumor

SS: Synovial Sarcoma

WDR5: WD Repeat Domain 5

WIN: WDR5 INteracting

WBM: WDR5 Binding Motif

MLLr: MLL1-rearranged

ER: Endoplasmic Reticulum

RPGs: Ribosomal Protein Genes

PSGs: Protein Synthesis Genes

NB: Neuroblastoma

SS: Synovial Sarcoma

WT: Wildtype

HHT: Homoharringtonine

DMEM: Dulbecco's Modified Eagle Medium

RPMI: Roswell Park Memorial Institute (media)

DMSO: Dimethylsulfoxide

IC_{50}: Half maximal Inhibitory Concentration

PBS: Phosphate Buffered Saline

PI: Propidium Iodide

OPP: O-propargyl-puromycin

CHX: cyclohexamide

FITC: Fluorescein Isothiocyanate

BrdU: Bromodeoxyuridine

7-AAD: 7-Aminoactinomycin D

EDTA: Ethylenediaminetetraacetic Acid

PMSF: Phenylmethylsulfonyl Fluoride

PVDF: Polyvinylidene Fluoride

DNA: Deoxyribonucleic Acid

RNA: Ribonucleic acid

qPCR: Quantitative Polymerase Chain Reaction

RT-qPCR: Reverse Transcriptase Quantitative Polymerase Chain Reaction

ChIP: Chromatin Immunoprecipitation

ChIP-Seq: Chromatin Immunoprecipitation coupled with Next Generation Sequencing

PRO-Seq: Precision Run-On Sequencing

RNA-Seq: RNA sequencing

FDR: False Discovery Rate

TSS: Transcription Start Site

ATP: Adenosine Triphosphate

G1: Gap 1

S: Synthesis

G2/M: Gap 2/Mitosis

POI: Protein of Interest

VANTAGE: Vanderbilt Technologies for Advanced Genomics

IGV: Integrated Genomic Viewer

ES: Enrichment Score

NES: Normalized Enrichment Score

DEGs: Differentially Expressed Genes

PCA: Principal Component Analysis

shRNA: Short Hairpin RNA

Scr: Scrambled

CRISPR: Clustered Regularly Interspaced Short Palindromic Repeats

CRISPRi: CRISPR interference

sgRNA: Short Guide RNA

HSA: Highest Single Agent

I. INTRODUCTION

Overview

In this chapter, I will first give an overview of rhabdoid tumors (RT), rare pediatric cancers with high rates of mortality and minimal treatment options [1]. While advances are being made in understanding these cancers and in potential therapeutic strategies, there is a desperate need for new treatment options for these patients. I will then introduce WDR5, a scaffolding protein that binds to chromatin to control the expression of a subset of protein synthesis genes, among other functions [2, 3]. In collaboration with the Fesik laboratory, we have developed small molecule inhibitors for WDR5 and previously tested their function in MLL1-rearranged (MLLr) leukemia [4] and neuroblastoma (NB) [3]. The goal of the work in this thesis is to determine if these WDR5 inhibitors have potential as a treatment strategy for patients with RT. In addition, this work with uncover more about the mechanism of action of these inhibitors in an additional cancer context. Finally, I present a summary of the work detailed throughout this thesis to understand the therapeutic potential of WDR5 WIN site inhibitors in RT.

Rhabdoid tumors

Introduction to rhabdoid tumors

Each year in the US, approximately 25 children receive a devastating rhabdoid tumor diagnosis [5]. These cancers can present in the brain, where they are termed atypical teratoid/rhabdoid tumor (AT/RT), or elsewhere in the body, specifically the kidneys and other soft tissues, where they are termed malignant rhabdoid tumor (MRT) [6]. RT typically afflict children under the age of two and most patients die within 18 months of diagnosis indicating how quickly these tumors progress [1]. Some improvements in patient survival have been made in recent years [6], but there are few effective treatment options for RT. Despite regimens that can involve combinations

of surgery, chemotherapy, and radiation, the five year survival rate of children diagnosed with RT is approximately 20% [1], highlighting the need for new targeted therapies that can substantively improve RT patient outcomes.

Histologically, rhabdoid tumors are characterized by a population of cells within the tumor with a rhabdoid-like appearance— abundant cytoplasm and prominent nucleoli within the nucleus [1]. While rhabdoid cells can be a feature of a variety of solid tumors, RT is distinguished by its unusually simple and specific genetic profile; MRT and AT/RT are defined by mutations in a single gene, SWI/SNF Related, Matrix Associated, Actin Dependent Regulator of Chromatin, Subfamily B, Member 1 (*SMARCB1*), which encodes the protein SNF5, a component of the SWI/SNF complex [1, 7-9].

SWI/SNF chromatin remodeling complex in cancer

Switchable/non-fermentable (SWI/SNF) is a chromatin remodeling complex responsible for mobilizing nucleosomes to control gene expression. SWI/SNF uses ATP to slide or eject nucleosomes from DNA [10-13]. The SWI/SNF family is also known as the BRG1/BRM-associated factor (BAF). There are three distinct SWI/SNF complexes: canonical BAF (cBAF), polybromo-associated BAF (PBAF), and non-canonical BAF (ncBAF). Each complex has a handful of common core subunits as well as some complex specific factors. The common subunits include one of the two mutually exclusive catalytic ATPase subunits, SMARCA2 or SMARCA4, as well as SMARCC1, SMARCC2, SMARCD1, ACT6L1, BCL7 , and β-actin (**Figure 1.1**) [14]. cBAF was the first defined SWI/SNF complex and is identified by the incorporation of ARID1A or ARID1B, and DPF2. cBAF also contains SMARCB1, SMARCE1, and SS18 (**Figure 1.1A**) [10, 14, 15] . The PBAF complex incorporates a distinct ARID protein, ARID2, in place of ARID1, and also uniquely includes PBRM1, BRD7, and PHF10. Like cBAF, PBAF incorporates SMARCB1 and SMARCE1 but is lacking SS18 (**Figure 1.1B**) [14, 16, 17]. More recently, a novel BAF complex was identified, termed ncBAF, which does not incorporate an ARID or PHF/ DPF subunit or SMARCB1 and SMARCE1, but instead uniquely contains the GLTSCR1/
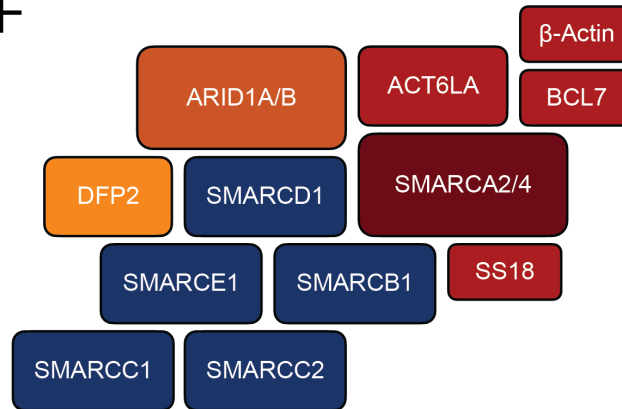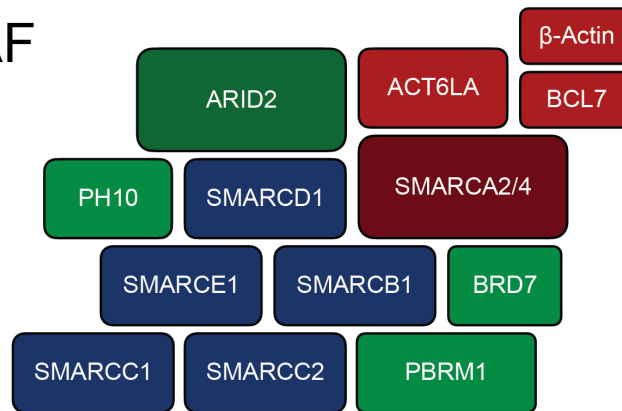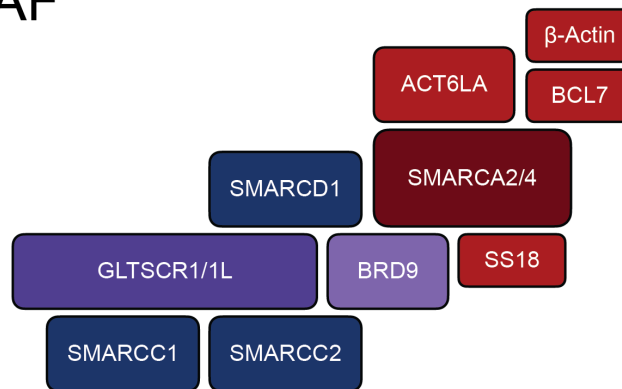
Figure 1.1 Model of SWI/SNF complexes (**A**) Canonical BAF (cBAF) is defined by the inclusions of ARID1A or ARID1B and DFP2 (**B**) Polybromo-associated BAF (PBAF) is defined by the inclusion of ARID2, PH10, BRD7, and PBRM1 and does not contain SS18 (**C**) Non-canonical BAF (ncBAF) is defined by the inclusion BRD9 and GLTSCR1/L1 and does not contain SMARCB1, SMARCE1, or an ARID subunit. [14]

GLSTCR1L and BRD9 subunits (**Figure 1.1C**) [14, 18-21].

SWI/SNF was first implicated in cancer with the discovery that *SMARCB1* is biallelically inactivated in nearly all cases of RT [22]. Since then, mutations in nine SWI/SNF subunits have been identified as recurrently mutated across a variety of cancer types. Mutations in SWI/SNF complex members can be found in approximately 20% of all cancers [13, 23]. Specifically, ARID1A is the most commonly deregulated SWI/SNF subunit and is found to be mutated in 50% of all ovarian clear cell carcinomas and ovarian endometriosis carcinomas [24, 25]. PBRM1 mutations are found in 41% of clear cell renal cell carcinomas [26]. Over 90% of small cell carcinoma of the ovary, hypercalcemic type have a SMARCA4 mutation [27]. As mentioned previously, 95% of RT cases have a mutation in *SMARCB1*. The remaining 5% of RT have a mutation in SMARCA4 [28, 29]. In addition to RT, another cancer type that involves the disruption of SNF5 from the SWI/SNF complex is synovial sarcoma (SS). SS is marked by the translocation between chromosomes 18 and X creating an SS18:SSX fusion protein [30]. When this SS18:SSX fusion protein participates in the SWI/SNF complex, it displaces the wildtype (WT) SS18 as well as SNF5 creating a pseudo-SNF5 knock out [30, 31]. The absence of SNF5 in both RT and SS compromises the expression and integrity of SWI/SNF complexes [32] but promotes the function of ncBAF. ncBAF is required for the survival of *SMARCB1*-deficient cancers cells as CRISPR screens and shRNA screens have revealed that RT and SS are selectively sensitive to loss of BRD9 [20, 21]. Because of the functional similarities between RT and SS, I thought it was valuable to evaluate SS cell lines alongside the RT cell lines in my work.

SNF5 loss causes rhabdoid tumors

Biallelic loss of *SMARCB1* is the only recurring mutation in rhabdoid tumors, and often the only mutation detected in RT genomes [7]. Although RT has a simple genetic basis, loss of SNF5 is associated with a complex set of molecular and phenotypic changes. Mouse models have been used to demonstrate the tumor suppressive function of SNF5. In fact, all mice with a

heterozygous knockout of *Snf5* develop tumors consistent with RT *in vivo* as early as five weeks old and at a median onset of only 11 weeks [33]. As further evidence that SNF5 loss is the driving force in maintaining the rhabdoid tumor state, groups have reintroduced SNF5 into patient-derived RT cell lines. They demonstrated that SNF5 reintroduction induces cell cycle arrest in G1 phase, apoptosis, and reversal of tumorigenicity [34-38], indicating that loss of SNF5 is responsible for the oncogenic state.

At the cellular level, SNF5 loss results in the the collapse of SWI/SNF complexes. This prevents SWI/SNF complexes from binding to enhancers required for the expression of differentiation programs but residual SWI/SNF complexes remain bound to super-enhancers essential for tumor maintenance [32, 39]. Super-enhancers are clusters of highly active enhancers that are occupied by master regulators [40]. In addition, SNF5 loss results in depletion of bivalent promoter activation [39]. Bivalent promoters are sites on chromatin bound by both an activating mark, histone H3 Lysine 4 trimethylation (H3K4me3) and a repressive mark, H3 Lysine 27 trimethylation (H3K27me3), a mark that seems to silence certain genes, especially those involved in development, while keeping them poised for activation [41]. SNF5 loss also induces endoplasmic reticulum (ER) stress and the unfolded protein response via the MYC–p19ARF–p53 axis [42], a process that protects RT cells from proteotoxic cell death and could explain the near-universal retention of wild-type *TP53* in RT genomes [43]. In all, loss of SNF5 promotes a number of cellular alterations that coalesce in driving and maintaining the malignant state of RT.

The role of MYC in RT

In addition to the molecular and phenotypic changes described above, multiple studies have shown a recurrent activation of MYC target gene signatures in *SMARCB1*-deficient cancers [44, 45]. MYC is an oncogenic transcription factor overexpressed in over half of all cancers, and it is estimated that inappropriate MYC expression contributes to one-third of all cancer deaths in the U.S. each year [46]. MYC proteins drive oncogenicity via their ability to bind DNA and regulate thousands of genes, most notably ones involved in cell growth, cell cycle progression,

metabolism, genome integrity, and stemness [47, 48]. Although the reason for MYC activation in RT was not initially understood, work from our laboratory has led to a new paradigm for how SNF5 loss drives RT, by activating MYC [49]. It has previously been shown that SNF5 interacts with the DNA binding domain (DBD) of MYC [50], and suggested that SNF5 is a co-activator of MYC function. We used a combination of biochemical and genomic approaches to discover, however, that SNF5 inhibits MYC by inhibiting its ability to bind DNA, both *in vitro* and in cells. Indeed, in MRT cells, the transcriptional effects of adding back SNF5 and inhibiting MYC are nearly identical [49]. These findings indicate that upon SNF5 loss, as is the case in RT, MYC has uninhibited access to its target genes where it can drive gene expression changes that maintain the tumorigenic state, a phenomenon presumably responsible for the recurrent activation of MYC target gene signatures in *SMARCB1*-null cancers [44, 45, 51].

Improving RT treatment strategies

The introduction of targeted therapies has revolutionized cancer treatment as new drugs are designed to target specific oncogenic drivers and mutations [52]. However, the unusually simple genomic profile of RT makes it challenging to develop new treatment strategies. In most cases of RT, the only mutation is the loss of *SMARCB1* and it is not possible to target the only driving mutation of RT as it is absent. Thus, a number of attempts have been made to identify new drug targets and improve therapeutic strategies to treat *SMARCB1*-deficient cancers. Interestingly, MDM2 and MDM4 have been identified as therapeutic vulnerabilities in RT and RT cells are sensitive to the HDM2 inhibitor idasanutlin, which blocks the ubiquitin-mediated destruction of p53 [53]. In addition, RT cells are sensitive to the FDA-approved translation inhibitor homoharringtonine (HHT) [54]. As far as targeted therapies, the EZH2 inhibitor, tazemetostat is being evaluated in clinical trials for the treatment of rhabdoid tumors, synovial sarcomas, and other cancers with a *SMARCB1* mutation. Enhancer of zeste homolog 2 (EZH2) is enzymatic catalytic subunit of polycomb repressive complex 2 (PRC2). PRC2 can repress gene expression via Histone 3 Lysine 27 trimethylation (H3K27me3). This is in opposition to the function of the

SWI/SNF complex as evidenced by loss of function mutations in SMARCA4, the catalytic subunit, and in *SMARCB1* resulting in increased levels of H3K27me3 [55]. In a trial involving patients with epithelial sarcoma, a cancer with consistent loss in SNF5 expression [56], only 15% of the 62 patients enrolled in the trial responded to treatment [57]. Because *SMARCB1*-deficient cells have a preferential dependence on the BRD9-containing ncBAF complex, targeting BRD9 is of particular interest [20, 21]. BRD9 inhibitors including I-BRD9 and BI-7273 have been developed and shown to have anti-cancer activity in AML [58, 59]. In addition, a "degron" compound for BRD9 (dBRD) has been developed which has shown to downregulate oncogenic transcriptional profiles in SS and disrupt tumor progression *in vivo* [19]. Unfortunately, RT cells were insensitive to BI-7273 [21] but degradation with dBRD9 is more potent than BI-7273 in colony forming assays of SS indicating that BRD9 depletion rather than inhibition may be required to treat *SMARCB1*-deficient cancers [20]. Other targeted treatments are under evaluation but to this point, there have yet to be any significant breakthroughs in improving treatments for RT [13].

WDR5 regulates gene expression

WDR5 as a scaffolding protein

WD Repeat Domain 5 (WDR5) is a WD40 repeat-containing protein that folds into a seven bladed β-propeller structure [2]. WDR5 is extensively conserved through evolution indicating its importance in cell function. Human and mouse WDR5 are identical and all vertebrates share over 90% sequence identity [2, 60]. WDR5 is most commonly considered a scaffolding protein and it has two binding motifs (**Figure 1.2A**). The first is a shallow hydrophobic cleft on the surface of the protein referred to as the "WDR5-binding motif" (WBM) site which is made up of the residues Asn225, Tyr228, Leu240, Phe266, Val268, and Gln289 (**Figure 1.2B**) [2]. The second site is an arginine-binding cavity on the opposite side known as the "WDR5-interacting" (WIN) site made up of residues Ala65, Ser91, Asp107, Phe133, Tyr191, Tyr260, and Phe263

A. WBM Site

WIN Site

B. 90°

C. 90°

D.
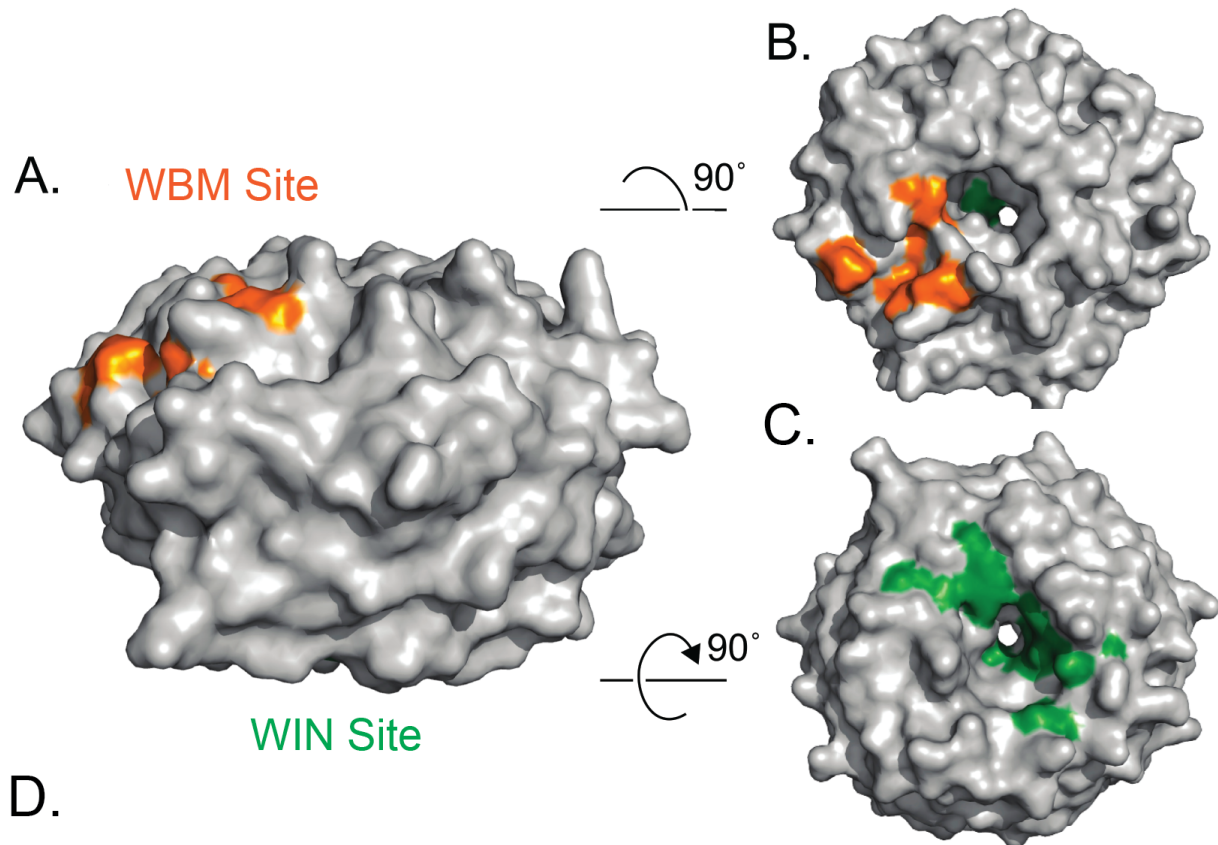
WIN site interactors:	WBM site interactors:
MLL1 (ARA)	RBBP5 (EEVDVT)
MLL2 (ARS)	c-MYC (EEIDVV)
MLL3 (ARS)	N-MYC (EEIDVV)
MLL4 (ARA)	L-MYC (EEIDVV)
SET1A (ARS)	KANSL2 (DDLDVV)
SET1B (ARS)	
H3 (ART)	
KANSL1 (ART)	
MBD3C (ARC)	
KIF2A (ARA)	
WDR5 (ARA)	
PDPK1 (ART)	

Figure 1.2. WDR5 has two interaction surfaces (**A**) Surface structure of WDR5 as shown from the side. The WDR5 binding motif (WBM) is on the top in orange and the "WDR5-interacting" (Win) is on the bottom. (**B**) Top view of WDR5 showing the WBM site highlighted in orange. (**C**) Bottom view of WDR5 showing the Win site highlighted in green. (**D**) Characterized WDR5 interacting partners and their WIN or WBM motifs. *Amended from [2].*

(**Figure 1.2C**) [2]. Proteins that interact with the WIN site of WDR5 contain a WIN motif consensus sequence of "ARA", an arginine between two small residues (**Figure 1.2D**). The center arginine engages the deep pocket of the WIN site [2]. All known proteins that interact with WDR5 do so through the WBM site or the WIN site (**Figure 1.2D**) [2]. The full interactome of WDR5 is still an expanding field of study but I will discuss some of the best understood and significant interaction partners of WDR5.

The "moonlighting" roles of WDR5

WDR5 is best understood for its role in scaffolding the assembly of complexes linked to gene activation but it also "moonlights" in other molecular processes, both on and off chromatin through its participation in proteins complexes and interaction with other partners [2, 61]. The most widely studied WDR5-containing complex is the SET1/MLL histone methyltransferase (HMT) complex that catalyzes histone H3 lysine 4 di- and tri-methylation (H3K4me2 and H3K4me3) . H3K4me2 and H3K4me3 mark transcriptionally active chromatin. In humans, there are six unique SET1/MLL catalytic components: SET1A, SET1B, MLL1, MLL2, MLL3, and MLL4. While the different complexes vary slightly in their members, each contains a core set of proteins known as "WRAD"— WDR5, RBBP5, ASH2L, and DPY30 [62]. WDR5 plays an important role in assembling these complexes as RBBP5 binds to the WBM site [63] and SET1/ MLL binds to the WIN site [64-66]. In the case of MLL1 and SET1B, binding to the WIN site of WDR5 is essential for HMT activity of these complexes [67].

WDR5 also interacts with other proteins and complexes [2]. It is important to note that both the WIN site and WBM site cannot be occupied by more than one protein simultaneously so the participation of WDR5 in these complexes are mutually exclusive. On chromatin, WDR5 has been shown to read and bind to specific histone modifications. WDR5 is able to bind to histone H3 arginine 2 dimethylation (H3R2me2) [68, 69]. Arginine 2 can be dimethylated in two different ways; asymmetrically in which both methyl groups are placed on the same terminal nitrogen or symmetrically in which a methyl group is placed one each of the two terminal nitrogens.

Asymmetrical dimethylation is a repressive mark where as symmetrical dimethylation marks sites of active transcription. WDR5 is able to bind to symmetrical H3R2me2 but not asymmetrical H3R2me2 [70] consistent with the notion that WDR5 is generally associated with transcriptional activity. WDR5 also assembles in the non-specific lethal (NSL) histone acetyltransferase (HAT) complex with MOF, KANSL1, KANSL2, KANSL3, PHF20, and MCRS1 [71]. WDR5 however does not participate in the other MOF containing complex, MSL [71]. Within the NSL complex, WDR5 binds directly to KANSL1 through the WIN site and to KANSL2 through the WBM site [72]. NSL acetylates histone H4 at lysines 5, 8, and 16 which also mark transcriptionally active chromatin [73]. In addition to the HMT and HAT complexes, WDR5 assembles into the Nucleosome Remodeling and Deacetylase (NuRD) complex which is capable of both remodeling chromatin and deacetylating histones [74]. The NuRD complex can be assembled into a few different varieties but WDR5 binds specifically to MBD3C which is expressed in embryonic stem cells (ESCs) and contributes to the stem-like state [75, 76].

Beyond its participation in chromatin regulatory complexes, WDR5 is able to bind to sequence specific transcription factors to promote their activity. Our laboratory discovered that recruitment of MYC to chromatin depends on an interaction with WDR5 at the WBM site [77]. Mutations that block the MYC-WDR5 interaction prevent MYC from driving tumorigenesis *in vivo* [77]. Further, we showed that WDR5 must bind to chromatin in order to recruit MYC to the MYC-WDR5 bound target genes [78, 79] and that genetic disruption of the MYC-WDR5 interaction in a Burkitt's Lympohoma xenograft promotes rapid and comprehensive tumor regression *in vivo* [78].

The variety of identified interaction partners of WDR5 underscores its importance in many epigenetic, transcriptional, and chromatin regulatory processes. There is still much to learn about the full functionality of WDR5 as many studies simply identify it as part of a complex without detailing how WDR5 contributes to the activity or localization of that complex. Additionally, the division of labor of WDR5 between each of its functions has not been fully

parsed out. The more we understand how WDR5 functions, the more we will understand the significance of WDR5 as an anti-cancer target.

WDR5 regulates protein synthesis gene expression

More recently, our laboratory performed a comparative genomic analysis to identify to conserved genes regulated by WDR5 across a diverse panel of cancer cell lines. These studies identified ~100 common WDR5-bound genes in a comparison of WDR5 chromatin binding in four human cell lines (MV4:11, K562, LoVo, and Be(2)C) and two mouse cell lines (MC-38 and NIH3T3) [3]. The majority of these genes are linked to protein synthesis, including half of the ribosomal protein genes (RPGs), as well as those encoding translation factors and nucleolar RNAs [3]. Protein synthesis is particularly important for cancer cell survival as cells must be able to produce enough protein to sustain the rapid rate of proliferation [80]. As such, cells increase the number of ribosomes in the cell to keep up with the increased protein synthesis. Our laboratory also demonstrated that WDR5 is tethered to chromatin at these universal PSGs via WIN site [3, 4]. Rapid and comprehensive depleting of WDR5 using the dTAG system [81] results in a decrease in expression of over half of the conserved WDR5-bound genes confirming that WDR5 is essential for controlling the expression of these genes [3]. Thus, the fact that WDR5 plays an important transcriptional role in biomass accumulation makes it a promising anti-cancer target.

WDR5 WIN site inhibitors

Due to the many connections between WDR5 and tumorigenic programs, targeting WDR5 is a promising therapeutic target for a variety of cancers. Specifically, the WIN site of WDR5 is a small arginine-binging pocket amenable to small molecule inhibition (**Figure 1.2C**) [2]. Several WDR5 WIN site inhibitors have been described. One of the earliest WIN site inhibitors tested in cells is OICR-9429 [82]. OICR-9429 was first studied in the context of acute myeloid leukemia expressing a C/EBPα p30 mutation where it decreases proliferation and induces differentiation.

In addition, OICR-9429 disrupts the interaction between WDR5 and MLL1. OICR-9429 has also been shown to have anti-proliferative effects in other cancer cell lines including MLLr leukemia [4], colon [83], bladder [84], and prostate [85] cancers. Another recently developed WIN site inhibitor is the cycle peptidomimetic MM-401 that binds WDR5 with a higher affinity than OICR-9429 [86]. MM-401 reduces proliferation in MLL cells and inhibits MLL1 mediated H3K4me2 and me3 [86] leading to the assumption that WIN site inhibitors function by blocking MLL HMT activity.

In collaboration with the Fesik laboratory, we have used fragment-based screening and structure-based design to develop a series of potent small molecule inhibitors of the WIN site of WDR5 [4, 87]. Our first-generation compound, C3, binds WDR5 with a K_d of 1.3 nM and was able to reduce proliferation of MLLr leukemia cells [4]. After further optimization, we developed a second generation compound, C6 (**Figure 1.3A**), that is able bind WDR5 with a K_d of 0.1 nM. To aid in our understanding of WIN site inhibitor function, members of the Fesik laboratory also developed a negative control compound, C6nc (**Figure 1.3B**), with the same molecular formula as C6 but with a reduced affinity due to a regioisomeric fluorine that blocks binding [4]. The Fesik laboratory further optimized the WIN site inhibitors to include a bicyclic core which allows for WDR5 binding with picomolar affinity [79]. This third-generation compound, C16 (**Figure 1.3C**), is the molecule used in the majority of my work.

Previous work from our laboratory has shown that MLLr leukemia cells are sensitive to our WIN site inhibitors [4]. WIN site inhibitors globally displace WDR5 from chromatin resulting in a reduction of WDR5-bound PSG transcription and expression. As a result, WIN site inhibitor treatment triggers a decrease in protein synthesis and induces p53 and the nucleolar stress response, ultimately pushing the cells to apoptosis [4]. This effect is not specific to leukemias, as a *MYCN*-amplified neuroblastoma (NB) cell line (CHP-134) responds similarly to WIN site inhibition in a p53-dependent manner [3]. Thus, although the many functions of WDR5 make it difficult to pinpoint a precise mechanism of action of WIN site inhibitors, a recurring theme is
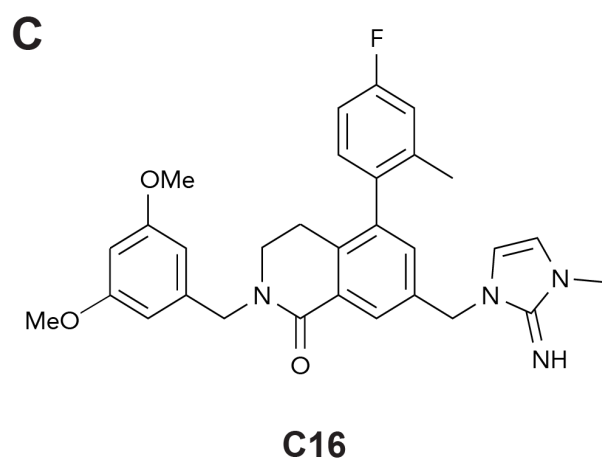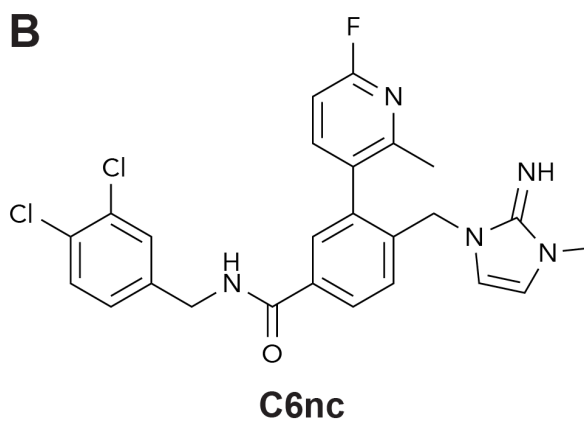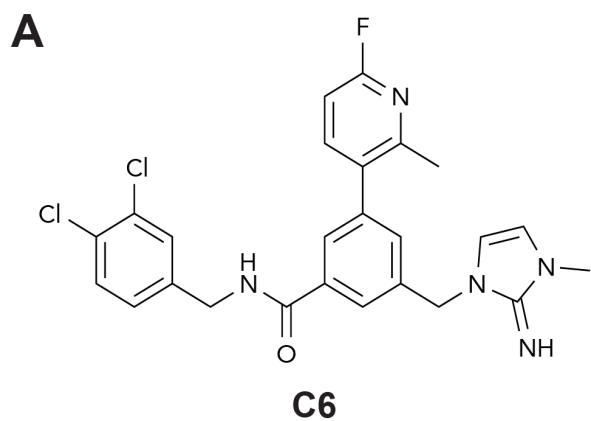
Figure 1.3. Chemical structures of WIN site inhibitors (**A**) Chemical structure of C6. (**B**) Chemical structure of negative control, C6nc. (**C**) Chemical structure of C16.

their ability to displace WDR5 from chromatin suppressing the expression of the protein synthesis machinery and activating p53.

Rationale

The goal of my work is to determine if *SMARCB1*-deficient cells are sensitive to WDR5 WIN site inhibitors to lay the groundwork for future preclinical evaluation in rhabdoid tumors. As previously discussed, several studies have shown that MYC is implicated in RT [44, 45]. Importantly, work from our laboratory showed that upon SNF5 loss, as is the case in RT, MYC has uninhibited access to its target genes where it can drive gene expression changes that maintain the tumorigenic state [49]. Consistent with this idea, we, and others [88], have shown that inhibiting MYC blocks RT cell viability, giving confidence that MYC inhibitors, when available, would be an effective treatment strategy for RT. However, MYC is often considered "undruggable" as it is unstructured and lacks a suitable binding pocket for pharmacological inhibition [89]. Our laboratory reported that recruitment of MYC to chromatin depends on interaction with WDR5 and that mutations that block the MYC–WDR5 interaction prevent MYC from driving tumorigenesis *in vivo* [77]. We determined that many of the PSGs at which WDR5 is bound are co-bound by MYC and that WDR5 must bind chromatin to recruit MYC to these targets [78] demonstrating that WDR5 participates in regulating a subset of MYC target genes related to protein synthesis. Importantly, preliminary work with our WIN site inhibitors shows that C16 is able to displace WDR5 and MYC from chromatin at sites where these proteins are co-bound [79]. As observed in previous work with WIN site inhibitors, I predict that WIN site blockade will displace WDR5 from chromatin and decrease the expression of PSGs and thus disrupt protein synthesis. Further, I predict that RT cells will be sensitive to the disruption of protein synthesis because they rely on upregulation of MYC target genes, like PSGs, to maintain their tumorigenic state [88].

Inhibition of protein synthesis is already a validated therapeutic strategy in RT cells. In fact, a genome-wide CRIPSR screen indicated that rhabdoid tumor cell lines are preferentially

sensitive to genetic loss of ribosomal subunits when compared to other cancer cell lines [54]. In addition, RT cells are sensitive to the protein-translation inhibitor homoharringtonine (HHT) [54]. HHT disrupts translation by blocking the site at which tRNAs bind within the ribosome and inhibiting the elongation phase [90]. Other work from the same group showed that RT cells are also preferentially sensitive to the HDM2 inhibitor, idasanutlin [53]. In an unperturbed cell, HDM2 maintains low levels of p53 by binding to and ubiquitylating p53, tagging it for degradation. Idasanutlin, like other HDM2 inhibitors, interacts with HDM2 and prevents it from binding p53, thus, stabilizing levels of p53 and activating the p53 pathway [91]. Our previous work has demonstrated that WIN site inhibitors behave in a manner similar to these compounds in that they disrupt protein synthesis and activate p53 [3, 4]. This prompted us to ask whether WIN site inhibitors are active against RT cell lines *in vitro.*

Summary of Thesis

RT is a rare pediatric cancer that desperately needs new treatment strategies. The work presented in this thesis explores the potential of WDR5 WIN site inhibitors for the treatment of RT. Two novel WIN site inhibitors developed by the Fesik laboratory, C6 and C16, were used to demonstrate that, despite a common genetic lesion, RT cells differ widely in their sensitivity to WIN site blockade, ranging from highly sensitive to functionally non-responsive. Using ChIP-Seq, we mapped the distribution of WDR5 on chromatin in RT cells, and found that WDR5 is bound to a specific set of PSGs, significantly overlapping with the set of genes we have previously defined as "universal" WDR5 binding sites. In addition, we were able to show that WDR5 is globally evicted from chromatin by treatment with WIN site inhibitor. Using PRO-seq, we defined a set of PSGs that are direct targets of WIN site inhibitor in which we see changes in gene transcription within two hours of treatment. As a companion data set, the use of RNA-seq allowed the elucidation of long-term secondary effects of WIN site inhibition. We determined that C16 treatment decreases the expression of PSGs and induces the expression of genes consistent with p53 activation. We observed that these gene expression changes overlap

remarkably with those seen with Nutlin-3a treatment. We asked whether or not p53 is required for the response of RT cells to WIN site inhibitor and were surprised to find that attenuating p53 expression does not impact the sensitivity of RT cells to C16. We exploit this observation to show that WIN site inhibitors act synergistically with HDM2 inhibitors, even in RT cells that are weakly sensitive to WIN site inhibition alone. These observations imply that a dual WDR5/HDM2 inhibition strategy could be deployed to one day treat these devastating childhood malignancies.

II. MATERIALS AND METHODS

Cell culture and transductions

G401, A204, HEK293, MV4:11, and BJ Fibroblasts cells were from ATCC. JMU-RTK-2 and KYM-1 cells were from the JCRB Cell Bank. Aska-SS and HS-SY-II cells were obtained from the RIKEN Cell Bank. TTC642, TTC549, and TM87-16 cells were a gift from Bernard E. Weissman. CHLA-266 and BT-12 cells were gifted from the Children's Oncology Group. G401, JMU-RTK-2, Aska-SS, HS-SY-II, BJ Fibroblasts, and HEK293 cells were maintained in DMEM supplemented with 10% FBS and 1% penicillin/streptomycin. A204, TTC642, KYM-1, TTC549, TM87-16, and MV4:11 cells were maintained in RPMI-1640 supplemented with 10% FBS and 1% penicillin/ streptomycin. CHLA-266 and BT-12 cells were maintained in DMEM supplemented with 20% FBS, 1% penicillin/streptomycin, and 1x Insulin-Transferrin-Selenium (ThermoFisher). Viral vector pLKO-p53-shRNA-941 was a gift from Todd Waldman (Addgene plasmid #25637; http:// n2t.net/addgene:25637; RRID:Addgene_25637; [92]); pLKO-shRNA-scramble was a gift from David Sabatini (Addgene plasmid #1864; http://n2t.net/addgene:1864; RRID:Addgene_1864; [93]); pXPR_050 was a gift from John Doench and David Root (Addgene plasmids #96925; http://n2t.net/addgene:96925; RRID:Addgene_96925; [94]); pLX_311-KRAB-dCas9 was a gift from John Doench, David Root, and William Hahn (Addgene plasmid #96918; http://n2t.net/ addgene:96918; RRID:Addgene_96918; [95]). The sgRNA targeting sequence for TP53 (CAGGTAGCTGCTGGGCTCCG) was cloned into pXPR_050 via *BsmBI* restriction enzyme (NEB) digestion. To prepare virus, Lipofectamine (ThermoFisher) was used to transfect plasmids into HEK293T cells with psPAX2 packaging (Addgene plasmid #12260; http://n2t.net/ addgene:12260; RRID:Addgene_12260) and pMD2.G envelope (Addgene plasmid #12259; http://n2t.net/addgene:12259; RRID:Addgene_12259) plasmids—both gifts from Didier Trono. Transduced cells were selected for six days with 1 µg/mL of puromycin or 10 µg/mL of blasticidin. For shRNA assays, published MV4:11 cells expressing scrambled shRNA or p53 shRNA #941 were used [4].

Proliferation assays

For proliferation assays, cells were plated in 96-well plates and treated with 0.1% DMSO or increasing concentrations of C6nc, C6, C16, or Nutlin-3a (Cayman Chemicals) for five days. Based on cell size and growth rate, 500 cells per well were plated for G401, TTC642, KYM-1, JMU-RTK-2, A204, HS-SY-II, and Aska-SS cells; 1000 cells per well were placed for TTC549, TM87-16, BT-12, CHLA-266 cells. Cells were quantified using the CellTiter-Glo Luminescent Assay (Promega) according to the manufacturer's instructions. IC50 values were calculated using GraphPad Prism software by fitting the data to a normalized-response model. For time course assays, G401 or TTC642 cells were treated with 0.1% DMSO or varying concentrations of C16, beginning at 5 µM followed by four 3-fold dilutions (1.67 µM, 0.556 µM, 0.185 µM, and 0.0617 µM). Cultures were quantified daily for five days with CellTiter-Glo assays. For synergy assays, cells were plated in 384-well plates and treated with a 7x7 matrix of varying concentrations of C16 (50 µM - ~70 nM) and Nutlin-3a (10 µM - ~15 nM) as well as each compound alone and 0.1% DMSO controls. Based on cell size and growth rate, 125 cells per well were plated for G401 and TTC642 cells; 250 cells per well were placed for TTC549, and TM87-16 cells. After five days, cells were quantified by CellTiter-Glo and the synergy was calculated using the Highest Single Agent Method via the SynergyFinder software [96].

Soft-agar Assays

For soft-agar assays, G401, TTC642, or KYM-1 cells were resuspended in 0.4% agarose-supplemented media with varying concentrations of C16 or 0.1% DMSO control. Cells were added on top of a layer of solidified 0.8% agarose. Fresh C16 or DMSO was added every 2–3 days for a total of 14–21 days. Cells were stained using 0.05% crystal violet in 70% methanol and destained with extensive washing with water. Plates were photographed and colonies counted (blinded) using ImageJ software.

Multiplex gene expression

Cells were treated with 0.1% DMSO or varying concentrations of C16 in a 96-well plate for 72 hours. To quantify transcripts, a custom QuantiGene™ Plex Assay panel from Thermo Fisher Scientific was used. For the assay, cells were lysed and lysates were incubated overnight with the probes and beads at 54°C while shaking. The beads were washed, incubated with PreAmplifier solution for 1 hr at 50°C while shaking, washed, incubated with Amplifier solution for 1 hr at 50°C while shaking, washed, incubated with Label Probe solution for 1 hr at 50°C while shaking. After an additional wash, beads were incubated with Streptavidin PER (SAPE) for 30 min at room temperature while shaking. After washing, Fluorescence signal was read on a Luminex MAGPIX. Signals from RPGs were normalized to those from *GAPDH* and *HPRT1*, and then to the DMSO control. IC50 values were calculated using R package dr4pl (Version 1.1.11; [97]).

Probe regions and accession numbers were: *RPS24* (NM_001026, region 5-334), *RPL35* (NM_007209, region 2-430), *RPL26* (NM_000987, region 37-445), *RPS14* (NM_005617, region 61-552), *RPL32* (NM_000994, region 95-677), *RPS11* (NM_001015, region 139-634), *RPL14* (NM_003973, region 108-530), *GAPDH* (NM_002046, region 2-407) and *HPRT1* (NM_000194, region 102-646).

Flow cytometry

For cell cycle analysis, 1×10^6 cells were collected after treatment with 0.1% DMSO or C16, fixed in ice-cold 70% ethanol, and stored at -20°C for at least four hours prior to staining. Fixed cells were washed with 1 X phosphate buffered saline (PBS), resuspended in propidium iodide (PI) staining buffer (1X PBS + 10 μg/ml PI + 100 μg/ml RNAse A + 2 mM $MgCl_2$) and stained overnight at 4°C. Cells were filtered through a 35 μm nylon mesh Falcon round bottom test tube and cell cycle distribution quantified using a Becton Dickinson LSRFortessa instrument. For each time point, at least 10,000 cells were counted using forward and side scatter pulse geometry gating to select single cells.

Protein synthesis was measured using the Click-iT Plus OPP Alexa Fluor 488 Protein Synthesis Analysis Kit (ThermoFisher). Cells were treated with either 0.1% DMSO or 500 nM C16 for four days. As a control, a culture of cells were treated with 50 µg/mL of cycloheximide for 30 minutes. Cells were pulsed with 20 µM O-propargyl-puromycin (OPP) for one hour, collected in PBS and fixed with ice-cold 70% ethanol. To control for background, a sample of DMSO- and C16-treated cells were subject to staining without OPP. A Click-iT reaction was then used to conjugate Alexa Fluor488-Azide (1:100 dilution). AlexaFluor488 fluorescence was quantified using a BD LSRFortessa instrument. For each sample, 10,000 single cell events were recorded using forward and side scatter pulse geometry gating to select single cells. An unstained control sample was used to identify and exclude autofluorescence in the AlexaFluor488 channel.

The percent of cells progressing through synthesis (S) phase was measured using the FITC BrdU Flow Kit (BD Biosciences). Cells were treated with either 0.1% DMSO or 500 nM C16 for two, four, or seven days then pulsed with BrdU for 30 minutes, collected in PBS, then processed to stain BrdU. Cells were fixed and permeabilized, treated with DNase, incubated with an anti-BrdU antibody conjugated to FITC, and resuspended in 7-AAD solution to stain DNA. FITC and 7-AAD fluorescence were quantified using a BD LSRFortessa instrument. For each sample, 10,000 single cell events were recorded using forward and side scatter pulse geometry gating to select single cells. Unstained control samples were used to identify and exclude autofluorescence.

Western blotting

Cells were washed with PBS and collected in Kischkel Lysis Buffer (150 mM Tris-HCl pH 8.0, 150 mM NaCl, 5 mM EDTA, 1% Triton X-100 with Protease Inhibitor Cocktail (Roche), and PMSF), sonicated, and lysates clarified by centrifugation. Lysates were resolved by SDS-PAGE, transferred to PVDF membrane, and blocked in 5% milk in TBS-T (50 mM Tris, pH 7.5, 150 mM NaCl, 0.1% Tween-20) for one hour. Immunoblotting was performed using the following antibodies: p53 (Santa Cruz sc-126, 1:200), p21 (Cell Signaling #2947, 1:1000), p73 (AbCam

ab40658, 1:1000), WDR5 (Cell Signaling #13105, 1:1000), Histone H3–HRP (Cell Signaling #4499, 1:5000), GAPDH–HRP (Cell Signaling #5174, 1:5000), Goat anti-Rabbit Fc Secondary (ThermoFisher, 1:5000), and Goat anti-Mouse Fc Secondary (Jackson ImmunoResearch, 1:5000). Proteins were visualized using Supersignal West Pico PLUS reagent (Pierce).

RT-qPCR Quantification of mRNA Expression

Cells were lysed in 500 ml Trizol, after which total RNA was extracted using the Zymo Research Direct-zol RNA MiniPrep kit with on-column DNase digestion. After extraction, 1 mg of RNA was reverse transcribed using MuLV reverse transcriptase (Life Tech N8080018) in 20 µl reaction, then diluted five-fold with nuclease-free water. 2 µl of cDNA was used in a 15 µl qPCR reaction using KAPA SYBR FAST qPCR 2x Master Mix and gene-specific primers against *RPL35, RPS24, RPL14, RPS11, TP53, CDKN1, HDM2, TP53INP1,* and *BGT2* (**Table 2.1**). Relative mRNA expression of genes of interest was quantified using the CT method, normalized to signals from *GAPDH*. mRNA expression studies were completed in triplicate with error bars representing the standard error of the mean.

Table 2.1 Primers for RT-qPCR

Gene	Forward Primer	Reverse Primer
RPL35	AACAGCTGGACGACCTGAAG	ACTGTGAGAACACGGGCAAT
RPS24	GACACCGTAACTATCCGCACT	TCTTAGGCACTGTCGCCTTC
RPL14	GTCTCCTTTGGACCTCATGC	ATGGCCTGTCTCCTCACTTG
RPS11	TCCCGCGGTACTACAAGAAC	ACCAGTGAAGGGGCATTTC
TP53	AATTTGCGTGTGGAGTATTT	GTACAGTCAGAGCCAACCTC
CDKN1A	AACAAAGCTGCTGCAACC	ATGGGTTCTGACGGACAT
HDM2	ACCTCACAGATTCCAGCTTCG	TTTCATAGTATAAGTGTCTTTTT
TP53INP1	CTTCCTCCAACCAAGAACCA	CTGCTGAGAAACCAGTGCAA
BTG2	CGAGCAGAGGCTTAAGGT	CTTTTCGGGAAACCAGTG
GAPDH	AAGGTGAAGGTCGGAGTCAAC	GTTGAGGTCAATGAAGGGGTC

Chromatin immunoprecipitations (ChIP)

ChIP-Seq experiments were performed with the help of Drs. April Weissmiller and Gregory Caleb Howard. For each reaction, 1 x 10^7 cells were treated with 500 nM C16 or 0.1% DMSO for four hours. To prepare chromatin, cells were crosslinked using 1% formaldehyde for 10 min, quenched with 0.125 M glycine for 10 min, washed with ice-cold PBS two times, and collected by centrifugation. Nuclei were extracted in 10 mM HEPES, pH 7.9, 10 mM KCl, 0.4% NP-40 and then incubated in 1× TE (10 mM Tris, pH 8.0, 1 mM EDTA) with 1% SDS for 15 min on ice. Chromatin was fragmented using sonication with a Diagenode Biorupter, and debris was removed by centrifugation. Immunoprecipitation was performed using antibodies against WDR5 (Cell Signaling #13105, 5uL per ChIP) or a rabbit IgG control (Cell Signaling #2729). Co-precipitating DNA was quantified using qPCR with primers against *SNHG15, RPS24, PUM1, RPL35, CCT7,* and *METTL1* (**Table 2.2**).

Table 2.2 Primers for ChIP-qPCR

Gene	Forward Primer	Reverse Primer
SNHG15	CGCCACTGAACCCAATCC	TCTAGTCATCCACCGCCATC
RPS24	TTGGCTGTCTGAAGATAGATCG	CGCGTGCCTATAGCTCAAGT
RPL35	CTTGTGCAGCAATGGTGAGA	GCCTAGGTGGCAGATAGAATC
PUM1	TATGAAGGGACAATCTGCTC	AATCCATCTTCATCCTACCG
METTL1	GCATGGCTGCGTCATTAACT	GAGTCTCGGCTGCCATGAT
CCT7	TTCCAAAATGATGGTGAGTG	AGAGGGTCCTACAGAGCAAG

ChIP signals were calculated as percent input. For ChIP coupled to next generation sequencing (ChIP-Seq), DNA from three ChIP reactions was pooled and purified using a QIAquick PCR Purification kit (Qiagen). DNA was eluted, size-selected via AMPure XP (Beckman Coulter), and used to generate libraries with the Ultra II DNA library Prep protocol with Multiplex Oligos for Illumina (New England BioLabs). Libraries were sequenced on an Illumina NovaSeq 6000

instrument (150 bp paired-end) by the VANTAGE Core at Vanderbilt University. Three biological replicates for all ChIP-Seq experiments were performed.

RNA-Seq and PRO-Seq

For RNA-Seq, cells were treated with 0.1% DMSO, 500 nM C16, or 500 nM Nutlin-3a for 72 hours. They were collected in Trizol and RNA purified using a Direct-zol RNA Miniprep kit (Zymo Research) following the manufacturer's instructions. After purification, 2 μg of RNA was submitted to the VANTAGE Core who performed ribosomal RNA depletion, library preparation, and sequencing on an Illumina NovaSeq 6000 (150 bp paired-end reads).

PRO-Seq was performed by Dr. April Weissmiller. For PRO-Seq, cells were treated with 0.1% DMSO or 500 nM C16 for two hours, at which point cells were harvested. Nuclei were extracted in 10 mM Tris-HCl, pH 7.4, 300 mM sucrose, 10 mM KCl, 5 mM MgCl2, 1 mM EGTA, 0.05% Tween, 0.1% NP-40, 0.5 mM DTT, RNAse inhibitor and protease inhibitor cocktail (Roche) and then snap-frozen in 10 mM Tris-HCl, pH 8.0, 25% glycerol, 5 mM MgCl2, 0.1 mM EDTA, 5 mM DTT with protease inhibitor cocktail and stored at −80 °C until ready to use. Biotin run-on reactions were performed on thawed nuclei in a reaction buffer containing Biotin-11-CTP (PerkinElmer, NEL542001) for 3 min at 30 °C. Reactions were stopped by adding Trizol LS (Thermo Scientific) then RNA was purified by chloroform and isopropanol extraction. Resuspended RNA pellets were heated at 65 °C for 40 sec then 1 M NaOH was added, followed by incubation on ice for 10 min. Base hydrolysis was neutralized by addition of 1 M Tris (pH 6.8) then the sample was run over a Micro Bio-Spin P-30 gel column (Bio-Rad). Strepavidin Dynabeads (ThermoFisher, 65601) were incubated with collected material to bind biotinylated RNA to the beads. Bound, biotinylated, RNA was eluted by extracting beads with Trizol then purified using chloroform and isopropanol. RNA adaptors (IDT) were added to the 3′ terminus of the biotinylated RNA. After a second round of biotin-RNA purification, 5′ RNA caps were removed using CAP CLIP (CellScript, C-CC15011H). 5′ RNA adaptors (IDT) were then added. One additional biotin-RNA purification was performed. The purified RNA was used in a reverse

transcriptase reaction to generate cDNA. Libraries were amplified using the generated cDNA and a PCR cycle number determined from a test analysis of a portion of sample. Library amplification was performed with Phusion high-fidelity polymerase (NEB) and customized Illumina-based index primers (*IDT*). PRO-Seq libraries were submitted to the VANTAGE Core at Vanderbilt University for sequencing on an Illumina NovaSeq 6000 with 150 paired-end reads.

Bioinformatics analyses

ChIP-Seq: ChIP-Seq reads were aligned to the human genome hg19 using Bowtie2 [98]. Narrow peaks for each sample were called using MACS2 with the options of "-B -q 0.05 -g hs -f BAMPE" [99]. Peaks were annotated using Homer (http://homer.ucsd.edu/homer/). Consensus peaks in each condition were identified using DiffBind [100]. Differential peaks were determined by DESeq2 [101]. False Discovery Rate (FDR) < 0.05 was used to identify significantly changed peaks.

RNA-Seq: After trimming by Cutadapt [102], RNA-Seq reads were aligned to hg19 using STAR [103] and quantified by featureCounts [104]. Differential analysis was performed by DESeq2 [101]. FDR < 0.05 was used to identify significantly changed genes.

PRO-Seq: Adapters were trimmed and low-quality sequences removed by Cutadapt [102]. Reverse complements for reads > 15 bp were generated using FASTX-Toolkit (http://hannonlab.cshl.edu/fastx_toolkit). Reverse-complemented reads were aligned to hg19 using Bowtie2 [98]. Reads mapping to rRNA loci and reads with mapping quality < 10 were removed. Reads were normalized by the RLE implemented in DESeq2 [101]. Alignment files were used as inputs to NRSA (http://bioinfo.vanderbilt.edu/NRSA/) for estimating alterations of RNA polymerase abundance in proximal-promoter and gene body regions [105]. The promoter-proximal region was defined by examining each 50 bp window with a 5 bp sliding step along the coding strand spanning ± 500 bp from known TSSs; the 50 bp region with the largest number of reads was considered as the promoter-proximal region and its read density was calculated [106]. Gene body was defined as the region from +1 kb downstream of a transcription start site

(TSS) to its transcription termination site. DESeq2 [101] was implemented to detect significant transcriptional changes for promoter-proximal and gene body regions accounting for the batch effect. Transcriptional changes with an FDR < 0.05 were considered significant.

III. SENSITIVITY OF *SMARCB1*-DEFICIENT CELLS TO WIN SITE INHIBITORS

Introduction

In the introduction to this thesis, I outlined the evidence that lead to the potential of WDR5 WIN site inhibitors for the treatment of rhabdoid tumors (RT). RT is a rare and aggressive childhood cancer with an exceptionally high mortality rate and minimal treatment options. RT is caused by the inactivation of *SMARCB1* [1, 6]. It is imperative that we learn more about potential treatment strategies for this cancer to improve outcomes for patients with this devastating diagnosis. Recent work has shown that rhabdoid tumors are sensitive to two small molecule inhibitors: Nutlin-3a, an HDM2 inhibitor, and homoharringtonine (HHT), a translation inhibitor [53, 54]. These sensitivities are particularly interesting because they align with the mechanism of action our laboratory has identified for WDR5 WIN site inhibitors. WIN site inhibitors are able to displace WDR5 from chromatin and decrease expression of a subset of ribosomal protein genes (RPGs). Disrupting this subset of RPGs causes a translational stress response and induces p53 and apoptosis [3, 4]. I hypothesized that because RT cells are sensitive to translational stress and p53 activation, they would be sensitive to WIN site inhibition as well. The primary goal of this portion of work is to determine if *SMARCB1*-deficient cells are sensitive to WIN site inhibitors and compare the sensitivities to that of MV4:11, the prototypical cell line for testing WDR5 WIN site inhibition.

RT is unusual among malignancies in that often the only mutation in these cancers is the biallelic deletion of *SMARCB1*. Because of the similar genetic profiles among RT, I hypothesized that the panel of RT cells that I assembled would exhibit similar sensitivities to WIN site inhibitors. To determine the effect of WIN site inhibition on RT growth, I performed proliferation assays with two chemically distinct WIN site inhibitors, C6 and C16, along with the negative control compound, C6nc. While screening compounds in cell lines does not accurately predict the success of a drug in clinical trials because it does not recapitulate the tumor

microenvironment, it is a necessary first step to demonstrate anti-cancer activity of a compound before moving into costly pre-clinical animal studies.

RT cells are in fact sensitive to WIN site inhibition albeit to varying degrees, with some of the cell lines having C16 IC_{50} values in the low nanomolar range, a value comparable to MV4:11 cells [79]. C16 treatment is also able to disrupt anchorage-independent growth, an important feature of malignant tumors. To try to explain the differences in sensitivity to WIN site inhibitors within the RT panel, I tested WDR5 engagement indirectly by measuring the expression of five universal WDR5 target genes at increasing concentrations of C16 using the QuantiGene™ Plex assay. I show that RT cell lines have nearly identical effect on WDR5 target gene expression despite differences in sensitivity. To determine if the decrease in cell proliferation with WIN site inhibitor treatment is due to an arrest or cell death, I performed a time course study and cell cycle analysis. These data reveal that the primary mode of response of sensitive RT lines to WIN site inhibition is not cell cycle arrest or cell death, but due to a reduction in the rate of proliferation.

Results

Sensitivity of SMARCB1-deficient cell lines to WDR5 WIN site inhibitors

I compiled a panel of eleven *SMARCB1*-deficient cell lines: nine RT cell lines from varying tissue origins including AT/RT from the brain and MRT from kidney, liver, muscle, and other soft tissues as well as two SS lines [107-112] (**Table 1.1**). I intentionally included RT lines from different tissue origins and the SS lines to recapitulate the variety of tumors seen in the clinic, as RT can be found in the brain, kidneys, liver, muscle, and other soft tissues. In my panel, I also included normal diploid BJ fibroblasts derived from the foreskin [113]. Of note, the majority of the cells in this panel express WT p53 (**Table 1.1**) which is an uncommon feature among cancers because p53 is the most frequently altered gene in cancer [114]. However, WT p53 is retained in almost all cases of RT in the clinic. Additionally, prior work has shown that expression of WT p53

Cell Line	C6nc (µM)	C6 (µM)	C16 (µM)	Tumor Type	Location	Lesion	CCLE *TP53* status	Reference
MV4:11	>25	3.2	0.038 ± 0.009	Leukemia (AML)	Blood (P)	MLL–AF4, FLT3/ITD	no mut	4
G401	>25	2.4 ± 0.35	0.098 ± 0.031	MRT	Kidney (P)	SMARCB1 deletion, homozygous	C277F	112
TTC642	>25	1.8 ± 0.34	0.138 ± 0.045	MRT	Soft Tissue, Muscle (P)	SMARCB1, nonsense mutation	no mut	112
HS-SY-II	>25	2.6 ± 0.61	0.309 ± 0.136	Synovial Sarcoma	Soft Tissue (M)	SS18-SSX1 fusion	no mut	107
JMU-RTK-2	>25	16 ± 3.7	0.315 ± 0.075	MRT	Kidney (M)	No SMARCB1 mRNA expression	no mut	108
KYM-1	>25	11.2 ± 3.0	0.555 ± 0.098	MRT	Neck (P)	SMARCB1 deletion, homozygous	no mut	112
A204	>25	5.9 ± 1.1	0.825 ± 0.187	MRT	Soft Tissue (P)	SMARCB1 deletion, homozygous	no mut	112
TTC549	>25	>25	4.5 ± 0.606	MRT	Liver (P)	SMARCB1 deletion, homozygous	no mut	112
TM87-16	>25	19.7 ± 9.1	4.6 ± 0.709	MRT	Retroperitoneum, muscle (M)	SMARCB1 deletion, homozygous	no mut	112
CHLA-266	>25	>25	7.5 ± 0.525	AT/RT	Brain (P)	SMARCB1 deletion, SMARCB1 mutation	no mut	111
Aska-SS	>25	>25	10.4 ± 1.1	Synovial Sarcoma	Soft Tissue (P)	SS18-SSX1 fusion	unreported	109
BT-12	>25	6.8 ± 1.1	11 ± 3.3	AT/RT	Brain (P)	SMARCB1 deletion, homozygous	no mut*	109
BJ	>25	>25	8.7 ± 1.40	Normal diploid fibroblasts	Foreskin	None	NA	113

Table 3.1. Sensitivity of *SMARCB1*-deficient cell lines to WIN site inhibitors Cell lines were treated with seven-point serial dilution set of compounds for five days, and cell numbers determined by CellTiter-Glo. Cell numbers for each dose were normalized to those from DMSO-treated samples and used to calculate mean IC_{50} values, which are shown along with SEM ($n \geq 3$). >25 indicates that the top concentration of compound used (25 µM) did not reduce cell number below 50%. (P) or (M) in Location column indicates if cell line was derived from the primary tumor (P) or a metastatic (M) site. Lesion indicates relevant mutation or *SMARCB1* expression status. Note that CHLA-266 cells have two distinct lesions in *SMARCB1*. *TP53* mutational status is taken from the Cancer Cell Line Encyclopedia [110]. "no mut" indicates no *TP53* mutation reported in that line. *Note that BT-12 cells do not express mutant p53, but have an impaired p53 response, likely due to deletion of CDKN2A [53].

confers sensitivity to WIN site inhibitors in MLLr leukemias and NB [3, 4] so the fact that these RT cell lines have WT p53 increases the likelihood that they will be sensitive to WIN site inhibitors. I tested the sensitivity of this panel to an early generation WIN site inhibitor, C6, and its negative control C6nc [4]. C6 and C6nc have the same molecular formula but slightly difference structures so that C6nc has a >1000-fold reduction in binding affinity compared to C6 [4]. I also tested a next-generation inhibitor with a chemically distinct structure, C16 [79]. C16 is able to bind WDR5 with at least 10 times higher affinity than C6. C6 has a binding affinity of 0.1 nM [4] and C16 has a binding affinity below the limit of detection of the assay used, <0.02 nM [79].

$SMARCB1$-deficient cell lines were treated with a seven point serial dilution of C6nc, C6 or C16 for five days and CellTiter-Glo reagent was used to determine viable cell numbers. CellTiter-Glo is a simple and quick method for quantifying viable cell number. The reagent works by adding the CellTiter-Glo reagent directly to the cultured cells. The CellTiter-Glo reagent is able to lyse the cells and supply luciferase, luciferin, and other proprietary reagents that will react in the presence of ATP to produce a luminescent signal which is proportional to the amount of ATP present in the well. The amount of ATP is directly proportional to the number of metabolically active cells in the culture [115]. This method is high throughput so I was able to screen several compounds in my cell lines rapidly. Cell numbers for each dose were normalized to DMSO-treated control samples. For each compound in each cell line, I calculated the concentration at which proliferation was inhibited by 50% compared to the DMSO control, (IC_{50}). The IC_{50} value is one of the most commonly used metrics of drug potency in pharmacological research. The IC_{50} values of C6nc, C6, and C16 are listed in **Table 3.1**. In addition, the dose response curves for each compound in each cell line are shown in **Figure 3.1**.

I can make three important observations from this analysis. First, the negative control compound, C6nc has little activity, if any, in these cell lines. The IC_{50} was not able to be calculated because it was higher than the concentrations tested. Second, the IC_{50} values for
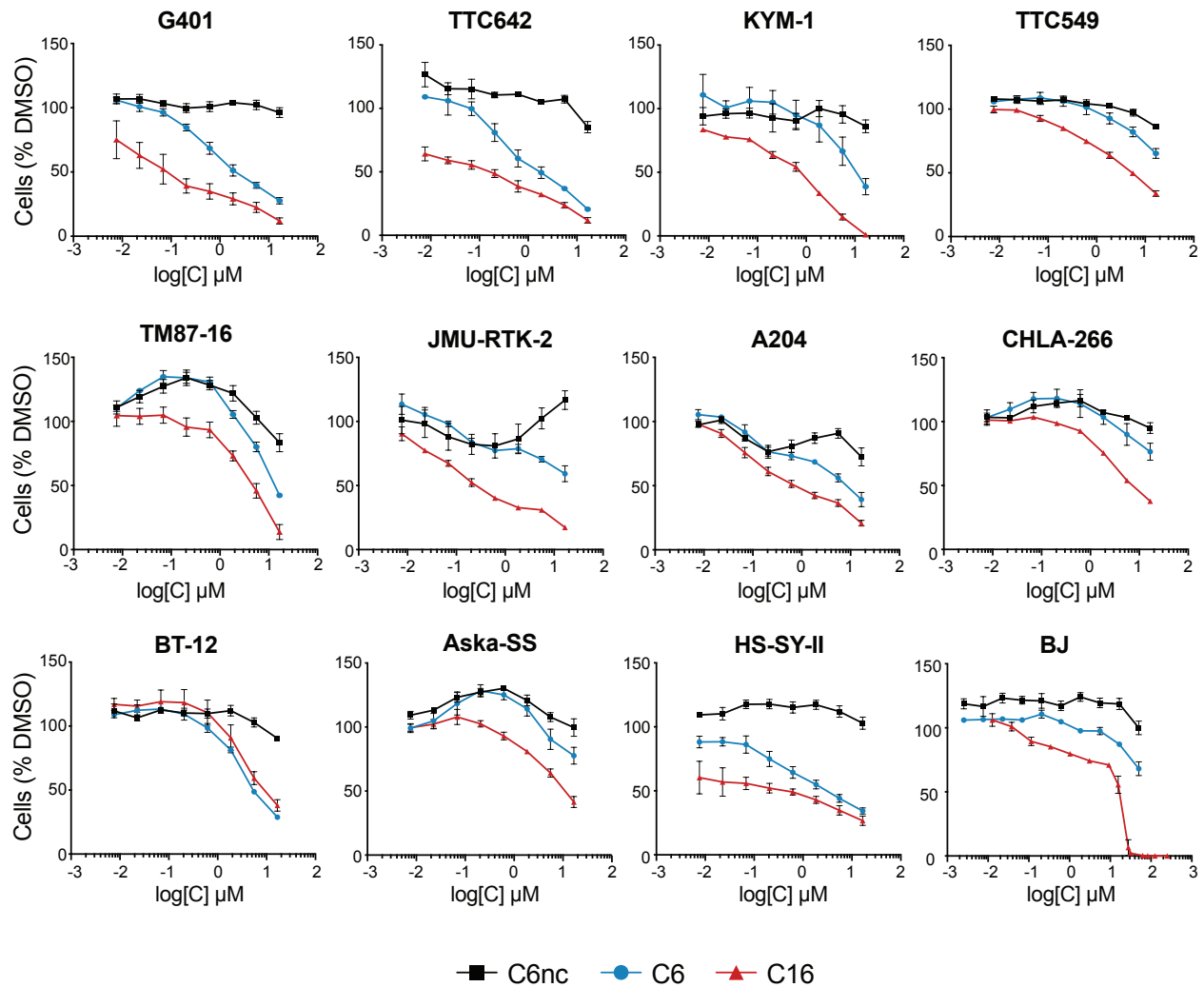
Figure 3.1. WDR5 WIN site inhibitors block proliferation of *SMARCB1*-deficient cells Dose response of indicated cell lines to C6nc, C6, or C16 in a five day treatment. Data are expressed as the percentage of cells remaining at day five, compared to the DMSO control. n=3, error bars represent standard error of the mean (SEM).

C16 are generally lower than those for C6, consistent with its higher affinity for the WIN site [79]. The only exception to this pattern is the BT-12 cells where C6 and C16 have similar potencies, possibly an indication of off target activity in these cells (**Table 3.1, Figure 3.1**). Finally, these cell lines exhibit a 100-fold range in sensitivity to WIN site inhibitors. I set an arbitrary cut-off to define cells that are sensitive to C16 at IC_{50} values less than 1 µM. I chose a more stringent cut-off for sensitivity than used in work with C6 in MLLr cancers due to the increased potency of C16. In general, IC_{50} values in the single digit micromolar range are considered acceptable for anti-cancer therapies [116]. This cut-off divides the panel in half with six sensitive cell lines and six insensitive cell lines. The sensitive cell lines include G401 (IC_{50} = 98 nM), TTC642 (IC_{50} = 138 nM), HS-SY-II (IC_{50} = 309 nM), JMU-RTK-2 (IC_{50} = 315 nM), KYM-1 (IC_{50} = 555 nM), and A204 (IC_{50} = 825 nM). The most sensitive lines respond almost as well as our benchmark leukemia line MV4:11 (IC_{50} = 38nM) [4, 79]. The insensitive lines include TTC549 (IC_{50} = 4.5 µM), TM87-16 (IC_{50} = 4.6 µM), CHLA-266 (IC_{50} = 7.5 µM), Aska-SS (IC_{50} = 10.4 µM), BT-12 (IC_{50} = 11 µM), and BJ fibroblasts (IC_{50} = 8.7 µM). There is no trend between sensitivity and the different RT types or the site of tumor origin. (**Table 3.1**).

A limitation of the proliferation assays is that the treated samples are normalized to the DMSO control. I cannot determine if the decrease in proliferation is because of a slowing or halting of proliferation or because of cell killing. I treated RT cell lines with DMSO or increasing concentrations of C16 and measured the cell number each day for five days using CellTiter-Glo. I also set up an ATP standard curve in order to measure absolute cell number at each day. I treated G401, TTC642, KYM-1, TTC549, and TM87-16 cells. As I move through this project, I will use this abbreviated panel of five cell lines because it encompasses a wide range of sensitivities, highly sensitive (G401 and TTC642), moderately sensitive (KYM-1) and insensitive (TTC549 and TM87-16). Over the course of a five day treatment, C16 induces a dose-dependent and progressive decrease in cell number compared to the DMSO control in G401, TTC642, and KYM-1 cells (**Figure 3.2A**). This means that at each day, there are progressively fewer cells when compared to DMSO. However, in KYM-1 cells, it takes at least two or three
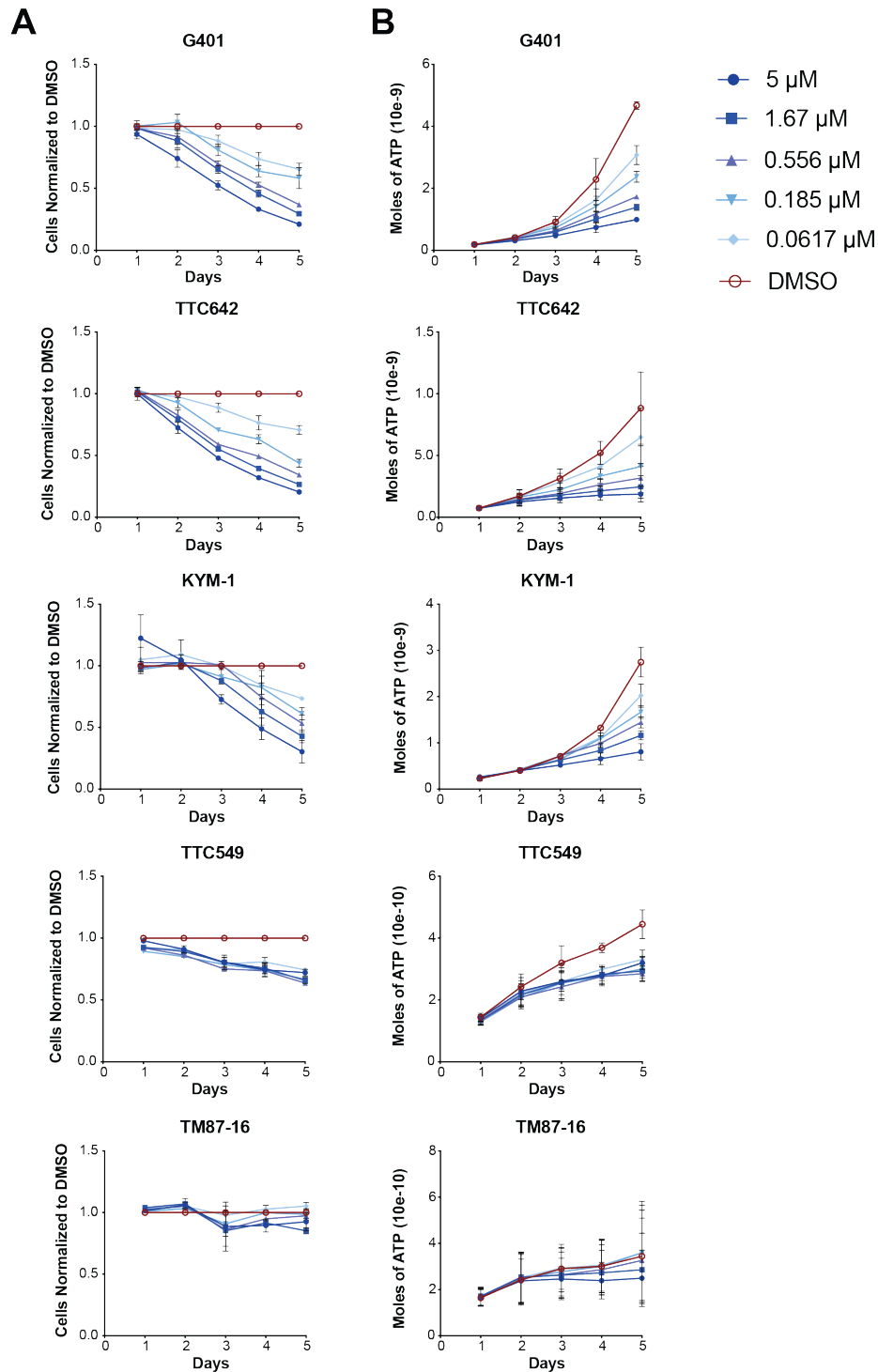
Figure 3.2. WIN site inhibitors decrease proliferation of RT cells (**A**) Cells were treated with the indicated concentrations of C16 for the indicated number of days. Data are expressed as the percentage of cells remaining at each day, compared to the DMSO control. n=3, error bars represent standard error of the mean (SEM). (**B**) As in (A) except that the cell number is expressed as absolute moles of ATP, determined using CellTiter-Glo Luminescent assay against an ATP standard curve. n=3, error bars represent standard error of the mean (SEM).

days to see the difference between DMSO and treated samples. On the other hand, TTC549 and TM87-16 do not demonstrate a growth deficit with C16 treatment. In TTC549 cells, there is only a small difference between the DMSO and the C16 treated samples. All the TTC549 cells that were treated with C16 responded similarly without an obvious difference in cell number for the different concentrations of C16 indicating that the inhibition is probably due to off-target activity. The TM87-16 cells show almost no difference between the DMSO and C16 treated samples. Normalizing the cell numbers to DMSO fails to give an indication of the absolute number of cells present in the well and if there are more, the same, or less cells present compared to the previous day. This is important because it will give an indication of if the inhibitors are slowing proliferation compared to the DMSO treated sample, stoping proliferation, or killing the cells. Because CellTiter-Glo measures ATP present in the well, I was able to set up an ATP standard curve to quantify the absolute amount of ATP each well, a proxy for cell number. At all dose levels in all cell lines, absolute cell numbers at the end of treatment are higher than at the beginning, indicating that the cells are able to continue to proliferate while being treated with WIN site inhibitors (**Figure 3.2B**). This observation is consistent with a decrease in proliferation as a result of WIN site blockade, rather than a cell death response.

In addition to disrupting cell proliferation in 2D culture, I wanted to know if WIN site inhibitors could disrupt anchorage independent growth. Normal cells require interactions with neighboring cells and extracellular matrix to be able to grow. Cancer cells on the other hand are able to grow in the absence of these interactions, a property referred to as anchorage-independent growth [117]. The ability of these cells to grow independently of a solid surface reflects the ability of cancer cells to grow in incorrect locations *in vivo* as is the case in cancers that invade beyond their tissue of origin into neighboring tissue or in the case of metastasis [118]. The ability of a cancer cells to invade and metastasize distinguishes a malignant tumor from a benign one. To evaluate anchorage-independent growth, Kiana Guerrazzi performed a soft agar colony formation assay. Soft agar colony formation assays are used to evaluate anchorage-independent growth *in vitro* [119]. We grew cells in a layer of soft agar mixed with culture

medium on top of a denser layer of soft agar and culture medium so that the cells cannot adhere to the culture plate but instead grow in visible colonies throughout the agar, independent of interactions with the culture plate. We were able to evaluate the ability of RT cells to form colonies in the presence of WIN site inhibitors compared to a DMSO control. In the three sensitive cell lines tested, G401, TTC642, and KYM-1, we see colony formation in the DMSO sample indicating that these cell lines are transformed and capable of anchorage-independent growth (**Figure 3.3**). When treated with increasing concentrations of C16, the cells develop fewer and smaller colonies compared to control (**Figure 3.3**). This is visible by eye but when we blindly counted the number of colonies at each treatment in the G401 and TTC642 cells lines to quantify the difference in anchorage-independent growth with C16 treatment, we found that colony formation significantly decreases in a dose-dependent manner (**Figure 3.3**). We did not quantify the colonies in KYM-1 cells because there were very few colonies even in the DMSO sample so the differences in colony formation between the treatments could easily be seen by eye. This experiment demonstrates that WIN site inhibitors are able to disrupt anchorage-independent growth, a hallmark of carcinogenesis.

Evaluation of WDR5 target engagement by WIN site inhibition

It is possible that the differential response of *SMARCB1*-deficient cells to WIN site inhibitors stems from differences in the ability of the compounds to access and engage WDR5. Potential loss in activity of the WIN site inhibitors could be due to failure of the drugs to get into the cells due to variance in membrane permeability or ability to reach their target due decreased rate of diffusion, increased non-specific binding, or metabolism, among other things [120]. In order to determine the efficiency with which WIN site inhibitors engage WDR5 in sensitive and insensitive cells, I quantified the effects of WIN site inhibition on the expression of a set of known direct WDR5 targets, a selection of RPGs. I developed a WDR5 target engagement assay that uses QuantiGene™ Plex technology to assess multiple transcript levels simultaneously. The QuantiGene™ Plex assay is a hybridization based technique that involves
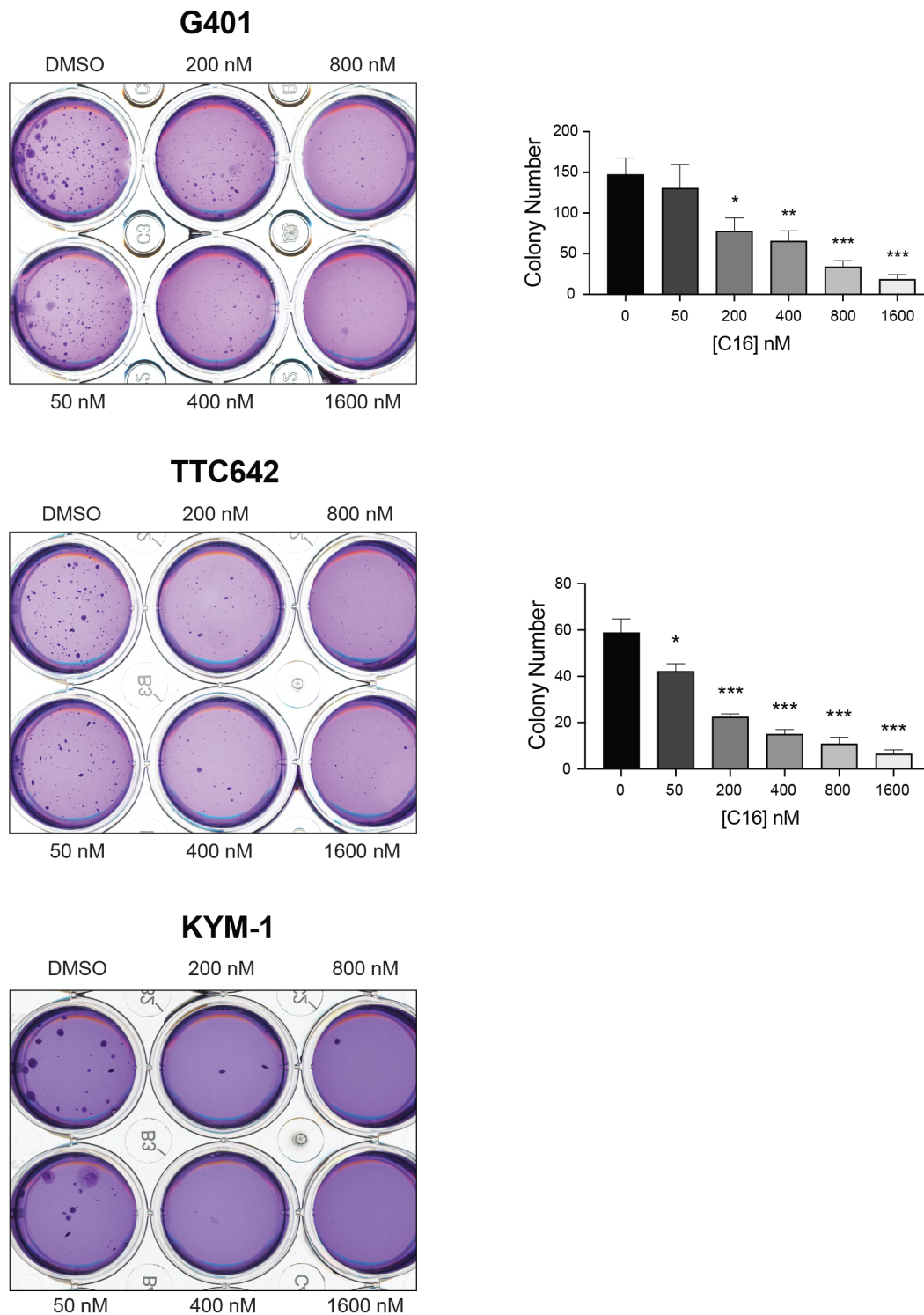
Figure 3.3. WIN site inhibitors prevent RT cell colony formation in soft agar assays
G401, TTC642, and KYM-1 cells were grown in soft-agar and treated with the indicated concentrations of C16 for 14 days. Cultures where then stained with crystal violet to visualize colonies. Left; representative images from analysis of each line. Right; quantification of colony number per well. Colonies were counted blind. *p = <0.05, **p =<0.01, ***p = <0.001, as determined by student's t-test. n=3, error bars represent standard error of the mean (SEM).

lysing cells to release RNA and incubating with a target specific probe set each with a unique Luminex capture bead. Once the RNA has been captured by the gene specific probe and bead, a signal amplification tree is built resulting in a 2,400x amplification per copy of RNA which can then be detected using a Luminex instrument. My target gene panel included seven RPGs, five of which are universally bound by WDR5 and suppressed by WIN site inhibitor (*RPS14, RPS24, RPL26, RPL32*, and *RPL35*) and two of which are never bound and are unresponsive to WIN site blockade (*RPS11* and *RPL14*) [3, 4]. I treated my abbreviated panel of five RT cell lines for three days with increasing concentrations of C16 as well as MV4:11 and BJ fibroblasts so that I could compare target engagement to our most responsive cell type as well as to a "normal" cell. I then used the QuantiGene™ Plex assay to measure relative expression levels of the selected RPGs at each concentration.

Previous work has shown that WIN site inhibitors reduce RPG expression two-fold [4]. As expected, WDR5-bound RPGs are suppressed by a factor of two compared to DMSO treated control samples in all lines examined (**Figure 3.4**), while the non-WDR5-bound RPGs do not change or are modestly induced at the highest concentrations. I was able to calculate IC_{50} values for RPG suppression in all of the cell lines (**Table 3.2**). The IC_{50} in this case is measuring the concentration at which the RPGs are inhibited to half of their maximum suppression, which allows for reliable comparison between cell lines. The concentration of maximal inhibition is helpful for identifying the minimal dose at which cells experience maximum activity to be able to treat cells in subsequent experiments with a dose that avoids off-target effects. In most cases, IC_{50} values for RPG suppression are in the double digit nanomolar range, values smaller than the cellular growth IC_{50} values. This result is not surprising because the cells may require RPGs to be maximally inhibited to disrupt proliferation rather than 50%, so the cellular IC_{50}s are higher than the RPG IC_{50} values. There are differences in the efficiency with which each of the RPGs are suppressed by C16 in each line, but these differences are generally relatively small, and do not correlate with cellular growth response. Thus, although cellular context can impact the efficiency with which WIN site inhibitors inhibit proliferation, differences in the ability of
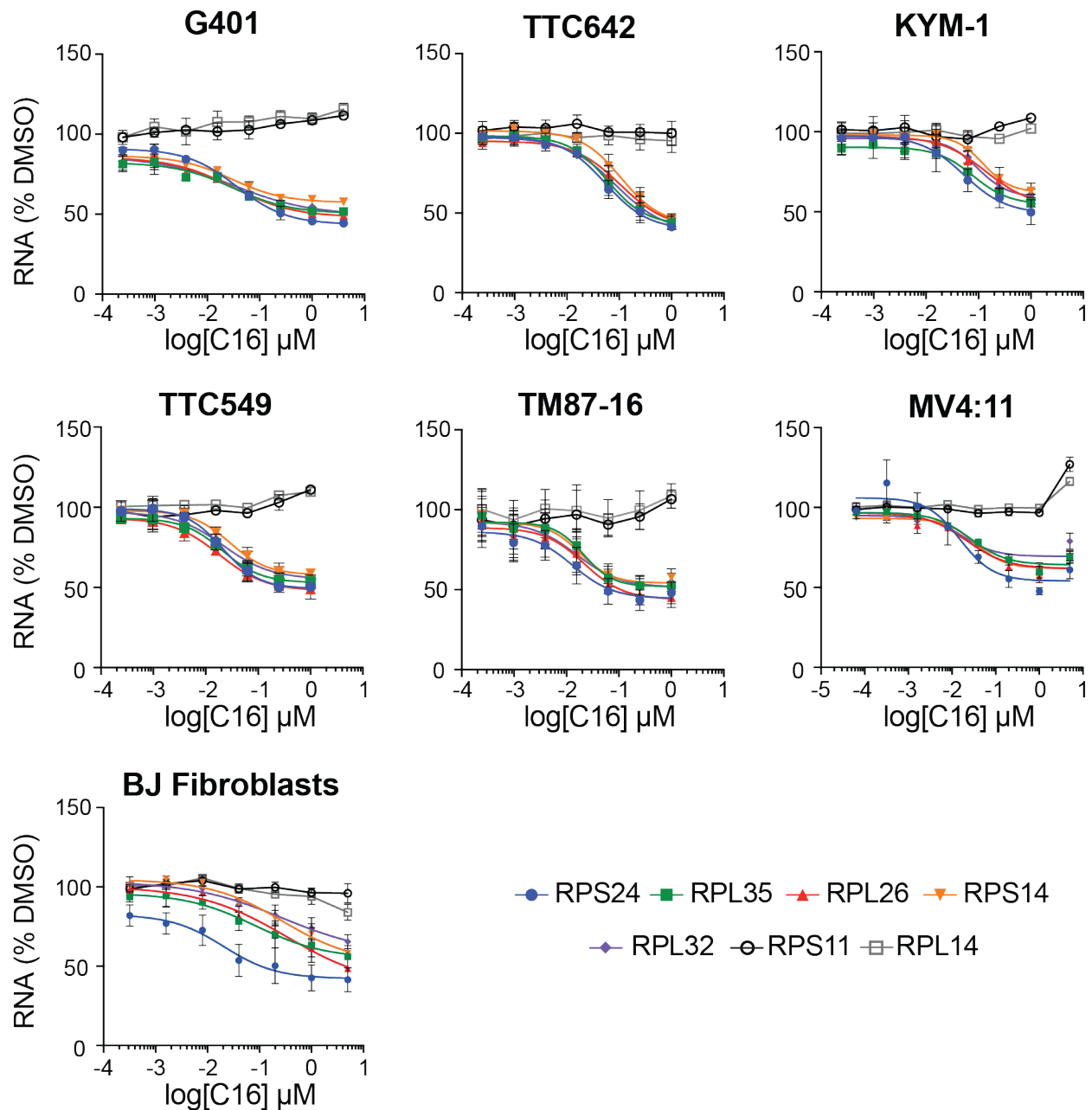
Figure 3.4. WIN site inhibitors engage WDR5 to decrease target gene expression
Indicated cell lines were treated for three days with increasing concentrations of C16, and RNA levels for RPGs determined via QuanitGene™ Plex arrays. RNA signal is expressed as a percentage of the equivalent DMSO control for each RPG in each line, normalized to *GAPDH* and *HPRT1*. RPGs with colored lines bind WDR5 and are suppressed two-fold by WIN site inhibitor; those in black and gray are unbound and not suppressed. n=3, error bars represent standard error of the mean (SEM).

IC$_{50}$ (nM) →	Cell proliferation	RPS24	RPL35	RPL26	RPS14	RPL32
G401	98	36.7 23.3 - 57.9	31.2 11.3 - 85.9	30.4 9.8 - 93.9	29.4 8.1 - 107	33.4 8.2 - 135
TTC642	138	54.2 28.8 - 102	58.9 25.9 - 134	105 34.5 - 320	108 45.2 - 257	85.3 32.2 - 226
KYM-1	555	52.5 69.4 - 397	79.0 34.8 - 179	139 16.0 - 1210	123 51.6 - 293	94.9 43.3 - 208
TTC549	4500	21.3 10.3 - 44.1	20.8 10.0 - 43.6	18.0 7.1 - 46.0	29.1 11.8 - 71.8	21.7 7.1 - 66.4
TM87-16	4600	13.0 1.8 - 91.0	21.2 5.8 - 77.3	21.7 3.5 - 133	18.0 3.3 - 99.8	15.6 1.5 - 165
MV4:11	38	21.6 4.46 - 104	52.8 17.2 - 162	73.8 6.56 - 831	74.6 26.5 - 210	47.1 12.3 - 180
BJ	8700	20.6 2.1 - 199	83.4 3.99 - 1747	333 11.0 - 1007	278 3.70 - 2090	277 1.69 - 4551

Cell line

Table 3.2. Summary of RPG IC$_{50}$ values obtained in QuanitGene™ Plex Assay Cell proliferation and RPG expression IC$_{50}$ values for C16 in the indicated cell lines. 95% confidence intervals for IC$_{50}$ values for RPG expression are shown in gray below the IC$_{50}$ in black.

compounds to engage WDR5 cannot explain the differential cellular sensitivities to WIN site inhibitors I observe in the *SMARCB1*-deficient cells.

Effect of WDR5 inhibition on the cell cycle

In order to understand if the reduction in proliferation in cells treated with WIN site inhibitors is due to an arrest in a specific phase of the cell cycle or the result of a general decrease in the rate of proliferation, I performed a cell cycle analysis. I treated cells with 500 nM C16—the minimum concentration sufficient to maximally inhibit RPG transcripts in all lines (**Figure 3.4A**) and stained the cells with propidium iodide which intercalates into DNA. By flow cytometry, I can quantify the amount of DNA in each cell to determine which phase of the cell cycle the cell is in. Cells in the quiescent non-dividing state (G_0) and the first gap phase (G_1) will have a single copy of each chromosome. During synthesis (S) phase, cells are dividing so the amount of DNA in the cell is increasing as the cell progresses through S phase. Cells in the second gap phase (G_2) have two copies of each chromosome so have twice as much DNA as they do in G_1. Cells with DNA content less than that of G_1 cells are termed sub-G_1 and are considered apoptotic or necrotic because cells undergo DNA fragmentation as they die. I treated G401 and TTC642 cells for two, four, and seven days in order to look for changes in cell cycle distribution at a relatively early point, day two, before there is a big difference in growth inhibition between DMSO and treated samples as seen in the timecourse experiments in **Figure 3.2B**. By day four, there is a greater difference in cell number between the DMSO control samples and the treated samples so there is greater chance that there will be a noticeable difference in cell cycle distribution at this point. Finally, looking for changes in cell cycle at seven days will show whether or not any changes in cell cycle distribution persist. When comparing DMSO and C16 treated samples, there are only modest changes in cell cycle phase distribution (**Figure 3.5A**). G401 cells display a small but significant increase in the percentage of cells in G1 phase at day two with decrease in S and G2/M phase cells. These differences resolve at day four and day seven with a lingering decrease in S phase cells. In TTC642 cells however, there are no
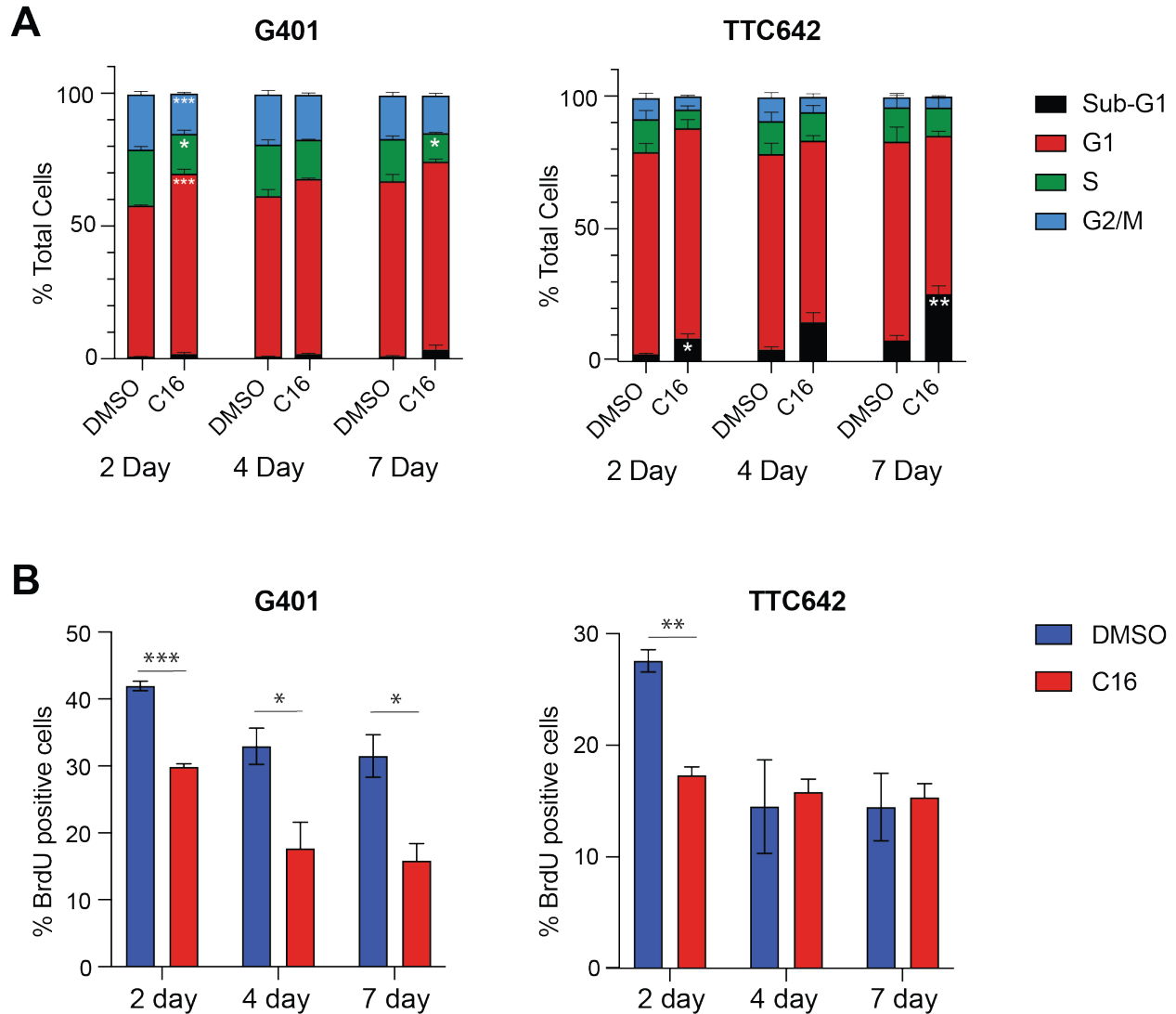
Figure 3.5. WIN site inhibition modestly affects cell cycle profile (**A**) Stacked bar graph, showing distribution of cell cycle phases as determined by flow cytometry for G401 and TTC642 cells treated with DMSO or C16 for two, four, or seven days. *p < 0.05. **p < 0.01, ***p < 0.001 as determined by students t-test. n=3, error bars represent standard error of the mean (SEM). (**B**) Bar-graph showing the percentage of BrdU positive cells as determined by flow cytometry in G401 or TTC642 cells treated with DMSO or C16 for two, four, or seven days. *p < 0.05. **p < 0.01, ***p < 0.001 as determined by students t-test. n=3, error bars represent standard error of the mean (SEM).

significant differences in cell cycle distribution with the exception of the sub-G1 population, which accumulates over time and likely corresponds to apoptotic or necrotic cells. This demonstrates that not all of the RT cell lines have an identical cellular response and that WIN site inhibition may induce apoptosis in certain RT contexts. Together this indicates that G401 and TTC642 cells are not undergoing a significant cell cycle arrest upon treatment with WIN site inhibitor.

I then performed BrdU-pulse labeling experiments to more accurately measure the percentage of cells actively undergoing DNA replication in S phase. For these experiments, I treated G401 or TTC642 cells with DMSO or 500 nM C16 for two, four, or seven days as I did in the cell cycle analysis experiment. I then added BrdU to the media for 30 minutes before harvesting the cells. The BrdU is incorporated into the DNA in the place of thymidine during DNA replication. I can use a fluorescently labeled anti-BrdU antibody to measure the percentage of cells incorporating the BrdU, meaning they are undergoing DNA replication, by flow cytometry. In G401 cells, DNA synthesis is significantly decreased by C16 at two, four, and seven days. However, a significant percentage of cells (~15%) are still progressing through S phase (**Figure 3.5B**). In TTC642 cells, there is a similar decrease in the percentage of BrdU positive cells at day two but then no significant difference between DMSO and C16 treated cells at days four and seven (**Figure 3.5B**). Taken together, these data indicate that the primary mode of response of sensitive cell lines to WIN site inhibition is a reduction in the rate of proliferation, rather than cell cycle arrest or cell death.

<center>Discussion</center>

RT is an aggressive pediatric cancer in desperate need of novel treatment strategies. WDR5 WIN site inhibitors have the potential to be an effective treatment strategy in RT. Studies have already shown that RT is sensitive to the translation inhibitor, HHT [54], and to the HDM2 inhibitor, idasanutlin [53] indicating that small molecules that disrupt protein synthesis or induce p53 may be affective treatment strategies for RT. Previous studies from our laboratory in

MV4:11 cells have shown that WDR5 WIN site inhibitors act by displacing WDR5 and decreasing the expression of PSGs [4]. This results in a decrease in protein synthesis, a similar functional mechanism to that of translation inhibitors. In addition, WIN site inhibitors induce p53 and promote apoptosis, a mechanism that reflects the mechanism of HDM2 inhibitors. To determine if RT cells are sensitive to WIN site inhibitors, I assembled a panel of *SMARCB1*-deficient cell lines including AT/RT, MRT from the kidney, liver, muscle, or soft tissue, and SS. I tested the sensitivity of these cells to two molecularly distinct WIN site inhibitors, C6 and C16 and a negative control compound, C6nc. All of the *SMARCB1*-deficient cell lines demonstrated some sort of sensitivity to the WIN site inhibitors, and in general, the IC_{50} value of C16 was an order of magnitude lower than C6. This alludes to the structure activity relationship (SAR) of C6 and C16, which is the relationship between the chemical structure and the biological activity of the drug. For the WIN site inhibitors, as the *in vitro* binding affinity of the inhibitors increases, the cellular growth inhibition also increases [4, 79]. The SAR provides evidence that the WDR5 WIN site inhibitors are acting on target and that any biological response is due to WDR5 inhibition.

Because of the unusually simple genetic profile of RT and the retention of WT p53 in almost all cell lines tested, a gene important for conferring sensitivity to WIN site inhibitors, I predicted that the *SMARCB1*-deficient cells in my panel would have similar sensitivity to WIN site inhibitors. Despite a common genetic (MRT and AT/RT) or functional (SS) perturbation, I was surprised to see a 100-fold range of sensitivities to WIN site inhibitors among the panel tested. G401 and TTC642 cells, for example, are almost as sensitive to C6 and C16 as MV4:11 leukemia cells, which are often considered the prototype for a WIN site inhibitor-sensitive cell line [4, 86] with IC_{50} values for C16 in the low nanomolar range. TTC549 and TM87-16 cells, in contrast, display IC_{50} values close to those obtained in K562 cells [4, 79], which our laboratory and others classified as least sensitive to WIN site inhibition. This is not unprecedented as work done with HHT and idasanutlin in a similar panel of RT cell lines also demonstrate ~100-fold range in sensitivities [53, 54]. One possible explanation for the differential response to WIN site inhibitors is because of differences in intracellular compound accumulation or access to WDR5. My use of

the QuanitGene™ Plex Assay to determine RPG target engagement demonstrates that differences in the extent of WDR5 inhibition do not account for the wide differential in cellular response across the panel. The differential sensitivities must be the result of distinct the downstream responses to WIN site inhibition in each cell line. Understanding the responses of WIN site inhibition in both sensitive and insensitive lines will be a major focus of this work.

Although it is true that sequencing of patient tumors reveals a clean background with a single genetic lesion, this may not be the case in the RT cell lines. Indeed, this is a major limitation of working with cell lines; cell lines may have diverged from the original patient sample and from each other in culture. This will be the subject of Chapter VI where I will compare the transcriptomes of sensitive and insensitive cell lines to determine if there are differences in the expression profiles that can account for the differences in cellular sensitivity. Another possibility for the differences in cellular sensitivity could be due to differences in the distribution of WDR5 on chromatin in different cell lines. Our laboratory has identified a "universal" set of WDR5 bound genes so we can predict where WDR5 is on chromatin but validating that WDR5 is actually at these sites in both sensitive and insensitive RT lines is essential for predicting the mechanism of response to WIN site inhibitors. This will be addressed in Chapter IV. Another explanation for the differences in sensitivity is that the primary transcriptional responses with WIN site blockade in these cell lines are different. The QuantiGene™ Assay only allowed me to look at a small subset of WDR5 target genes to confirm WDR5 engagement but the complete transcriptional response to WIN site inhibition might vary between cell lines. Exploring the transcriptional response both at the transcriptional level in Chapter V and the expression level in Chapter VI will be important for defining the full response to WIN site inhibition in RT cells. In my panel of *SMARCB1*-deficient cell lines, almost all of the cell lines have WT p53 (**Table 3.1**), a protein shown to be important for cells to respond to WIN site blockade [3, 4]. It is important that I confirm that p53 and the p53-pathway are functional as that may be contributing to differences in sensitivity. For example, BT-12 cells are the least sensitive to WIN site inhibition (**Table 3.1**) but its been shown that they have a mutation in CDKN2A leading to increased HDM2 activation

43

and decreased p53 pathway function [53]. If the p53 pathway is not intact in any of these cells lines, that may provide an explanation for the differential sensitivity.

In addition to exploring the variability in response to WIN site inhibitors among *SMARCB1*-deficient cells, another major focus of my work is to identify if and how the response differs from that of MV4:11, our premier responding cell line. When examining how RT cells respond to WIN site inhibition over time, I did not find evidence that the cells were undergoing a cell cycle arrest or cell death but instead slowing their rate of proliferation. In time course assays, samples treated with C16 have fewer cells compared to DMSO controls but still demonstrate an increase in cell number over the course of the experiment. While this does not rule out the possibility that the rate of proliferation outpaces at the rate of apoptosis, cell cycle analysis in G401 cells failed to show an accumulation of cells in sub-G1 suggesting that cells are not undergoing cell death. Overall, the changes in the cell cycle profile are subtle which indicates that cells are not arresting in any single phase. In fact, BrdU pulse-labeling experiments show that while there is a decrease in the percentage of cells undergoing DNA replication, cells continue to pass through the cell cycle despite WIN site inhibitor treatment. Together this suggests that the response of RT cells to WIN site inhibition is not via apoptosis as is the case in MLLr and NB cell lines [3, 4], but is instead due to a decrease in proliferation. Slowing the rate of growth is an effective anti-cancer treatment strategy as there are a number of therapeutics that are cytostatic in response rather than cytotoxic [121]. For example, the mechanism of action for most chemotherapies is cytostatic in nature and involves disrupting an essential program to prevent the growth and division of the cancer cell [121]. Along these lines, progression-free survival, the amount of time a patient lives with the disease without it getting worse, is still a common metric for drug efficacy in clinical trials. Due to the aggressive nature of RT in the clinic, a cytostatic or progressive-free response would be a vast improvement over current treatment strategies.

The perplexing result from these early cellular sensitivity studies is that despite a common genetic lesion amongst the *SMARCB1*-deficient cells, they have a considerable range of

sensitivities. The universal retention of WT p53 in the panel can not explain the differences in cellular sensitivity. The concept that WT p53 alone may not be an accurate predictor of sensitivity will be explored in Chapter VII but it opens the possibility for a broader utility of WDR5 WIN site inhibitors in the clinic should they become available. In addition, the range in cellular sensitivities can not be explained by differences in WDR5 target engagement between sensitive and insensitive lines because I do not observe a difference in RPG inhibition between cell lines. While this result may initially be discouraging because it indicates that there is some yet to be discovered factor that is conferring sensitivity, it also leads to more informed decisions about therapies because we know that there may be variable responses in the clinic. Perhaps a combination therapy may be an effective treatment strategy to improve the response of the less sensitive and insensitive cell lines. This possibility will be explored in Chapter VI.

Our understanding of the understanding the mechanism of action of our WDR5 WIN site inhibitors is entirely based on work done in MLLr leukemia cells and NB cells [3, 4]. In those contexts, WIN site inhibition displaces WDR5 from chromatin, decreases PSG expression, and induces translational stress and p53-mediated apoptosis. Early experiments with WIN site inhibitors in the context of *SMARCB1*-deficient cancer already deviate from the expectation in that WIN site inhibition fails to induce apoptosis and instead slows the rate of cellular proliferation. By understanding how *SMARCB1*-deficient cells respond to WIN site inhibitors and how it differs from previous studies, we will be able to expand our understanding of WDR5 WIN site inhibitor function in a novel context. Much of the rest of my work throughout this thesis is focused on understanding how *SMARCB1*-deficient cells respond to WIN site inhibitors through changes in WDR5 chromatin binding and the transcription and gene expression of WDR5 target genes. I will highlight instances in which RT cells respond similarly and differently from our preconceived understanding of the mechanism of action of these inhibitors.

IV. WIN SITE INHIBITORS DISPLACE WDR5 FROM CHROMATIN IN RHABDOID TUMOR

CELLS

Introduction

The central objective of this thesis work is to explore the potential of WDR5 WIN site inhibitors to treat rhabdoid tumors. Previous work in our laboratory has shown that WDR5 is tethered to chromatin via the WIN site and that the primary mechanism through which WIN site inhibitors function in MLLr leukemia cells is through the displacement of WDR5 from its sites on chromatin [3, 4]. I predict that WIN site inhibitors will behave the same way in the context of RT cells and that WDR5 will be globally displaced in RT cell lines, regardless of sensitivity. Before we test if WDR5 is displaced from chromatin with WIN site inhibitor, it is important to understand where WDR5 binds to chromatin in unperturbed RT cells. Defining the sites of WDR5 chromatin localization in RT cells and comparing it to where WDR5 is bound in other contexts is important for predicting cellular changes as a result of WIN site inhibition. WDR5 chromatin association studies have revealed a conserved set of WDR5 binding sites which consists of ~100 genes enriched in genes that encode PSGs [3]. I predict that WDR5 will be bound to these universal target genes in RT cells but that there may be some cell type to cell type variability in other locations at which WDR5 is bound. We know that WDR5 is comprehensively displaced from chromatin with WIN site inhibitor treatment in MV4:11 and K562 cells regardless of cellular sensitivity to WIN site inhibitors [3, 4]. MV4:11 cells have comparable cellular IC_{50} values to the most sensitive *SMARCB1*-deficient cell lines and K562 cells have cellular IC_{50} value comparable to the insensitive *SMARCB1*-deficient cell lines (**Table 3.1**) [4]. I hypothesize that WDR5 will be globally displaced from WDR5 target genes with WIN site inhibition regardless of cellular sensitivity.

The ChIP-Seq experiments in this chapter were performed by Dr. April Weissmiller and Dr. Caleb Howard and the in-depth analysis was done by Dr. Jing Wang in the Department of

Biostatistics at Vanderbilt University. We first performed ChIP-Seq for WDR5 in both sensitive and insensitive RT cell lines, G401, KYM-1, and TTC549. This analysis revealed that WDR5 is bound to the universal WDR5 target genes in each cell type but that there is some variability in WDR5 binding between the cell lines. As has been observed in other cell types [3, 4], WDR5 is bound to genes related to protein synthesis. We then tested how WIN site inhibitor treatment affects WDR5 localization to chromatin. Upon treatment with WIN site inhibitors, WDR5 is globally displaced from chromatin at WDR5-bound genes. These data confirm that WDR5 is bound to universal WDR5 target genes in RT cells and that the WIN site is required to tether WDR5 to chromatin. As is the case in other contexts [4], treatment with WIN site inhibitor globally displaces WDR5 from chromatin in RT cells.

<div align="center">Results</div>

Genome-wide localization of WDR5 on chromatin in RT cells

Chromatin-immunoprecipitation coupled to next generation sequencing (ChIP-Seq) was used to track the location of WDR5 on chromatin. ChIP is a technique to investigate the interaction between a protein of interest (POI), in this case WDR5, and genomic DNA. For this assay, cells are harvested and treated with formaldehyde which cross-links protein-DNA interactions. The chromatin is then fragmented using sonication and then the POI and the DNA it is bound to are pulled down using an antibody for the POI. After the pulldown, the protein-DNA cross-links are reversed and the precipitated DNA fragments are purified. These purified DNA fragments correspond to locations at which the POI is bound to DNA. The genomic loci can be identified using Next Generation Sequencing by Vanderbilt Technologies for Advanced Genomics (VANTAGE). Dr. April Weissmiller and Dr. Caleb Howard performed ChIP-seq in three RT lines, G401, KYM-1, and TTC549. These lines were chosen because they represent three different sensitivities to the WIN site inhibitor, C16. G401 cells are highly sensitive, KYM-1 cells are moderately sensitive, and TTC549 cells are insensitive (**Table 3.1**). This will allow us to

determine if the differences in cellular sensitivity with WIN site inhibitors is because of differential WDR5 chromatin localization between cell lines.

Consistent with studies in other cell lines [3, 4, 78], there is a difference in the number of WDR5 binding sites in the three RT lines, ranging from ~160 in G401 to ~700 in KYM-1 cells and ~1000 in TTC549 cells (**Figure 4.1**). Despite the disparate number of binding sites, there is a high degree of overlap between the three lines such that the commonalities encompass almost all of the G401 binding sites (**Figure 4.1**). The overlap is not surprising based on the previous work demonstrating that WDR5 is bound to a conserved set of binding sites in many cell types [3]. However, the differences in WDR5 binding between the cell lines could be responsible for the differences in cellular sensitivity to WIN site inhibition.

WDR5 is bound to protein synthesis genes in RT cells

We were then interested in identifying where WDR5 is bound in relation to transcriptional start sites (TSS) of genes in each of the cell lines. We found that as with earlier studies [3, 4, 78], binding sites for WDR5 in all RT lines are predominantly promoter proximal, with a majority occurring within 1 kb of an annotated TSS (**Figure 4.2**). WDR5 binding with respect to the TSS is similar between G401, KYM-1, and TTC549 which corroborates the idea that WDR5 is a predominantly promoter proximal binding protein. Due to the extensive overlap of WDR5 chromatin localization in the three RT cell lines tested, I assumed that WDR5 would be bound at the sites we have previously characterized as "universal" WDR5 target genes. In human cell lines, this set is made up of ~100 binding sites [3]. We observed that almost all the universal sites are bound in all three RT cell lines (**Figure 4.3**), extending the presence of these near-ubiquitous binding sites to the RT context.

I was then interested in seeing if the genes at which WDR5 is bound have any common functionality or are involved in a specific pathway. Based on previous work, I predicted that WDR5 binds at genes related to protein synthesis. I used gene ontology (GO) enrichment
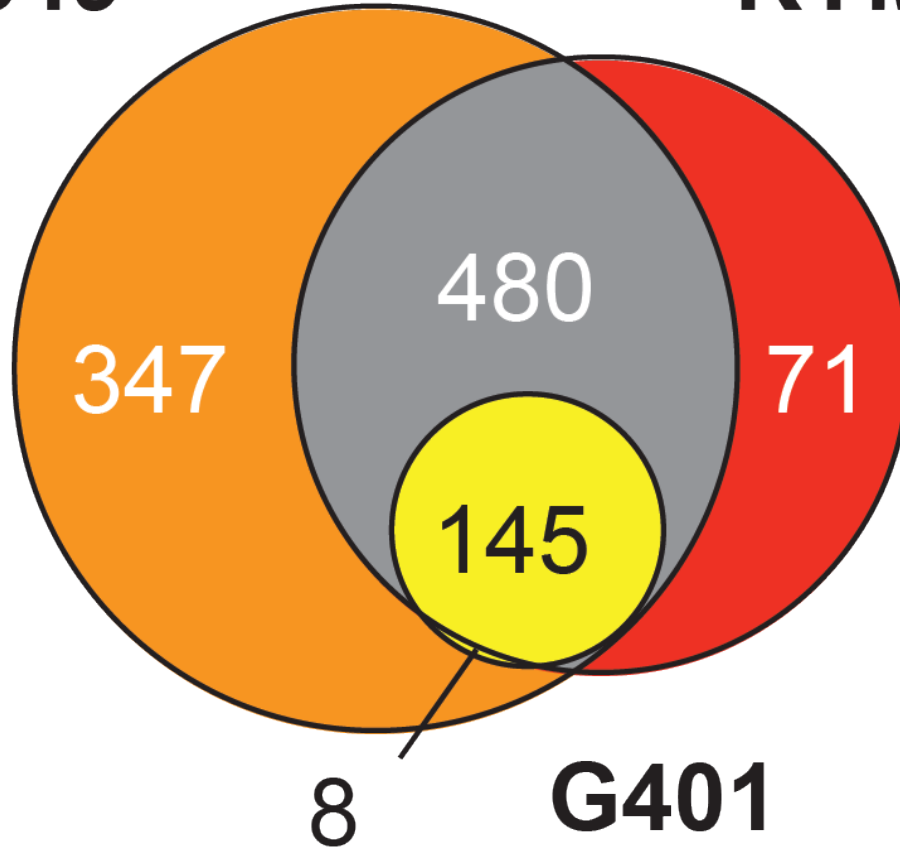
Figure 4.1. Overlap of WDR5 binding peaks in RT cell lines Venn diagram showing the overall of binding sites for WDR5 in ChIP-Seq data in G401, KYM-1, and TTC549. Of note, there is 1 binding site unique to G401 and 2 binding sites shared by G401 and KYM-1 that were too small to show in the Venn diagram. Data are from the DMSO samples presented in **Figure 4.7**.
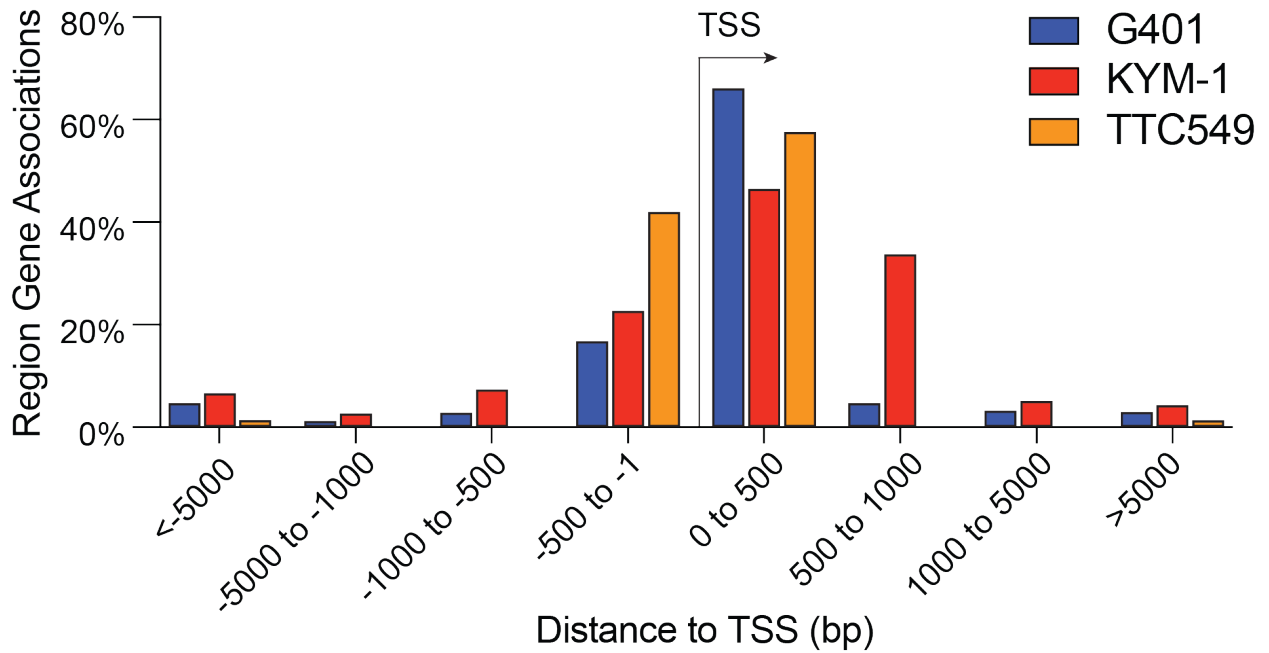
Figure 4.2. WDR5 binding on chromatin in RT cells is primarily promoter proximal
Distribution of WDR5 binding sites in G401, KYM-1, and TTC549 cells, binned according to the distance to the closest annotated transcriptional start site.
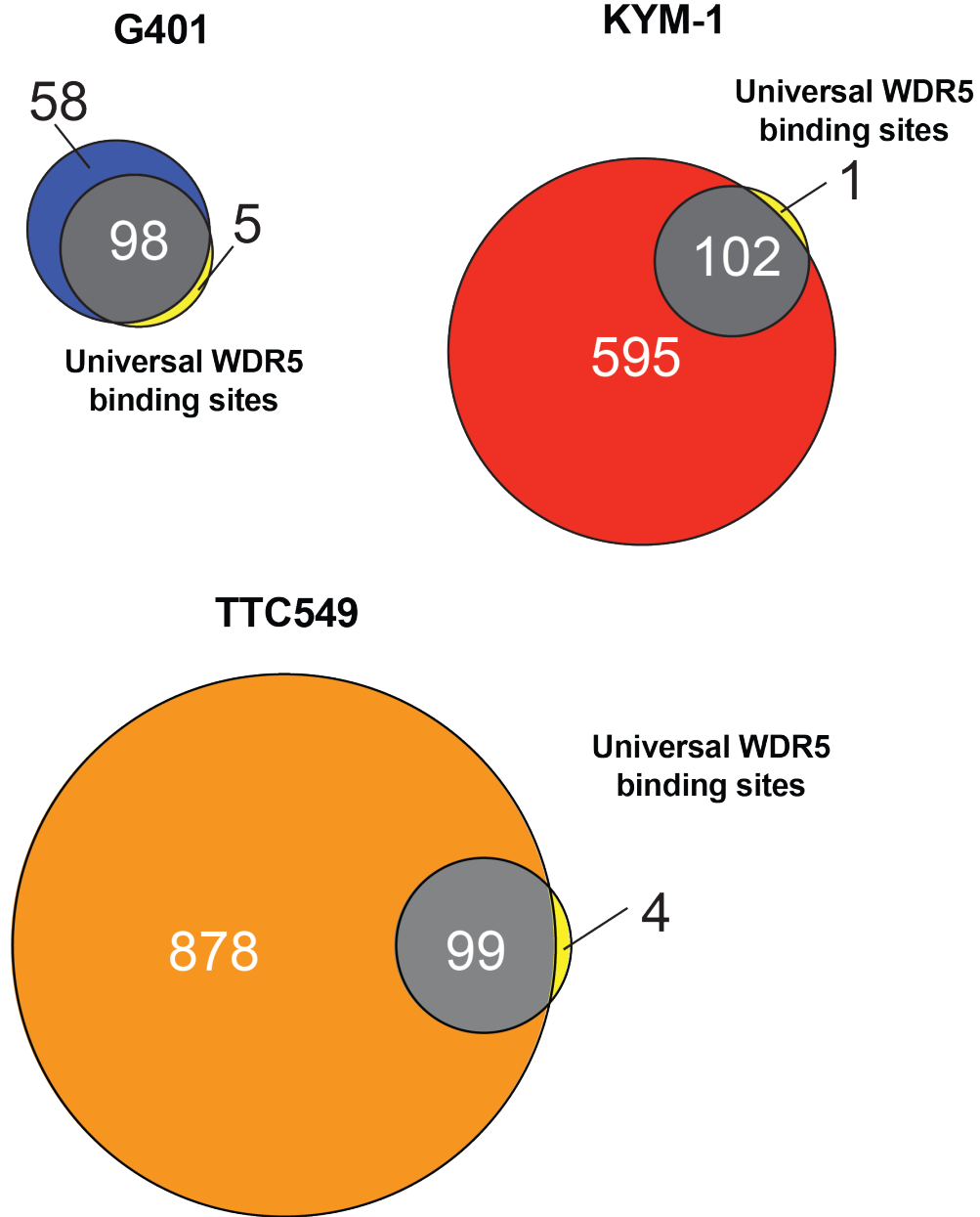
Figure 4.3. WDR5 binds universal WDR5 binding sites in RT cells Venn diagram showing the overlap of WDR5 peaks detected in G401, KYM-1, and TTC549 cells with the set of 103 "universal" human WDR5 binding sites identified in [3].

analysis to determine if the genes bound by WDR5 in G401, KYM-1, and TTC549 have a common functionality. GO terms are groups of related genes based on molecular function, cellular component, or biological process. GO enrichment analysis determines which GO terms appear more frequently than expected due to chance in a list of genes [122]. For this analysis, we assigned all genes within 2 kb upstream of an annotated TSS or within a transcription unit and identified ~148 genes in G401, ~649 genes for KYM-1, and ~980 genes in TTC549 cells which are bound by WDR5. The top eight most significant GO terms for WDR5-bound genes in G401, KYM-1, and TTC549 are shown in **Figure 4.4**. In these bubble plots, the size of the circle indicates how many genes in the data set fell within the indicated category. The color of the circle corresponds with the fold change and the x-axis represents the False Discovery Rate (FDR). The WDR5-bound genes cluster strongly in terms related to protein synthesis including ribosome biogenesis, translation, and mRNA catabolic process, among others. Notably, the categories in each of the RT cell lines are remarkably similar, regardless of sensitivity to WIN site inhibition. This was not surprising given that the overlapping WDR5 localization between the three cell lines encompassed nearly all of the G401 binding sites (**Figure 4.1**). This also demonstrates that the cell type specific binding sites in KYM-1 and TTC549 are at genes related to protein synthesis as well. As further proof, I performed a GO terms analysis on the genes at which WDR5 is bound in KYM-1 and TTC549 that do no overlap with G401 and it reveals similar categories related to nucleotide-containing metabolism (data not shown). Beyond RT, these ribosome-related and protein synthesis categories are nearly identical to those observed in all the cell lines in which we have probed WDR5 localization to date [3, 4, 78]. We have previously demonstrated that WDR5 binds a distinct subset of RPGs corresponding to about 40% of the small subunit RPGs and about 70% of the large subunit RPGs. The RPGs at which WDR5 is bound are nearly identical in all cell lines tested to date [3, 4]. In order to visually compare the WDR5-bound RPGs in RT cells to the other cancer cell types in which we have WDR5 ChIP-Seq data, I mapped the WDR5-bound RPGs on a ribosomogram (**Figure 4.5**). The ribosomogram lists all of the RPGs of the large and small ribosomal subunits and marks which
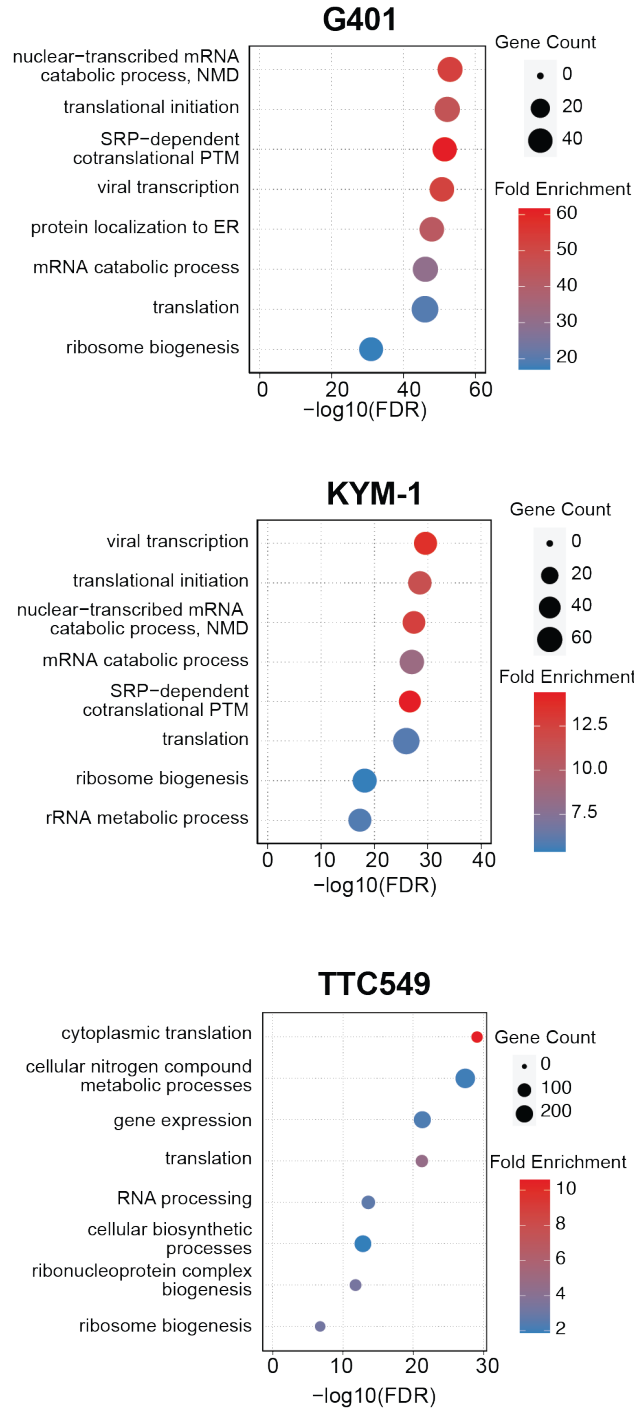
Figure 4.4. WDR5 binding is enriched at ribosomal protein genes in RT cells Gene Ontology (GO) term enrichment analysis of WDR5-bound genes in G401 cels (top), KYM-1 cells (middle), and TTC549 (bottom). The genes were defined as those in which a WDR5 binding site is located within 2 kb of an annotated TSS or within a transcription unit. Biological Process GO terms were ranked by False Discovery Rate (FDR). The eight most significantly enriched terms are shown. Color indicates fold enrichment, size indicates gene number, and the x-axis is the -log10(FDR). PTM post-translational modification; NMD nonsense-mediated decay; ER endoplasmic reticulum
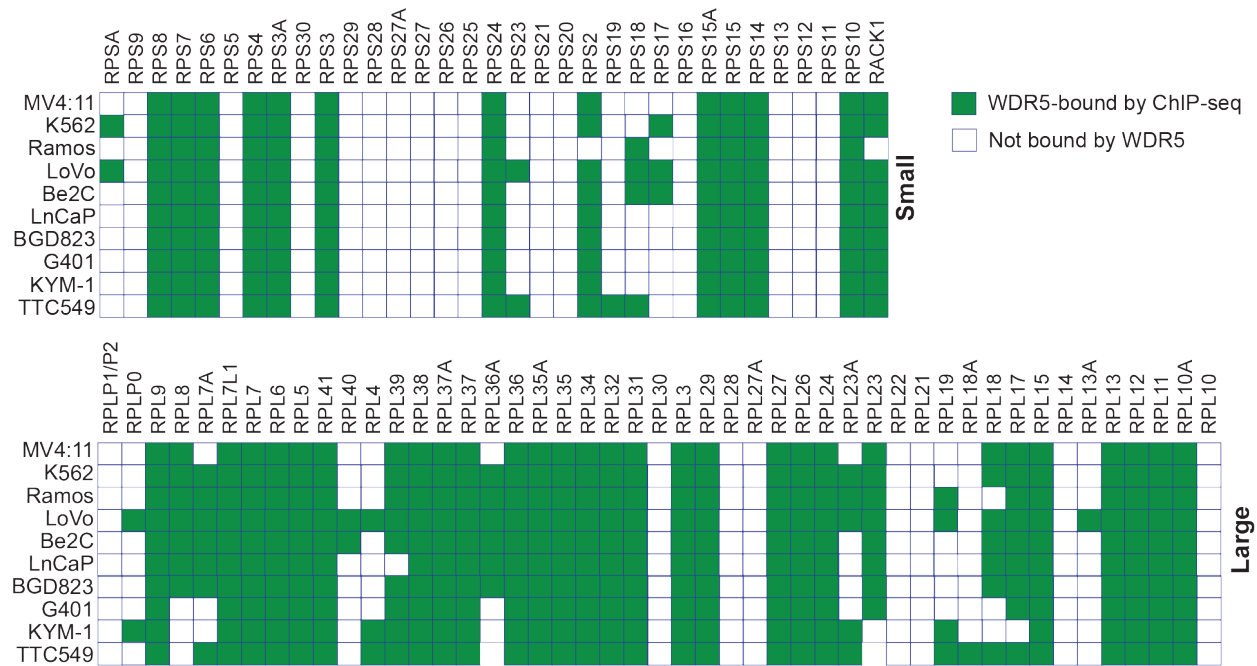
Figure 4.5. WDR5 is bound to a subset of ribosomal protein genes Ribosomogram showing small (top) and large (bottom) subunits of ribosomal protein genes (RPGs); a green box indicates whether WDR5 is bound to each RPG in the indicated cell type. MV4:11 and K562 data are from GSE115377. Ramos data are from GSE126207. LoVo and Be(2)C data are from GSE125451. LnCaP and BGC823 are from GSE55279 and GSE63763, respectively. G401, KYM-1, and TTC549 data are from this study.

54

are bound by WDR5 in each cell line. The RPGs at which WDR5 is bound is remarkably similar in the different cell types. From this analysis, we conclude that the pattern of WDR5 localization on chromatin in RT cells matches expectations from other cell lines in terms of both the location of WDR5 binding and the nature of genes bound.

Effect of WIN site inhibition on WDR5 chromatin binding

As previously mentioned, the primary mode of action for our WIN site inhibitors in MLLr leukemia and NB is through the global displacement of WDR5 from chromatin [3, 4]. I predicted that WIN site inhibitors will function in the same way in RT cells and that WDR5 will be displaced from chromatin in G401, KYM-1, and TTC549 despite differences in sensitivity as is the case in the sensitive MV4;11 cells [4] and the insensitive K562 cells [3]. We treated G401 and KYM-1 cells for four hours with DMSO or 500 nM C16, a concentration that maximally inhibits RPG transcript levels in both lines (**Table 3.2**). Four hour treatment was chosen because prior work has demonstrated that displacement of WDR5 happens rapidly, within four hours [3, 4]. To confirm that WDR5 is displaced from chromatin within four hours, we performed chromatin immunoprecipitation (ChIP) with a WDR5 antibody followed by quantitative polymerase chain reaction (qPCR) to detect changes in WDR5 binding to five WDR5 bound genes (*SNGH15, RPS24, PUM1, RPL35,* and *CCT7*) and a negative control gene that is not bound by WDR5 (*METTL1*) (**Figure 4.6**). Immunoprecipitation with a rabbit IgG antibody was used as a control for background binding. After four hours of C16 treatment, WDR5 binding was dramatically reduced at all five loci examined in both G401 and KYM-1 cells demonstrating the WIN site inhibitors are more than likely functioning by displacing WDR5 from its chromatin locations.

To validate that WIN site inhibitors globally displace WDR5 from chromatin in RT cell rather than only at the five loci examined, Dr. April Weissmiller and Dr. Caleb Howard performed ChIP-Seq in RT cells that had been treated for four hours with DMSO or 500 nM C16. Under these conditions, C16 treatment results in the global reduction of WDR5 association with chromatin. With the help of Dr. Jing Wang, we were able to generate heat maps displaying the WDR5 peak
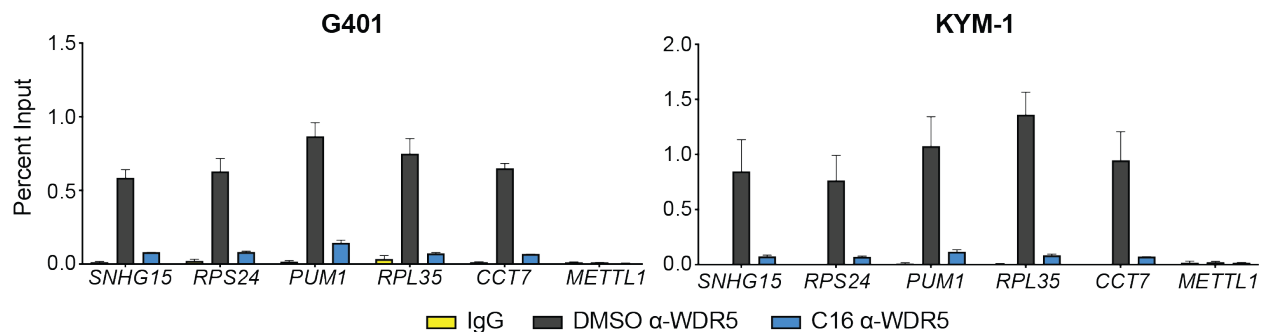
Figure 4.6. WDR5 is displaced from chromatin in G401 and KYM-1 cells ChIP for WDR5 was performed on G401 (left) of KYM-1 (right) cells treated with DMSO (gray) or 500 nM C16 (blue) for four hours. IgG (yellow) is a negative control ChIP, performed on DMSO-treated samples. WDR5 binding to the indicated loci was probed by qPCR. *SNHG15, RPS24, PUM1, RPL35,* and *CCT7* are part of the "universal" set of WDR5-bound genes; *METTL1* is a negative control locus. ChIP signals are calculated as percent input (n=3, mean ± SEM).

intensity from ChIP-Seq in all three cell lines (**Figure 4.7A**). The heat maps are ranked from the highest to lowest peak intensity in the DMSO samples. It is obvious from these heat maps that WDR5 peak intensity is reduced with WIN site inhibitor treatment in all three cell lines. We were also able to generate scatterplots displaying the normalized average read counts of each WDR5 peak after treatment with DMSO or C16 (**Figure 4.7B**). This shows a decrease in WDR5 read counts with C16 treatment compared to DMSO. This demonstrates that WDR5 is displaced from chromatin at sites that are shared between cell types and at cell type specific binding sites. The nature of the effect is similar to what we reported with C6 in MV4:11 and K562 leukemia cells [3, 4], both in terms of the magnitude of reduction in WDR5 binding, as well as the fact that WDR5 is displaced from both shared and cell-type specific WDR5 binding sites by C16. To visualize the ChIP-Seq data, we used the Integrative Genome Viewer (IGV) to examine the WDR5 binding at specific genes in G401, KYM-1, and TTC549 cells (**Figure 4.8**). IGV allows us to see the peak intensity from the WDR5 sequencing reads in any region of the genome. The gene of interest is along the top of the images and the DNA reads are represented below in blue for G401 cells, in red for KYM-1 cells, and in green for TTC549 cells. In these images, I am able to see peaks of DNA reads that were pulled down as being bound to WDR5 and then sequenced. I can see obvious peaks in all three cell lines at *SNGH15, PUM1*, and *RPL35* (*ARPC5L*) that are in close proximity to the TSS of each gene. More importantly, I can see the disappearance of the WDR5 bound DNA peaks with C16 treatment in all the cell lines. We also looked at a few cell type specific WDR5 peaks. For example, *RAD18* and *PDP1* are genes at which there is WDR5 binding in KYM-1 cells but not in G401 cells. In these cell-type specific peaks, we also observe that C16 disrupts WDR5 binding reveling that WIN site blockade globally disrupts WDR5 chromatin and is not specific to universal binding sites. Taken together with other studies, I can conclude from these ChIP-seq data that the WIN site tethers WDR5 to chromatin in RT cells as in MLLr leukemia cells and that WIN site inhibitors have a consistent ability to comprehensively evict WDR5 from all of its chromatin locations. WDR5 displacement due to WIN site blockade happens in both sensitive and insensitive RT cell lines indicating that the primary mechanism
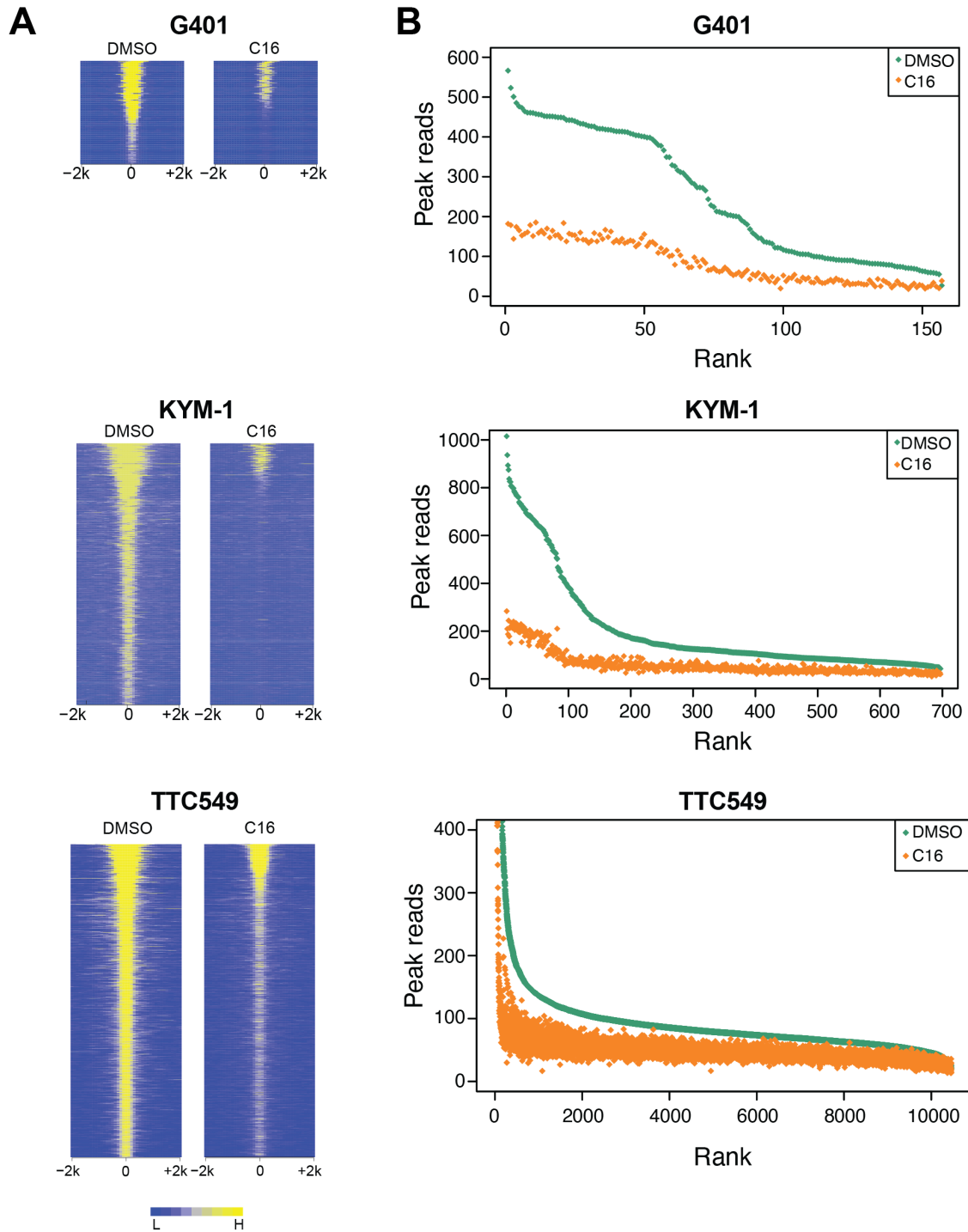
Figure 4.7. WIN site inhibition displaces WDR5 from chromatin genome-wide in RT cells
(**A**) Heatmaps of WDR5 ChIP-peak intensity in G401 (top), KYM-1 (middle), and TTC549 (bottom) cells treated for four hours with DMSO or 500 nM C16. Images represent the combined average of normalized peak intensity in 100-bp bins ± 2 kb around the center of peaks. Peaks are ranked based on the DMSO-treated samples. (**B**) Ranking of WDR5 peak intensities in G401 (top), KYM-1 (middle), and TTC549 (bottom) cells treated for four hours with DMSO (green) or 500 nM C16 (orange). Peaks are ranked according to peak reads in DMSO samples.

58
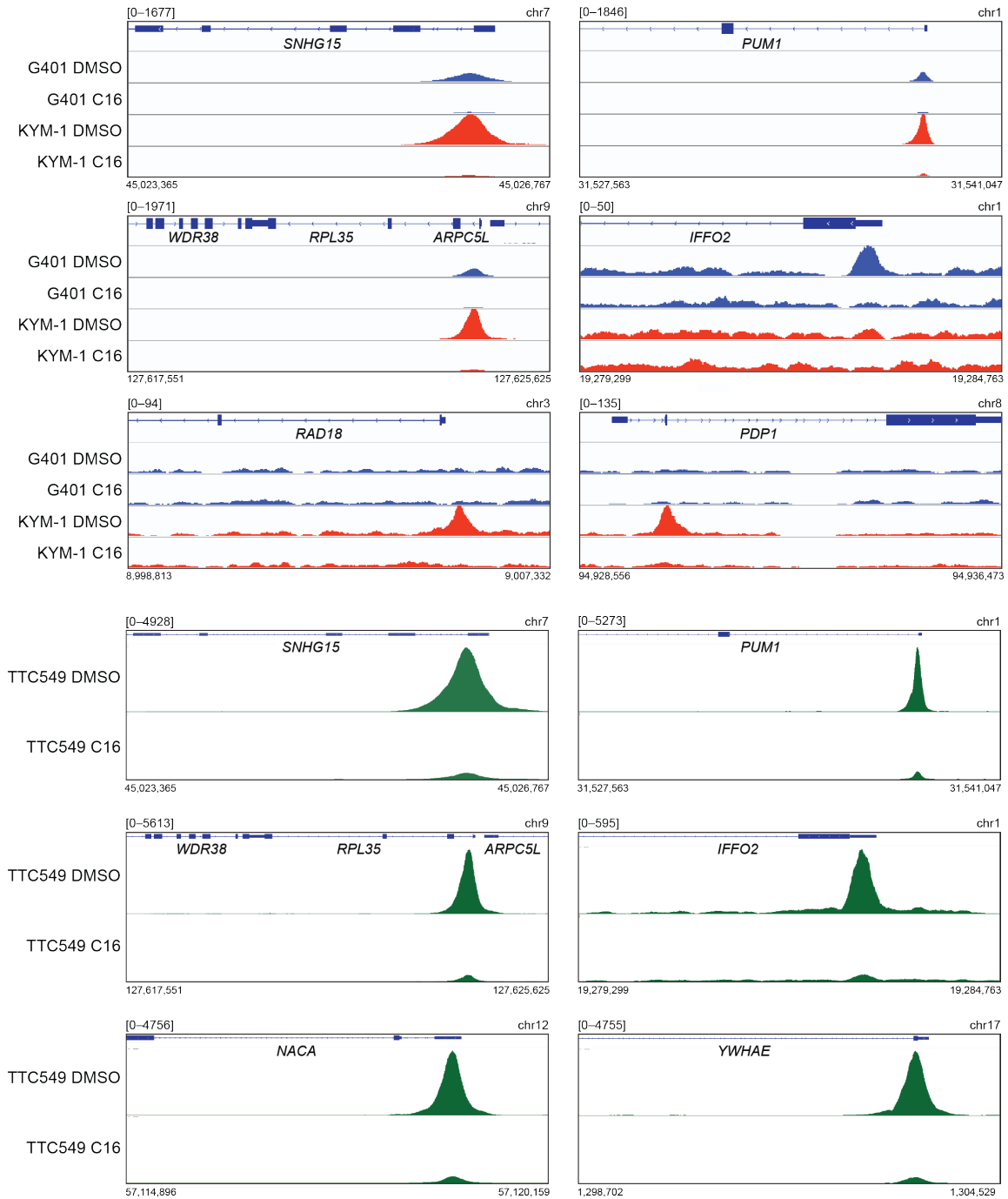
Figure 4.8. Visualization of WDR5 binding in RT cells Integrated Genomic Viewer (IGV) screenshots of representative ChIP-seq data for WDR5 in G401 (blue), KYM-1 (red), and TTC549 (green) cells treated with DMSO or 500 nM C16 for four hours. *SNHG15, PUM1,* and *RPL35* (*ARPC5L*) are bound by WDR5 in all three cell types. *IFFO2* is bound by WDR5 in G401 and TTC549. *RAD18* and *PDP1* are KYM-1 specific WDR5-bound genes. *NACA* and *YWHAE* are bound by WDR5 in TTC549. Scale is consistent within each screenshot, but differs between them as indicated.

through with WIN site inhibitors function is the same in different RT cell lines so whatever determines sensitivity must occurs downstream of WDR5 displacement from chromatin.

Discussion

WDR5 is known for its activity at chromatin where it functions as a transcriptional regulator through its partnerships with a number of chromatin regulatory complexes and transcription factors [2]. In order to predict how WDR5 WIN site inhibitors may act to reduce proliferation in RT cells, I must first identify the sites at which WDR5 is bound to chromatin as these genes are the most likely to be altered upon WIN site inhibition. Based on work in a number of other cancer contexts including acute myeloid leukemia (AML), chronic myeloid leukemia (CML), neuroblastoma, colorectal adenocarcinoma, as well as cell lines derived from mice, WDR5 is commonly localized to genes related to protein synthesis and the ribosome [3]. In fact, we were able to establish a cohort of "universal" WDR5 binding sites from these studies that include ~100 chromatin loci at which WDR5 is bound invariably in all human cell types [3]. Because of the consensus of WDR5 binding sites in all the cells lines we have tested, I predicted that WDR5 localization on chromatin would be similar in the context of RT cells. By ChIP-Seq for WDR5 in three RT cell lines with differing sensitivities to C16, we were able to establish that WDR5 localization is similar in sensitive and insensitive lines but does have some cell-to-cell variability. TTC549 had the largest number of chromatin sites at which WDR5 is bound compared to KYM-1 and G401 cells. However, despite the difference in number of binding sites, WDR5 is found at similar genes with similar functions. By GO terms enrichment analysis, WDR5 binding sites in G401, KYM-1, and TTC549 were enriched in nearly identical categories, terms related to ribosome biogenesis and translation. As seen in other cell types, WDR5 is bound to genes that encode RPGs which further validates that a major function of WDR5 is to regulate genes involved in protein synthesis and biomass accumulation. Importantly, increased ribosome biogenesis plays an essential role in tumor growth and proliferation as cancer cells need to have the machinery to synthesize greater numbers of proteins to sustain the rapid growth [80]. Drugs

that are able to disrupt protein synthesis are emerging as promising new anti-cancer agents [80].

We have already established that the primary mechanism through which WIN site inhibitors function is by globally displacing WDR5 from chromatin [3, 4]. This helped determine that the WIN site is responsible for tethering WDR5 to chromatin. WDR5 does not have a known DNA binding motif so WDR5 must interact with chromatin by engaging with a WIN motif in a chromatin bound protein. At this point, the factor(s) tethering WDR5 to chromatin have yet to be identified but it may be a previously known interaction partner of WDR5 or a novel interacting protein. There are thousands of proteins encoded in the human genome that contain a WIN motif (ARA) so there are many possibilities for what this linking protein(s) may be. Defining the WDR5 interactome both on and off chromatin is important to identify how WDR5 binds to chromatin and will be discussed in the Future Directions in Chapter IX.

Based on previous work, I predicted that displacement of WDR5 from chromatin in RT cells happens before any drastic changes in cellular response to the inhibitors. We treated RT cells for only four hours and were able to demonstrate that WIN site inhibition promotes the rapid, comprehensive, and persistent displacement of WDR5 from chromatin within this short time period. WDR5 is displaced from the common PSGs as well as the cell type specific binding sites meaning that WDR5 displacement is not specific to any WDR5 chromatin loci but is instead occurs irrespective of genomic location. This global WDR5 displacement occurs regardless of cellular sensitivity meaning that the lack of cellular response to WIN site inhibitors in TTC549 cells is not due to the lack of displacement of WDR5 from chromatin. There is thus no substantive difference in the effects of C16 in an insensitive RT line that can explain the lack of an overt cellular response to WIN site blockade. I conclude that differences in the way RT cells respond to WIN site inhibitor are likely a consequence of downstream cellular characteristics, rather than those related to the actions of WDR5 on chromatin or the primary response to WIN site inhibition.

Because of the role that WDR5 plays in regulating transcription, it is reasonable to predict that disrupting WDR5 binding to chromatin by WIN site inhibition will alter the transcription and expression of WDR5-bound genes. I further hypothesize that the changes in gene expression of the WDR5 bound genes that result from WIN site inhibition are what is ultimately responsible for the decrease in proliferation in RT cell lines. It is important that I explore how WDR5 affects gene expression at early time points to look for direct effects of WIN site inhibition as well as the effects from longer term WIN site inhibitor treatment to determine if the changes persist and to identify how the cell is responding. Both short term and long term gene expression changes as a result of WIN site inhibition in RT cells will be explored in Chapters V and VI respectively.

V. WDR5-BOUND PROTEIN SYNTHESIS GENES ARE DIRECT TARGETS OF WIN SITE INHIBITORS IN RHABDOID TUMOR CELLS

Introduction

In order to fully understand the utility of WDR5 WIN site inhibitors in RT, it is important to understand which genes are regulated by WDR5 and how they are affected by WIN site blockade. Only then can I connect the changes in gene expression from WIN site inhibition to the reduced proliferation in RT cell lines observed in Chapter III. WDR5 has been implicated in chromatin remodeling and in recruiting transcription factors to DNA to activate transcription and regulate gene expression [2]. I predict that displacing WDR5 from chromatin will decrease transcription of a portion of the genes bound by WDR5 and ultimately cause more global secondary changes in gene expression at longer time points. This prediction is supported with previous data in MV4:11 cells that shows that WIN site blockade inhibits the transcription of WDR5-bound genes and leads to long term decrease in expression in PSGs and other compensatory gene expression changes [4]. In order to validate that the previously described mode of action for WIN site inhibitors is the same in RT cells, I must examine both the early primary transcriptional effects and longer-term secondary gene expression changes. Transcriptional effects at shorter time points will define the direct effects of WIN site inhibition but changes in steady-state expression of mRNA expose compensatory consequences of WIN site inhibition and may provide insight as to how the compounds are suppressing proliferation. In this chapter, Precision nuclear Run-On coupled to next generation sequencing (PRO-Seq) is used to identify primary transcriptional changes with high temporal resolution. The effects of WIN site inhibition on gene expression at a later time point will be explored in Chapter VI.

The PRO-Seq experiments in this chapter were performed by Dr. April Weissmiller and the analysis performed by Dr. Jing Wang. By overlaying the ChIP-Seq data from Chapter IV and the PRO-Seq data gathered here, we show that WIN site inhibition decreases transcription of

WDR5-bound genes within two hours and that unsurprisingly, these genes are connected to protein synthesis. We performed these experiments in two RT cell lines with a five-fold differences in sensitivity to C16, G401 and KYM-1, and show that the genes that exhibit decreased transcription are similar between the two cell lines. We found that the primary transcriptional targets of WIN site inhibitors are a conserved set of WDR5-bound RPGs at which WDR5 is displaced upon inhibitor treatment.

Results

Early transcriptional changes from WDR5 WIN site inhibition in RT cells

Previous work has indicated that the primary transcriptional consequences of WDR5 WIN site inhibitor treatment is a decrease in transcription of a subset WDR5-bound genes. This work was done in MV4:11 cells with an early generation WIN site inhibitor, C3 [4]. I predict that the later generation WIN site inhibitor, C16, will have the same effect in RT cells because WIN site inhibitors globally displace WDR5 from chromatin in both contexts. To identify direct transcriptional targets of WIN site inhibitor in G401 and KYM-1 cells, we used PRO-Seq [123, 124] to ask how the distribution of active RNA polymerases is altered after two hours of exposure to C16. PRO-Seq is a global nuclear run-on assay that allows us to track the distribution of RNA polymerase that is actively transcribing with base-pair resolution. For these experiments, nuclei were isolated from cells and transcription is halted by carefully washing away the nucleotides. RNA polymerase remains active and engaged to DNA. A run-on reaction is performed by re-adding ATP, GTP, UTP, and biotinylated CTP to the nuclei. When the biotinylated nucleotide is incorporated into the nascent RNA by RNA polymerase, it terminates transcription at that point while simultaneously labeling all nascent RNA fragments with biotin. This biotin tagged RNA can then be isolated from the total RNA using streptavidin-conjugated beads. We can then use next generation sequencing (NGS) to identify the fragments that were being actively transcribed [123, 124]. NGS was performed by Vanderbilt Technologies for Advanced Genomics (VANTAGE).

We treated G401 and KYM-1 cells with DMSO or 500 nM C16 for two hours before isolating nuclei for PRO-Seq. We chose to treat cells for two hours because this time point is long enough to ensure that the inhibitors have gotten into the cells and displaced WDR5 from chromatin but short enough to keep the focus on primary responses. To understand how WDR5 displacement from chromatin as a result of WIN site inhibitor treatment affects transcription, we asked which genes showed a significant change in polymerase associated with gene bodies after C16 treatment compared to DMSO. Dr. Jing Wang used Nascent RNA Sequencing Analysis (NRSA) to detect C16-dependent transcriptional changes in gene body regions [105]. This analysis revealed a small set of transcriptional changes in both cell lines as measured by differences in gene body associated active RNA polymerases (**Figure 5.1A**). These heatmaps allow the visualization of active RNA polymerase after C16 treatment. Each row represents the region +/- 5 kb around the TSS of an individual gene found to have altered polymerase association after treatment with C16. The G401 heatmap has more rows than the KYM-1 heatmap because there are more significantly altered genes in the G401 cells. Each box indicated the $\log_2$-transformed fold change of read counts in 200 bp bins. Yellow boxes indicate an increase in RNA polymerase association and blue boxes indicate a decreases in RNA polymerase association. The changes in gene body associated active RNA polymerase are modest with the $\log_2$ fold change ranging from -0.7 to +0.7 (**Figure 5.1A**).

We identified 76 genes with decreased gene body associated polymerase in G401 cells and 71 in KYM-1 cells after C16 treatment (**Figure 5.1B**). Genes with decreased transcription in response to WIN site inhibition are almost identical between the two lines (**Figure 5.1B**) therefore, we can be confident that these genes are primary targets of WDR5 WIN site inhibition in RT cells. We did not expect to see any genes with increased gene body polymerase association because displacing WDR5 from chromatin is more likely to decrease transcription based on earlier observations using PRO-Seq in MV4:11 cells [4]. Surprisingly, we identified 50 genes in G401 cells and one gene in KYM-1 cells with increased polymerase engagement. Genes with increased transcription are dissimilar between G401 and KYM-1 cells; the single
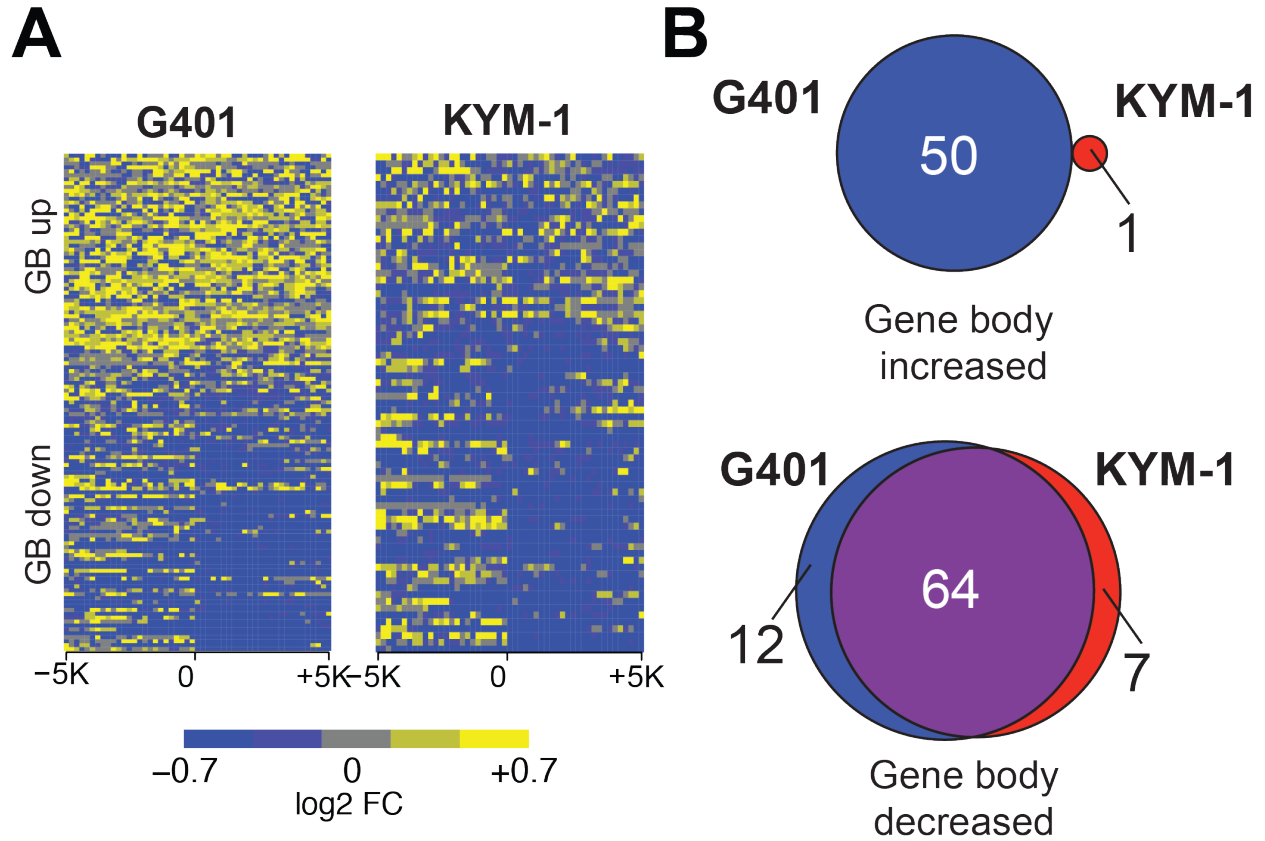
Figure 5.1. WIN site inhibition affects gene transcription in RT cells (**A**) Heatmaps displaying $\log_2$-fold change (log2 FC) of active polymerases in G401 or KYM-1 cells treated for two hours with 500 nM C16 compared to their respective DMSO controls, as determined by PRO-Seq. Maps are ranked individually within each cell type, and show changed in polymerase density in the promoter-proximal region and +/- 5 kb around the TSS (200 bp bins). The top of the figure shows genes where transcription in the gene body increased (GB up) and the lower part shows genes were gene body transcription decreased (GB down) (n=2). (**B**) Venn diagrams comparing the genes showing an increase (top) or decrease (bottom) in gene body associated polymerases in response to C16 in G401 versus KYM-1 cells.

gene with increased polymerase association in KYM-1 cells is not one of the 50 genes with increased transcription in G401 cells (**Figure 5.1B**). This demonstrates that an increase in transcription is not a bonafide response to WIN site inhibition and that WIN site blockade reduces transcription of common set of genes in RT cells.

WDR5-bound genes are direct targets of WDR5 WIN site inhibition in RT cells

I was interested in knowing whether the primary transcriptional targets of WIN site inhibition as determined by PRO-Seq are also bound by WDR5 in RT cells. Because we performed ChIP-Seq in both G401 and KYM-1 cells, I was able to manually inspect the ChIP-seq data to see if the genes with altered polymerase association with WIN site inhibition in PRO-Seq are bound by WDR5 in either G401 or KYM-1. All of the genes with reduced RNA polymerase association are bound by WDR5 —most of them in both G401 and KYM-1 cell with a few genes only bound in one of the lines (**Figure 5.2**). On the other hand, none of the genes induced by WIN site inhibition are bound by WDR5 in the same line (**Figure 5.2**). Beyond manual inspection, we used gene set enrichment analysis (GSEA) to compare the ChIP-Seq and PRO-Seq data in each cell lines. GSEA is a computational method to determine if there is an enrichment between two data sets which it quantifies as an Enrichment Score (ES) [125]. In this case, the two data sets are (1) the list of genes at which WDR5 is displaced by ChIP-Seq and (2) the genes at which transcription is significantly altered with C16 treatment by PRO-seq. The PRO-Seq data is ranked along the bottom of the plot with the increased genes on the left and the decreased genes on the right. GSEA calculates an ES by scanning the ranked PRO-Seq data and determining if the gene is present in the ChIP-Seq data. The ES deviates farther from zero if the genes are found in both data sets and moves closer to zero if they do not match. The GSEA determined that there is a strong tendency for WDR5-bound genes to have decreased RNA polymerase association by PRO-Seq in both G401 and KYM-1 cells (**Figure 5.3**). However, WDR5 is bound to ~160 loci in G401 cell and ~700 loci in KYM-1 cell so only a portion of the WDR5-bound genes in each cell line respond transcriptionally to WIN site inhibition within two

67
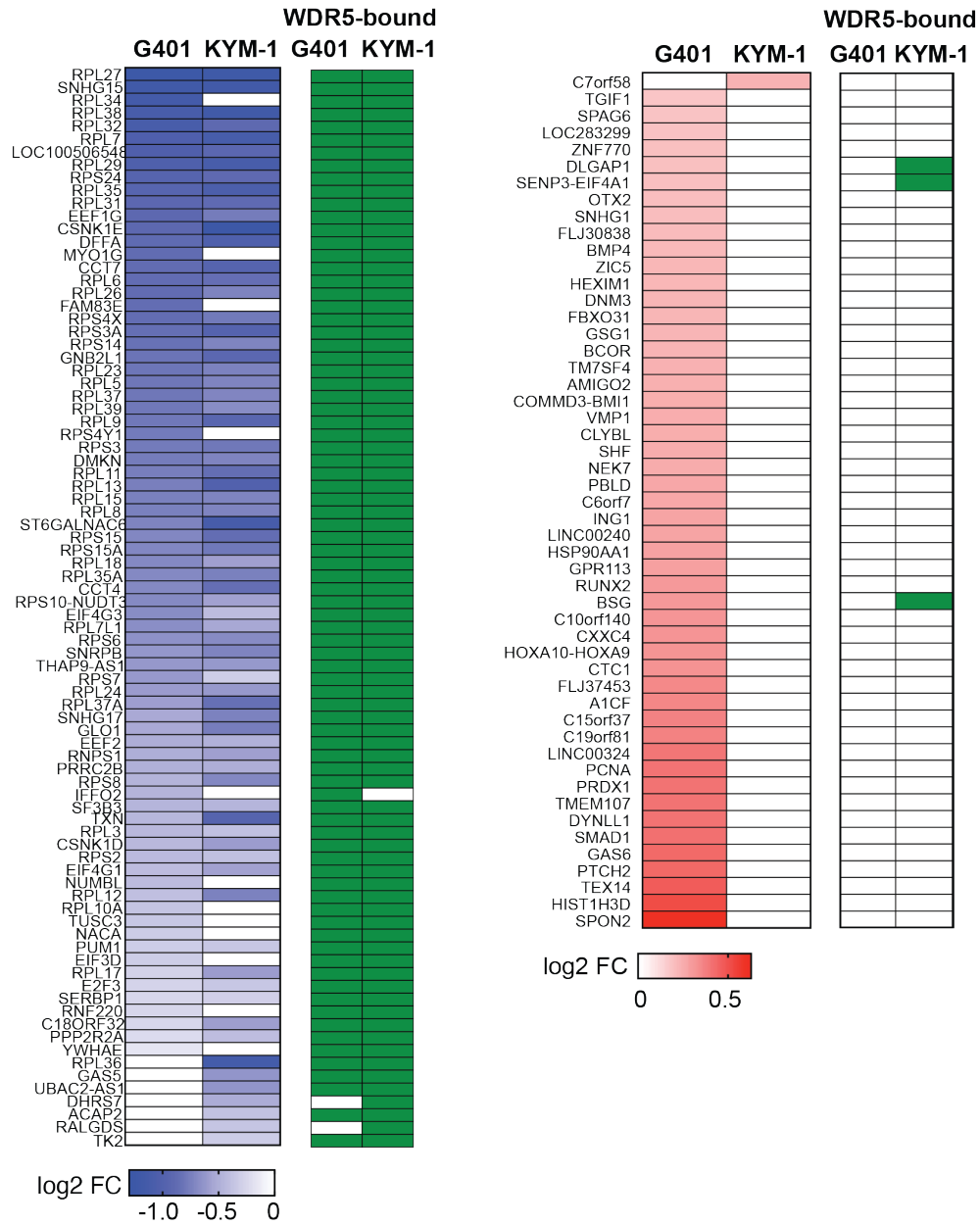
Figure 5.2. Genes with decreased transcription with C16 are bound by WDR5 Heatmaps showing genes with significant decrease (blue) or increase (red) in gene body-associated polymerases in G401 or KYM-1 cells treated with 500 nM C16. The green bars to the right indicate if WDR5 is bound to that locus in each cell type (ChIP-Seq). *LOC100506548* is a read-through transcription from RPL37.
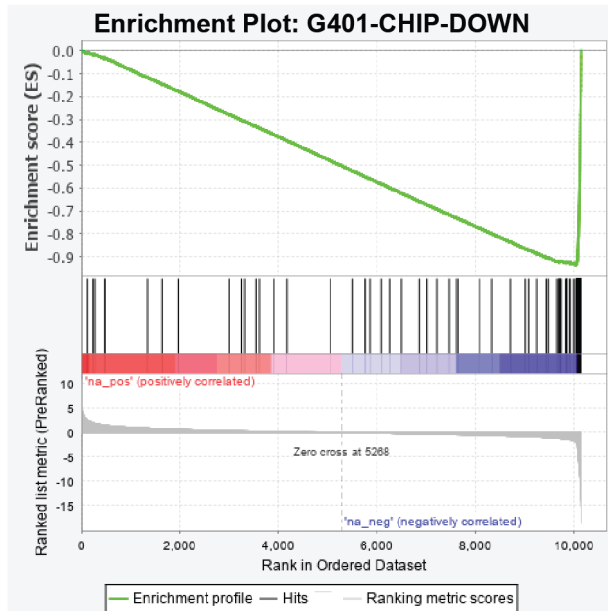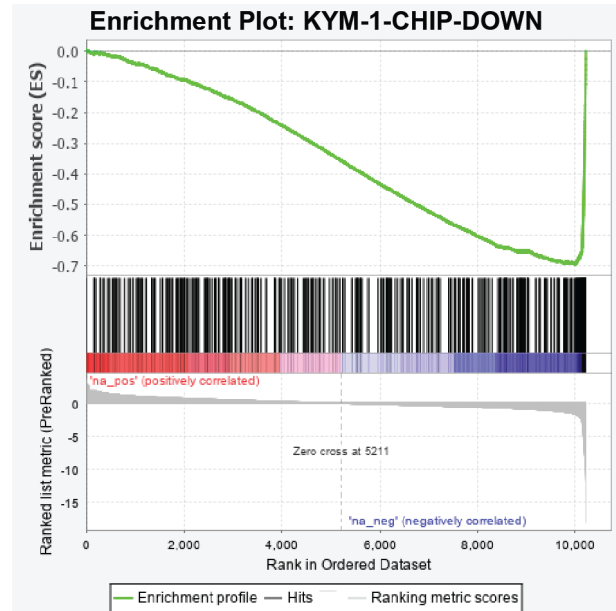
NES: -3.55   NES: -3.31

Figure 5.3 WDR5-bound genes are direct targets of WIN site inhibition in RT cells Gene set enrichment analysis (GSEA) comparing genes with a reduction WDR5 binding by ChIP-Seq against a gene list ranked by alteration in the density of gene body-associated transcribing polymerases in C16-treated G401 and KYM-1 cells. FDR q = 0.0 in both cases. NES = Normalized Enrichment Score

hours of treatment. In fact, only about 50% of the genes bound by WDR5 respond transcriptionally at two hours and only about 10% in KYM-1 cells. Together, this indicates that the primary mechanism by which WIN site inhibitors function is to decrease the transcription of the WDR5-bound genes, although it is only a portion of the genes bound by WDR5 in each of these RT cell lines.

WIN site inhibition decreases transcription of protein synthesis genes in RT cells

After demonstrating that all of the genes with decreased gene body-associated polymerase are bound by WDR5, I used GO terms enrichment analysis to determine if the genes showed altered transcription with WIN site inhibitor treatment clustered into any functional category. Because there is no precedent for genes with increased RNA polymerase occupancy with WIN site inhibition, I was surprised to see 50 genes at which the gene body associated polymerase increased. I predicted that these genes would not cluster into any meaningful category by GO terms enrichment analysis because this response is not recapitulated in any other context tested and thus, not a high confidence mechanism of response to WIN site inhibition. As predicted, the genes in G401 cells with increased polymerase occupancy failed to be significantly enriched in any meaningful GO term. I predicted based on previous work [4] and the similarity between genes bound by WDR5 with altered transcription (**Figures 5.2 and 5.3**) that the gene body decreased genes would be involved in protein synthesis. Because genes with decreased transcription were nearly identical in G401 and KYM-1 cell lines, I deemed the 64 shared genes high confidence primary targets of WDR5 WIN site inhibition (**Figure 5.1**). I performed GO terms enrichment analysis on these 64 high confidence genes. As expected, GO analysis reveals enrichment in genes connected to protein synthesis (**Figure 5.4**). These categories included genes encoding the nucleolar RNAs SNHG15 and SNHG17, the cell cycle transcription factor E2F3, and translation initiation factors EIF4G3, EIF4G1, and EIF3D, and the elongation factor EEF1G (**Figure 5.2**). Further, the high confidence genes included about half of the RPGs (**Figure 5.5**), a pattern remarkably similar the one seen in MV4:11 cells [4]. Together
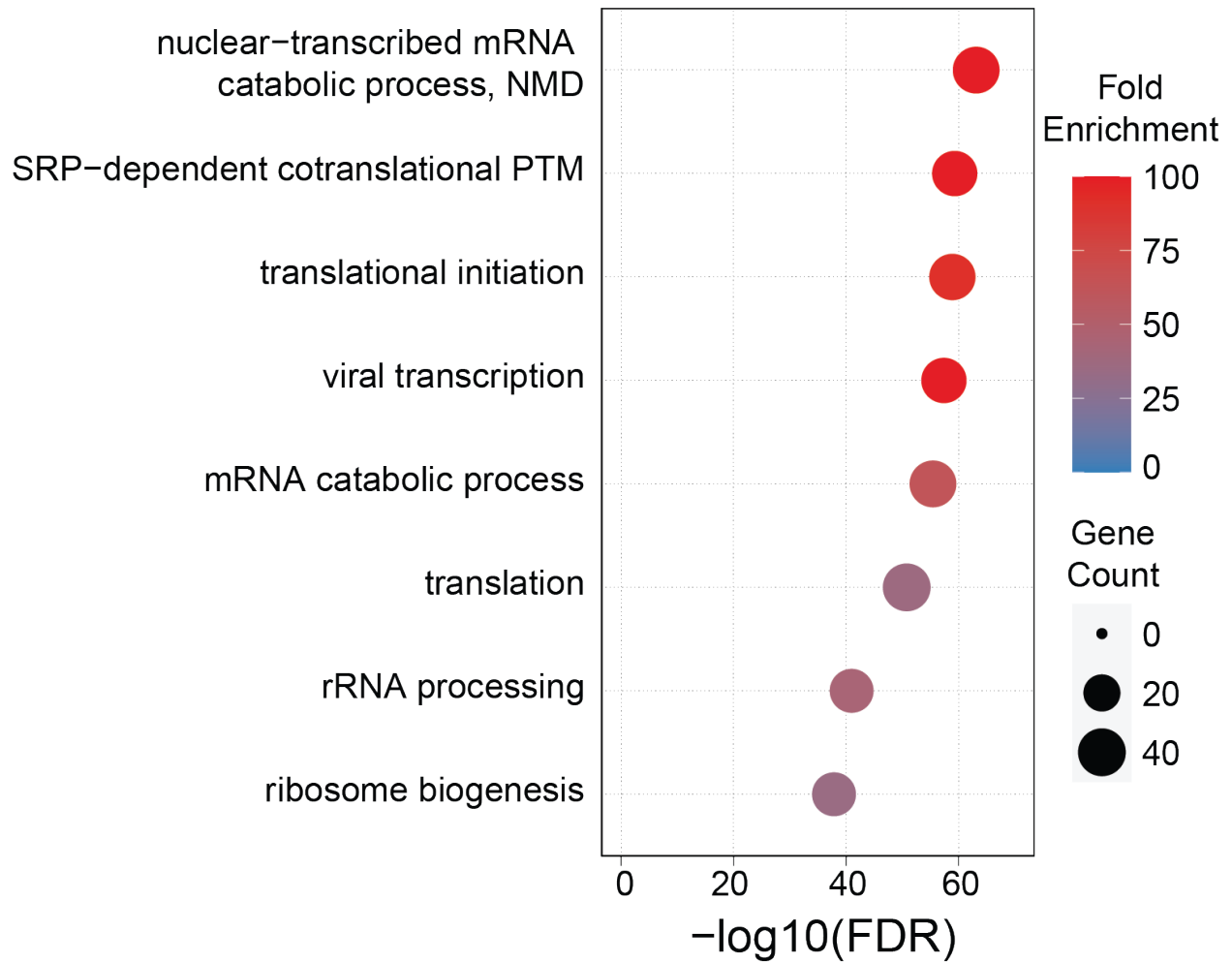
Figure 5.4 GO analysis of genes with decreased gene body-associated polymerase with WIN site inhibition in RT cells GO terms enrichment analysis of genes showing a significant decrease in gene body associated polymerase in both G401 and KYM-1 cells in response to C16 treatment. Biological Processed GO terms were ranked by false discovery rate (FDR). The eight most significantly enriched terms are shown. Color indicates fold enrichment, size indicates gene number, and the x-axis is the -log10(FDR). PTM post-translational modification; NMD nonsense-mediated decay.
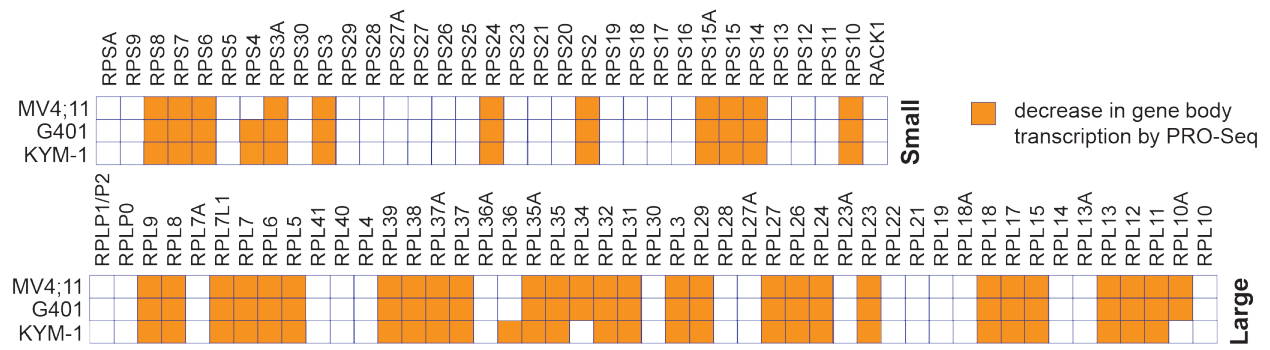
Figure 5.5. WIN site inhibitor treatment decrease transcription of a discrete set of ribosomal protein genes Ribosomogram showing small (top) and large (bottom) subunit RPGs; an orange box indicates whether that specific RPG is inhibited by WIN site inhibitor C3 in MV4:11 cells (GSE115377) or WIN site inhibitor C16 in G401 and KYM-1 cells (this study), as determined by PRO-Seq.

this demonstrates that as in other cell types [3, 4] these PSGs are the primary transcriptional targets of WIN site inhibitor in RT cells.

Discussion

In order to understand the potential of WDR5 WIN site inhibitors to treat rhabdoid tumors, it is vital that we define the primary transcriptional consequences of WIN site blockade in RT cells to help uncover the mechanism of action of these inhibitors. I have a proposed mechanism of action based on our work in MLLr leukemia [4] and NB [3] but it is important that we show that the mechanism extends to the RT context as well. PRO-Seq is a helpful technique because allows us to capture the transcriptional response to WIN site inhibition with high temporal resolution. The real power is when we couple the data gathered in PRO-Seq with ChIP-Seq to identify direct targets of WDR5 WIN site inhibition. The predominant transcriptional response to WIN site inhibitors in RT cells is repression of transcription at WDR5-bound genes. Importantly, after WDR5 is displaced due to WIN site inhibition, we observe a change in RNA polymerase occupancy at many of these genes implying a decrease in active transcription of these WDR5-target genes.

In both G401 and KYM-1, the impact of WIN site inhibitor on gene transcription is small, both in terms of the number of genes involved and the magnitude of the response. The implication of this is that WDR5 functions to modulate the expression of specific RPGs within a fairly narrow window rather than turning them on or off. However, this subtle change appears to be enough to elicit a cellular response because both G401 and KYM-1 cells are sensitive to WIN site inhibition. In addition, even though WDR5 is displaced from chromatin at all of its binding sites, the majority of genes bound by WDR5 do not rapidly respond transcriptionally to WIN site inhibition. Only 50% of WDR5-bound genes in G401 and 10% of WDR5-bound genes in KYM-1 exhibit a decrease in gene body-associated polymerase. This indicates that there is a specific subset of genes affected by WIN site blockade that does not make up all of the WDR5-bound genes. Perhaps WDR5 has a different function at the genes not transcriptionally altered by WIN

73

site inhibition. Because of the vast array of functions of WDR5, determining what WDR5 is doing at each of these site is not straight forward. There are a number of ways that WDR5 could be influencing transcription at each of these sites and WDR5 does not have to behave the same way at each of its loci. WDR5 is a member of the SET1/MLL complexes which are responsible for histone H3 lysine 4 trimethylation, a marker of transcriptionally active chromatin [62]. It is possible that displacement of WDR5 from chromatin with WIN site inhibition displaces the SET/ MLL1 complex resulting in a decrease in H3K4me3. However, this is not likely to happen within two hours of treatment. I did not specifically test how WIN site inhibition affected H3K4me3 but our laboratory has evidence that suggests that WIN site inhibitor treatment does not alter H3K4me3 at this short time point. In MV4:11 cells treated with C3 for 4 hours, H3K4me3 ChIP-qPCR at five WDR5-bound loci showed no differences in this histone modification compared to the negative controls [4]. In addition, we measured bulk H3K4me3 levels by western blot in Burkitt's lymphoma cells (Ramos) treated with C16 for two, four, six, eight, and ten hours and did not see any alterations in H3K4me3 at any of these timepoints [126]. Thus, it is unlikely that the decrease in transcription resulting from WIN site blockade at these WDR5 bound sites is because of loss of the H3K4me3 mark. WDR5 is also essential for recruiting the oncoprotein MYC to chromatin, especially at PSGs [77, 78]. Moreover, WIN site inhibition displaces MYC along with WDR5 in MV4:11 cells [79]. It is plausible that as WIN site inhibitor displaces WDR5 from chromatin, it also displaces MYC to decrease transcription of RPGs. Further investigation is needed to confirm this hypothesis. WDR5 is known to participate in a number of other chromatin regulatory complexes and to act as an epigenetic reader. WDR5 could also be functioning in a novel and undiscovered way at these binding sites. Any number of these functions could be disrupted by WIN site inhibition and thus alter transcription. Elucidating what WDR5 is doing at each of its binding sites is beyond the scope of this project but approaches to understand this open question will be discussed in the Future Directions portion of Chapter IX.

The majority of the genes at which WDR5 is bound and thus displaced with WIN site inhibitor treatment are linked to protein synthesis and include a specific subset of RPGs. The genes that

do respond transcriptionally to WIN site inhibition are nearly identical between G401 and KYM-1 despite a five-fold difference in cellular sensitivity to C16. Genes with decreased gene body-associated polymerase in the RT cells are remarkably similar to those seen in MV4:11 cells treated with C3 for one hour. From this I can conclude that the RPGs within this subset are the predominant targets of WDR5 and thus the primary targets of WIN site inhibition in the context of RT. In addition, expanding the primary targets beyond MLLr and NB to yet another cellular context allows us to confidently predict which RPGs will be repressed by WIN site inhibition in other cellular settings. The similarities in different cell types and with different WIN site inhibitors confirms that that repression is due to on-target action of these inhibitors.

As discussed in Chapter IV, disruption of protein synthesis and ribosome biogenesis is a promising cancer therapeutic strategy [80]. In order to sustain the enhanced growth, cancer cells need to increase protein synthesis, cells rely on their ability to ramp up production of protein synthesis machinery, including ribosomes [80]. Therefore, inhibitors that disrupt protein synthesis could preferentially target the growth of cancer cells. In fact, RT cells have been shown to be sensitive to the FDA-approved protein synthesis inhibitor homoharrringtonine (HHT) [54]. HHT functions by inhibiting the elongation phase of translation by blocking the site at which tRNAs bind within the ribosome [90]. This demonstrates that disrupting protein synthesis in RT cell is a validated treatment strategy for inhibiting proliferation.

Although I observe a decrease in the transcription of PSGs, I need to determine if this translates to a decrease in expression of PSGs and identify what other gene expression changes result from WIN site inhibition at longer time points. Presumably, under longer treatments with WIN site inhibitors, there will be additional gene expression changes beyond the PSGs that will reveal additional cellular changes to account for decreased cell proliferation. In addition, I must determine if the decrease transcription of PSGs translates to a sustained decrease in expression of these genes. Also, it will be interesting to see if the genes that demonstrate an increase in transcription in G401 cells persist to longer time points as this has never been seen

in other cellular contexts. Long term gene expression changes that result from treating RT cells with WIN site inhibition will be the topic of Chapter VI. Finally, I need to connect changes in gene expression to the cellular response that reduces proliferation in RT cells and makes them sensitive to WIN site inhibitors.

VI. WIN SITE INHIBITORS SUPPRESS WDR5-BOUND PROTEIN SYNTHESIS GENES AND INDUCES P53 TARGET GENES IN RHABDOID TUMOR CELLS

Introduction

The major goal of this work is to understand the function of WDR5 WIN site inhibitors in *SMARCB1*-deficient cell lines. To do so, it is important to understand how the expression of WDR5 target and non-target genes respond to WIN site blockade. In Chapter V, I explored the primary transcriptional responses of WIN site inhibitors and showed that WIN site inhibition decreases transcription of a specific set of PSGs in both of the RT cell lines tested. Short-term transcriptional changes are not sufficient to understand the whole picture of the response to WIN site inhibitors in RT cells because secondary gene expression changes play a major role in determining cellular response. The purpose of this chapter is to use RNA-Seq to look at gene expression changes after longer treatment with WIN site inhibitors. By comparing these gene expression changes to ChIP-Seq, I can determine if the changes observed at later time points are in genes bound by WDR5. In addition, I can compare the differentially expressed genes to the PRO-Seq data to determine if the primary transcriptional changes persist to longer treatment and reveal secondary consequences of WIN site blockade that may predict the cellular response. I hypothesize that many of the early transcriptionally responsive genes will persist at a later time point and that the majority of the differentially expressed genes will not be bound by WDR5 because they are a result of the cells' compensatory mechanisms to WIN site inhibition rather than the primary response.

To test my hypothesis, Dr. April Weissmiller, Chase Woodley, and I used RNA-Seq in the abbreviated *SMARCB1*-deficient cell line panel comprised of G401, TTC642, KYM-1, TTC549, and TM87-16 cells so that we could compare the response to WIN site blockade in cells with a variety of sensitivities. We were hopeful that longer term gene expression changes would reveal the reason for the differential cellular sensitivity to C6 and C16. As expected, the decrease in

PSGs seen in G401 and KYM-1 with WIN site inhibition with PRO-Seq persists to three days and is observed in the other three cell lines as well. We also observe gene expression changes beyond the WDR5-bound genes. WIN site inhibition results in thousands of differentially expressed genes in each cell type. Notably, very few of the gene expression changes were observed in all five cell lines. The genes with decreased expression in all five cell lines are highly enriched in PSGs. In the genes that are increased in all five cell types, the p53 pathway is induced. TP53 is a gene that codes for the tumor suppressor p53. Under normal conditions, p53 levels are low because it is targeted for degradation by HDM2. However, under stress conditions or after DNA damage, p53 becomes activated and can promote cell cycle arrest, DNA repair, apoptosis, or a number of other functions [127]. The ability to detect DNA damage and promote either repair or programmed cell death has earned p53 the nickname "the guardian of the genome" [128]. However, the level of p53 induction can determine the cellular outcome. Studies have shown that high levels of p53 expression induce apoptosis while lower levels of p53 results in cell cycle arrest [129]. These observations align well with the response to WIN site inhibition we observe in other cellular contexts [3, 4].

Results

Long term effects of WDR5 WIN site inhibition on gene expression in RT cells

To expose transcriptomic changes induced by C16 in RT cells, Dr. April Weissmiller, Chase Woodley, and I performed whole transcriptome sequencing (RNA-Seq) to identify changes in levels of mRNA after WIN site inhibition. We profiled two sensitive cell lines (G401 and TTC642), a moderately sensitive cell line, (KYM-1) and two less sensitive cell lines (TTC549 and TM87-16). We chose these cell lines because it would allow us to compare differences in the response to WIN site inhibition in cell lines with varying sensitivity. We treated these five cell lines with DMSO or 500 nM C16 for three days and isolated RNA for RNA-Seq. As before, 500 nM C16 was chosen because it is the lowest concentration at which we see maximal reduction of WDR5-target genes in the QuantiGene™ Plex assay (**Figure 3.4**). Following three day

treatment, we isolated and purified RNA and sent the samples to Vanderbilt Technologies for Advanced Genomics (VANTAGE) who performed ribosomal RNA depletion, library preparation, and next generation sequencing (NGS). We performed the experiment three times in all five cell lines. However, one replicate in each of G401, TTC642, and KYM-1 was an outlier and did not resemble the other two replicates. We were able to remove the replicate and perform the analysis with only two because of the extensive similarity between the first two replicates. The number of differentially expressed genes (DEGs) in each cell line as a result of WIN site inhibition is summarized in **Figure 6.1A**. Heatmaps were generated of all the significantly changed genes (FDR < 0.05) comparing C16 treated RT cells to DMSO for all of the replicates to look for variability in the replicates (**Figure 6.1B**). In all cell lines, we see a high degree of consistency in the pattern of gene expression change between each of the replicates, especially among the cell lines in which we only used two replicates. These heatmaps also demonstrate that the pattern of gene expression changes with C16 treatment is distinct from the DMSO treated samples.

We identified thousands of DEGs, depending on the cell type (**Figure 6.1A**). This is many more gene changes than observed in MV4:11 and CHP-134 cells treated with C6 [3, 4]. In general, the more sensitive lines have a greater response than that of the less sensitive in terms of the number of genes with TTC642 having nearly 5,700 DEGs and TTC549 and TM87-16 both having about 1,700 DEGs each. In addition, there seems to be a difference in the magnitude of gene expression changes between sensitive and insensitive cell lines. In a violin plot showing the $\log_2$fold changes as a result of C16 treatment in each cell line, TTC642 cells extend the furthest with $\log_2$fold change extending from approximately -6 to +6 while TTC549 and TM87-16 cells only extend from about -4 to +3 (**Figure 6.2A**). The same trend is observed in the volcano plots in which demonstrate a greater magnitude of changes in the sensitive cell lines (G401, TTC642, and KYM-1) than observed in the insensitive cell lines (TTC549 and TM87-16) (**Figure 6.2B**).

A Cell lines

DEGs	G401	TTC642	KYM-1	TTC549	TM87-16
UP	2190	3032	1467	899	892
DOWN	1658	2643	1342	854	841
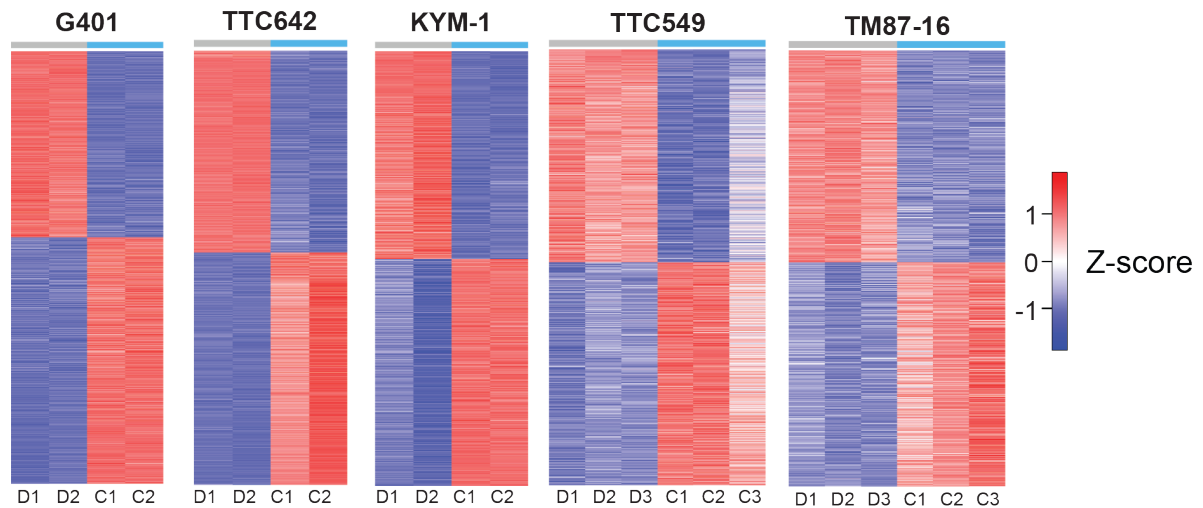
Figure 6.1. Summary of gene expression changes in RT cells treated with WIN site inhibitor (**A**) Table shows the number of differentially expressed genes (DEGs; FDR < 0.05) altered at 3 days of treatment in the indicated cel lines with 500 nM C16, compared to their respective DMSO control (n = 2 for G401, TTC642, and KYM-1 cells; n = 3 for TTC549 and TM87-16 cells). (**B**) Heatmaps displaying consistency amongst replicates of RNA-Seq for three day C16-treated cell lines; Z-transformation and ranking by fold-change. Transcripts that are significantly (FDR < 0.05) impacted by C16, compared to DMSO are shown (n = 2 for G401, TTC642, and KYM-1 cells; n = 3 for TTC549 and TM87-16 cells).
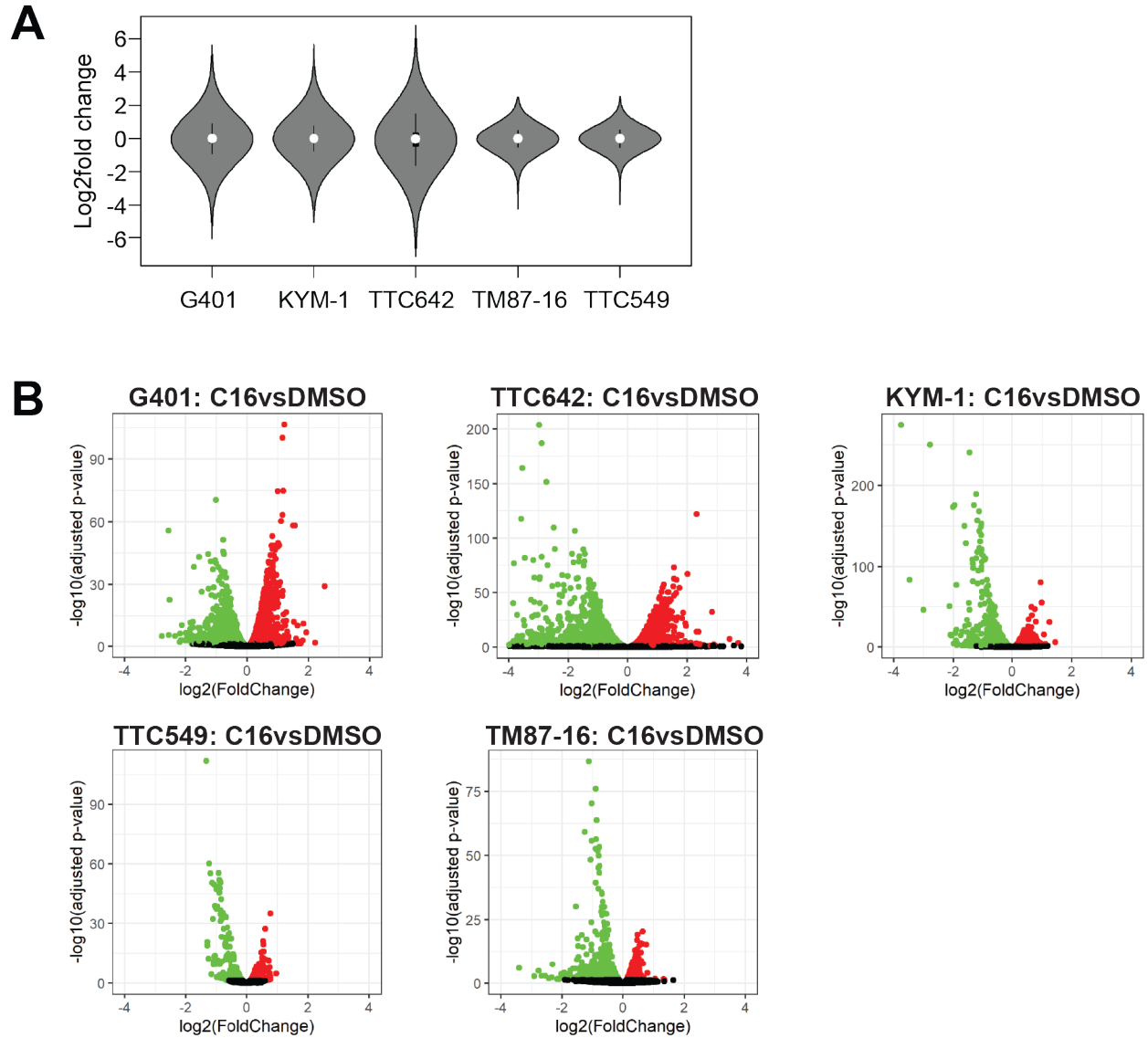
Figure 6.2. Magnitude of gene expression changes in RT cells with C16 treatment (**A**) Violin plot showing the distribution of $\log_2$-fold transcript changes elicited by C16 (RNA-Seq) in each cell line. (**B**) Volcano plots comparing $\log_2$-fold transcripts changes against $-\log_{10}$ adjusted p-values (C16vsDMSO) for each of the RNA-Seq experiments in the five RT cell lines.

I next compared the DEGs between cell lines to look for similarities and differences between the genes that were significantly changed with C16 treatment. This is especially important to identify gene expression changes that are common to all RT cell lines tested to define a common response to WIN site inhibition and to identify changes that are seen in sensitive cells but not insensitive cells to reveal as a possible explanation for the differences in cellular sensitivity. Upset plots were used to visualize the comparison of the genes that increased or decreased in response to C16 treatment in all five cell lines (**Figure 6.3**). The total number of gene changes in each cell lines is represented in the bars on the left. Every possible overlap of cell lines is represented by the colored dots in the bottom plot, and the number of genes in each overlap is shown in the top bars. Genes differentially expressed in only a single cell line are shown on the left and the DEGs that are common to all five cell lines are on the right. Genes that are changed in two, three, or four cell lines are represented in the middle. From this comparison, we observe a similar pattern in the genes that are decreased (**Figure 6.3A**), and increased (**Figure 6.3B**) A small number of genes changes are shared amongst all five cell types with only 69 genes decreased in all five cell lines and only 23 genes increased in all five cell lines. The majority of the gene changes are unique to a single cell lines. In fact, between 25% and 60% of the DEGs are cell type-specific illustrating the diversity of the transcriptional response to C16 within this panel. The variety of gene expression changes between cell types could be because of different responses to the WIN site inhibitor in each cell type or due to differences in the unperturbed transcriptomes of each cell type because these cell lines were derived from different tissues (**Table 3.1**). Principal component analysis (PCA) reveals that the diversity in gene expression changes is likely a consequence of the diverse native transcriptomes of the five lines, rather than disparate responses to C16 (**Figure 6.4**). The PCA shows that the samples cluster by cell line rather than by treatment group.

Contrasting the more sensitive with the less sensitive lines, we looked for gene expression changes that are common among G401, TTC642, and KYM-1 but not observed in TTC549 or TM87-16 to see if we could pinpoint a response that is unique to the sensitive cell lines that may

Figure 6.3. Summary of gene expression changes in RT cell lines after C16 treatment
(**A**) UpSet Plot comparing the genes with decreased expression in response to C16 in all five cell lines after three day treatment. (**B**) As in (A) but genes with increased expression.
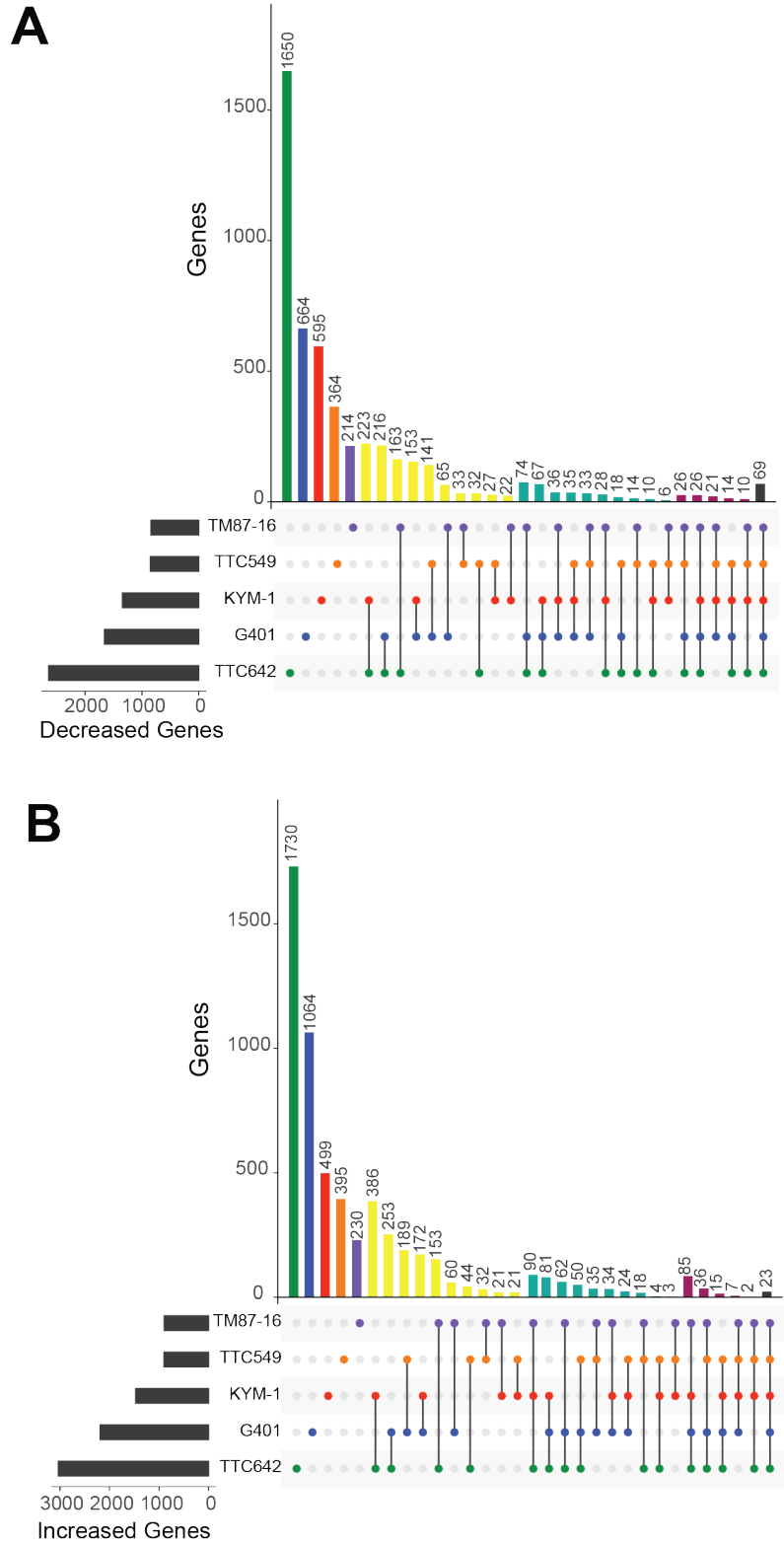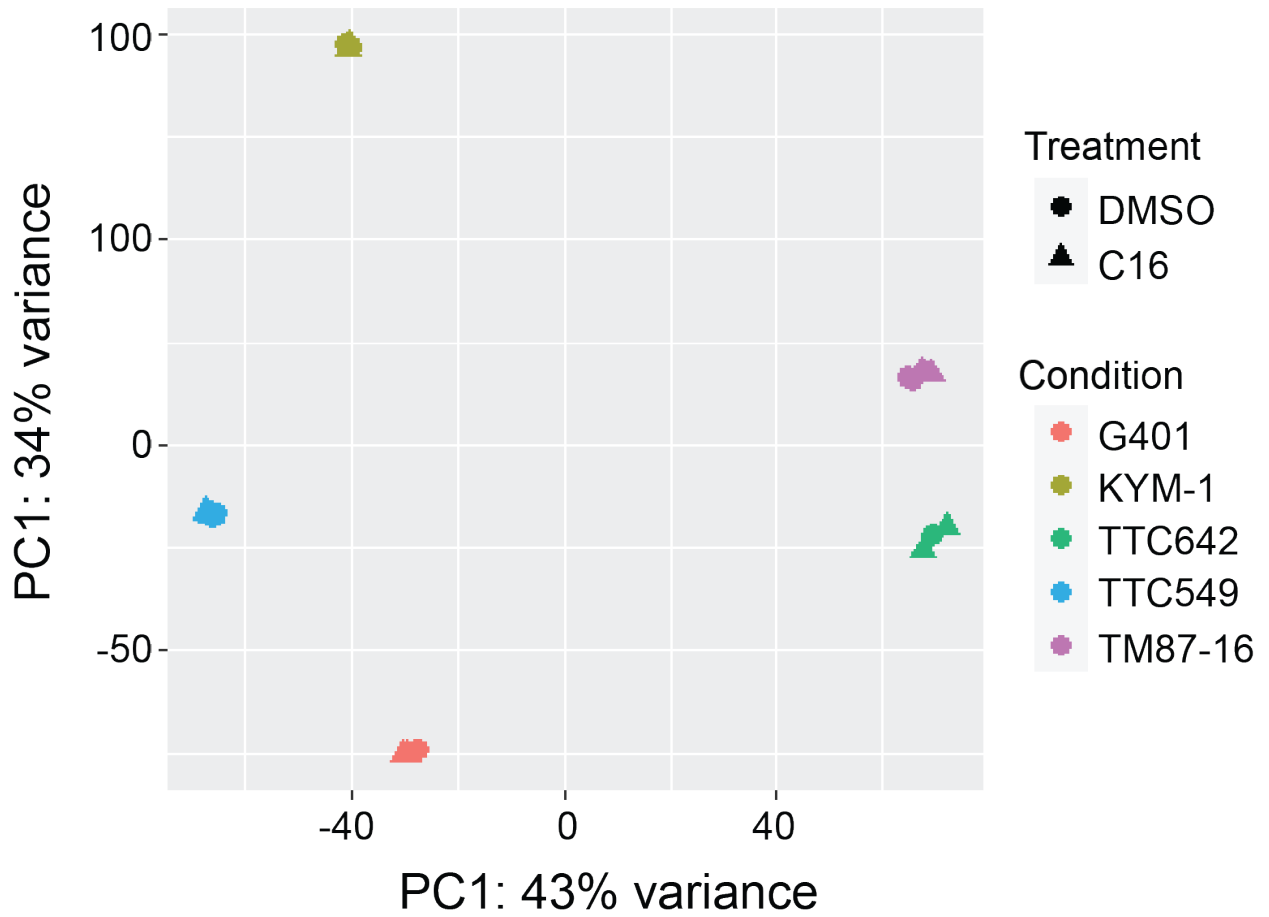
Figure 6.4. Comparison of transcriptomes of RT cells lines with and without C16 treatment Principal Component Analysis (PCA) plot based on RNA-Seq in all five cell lines. The samples are clustered by cell types rather than treatment.

explain their preferential cellular sensitivity to WIN site inhibition. There are 67 genes with decreased expression only in the more sensitive cells (**Figure 6.3A**) but these genes fail to cluster into any biological category by GO analysis to give ay meaningful biological significance. There are 81 genes induced only in more sensitive cells (**Figure 6.3B**). including a small but highly enriched set encoding mitochondrial respiratory chain complex I, a member of the electron transport chain (**Figure 6.5**). One explanation for this increase in mitochondrial complex genes could be due to a shift from glycolysis to oxidative phosphorylation under WIN site blockade. Tumors are known to preferentially utilize anaerobic glycolysis for energy to maintain the rapid growth and proliferation that define cancer cells, a phenomenon known as the Warburg effect [130]. WIN site inhibitor treatment could be causing a decrease in glycolysis forcing the cells to utilize oxidative phosphorylation thereby slowing their growth. Further studies need to be done to tease apart the intricacies and validity of this hypothesis.

A powerful facet of performing multiple types of genomic analysis in these cell lines is that we can compare the long term gene expression changes for the RNA-Seq experiments to the WDR5 binding data from the ChIP-Seq experiments in Chapter IV and the early transcriptional response data from the PRO-Seq experiments in Chapter V. These comparisons will showcase if the long term transcriptional response is in genes that are bound by WDR5 and if the early primary transcriptional changes from WIN site inhibitor treatment persists to three days. In G401, KYM-1, and TTC549 cells in which we have WDR5 binding data, only about half of the WDR5-bound genes respond transcriptionally to WIN site inhibition at the three day time point (**Figure 6.6A**). Even fewer of the WDR5 bound genes in KYM-1 and TTC549 responded to WIN site blockade transcriptionally with only about 30% of genes bound by WDR5 in KYM-1 cells and 20% of genes bound by WDR5 in TTC549 cells demonstrating changes in expression. However, in a GSEA ranking DEGs in each cell type against WDR5 binding sites, there is a tendency of WDR5-bound genes to be persistently suppressed by C16 in all three cell lines (**Figure 6.6B**). In each cell type, a greater number of WDR5-bound genes have decreased expression rather than increased expression. This is most likely because WDR5 is playing a
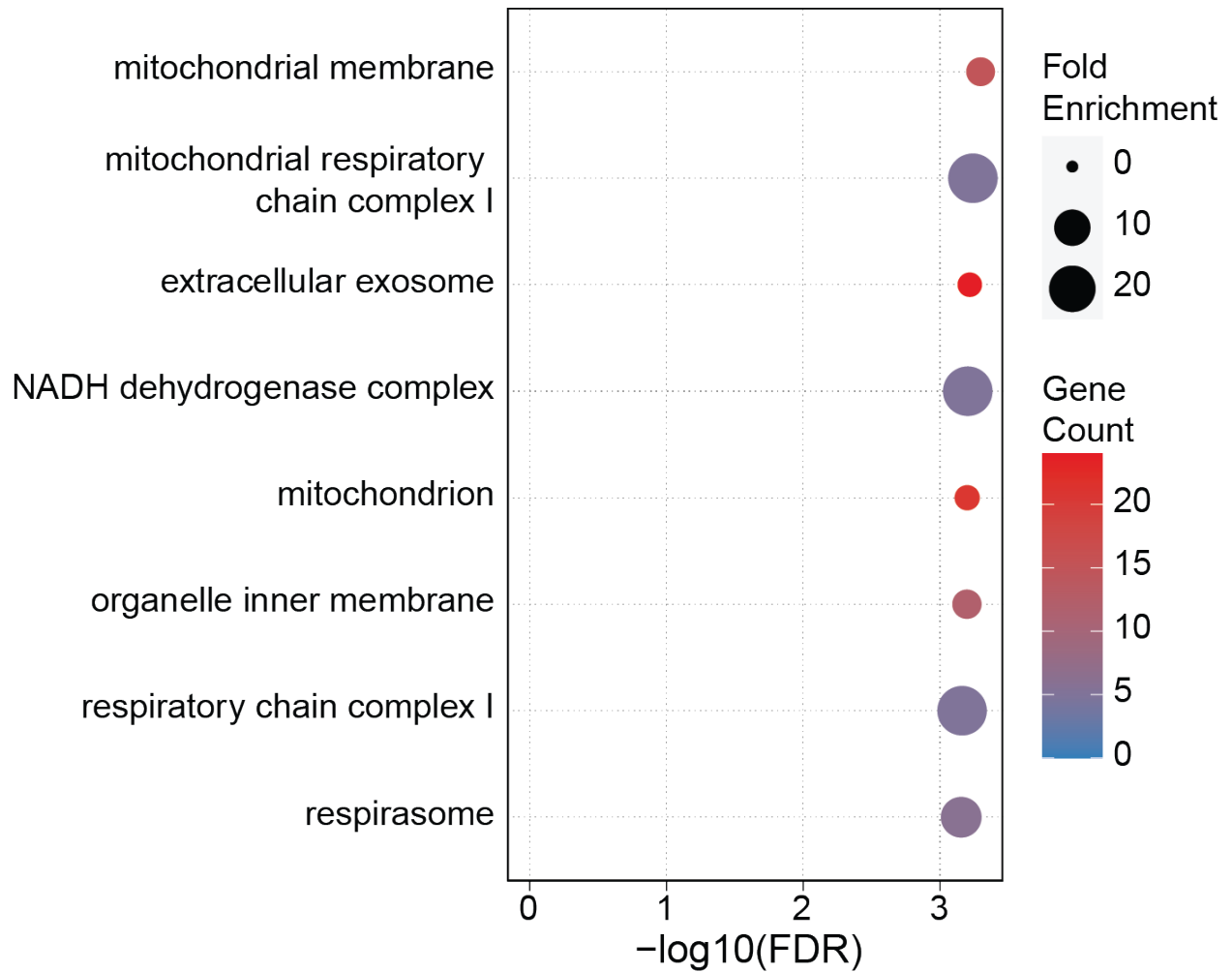
Figure 6.5. GO terms enrichment analysis of genes uniquely induced in sensitive cell lines Bubble plot showing GO terms enrichment analysis of the 81 genes uniquely induced by C16 in G401, TTC642, and KYM-1 cells. Cellular Component GO terms were ranked by false discover rate (FDR). The eight most significantly enriched terms are shown. Size indicates fold enrichment, color indicates gene number, and the x-axis is the -log$_{10}$(FDR).
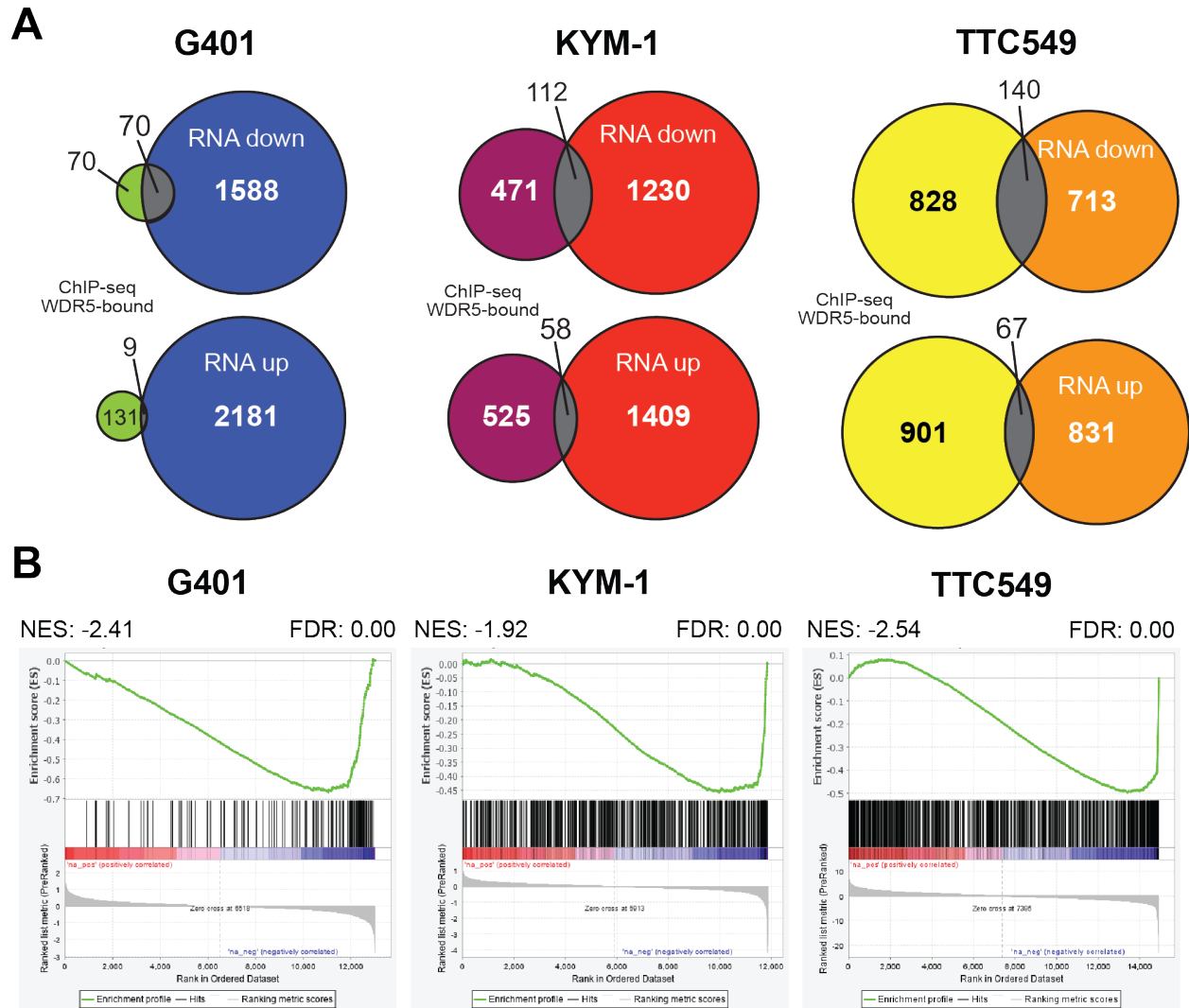
Figure 6.6. Comparison of WDR5-bound genes by ChIP-Seq and genes altered with C16 treatment by RNA-Seq (**A**) Venn diagram showing the overlap of genes bound by WDR5 in G401, KYM-1 and TTC549 cells (ChIP-Seq) with those that are suppressed ("RNA down") or induced ("RNA up") by three days of C16 treatment. (**B**) GSEA comparing genes bound by WDR5 in ChIP-Seq against a gene list ranked by alteration in expression, as determined by RNA-Seq. G401 cell data is on the left, KYM-1 cell data is in the middle. TTC549 cell data is on the right. "NES" is normalized enrichment score. "FDR" is False Discovery Rate.

role in activating expression of these genes under normal conditions so when WDR5 is displaced from chromatin from WIN site blockade, expression of these genes decreases as a result. When we look to see if the genes that responded transcriptionally to WIN site inhibition in two hours persist to three days, a majority of genes with decreased transcription by PRO-Seq are also decreased in RNA-Seq (**Figure 6.7**). This is in line with what we have observed in MV4:11 cells treated with C3 and C6 [4]. Very few genes with increased RNA polymerase occupancy in PRO-seq have a corresponding increase in gene expression from WIN site inhibitor treatment at a longer time point. In fact, only 18 of the genes in G401 that were increased by PRO-Seq were also increased in RNA-Seq and the single gene in KYM-1 cells increased at two hours did not remain increased at three days. We have not seen evidence of genes with increased transcription as a result of WIN site inhibition by PRO-Seq or SLAM-Seq in previous cell lines that we have tested [3, 4] indicating that these transcriptional changes are not required for cells to respond to WIN site inhibitors so I am not surprised that most of these transcriptional changes did not persist to longer treatment times. From comparing various genomic data sets in RT cell lines, we can conclude that a considerable percentage of WDR5-bound genes do indeed have altered gene expression as a result of WIN site inhibition (**Figure 6.6A**). In addition, the majority of the genes that decrease expression at two hours of WIN site inhibitor treatment persist to three days (**Figure 6.7**). However, most genes with altered expression in RNA-Seq are neither bound by WDR5 nor respond early (**Figure 6.6A** and **Figure 6.7**), indicating that the predominant long term transcriptional response to C16 in these cells is likely a secondary consequence of WIN site blockade, rather than due to differences in primary transcriptional effects. This is especially true in the genes with increased expression at three days of inhibitor treatment because a smaller percentage of the genes that are induced with WIN site inhibitor treatment are bound by WDR5 or respond early. This indicates that almost all of the genes with increased expression are secondary consequences of the WIN site inhibitor treatment.
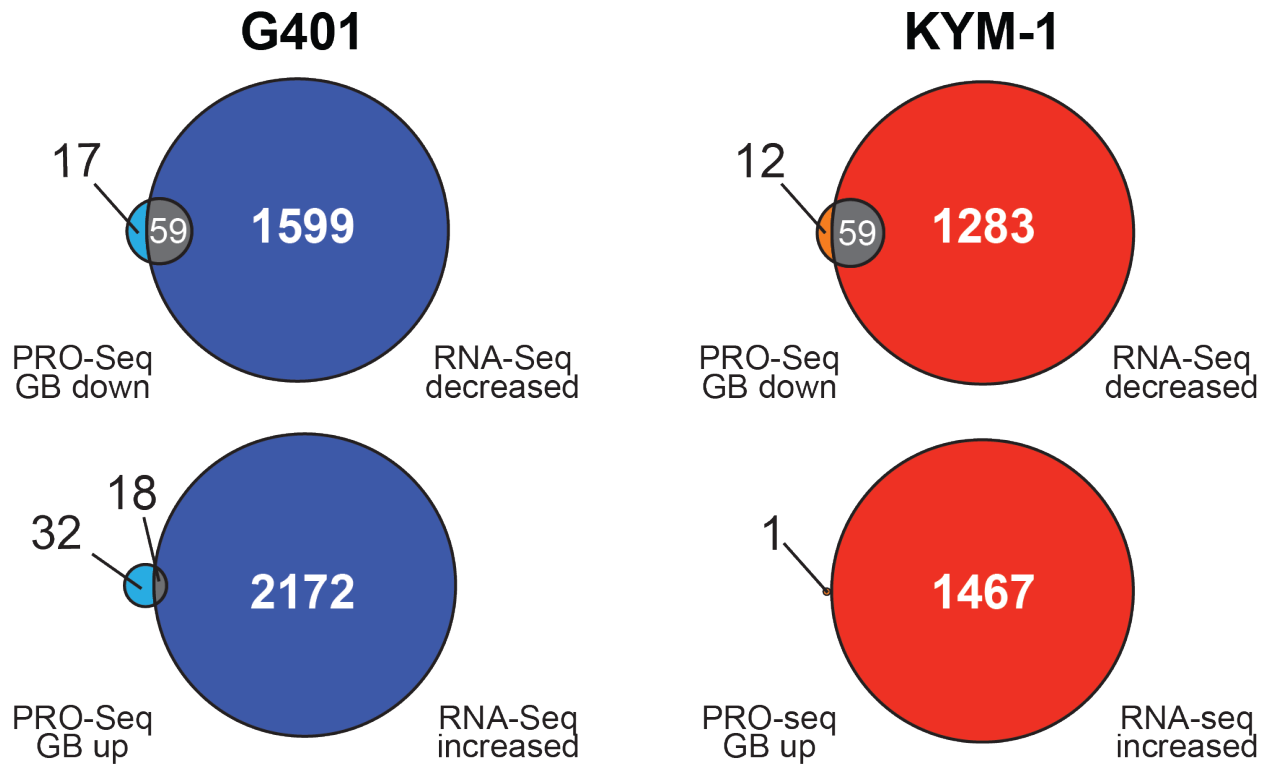
Figure 6.7. Comparison of genes that respond to C16 in two hours and at three days Venn diagram showing the overlap of genes that respond to C16 treatment in two hours (PRO-Seq) with those that respond to C16 in three days (RNA-Seq). G401 cell data are presented on the left. KYM-1 cell data are presented on the right. Genes with decreased expression are at the top, genes with increased expression are at the bottom.

WIN site inhibition decreases expression of PSGs in RT cells

To understand how *SMARCB1*-deficient cells are responding to WIN site inhibitors, it is imperative that we examine genes that are significantly altered with WIN site inhibition in all five cell lines. Only about 90 genes are differentially expressed in response to C16 in all lines (**Figure 6.3**). The heatmap in **Figure 6.8** shows the similarities in the gene expression changes resulting from WIN site inhibition in all five cell lines. The majority of the genes change in the same direction and within a factor of two (**Figure 6.8**). An exception to this trend is a group of ten genes induced in TTC642 but suppressed in all other lines, most of which encode variants of histone H2A and H2B. The majority of the genes with common alterations in the five cell lines show decreased expression rather than increased expression. GO terms enrichment analysis of the ~70 genes with decreased transcription in all lines reveals strong enrichment in terms connected to protein synthesis (**Figure 6.9**), a pattern that is expected based of the categories of genes that are bound by WDR5 (**Figure 4.4**) and that decrease transcription with two hours of WIN site inhibition (**Figure 5.4**). This is also expected based on the gene expression changes from WIN site inhibition that we see in other cancer cells such as MLLr leukemia and NB [3, 4]. Significantly enriched GO terms in the genes with decreased expression include categories related to translation, RNA processing, and ribosome biogenesis. The same set of ~40 C16 repressed genes were represented in all the most significant categories. They include the recurrent set of ~38 RPGs (**Figure 6.10**) and a handful of transcription factors. These same RPGs responded to C16 treatment at two hours with decreased transcription demonstrating that RPG repression is a primary response to WIN site inhibition and that the decreased expression of these genes is common to all RT cell lines tested regardless of cellular sensitivity to WIN site inhibitors. In addition, the decrease in RPGs is a mechanism shared with other cell lines in which we have tested the effects of WIN site inhibition [3, 4] furthering the notion that suppression of the RPGs is a prevailing response to WIN site inhibition regardless of cell type.
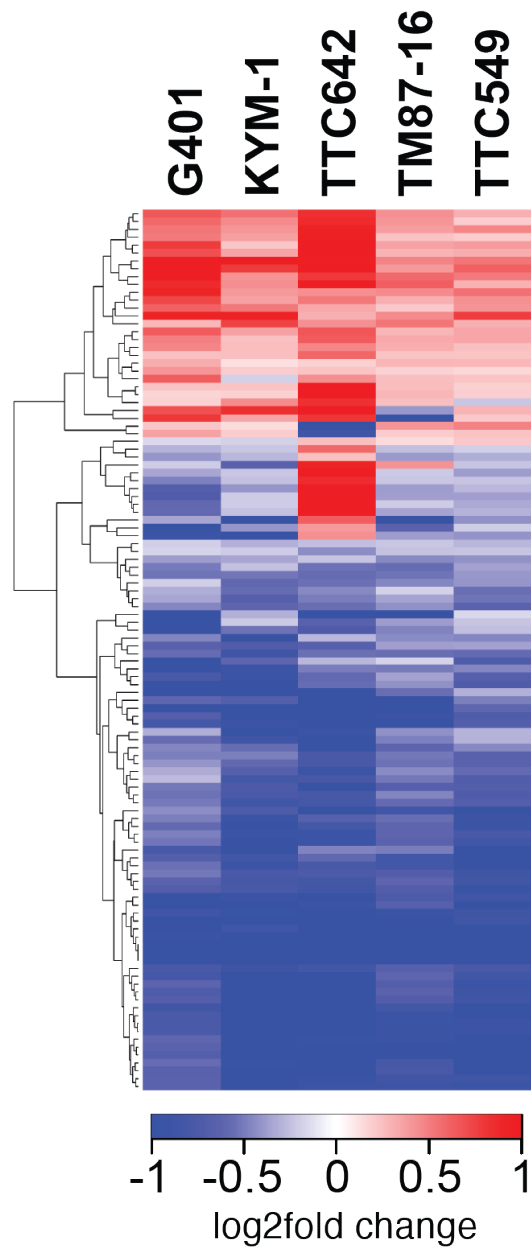
Figure 6.8. Comparison of genes differentially expressed in all five RT cell lines Heatmap showing the log$_2$fold change of significantly (FDR < 0.05) changed transcripts that are altered by C16 in all five RT cell lines. Transcripts are clustered according to the relationship between the cell lines.

Figure 6.9 GO terms enrichment analysis of genes with decreased expression with C16 in RT cell lines GO terms enrichment analysis of genes showing a significant decrease in expression in all five cells lines, as determined by RNA-Seq. Biological Process GO terms were ranked by false discovery rate (FDR). The eight most significantly enriched terms are shown. Color indicates fold enrichment, size indicates the gene number, and the x-axis is the -log$_{10}$(FDR). PTM post-translational modification; NMD nonsense-mediated decay.
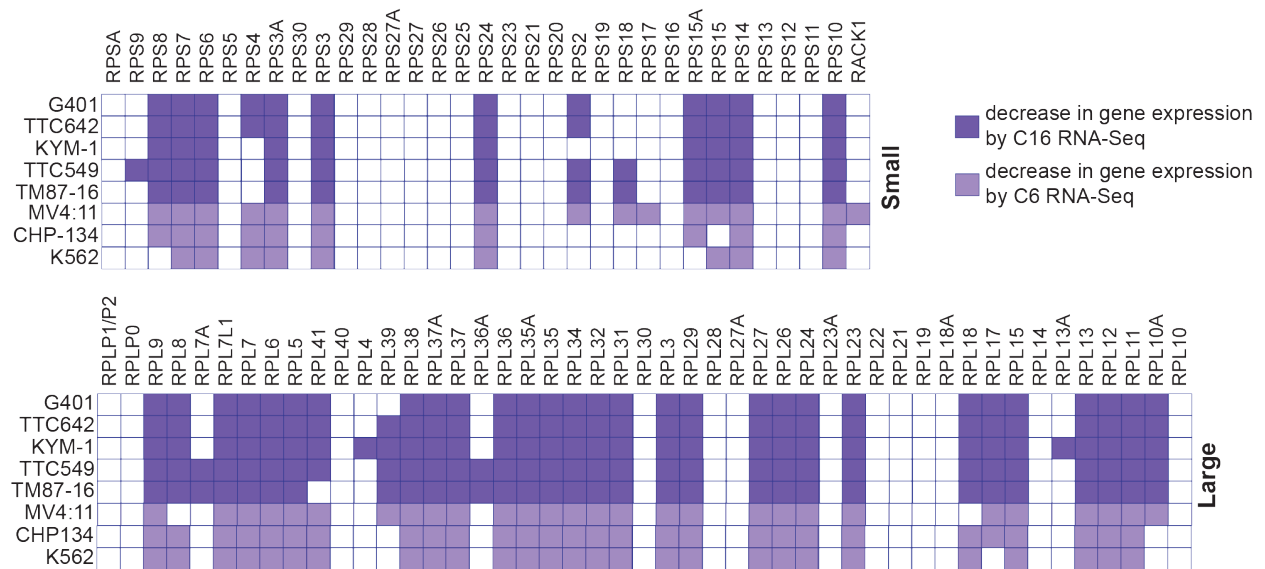
Figure 6.10. WIN site inhibitor decreases expression of a discrete set subset of ribosomal protein genes Ribosomogram showing the small (top) and large (bottom) subunit RPGs. A purple box indicates whether that specific RPG is suppressed by C16 in the indicated cell line. A lighter purple box indicates whether that specific RPG is suppressed by C6 in the indicated cell line. MV4:11 and K562 data (GSE115377), CHP-134 data (GSE136451); all other data this study.

After validating that the primary mode of action of WDR5 WIN site inhibitors is to reduce the transcription and steady state expression of PSGs, I predicted that this would impede the translational capacity of treated cells resulting in inhibited growth. The relative protein translational capacity of cells can be quantified by fluorescently labeling all the newly synthesized proteins in a cell during a given time and measuring the relative fluorescence by flow cytometry [131]. To do this, we used the compound O-propargyl-puromycin (OP-Puro or OPP) to label nascent polypeptides produced during a one hour pulse with OP-Puro. OP-Puro is an analog of puromycin, a protein synthesis inhibitor that prematurely terminates the nascent polypeptide when it is incorporated in the place of an amino acid [132]. This premature termination releases the OP-Puro labeled peptide from the ribosome where is can be labeled with a fluorophore using a "click" reaction. The relative rate of protein synthesis can be quantified by measuring the relative fluorescence of the labeled nascent peptides using flow cytometry. Chase Woodley performed OP-Puro labeling experiments in G401 and TTC642 cells treated for four days with DMSO or 500 nM C16. A four day treatment ensured that any gene expression changed observed at the three day treatment by RNA-Seq would have time to elicit changes in the cell. As a positive control for translation inhibition, cyclohexamide (CHX) was added to the cells 30 minutes prior to the OP-Puro pulse. As a control for background Alexa488 staining, OP-Puro was withheld from a DMSO treated and C16 treated sample. We found that there is a significant decrease in OP-Puro incorporation in the C16 treated samples and that the result is similar in both G401 and TTC642 cells (**Figure 6.11**). However, the effect of C16 on protein translation is modest compared to CHX but is consistent with what we see in MV4:11 cells. Thus, WIN site inhibitors lead to a moderate but significant decrease in protein translational capacity in G401 and TTC642 cells. Taken together, as observed in other cell types, the mode of action for WIN site inhibitors in RT cells is to suppress the expression of ribosomal protein genes which corresponds to a reduction in protein translational capacity.
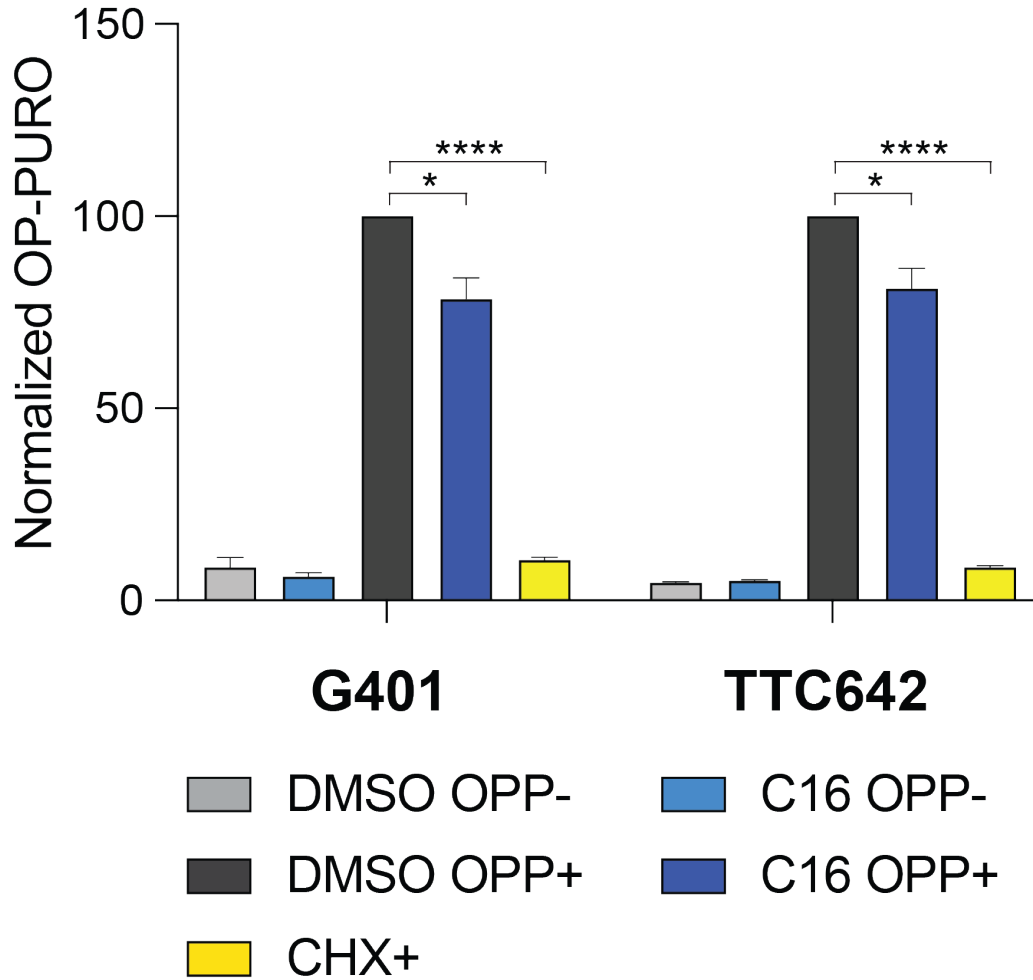
Figure 6.11. C16 treatment suppresses protein synthesis in RT cells Alexa488 labeled-OPP (OPP+) incorporation into nascent polypeptides of G401 or TTC642 cells treated with DMSO or 500 nM C16 for four days. As a positive control for protein translation inhibition, 50 µg/mL of cyclohexamide (CHX) was added to a sample of DMSO treated samples for 30 minutes prior to addition of OPP. No OPP (OPP-) samples were processed for both DMSO and C16 treated cells for background staining. Mean Alexa488 fluorescence measurements were normalized to DMOS treated OPP+ samples. *p<0.05, ***p<0.001 (n=3, mean ± standard error of the mean (SEM))

WIN site inhibition induces p53 target genes in RT cells

To further dissect the response to WIN site inhibitors in RT cells, I next examined the genes with increased expression in all five cell lines. Because there were very few genes with increased transcription with WIN site inhibition in both G401 and KYM-1 cells (**Figure 5.4**), the genes that are induced with WIN site inhibitor treatment at three days are secondary consequences of WIN site blockade rather than a primary response. Only 23 genes are induced in all lines (**Figure 6.3**). Although this set is small, a GO terms analysis reveals that the list is significantly enriched in genes linked to p53 signaling, DNA damage, and apoptosis (**Figure 6.12**). This is to be expected because prior work exploring the effect of WIN site inhibitors in MV4:11 cells reveals that C6 treatment induces p53 expression at the protein level [4]. However, the GO terms analysis from the DEGs from RNA-Seq in MV4:11 cells following three day C6 treatment did not reveal the p53 pathway as significantly enriched [4]. This could be due to the fact that there were fewer upregulated genes in the MV4:11 cells in response to C6 treatment so the GO analysis failed to reach significance for the p53 pathway categories. Manual inspection of the DEGs in response to C6 treatment in MV4:11 cells reveals that p53 target genes are induced. To further reinforce the connections to p53 in RT cells treated with WIN site inhibitor, we performed a Reactome Pathway analysis [133] which uses the over-representation analysis method to determine if a set of genes significantly associates with certain pathways [134]. We found that genes that are induced by C16 treatment are significantly enriched for the pathway "Transcriptional Regulation by p53" in all lines (**Figure 6.13A**). By this analysis, TTC642 cells show the highest enrichment for this category both in number of DEGs that fall into this category and in the FDR. Dr. Jing Wang also performed a Hallmark GSEA analysis [135]. In a hallmark GSEA, a list of ranked genes, in this case the DEGs elicited by C16 treatment in each cell line, are queried against a number of pre-defined hallmark gene sets that represent specific well-defined biological states or processes to determine if the genes in that hallmark set are over-represented beyond random chance in the data set of interest. GSEA will also determine if the genes in the category tend to have increased or decreased expression. We saw a positive
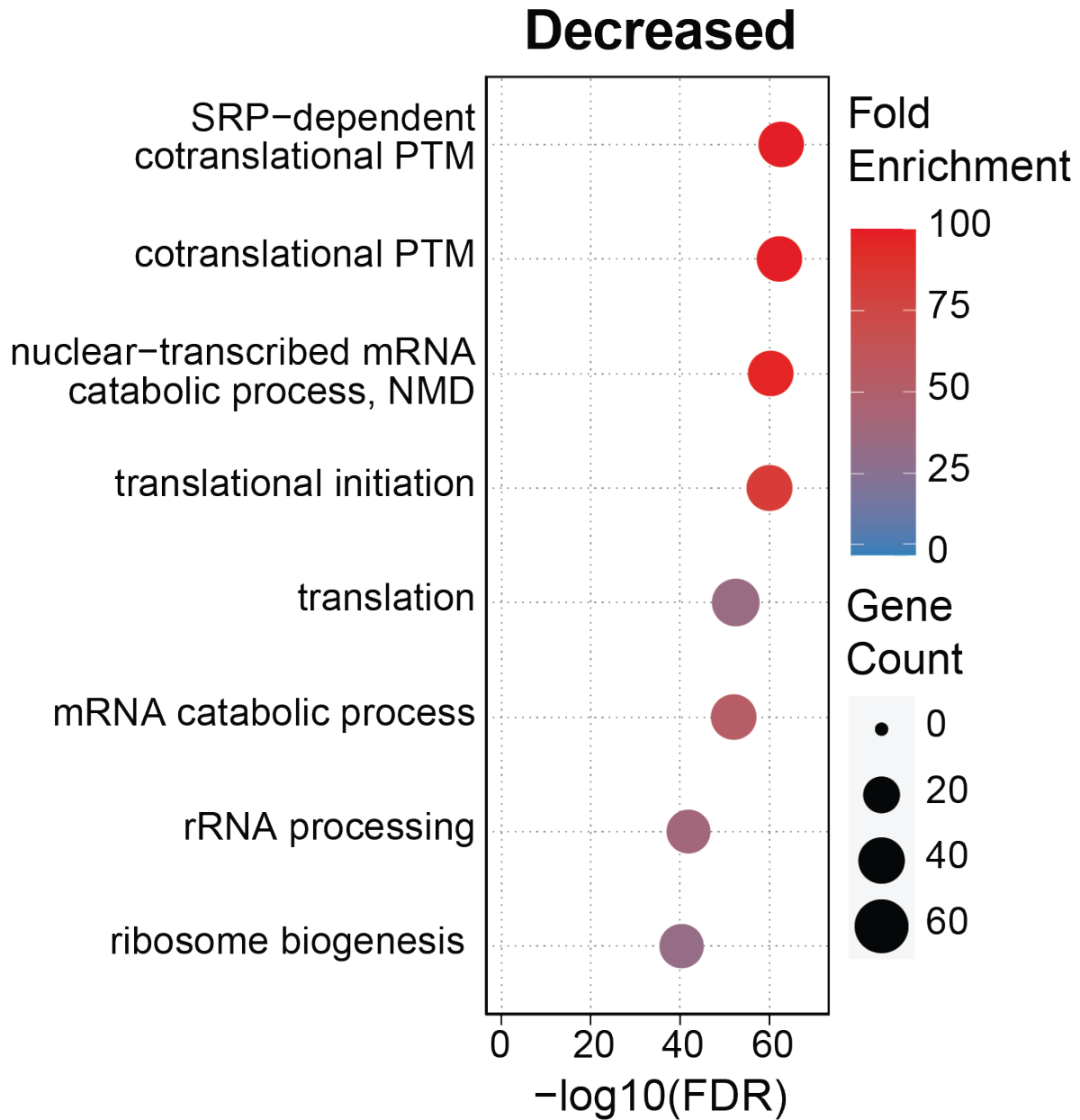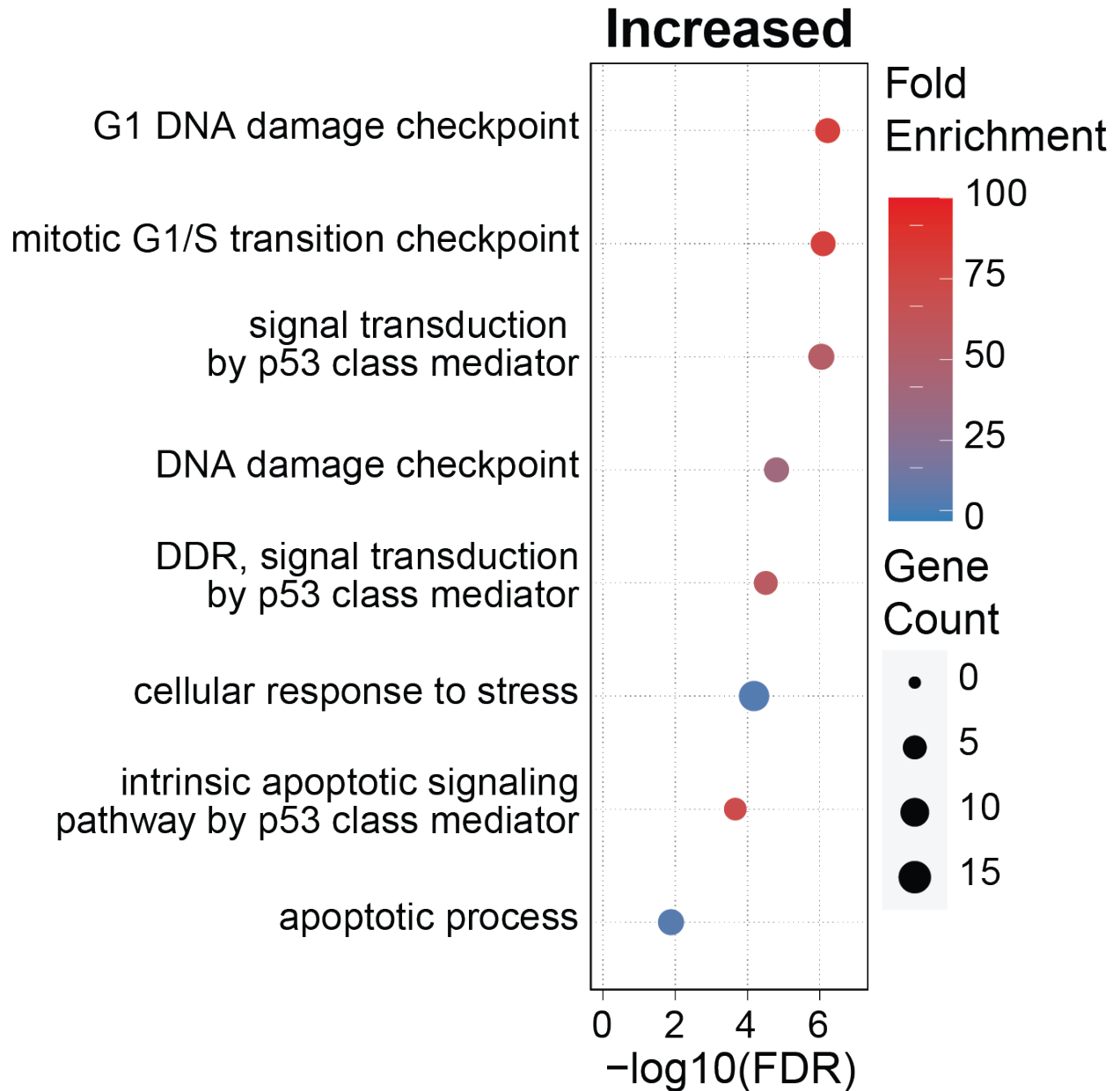
Figure 6.12. GO terms enrichment analysis of genes with increased expression with C16 in RT cell lines GO terms enrichment analysis of genes showing a significant increase in expression in all five cells lines, as determined by RNA-Seq. Biological Process GO terms were ranked by false discovery rate (FDR). The eight most significantly enriched terms are shown. Color indicates fold enrichment, size indicates the gene number, and the x-axis is the -$\log_{10}$(FDR).
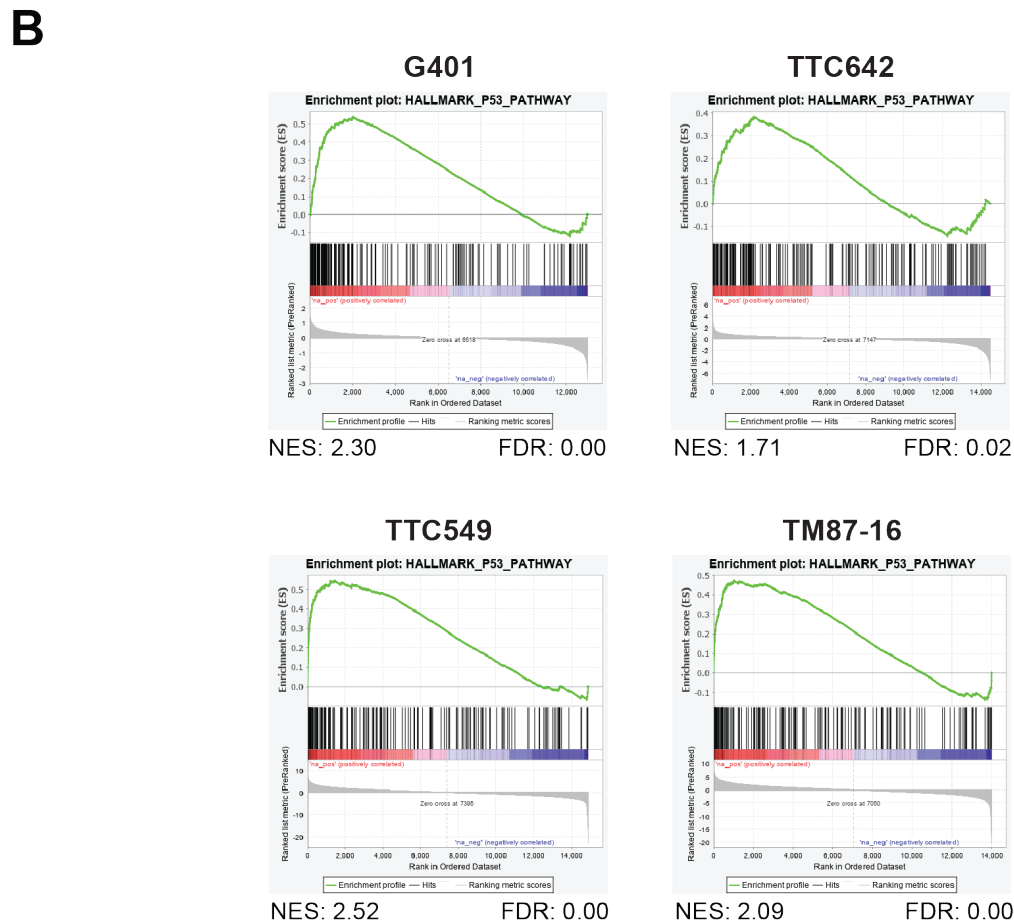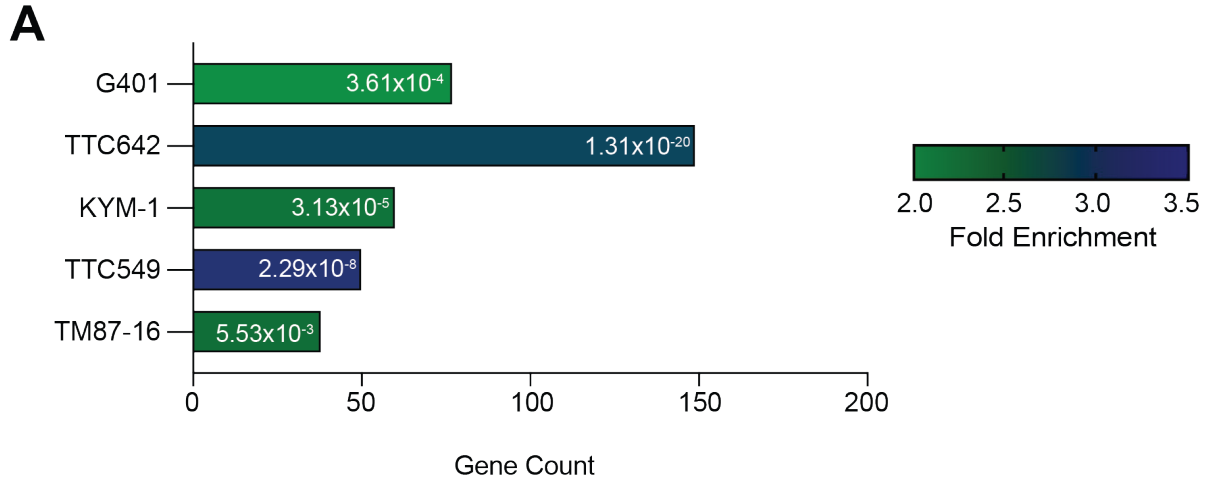
Figure 6.13. C16 treatment induces the p53 pathway in RT cells (**A**) Reactome pathway analysis on induced genes for each of the cell lines showing only "transcriptional regulation by p53" category. Color indicates fold enrichment, the x-axis is the gene number, and the number in each bar is FDR (**B**) Results of a genes set enrichment analysis (GSEA) of RNA-Seq data from C16 treated cells; only the results from the Reactome "Hallmark p53 Pathway" are shown. "NES" is normalized enrichment score; "FDR" is false discovery rate.

enrichment in "Hallmark p53 pathway" in all RNA-Seq datasets except for KYM-1 cells indicating that the p53 pathway is upregulated at three days in response to WIN site inhibitor treatment (**Figure 6.13B**). While the GSEA Hallmark p53 pathway failed to reach significance in KYM-1 cells, p53 target genes still appear in the set of upregulated genes and the "Transcriptional Regulation by p53" reactome pathway was significant. Indeed, curation of the list of 23 genes with increased expression in all five cell lines reveals that 16 of these 23 genes are induced by p53. This list includes *ZMAT3* [136], *CDKN1A* (p21), and *CCND1* (Cyclin D1) indicating that WIN site inhibition may be inducing p53 which promotes the expression of p53 target genes. Based on these analyses, I conclude that activation of p53 target genes is a recurring response to WIN site inhibition in this *SMARCB1*-deficient panel regardless of cellular sensitivity.

Discussion

Defining the long term gene expression changes in response to WIN site inhibitor treatment in *SMARCB1*-deficient cells serves as a good companion to the WDR5 binding data and the primary transcriptional response data we obtained in Chapter IV and V respectively to give a more complete picture of the mechanism of action to WDR5 WIN site blockade. The same subset of RPGs are consistently bound by WDR5 in RT cells and are suppressed by WIN site inhibition so I conclude that these RPGs are the predominant biological targets of WDR5 and thus WDR5 WIN site inhibitors. We see a recurrent reduction in transcription of RPGs in G401 and KYM-1 cells that corresponds to a decrease in mRNA expression in all five of the RT cell lines tested, consistent with data collected in MLLr leukemia, NB, and Burkitt's lymphoma [3, 4, 126]. We can confidently predict that other cell types treated with WDR5 WIN site inhibitors will respond in the same way. Interestingly, WIN site inhibitors only promote a two-fold decrease in RPG expression and only affect about half of the ribosomal encoding genes. While this change appears modest, prior work from our laboratory has shown that this is sufficient to elicit a

99

cellular response [3, 4]. We were able to show that the decrease in RPGs translates to a reduction in protein translational capacity as G401 and TTC642 cells treated with WIN site inhibitor showed a decrease in nascent polypeptide production compared the DMSO control.

It is clear from our transcriptomic analyses that p53 target genes are induced in RT lines in response to C16 treatment. What is not clear, however, is the mechanism by which the p53 pathway is being activated. A variety of cellular stressors can induce p53. The most widely recognized activator of p53 is DNA damage but p53 can be activated by hypoxia, oncogene activation, nutrient deprivation, among other stressors [127, 137]. Interestingly, ribosomal imbalance has been shown to induce a nucleolar stress response that activates p53 [138, 139]. The best-characterized mechanism involves RPL5 and RPL11 which leave the nucleolus upon ribosomal protein imbalance [140-142]. Once in the nucleoplasm, RPL5 and RPL11 are able to bind directly to HDM2 preventing it from interacting with p53. Disruption of this interaction leads to stabilization of p53 and activation of the p53 pathway. While on the surface, this seems like a plausible explanation for how WIN site inhibition induces the p53 pathway, RPL5 and RPL11 are both bound by WDR5 and repressed by WIN site inhibition. It seems unlikely proteins with decreased expression could be binding HDM2 to activate p53. However, RPS27L has also been shown to bind to HDM2 in a manner that disrupts its interaction with p53, thus stabilizing the p53 protein and activating the p53 pathway [143]. RPS27L is located in the cytoplasm in an unperturbed cell but relocalizes to the nucleus where it interacts with HDM2 [143]. Unlike RPL5 and RPL11, WDR5 does not localize to RPS27L nor does the expression of RPS27L decrease with WIN site inhibition. In fact, RPS27L is one of the 23 genes that are induced in all five cell lines by WIN site blockade. It is possible that the ribosomal imbalance resulting from the decreased expression of only a subset of the RPGs causes RPS27L to relocalize to the nucleus where it interacts with HDM2 and activates the p53 pathway. In the future, further investigation into whether or not RPS27L is required for cells to respond to WIN site inhibition is needed to understand the accuracy of this hypothesis.

In this chapter, we have found that the transcriptional changes in response to WDR5 WIN site inhibitors occur in all five RT cells lines tested regardless of their C16 cellular IC_{50} values. This indicates that there is some yet to be determined characteristic(s) that occurs downstream of WDR5 displacement from chromatin and the transcriptional changes of RPGs that determines whether a cell line is sensitive to WIN site inhibition. In addition, the activation of p53 pathway cannot explain the variable cellular sensitivity to C16 observed in the *SMARCB1*-deficient cell line panel because it occurs in both the sensitive and insensitive cell lines. Now that we have observed increased expression of genes associated with the p53 pathway, the logical next step is to determine how p53 is involved in the cellular response to WIN site inhibitors. p53 levels can be induced on an continuum and the level of p53 induction will determine the outcome; higher levels of p53 have been shown to induce apoptosis while lower levels of p53 induce cell cycle arrest [129]. In the next chapter, I will explore the role of p53 in WIN site inhibitor function in RT cells by comparing C16 treatment to the response of a traditional p53 activator and by determining if p53 is required for RT cells to respond to WIN site inhibitors.

VII. THE CELLULAR RESPONSE TO WIN SITE INHIBITORS IS P53-INDEPENDENT IN RHABDOID TUMOR CELLS

Introduction

In the previous chapters, I have shown that the primary mechanism through which WDR5 WIN site inhibitors function in *SMARCB1*-deficient cell lines is through the comprehensive displacement of WDR5 from chromatin at a conserved set of protein synthesis genes which results in a decrease in expression of these genes, a mechanism which is consistent with observations in other cell lines [3, 4]. WIN site inhibition also induces the p53 pathway in these cell lines. Earlier studies have also shown that p53 is induced with WIN site inhibition in MV4:11 and CHP-134 cells and that p53 is required for a robust response [3, 4]. Because of the simple genetic profile of RT, WT p53 is retained in nearly all cases of RT [1]. I predict that p53 is involved in the cellular response to WIN site inhibition in RT cells. To test this hypothesis, I will look for induction of p53 at the bulk protein level. I will then look for similarities between the transcriptional response to WIN site inhibition and an HDM2 inhibitor. I will then determine if RT cells are able to respond to WIN site inhibition in the absence of p53.

I found that despite the activation of the p53 pathway observed in samples treated with WIN site inhibitors, I do not see a robust induction of p53 at the protein level. It is possible that induction of p53 by C16 is too small to detect by Western blotting, as opposed to the more sensitive output provided by p53 target gene expression. To test if p53 target gene activation can be measured in the absence of robust changes in p53 protein, I treated RT cells with the HDM2 antagonist Nutlin-3a. In an unperturbed cell, HDM2 binds to p53 to mark it for degradation and maintain low levels of p53 in the cell. Nutlin-3a binds to HDM2 and disrupts its interaction with p53, thus stabilizing p53 and activating the p53 pathway. I treated RT cells with Nutlin-3a at a dosage that fails to induce detectable changes in p53 protein levels, but is close to the IC_{50} for cellular proliferation for each line. When comparing the transcriptional response of RT cells to

C16 and Nutlin-3a treatment, I found a considerable overlap in the differentially expressed genes, suggesting that the p53 pathway is involved in the WIN site inhibitor response even in the absence of p53 induction at the protein level. When I knocked down p53 in the RT cell lines, it did not change their sensitivity to C16 indicating that p53 is not required for RT cells to respond to WIN site inhibition. I concluded that WIN site inhibitor modestly induces the p53 pathway but unlike in MLLr leukemia and NB, the response of RT cells to WDR5 WIN site inhibition is p53-independent.

Results

Effects of WIN site inhibition on p53 levels in RT cells

After demonstrating an induction of genes involved in the p53 response pathway with WIN site inhibitor treatment, I was interested to know whether p53 is induced at the protein level. I treated G401, TTC642, KYM-1, TTC549, and TM87-16 cells with DMSO or C16 for three days and performed a western blot to look for induction of p53. It is important to test for p53 induction at the protein level in cell lines with varying cellular sensitivities as it may explain the differences in C16 IC_{50} values. I chose three day treatment because I see considerable differences in proliferation between the DMSO and C16 treated samples in G401, TTC642, and KYM-1 cells by three days (**Figure 3.2**) and there is a transcriptional induction of genes involved in the p53 pathway at this point. After three day treatment with DMSO or 500 nM C16, I isolated protein from these cells and ran the lysates on an SDS-PAGE gel, transferred them to a PDVF membrane, and probed the membrane with antibodies specific for p53 and histone H3 as a loading control (**Figure 7.1**) Curiously, I observe only a subtle induction of p53 protein in G401 and TTC642 cells, but not in KYM-1, TTC549, and TM87-16. I also probed these lysates with an antibody specific for p21, a well known p53 target gene [144], to assess whether or not the p53 pathway activation results in the induction of p53-target genes at the protein level. I found that p21 is robustly induced in G401, TTC642, and KYM-1 cells but only subtly or not at all in TTC549 and TM87-16 cells.
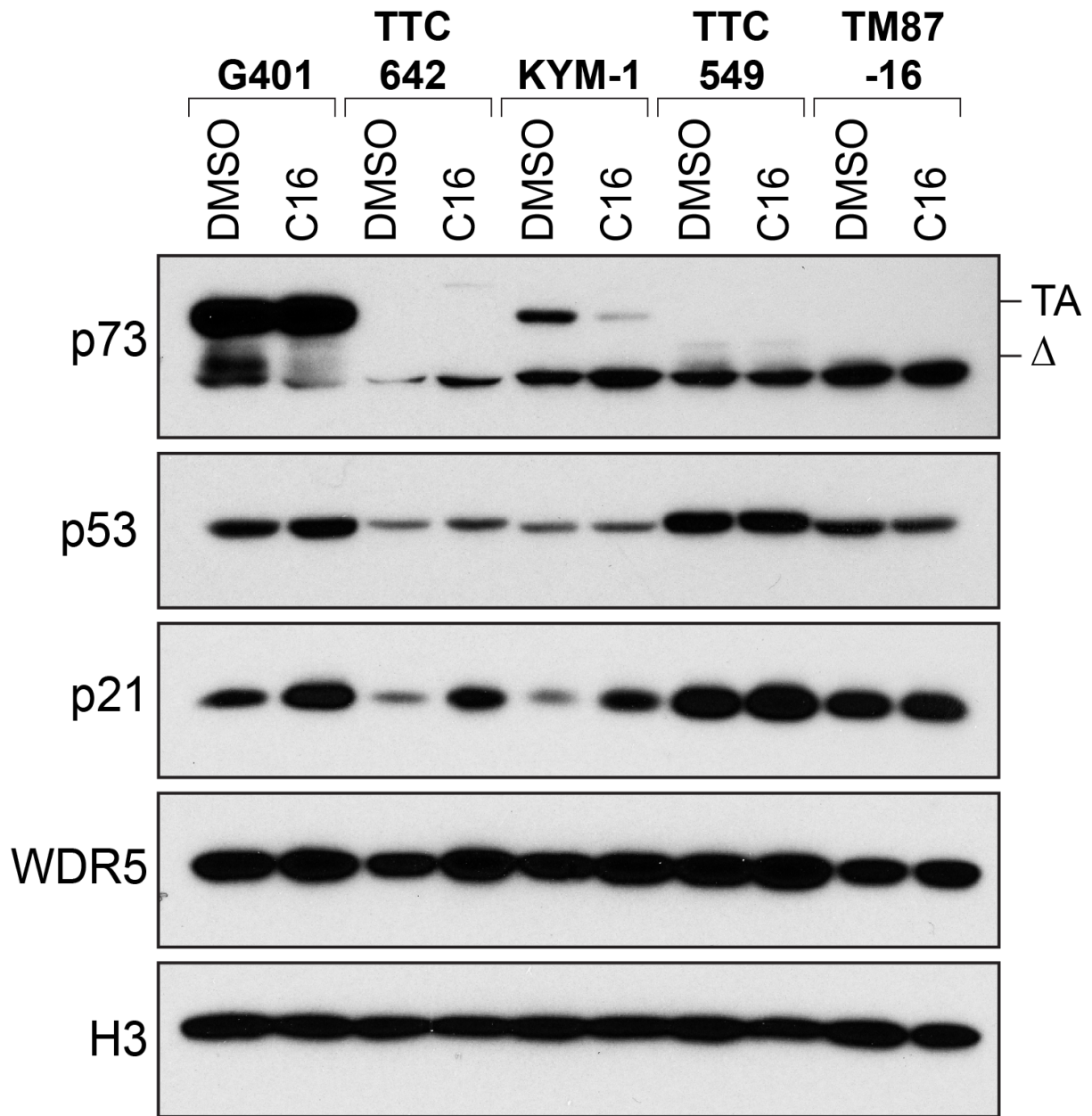
Figure 7.1. Effect of WIN site inhibition on p73, p53, and p21 protein levels Western blot performed on lysates from the indicated lines that were treated with DMSO or 500 nM C16 for three days. Lysates were probed with the indicated antibodies. For p73, isoforms carrying the transcriptional activation domain (TA), or lacking this domain (Δ), are visible. Histone H3 is a loading control. Image is representative of three biological replicates.

To determine if other p53 family members were contributing to the transcriptional p53 activation we observe, I examined whether or not p63 and p73 could account for the induction of the p53 pathway. By RNA-Seq, none of these lines express the p53 family member, *TP63*, indicating that p63 is not responsible for the p53 pathway transcriptional induction. *TP73* is expressed in all five cell lines so I probed the RT cell lysates with antibodies specific for p73. The p73 antibody is capable of detecting both the transcriptionally-active isoform of p73, TAp73 and the isoform lacking the transcriptional activation domain, ΔNp73 [145]. Importantly, TAp73 is either not expressed, unchanged, or decreased by C16 treatment (**Figure 7.1**) indicating that induction of p73 is unlikely to be responsible for the activation of the p53 pathway seen by RNA-Seq.

Despite the consistent activation of p53 target genes detected in the C16 RNA-Seq experiments, I was surprised to find that induction of p53 itself is minimally detected at the protein level, and only in G401 and TTC642 cells. Perhaps the level of p53 induction is relatively subtle and therefore not able to be detected by Western blotting. To determine whether p53 target genes can be induced and trigger a cellular response in the absence of robust changes in p53 protein, we can use an HDM2 inhibitor and compare the response to that of WIN site inhibitors.

Comparison of gene expression changes induced by WIN site inhibition and HDM2 inhibition in RT cells

To further validate the p53 pathway can be activated in the absence of robust p53 protein induction, I wanted to treat RT cells with an HDM2 antagonist, Nutlin-3a [146] as a dose that fails to induce detectable changes in p53 protein levels but is close to the IC_{50} for cellular proliferation. I began by determining the IC_{50} of Nutlin-3a in nine *SMARCB1*-deficient cell lines from my original panel (**Figure 7.2A**). As with WIN site inhibitors, there is a range in sensitivity of *SMARCB1*-deficient cell lines. However, the range in IC_{50} values is only about five-fold. Of note, the least sensitive cell line, BT-12, has an impaired p53 response, likely due to deletion of CDKN2A, a gene that encodes p14ARF which helps stabilize p53, which explains its poor

A Nutlin-3a

Cell line	IC$_{50}$nM
JMU-RTK-2	369 ± 22
A204	426 ± 64
TTC642	504 ± 79
KYM-1	654 ± 48
TTC549	742 ± 26
G401	743 ± 125
HS-SY-II	755 ± 220
TM87-16	1455 ± 227
BT-12	1654 ± 148

B
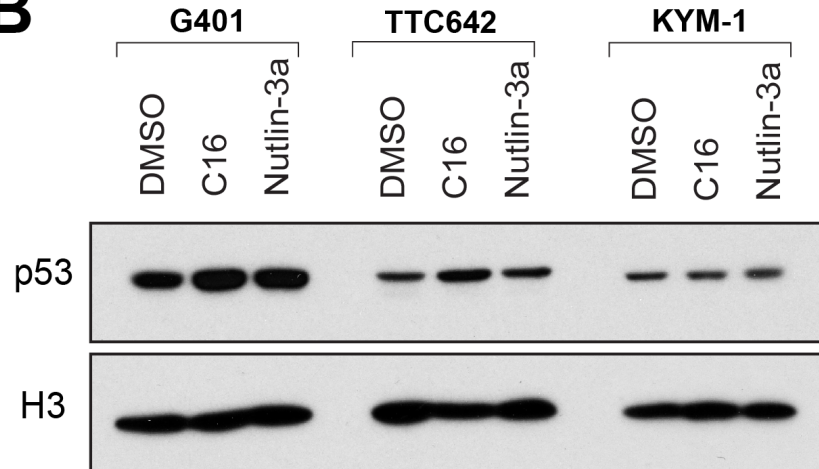
Figure 7.2. *SMARCB1*-deficient cells are sensitive to Nutlin-3a (**A**) Table showing the IC$_{50}$ values for Nutlin-3a in each cell line, calculated by performing a dose-response analysis in a five day treatment. The IC$_{50}$ column shows the IC$_{50}$ values ± SEM (n=3). (**B**) Western blot performed on lysates from the indicated cell lines that were treated with DMSO, 500 nM C16, or 500 nM Nutlin-3a for three days. Lysates were probed with the indicated antibodies. Image is representative of three biological replicates.

sensitivity to Nutlin-3a [53]. Overall, as seen by others [53], *SMARCB1*-deficient cells are sensitive to p53 activation which validates that the p53 pathway is functional in these cell lines. I next wanted to identify a concentration at which RT cells are responding to Nutlin-3a at the cellular level but have a change p53 protein levels comparable to what we observe with C16 treatment. Again, the goal is to determine if we can observe transcriptional induction of the p53 pathway without detectable induction of p53 protein. I treated G401, TTC642, and KYM-1 cells with DMSO, 500 nM C16, or 500 nM Nutlin-3a, a concentration close to the IC_{50} of these cell lines. I isolated protein from the cells and probed the lysates with antibodies specific for p53 and histone H3 as a loading control (**Figure 7.2B**). Indeed, cells treated with 500 nM C16 and 500 nM Nutlin-3a yielded similar p53 responses, a minimal induction in G401 and TTC642 cells and no change in expression in KYM-1 cells. Thus, this dose of Nutlin-3a that inhibits growth in these cell lines (**Figure 7.1A**) only results a subtle induction of p53 protein.

To test if p53 target gene activation can be measured in the absence of robust changes in p53 protein, I performed RNA-Seq in RT cells treated with DMSO or 500 nM Nutlin-3a to measure the transcriptional consequences and to look for induction of p53 target genes at this dose. As with the C16 RNA-Seq (Chapter VI), I treated G401, TTC642, and KYM-1 cells with DMSO or Nutlin-3a at 500 nM for three days and isolated RNA for sequencing. VANTAGE performed ribosomal RNA depletion, library preparation and next generation sequencing. Dr. Jing Wang identified the DEGs between DMSO and Nutlin-3a treated cells. Under these conditions, Nutlin-3a treatment results in between ~1,400 and ~6,500 DEGs, depending on cell type (**Figure 7.3A**). As before, Dr. Jing Wang generated heatmaps of all the significantly changed genes (FDR < 0.05) comparing Nutlin-3a treated RT cells to DMSO for all three replicates to look for variability (**Figure 7.3B**). As with WIN site inhibitor treatment, there is marked consistency in the response between replicates. As we observed with WIN site inhibitor, the magnitude of the response is modest. In a volcano plot showing the $\log_2$fold changes as a result of Nutlin-3a treatment in each cell line, the majority of gene expression $\log_2$fold changes only extend from about -2 to +2 in the three cell lines (**Figure 7.4A**). In a direct comparison of C16

107
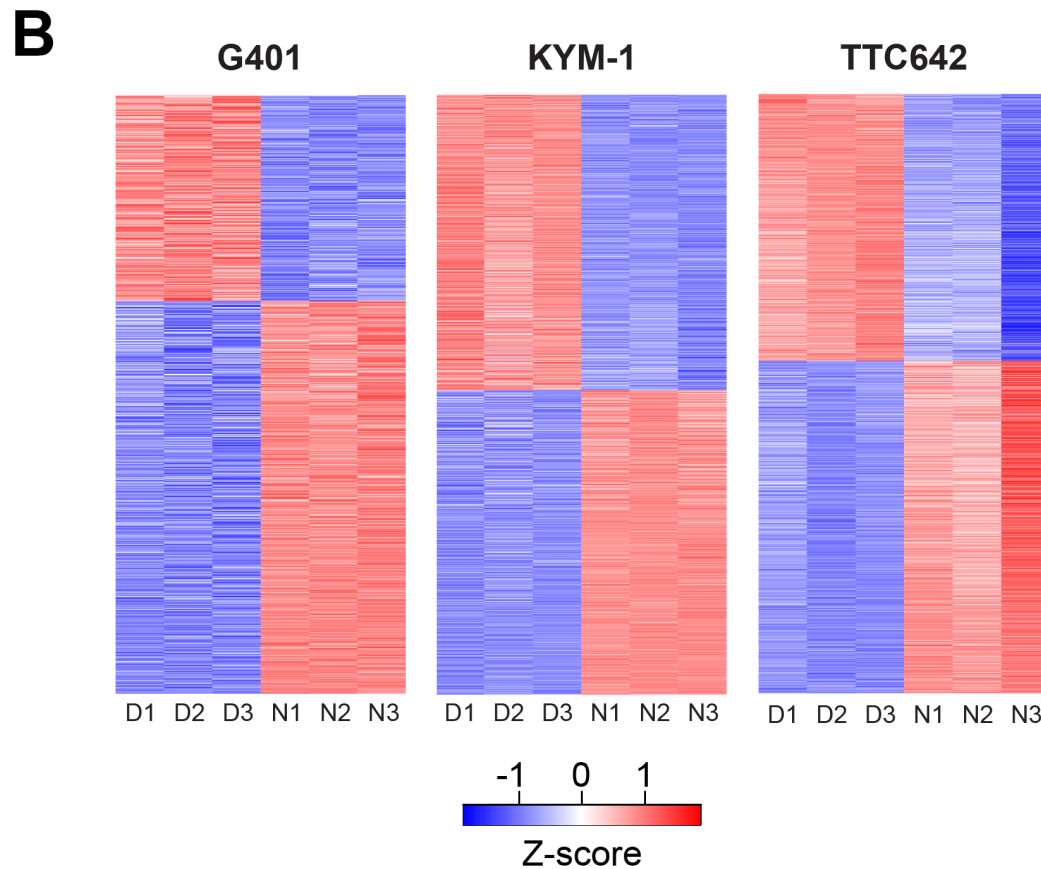
Figure 7.3. Summary of gene expression changes in RT cells treated with Nutlin-3a (**A**) Table showing the number of transcripts significantly altered (FDR < 0.05) altered by three days of treatment of cell lines with 500 nM Nutlin-3a, compared to respective DMSO controls, as determined of RNA-Seq. "DEGs"; differentially expressed genes (n=3). (**B**) Heatmaps displaying consistency amongst replicates of RNA-Seq for the three day Nutlin-3a-treated (500 nM) cell lines, by Z-transformation and ranking by fold-change. Transcripts that are significantly (FDR < 0.05) impacted by Nutlin-3a, compared to DMSO, are shown (n=3).
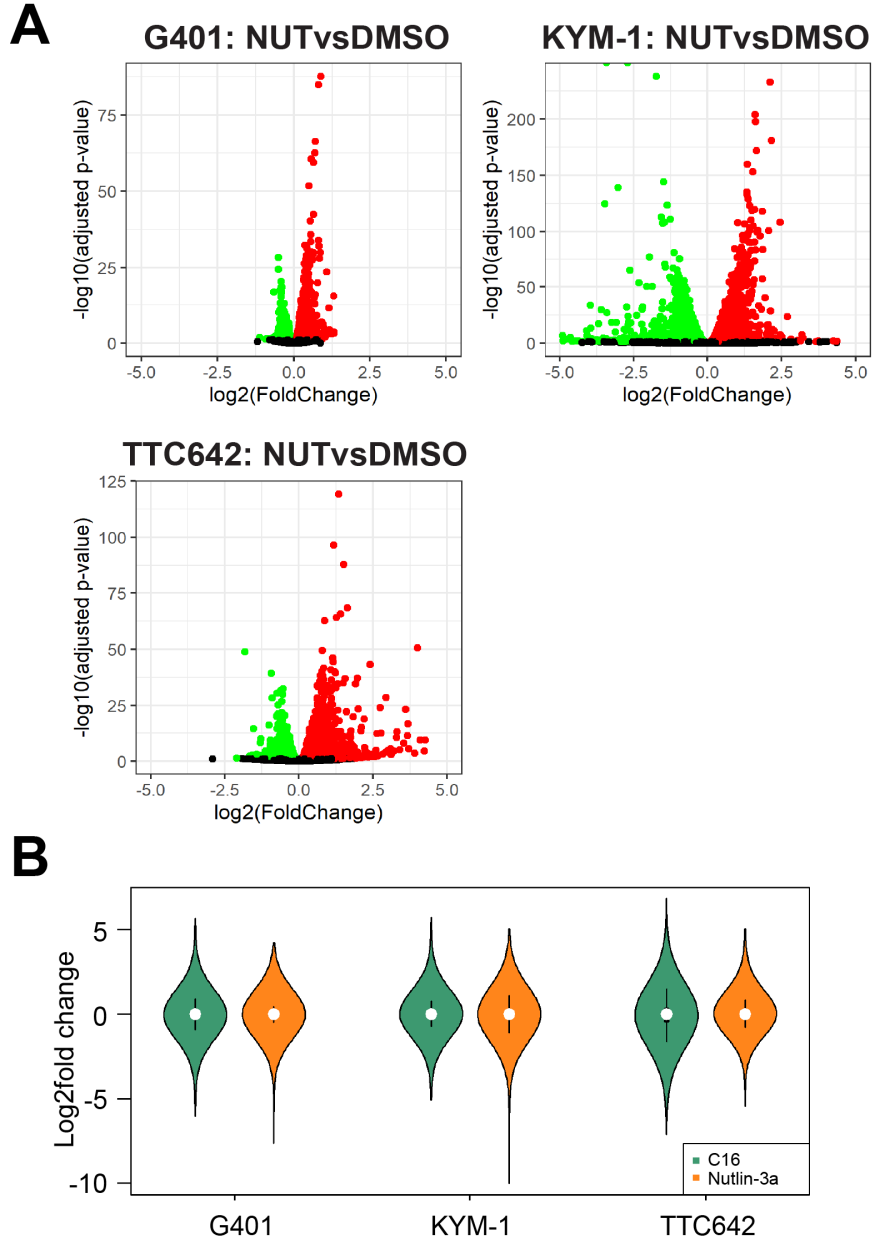
Figure 7.4. Magnitude of gene expression changes in RT cells with Nutlin-3a treatment
(**A**) Volcano plots comparing $\log_2$fold transcript changes against -log10 adjusted p-values (Nutlin-3a (NUT) vs DMSO) for each of the RNA-Seq experiments in the indicated RT cell lines. (**B**) Violin plot showing the distribution of $\log_2$-fold transcript changes elicited by either 500 nM C16 or 500 nM Nutlin-3a compared to DMSO in each cell line (three days).

treated and Nutlin-3a treated cell lines, the violin plots demonstrate that the magnitude of gene expression changes is very similar with both treatments (**Figure 7.4B**). Importantly, we do observe a transcriptional response to Nutlin-3a treatment in RT cells despite failing to see induction of p53 at the protein level.

When we compare the DEGs with Nutlin-3a treatment between the three RT cell lines tested, the DEGs are disparate across the three lines (**Figure 7.5**). There are only 49 genes with decreased expression in all three cell lines and only 206 genes with increased expression in all three cell lines. As was the case with WIN site inhibition, this indicates that the vast majority of the response is cell type-specific. This may be due to the fact that the location from which each of these cell lines were derived are different, G401 are from the kidney, TTC642 are from the muscle, and KYM-1 are from the neck. (**Table 3.1**). I expect that the common transcriptional response between the cell lines is the upregulation of the p53 pathway as the primary mechanism through which Nutlin-3a inhibits proliferation is by activating the p53 pathway. I performed GO terms enrichment analyses on the commonly suppressed and commonly induced genes to identify pathways that are downregulated or upregulated in all three cell lines. GO analysis of the 49 commonly suppressed genes reveals modest enrichment in categories related to G2/M cell cycle transition and generic metabolic processes (**Figure 7.6A**). As far as genes that are upregulated by Nutlin-3a treatment, GO terms analysis of the 206 commonly induced genes returns strong and significant enrichments in terms related to induction of p53 (**Figure 7.6B**). This observation is expected and it confirms that RT cells are responding to Nutlin-3a by upregulating p53 pathways. To further solidify the connection to p53, we performed a GSEA using the Hallmark data sets and see significant enrichment in "Hallmark p53 pathway" in each of the lines, again confirming that p53 target genes are upregulated with Nutlin-3a treatment (**Figure 7.6C**).

I have determined that both C16 and Nutlin-3a treatment induce a p53 transcriptional response but overlaying the RNA-Seq data will determine how similar the response is. Overlaying the
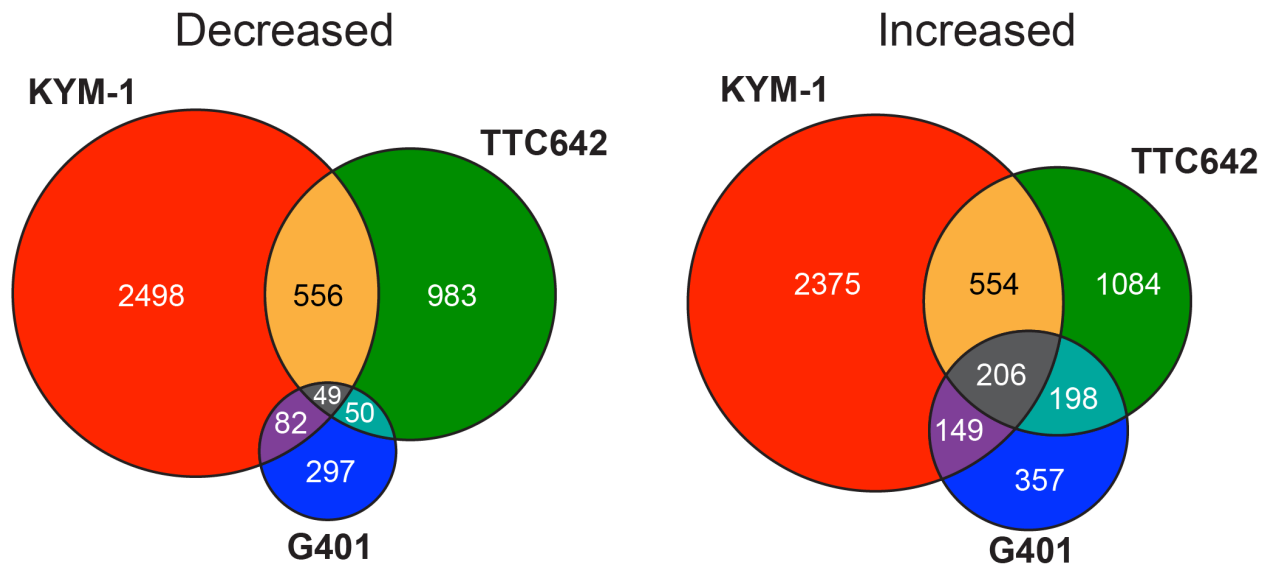
Figure 7.5. Comparison of differentially expressed genes from Nutlin-3a treatment in RT cells Venn diagrams comparing genes showing a significant decrease (left) or increase (right) in expression upon Nutlin-3a treatment (500 nM; three days) in each of the cell lines, as determined by RNA-Seq.
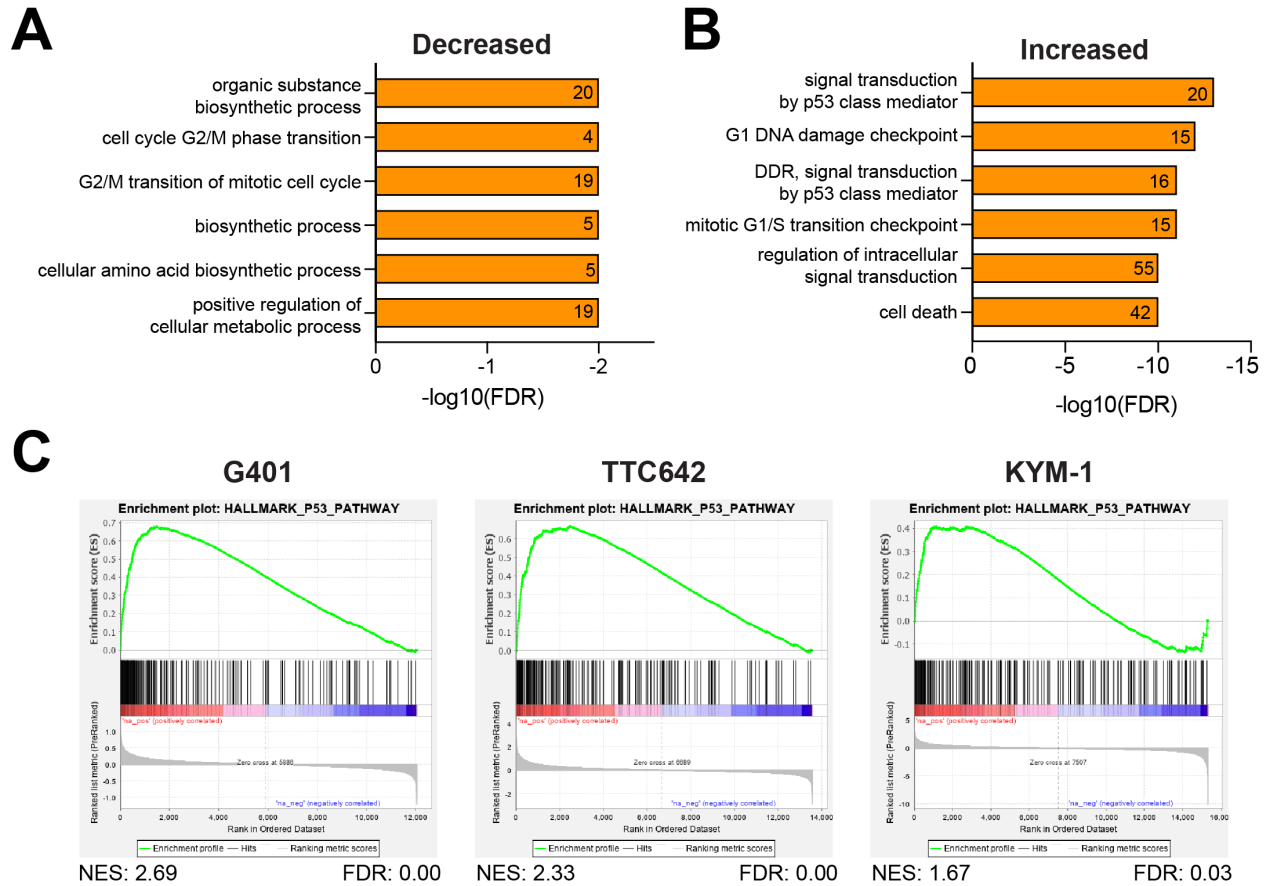
Figure 7.6. Nutlin-3a treatment induces the p53 pathway in RT cells (**A**) GO term (Biological Process) enrichment analysis of the 49 common genes suppressed by Nutlin-3a in G401, KYM-1, and TTC642 cells. The x-axis is the -log10(FDR) and the number of the bar is the gene count. (**B**) GO term (Biological Process) enrichment analysis of the 206 common genes induced by Nutlin-3a in G401, KYM-1, and TTC642 cells. The x-axis is the -log10(FDR) and the number of the bar is the gene count. (**C**) Results of Hallmark gene set enrichment analysis (GSEA) on RNA-Seq data from Nutlin-3a treated cells; only the results for the Reactome "Hallmark p53 Pathway" are shown. "NES"; normalized enrichment score. "FDR"; false discovery rate.

Nutlin-3a RNA-Seq with that of the C16 in each line reveals a high degree of similarity between the transcriptional responses to both treatments (**Figure 7.7**). In general, there was a greater overlap in the upregulated genes than in the downregulated genes in all three cell lines. When I compared the genes repressed with C16 to the genes repressed with Nutlin-3a, I found that the overlap accounted for a small percentage of the genes that were induced with C16 – almost 15% in G401 cells, about 25% in TTC642 cells, and over 40% in KYM-1 cells. Importantly, the WDR5-bound RPGs were not included in this overlap indicting that the repression of RPGs is unique to the response to WIN site inhibitors and not shared with Nutlin-3a. When I compared the genes induced with C16 to the genes induced with Nutlin-3a, I found that the overlap accounted for a larger percentage of the genes that were induced with C16 – over 25% in G401 cells, over 30% in TTC642 cells, and almost 45% in KYM-1 cells. When I performed a GO terms analysis on the commonly upregulated genes in each cell line, one of the most significantly enriched categories in all three cell lines was the Biological Process "Signal transduction by a p53 class mediator". This reinforces the concept that p53 target genes are induced by C16 and Nutlin-3a in RT cells even in the absence of a robust p53 protein response. However, the outstanding question is whether or not the induction of the p53 pathway is important for the cellular response.

Effect of p53 knockdown on cellular sensitivity to WIN site inhibition in RT cells

The data presented thus far demonstrates that WIN site inhibition upregulates the expression of p53 target genes in RT cells (Chapter VI). However, we observe only a subtle induction of p53 protein levels (**Figure 7.1**), indicating that the p53 response triggered by WIN site blockade is relatively subtle. This begs the question: Is p53 required for the overt cellular response of RT cells to WIN site inhibitors? Previous work has shown that knockdown or knock out of p53 significantly attenuates the sensitivity of MLLr and NB cell lines to WIN site inhibition indicating that p53 expression is required for a robust response [3, 4] so I predicted that depleting p53 expression in RT cells would reduce their sensitivity to WIN site inhibition.
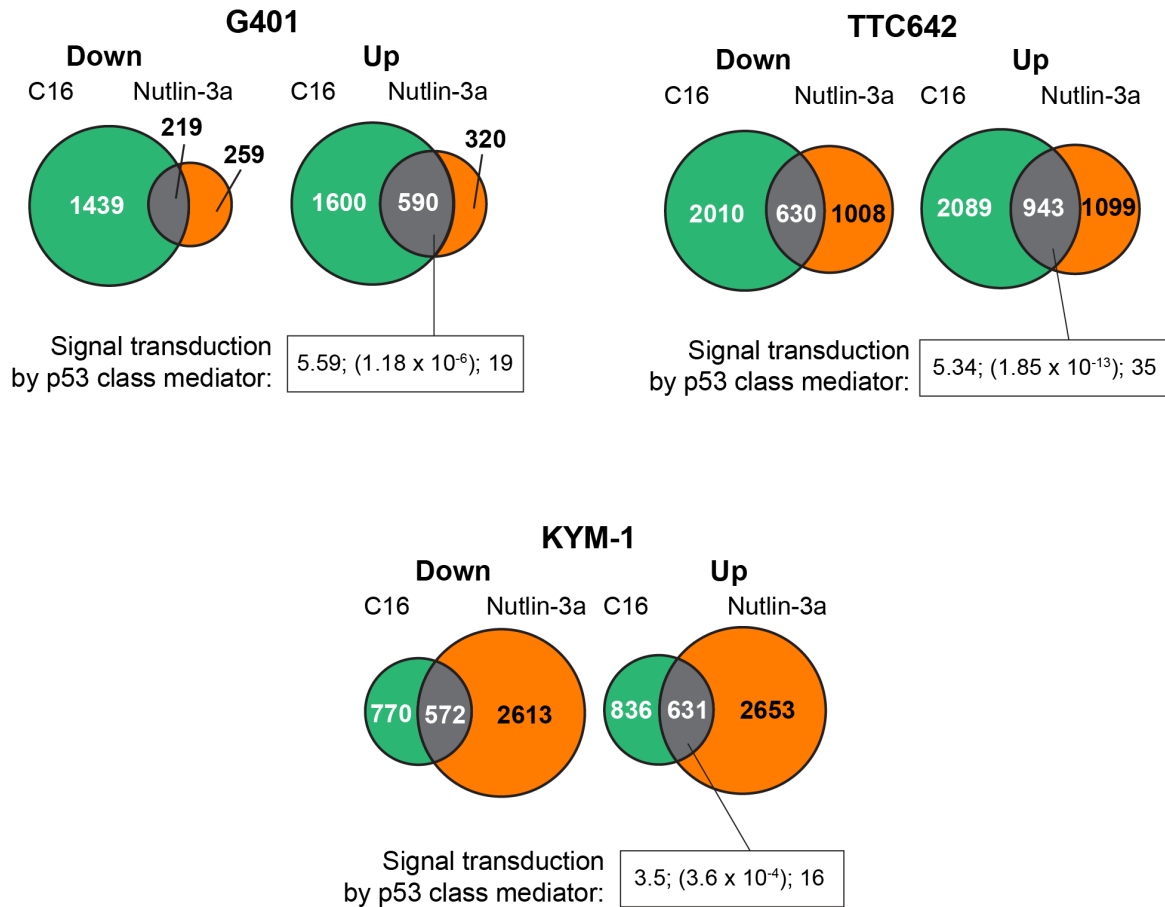
Figure 7.7. Comparison of differentially expressed genes from C16 and Nutlin-3a treatment in RT cells Venn diagrams showing the overlap of significantly differentially expressed genes ("Down"-decreased; "Up"-increased) in response to C16 or Nutlin-3a treatment in each line. For common induced genes, the fold enrichment, (FDR), and number of genes for the GO Biological Process term "Signal Transduction by class p53 mediator" are shown in the box below, separated by semi-colons.

We used RNA interference to reduce the expression of p53 in G401, TTC642, and KYM-1 cells. Specifically, we can deplete the expression of an mRNA of interest by introducing a short hairpin RNA (shRNA). An shRNA is made up of two complementary 19–22 bp RNA sequences, customized to an mRNA of interest, linked by a short 4-11 nucleotide loop [147]. Once the shRNA is transcribed, it is exported to the cytosol where it is processed and can then bind to the target mRNA. This shRNA/mRNA complex gets incorporated into the RNA-induced Silencing Complex (RISC) where it is cleaved and degraded and thus decreases expression of the mRNA of the gene of interest. We introduced shRNAs to the RT cells using a lentiviral transduction. First, a plasmid containing the shRNA sequence was transfected into HEK293T cells along with viral packaging plasmids so that the cells made lentivirus encoding the shRNA in their genome. We then infected the RT cells with the lentiviral particles where they incorporated the shRNA sequence into the cells' genomes so they stably express the shRNA. We used a previously published shRNA against p53 (sh_941) [92] as well as a negative control non-targeting "scrambled" shRNA (scr). We transduced G401, TTC642, and KYM-1 with lentiviral particles encoding the scr or p53 shRNA. The original shRNA plasmid also contained a puromycin resistance gene that was incorporated alongside the shRNA allowing us to add puromycin to the culture and kill any cells that did not incorporate the lentiviral genome. To confirm that p53 had been knocked down, we isolated protein from these cells and probed for p53 and GAPDH as a loading control (**Figure 7.8**). To see if p53 target genes could still be induced with WIN site inhibitor treatment after knockdown, we treated scr and p53 shRNA expressing cells with DMSO or 500 nM C16 for three days and performed a western blot probing for p53, p21, and GAPDH as a loading control (**Figure 7.8**). As expected, p53 is expressed in the scr cell lines and is minimally induced with C16 treatment as in the case in WT cells. We also see a robust induction of p21 with C16 treatment in the scr cell lines indicating that introduction of the scr shRNA did not affect the normal response to WIN site inhibition (**Figure 7.8**). In contrast, the p53 shRNA reduced the expression of p53 compared to the scr control, validating that the shRNA reduced expression of p53. When the p53 shRNA cells were treated with C16, there is not evidence of
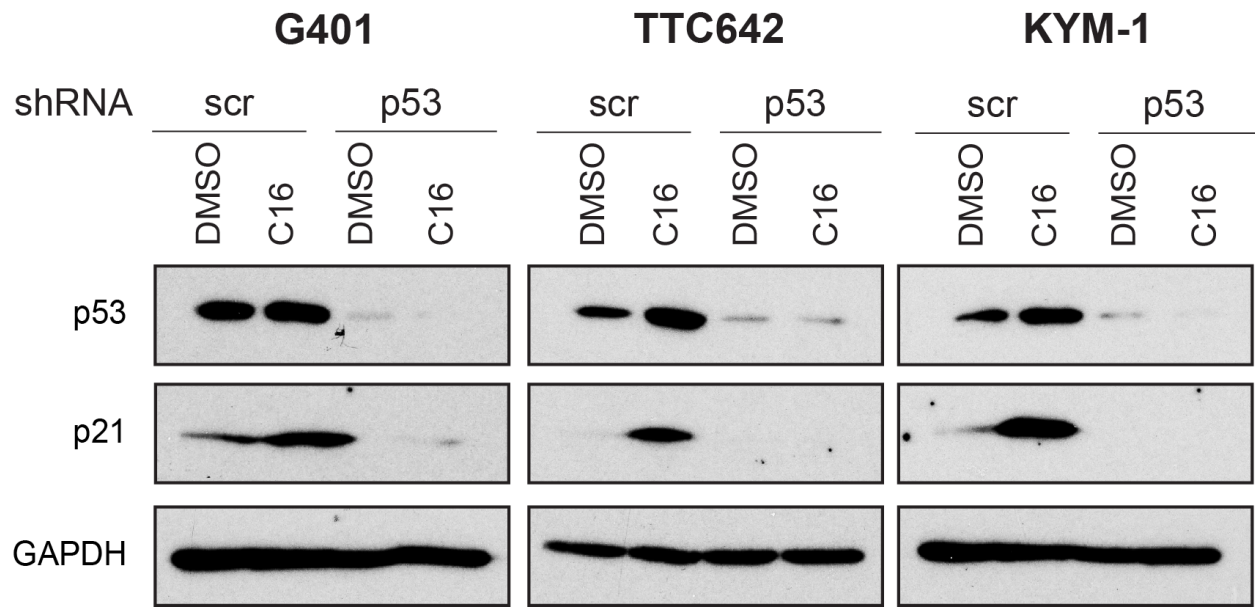
Figure 7.8. Validation of p53 knockdown in RT cells Western blot performed on lysates from the indicated cell lines that were treated with DMSO or 500 nM C16 for three days. Cells were stably transduced to expressed either a scrambled ("scr") or p53 shRNA. Blots were probed with antibodies against the indicated proteins. GAPDH is a loading control. Image is representative of three biological replicates.

p53 expression and we do not see p21 induction with the exception of a light band appearing in the G401 cells expressing p53 shRNA (**Figure 7.8**). This indicates that the p53 shRNA successfully depletes p53 and prevents induction of the p53 target gene, p21.

To validate that the p53 pathway had been inactivated by shRNA knockdown, I treated G401 cells with DMSO or C16 at 500 nM for three days and performed RNA-Seq to identify global changes in gene expression. As with the earlier RNA-Seq experiments, VANTAGE performed ribosomal RNA depletion, library preparation and next generation sequencing. Dr. Jing Wang identified the DEGs between DMSO and C16 treated cells. Under these conditions, C16 treatment results in 4,330 DEGs in the G401 cells expressing scr shRNA and 5,201 DEGs in the G401 cells expressing p53 shRNA (**Figure 7.9A**). As before, Dr. Jing Wang generated heatmaps of all the significantly changed genes (FDR < 0.05) comparing DMSO and C16 treated RT cells for all three replicates to look for variability (**Figure 7.9B**). As we observed with WIN site inhibitor in WT G401 cells, there is high consistency between the replicates. In a volcano plot showing the $\log_2$fold changes as a result of C16 treatment in both cell lines, the majority on gene expression changes extend from about -2.5 to +2 in both cells expressing the scr shRNA and the cells expressing the p53 shRNA (**Figure 7.9C**), consistent with what is observed in the WT G401 cells (**Figure 6.2B**). We compared the DEGs that were induced or repressed in both cell lines and performed GO terms enrichment analysis on each of the overlapping gene lists (**Figure 7.10A**). Curiously, there were only four terms that generated significant enrichments and they are shown in **Figure 7.10**. There were 574 genes that were induced in the C16-treated control cells but not in treated cells expressing the shRNA against p53. As expected, "Signal transduction by p53 class mediator" is only observed in this segment, likely because the p53 pathway cannot be induced in the absence of p53. Notably, "Cytoplasmic translation" is observed in both the scrambled- and p53-shRNA cells in response to C16 which confirms that the reduction in expression of RPGs resulting from the displacement of WDR5 from chromatin is a primary response to WIN site inhibition and occurs independent of p53. The category "DNA strand elongation involved in DNA replication" is enriched in the genes that are
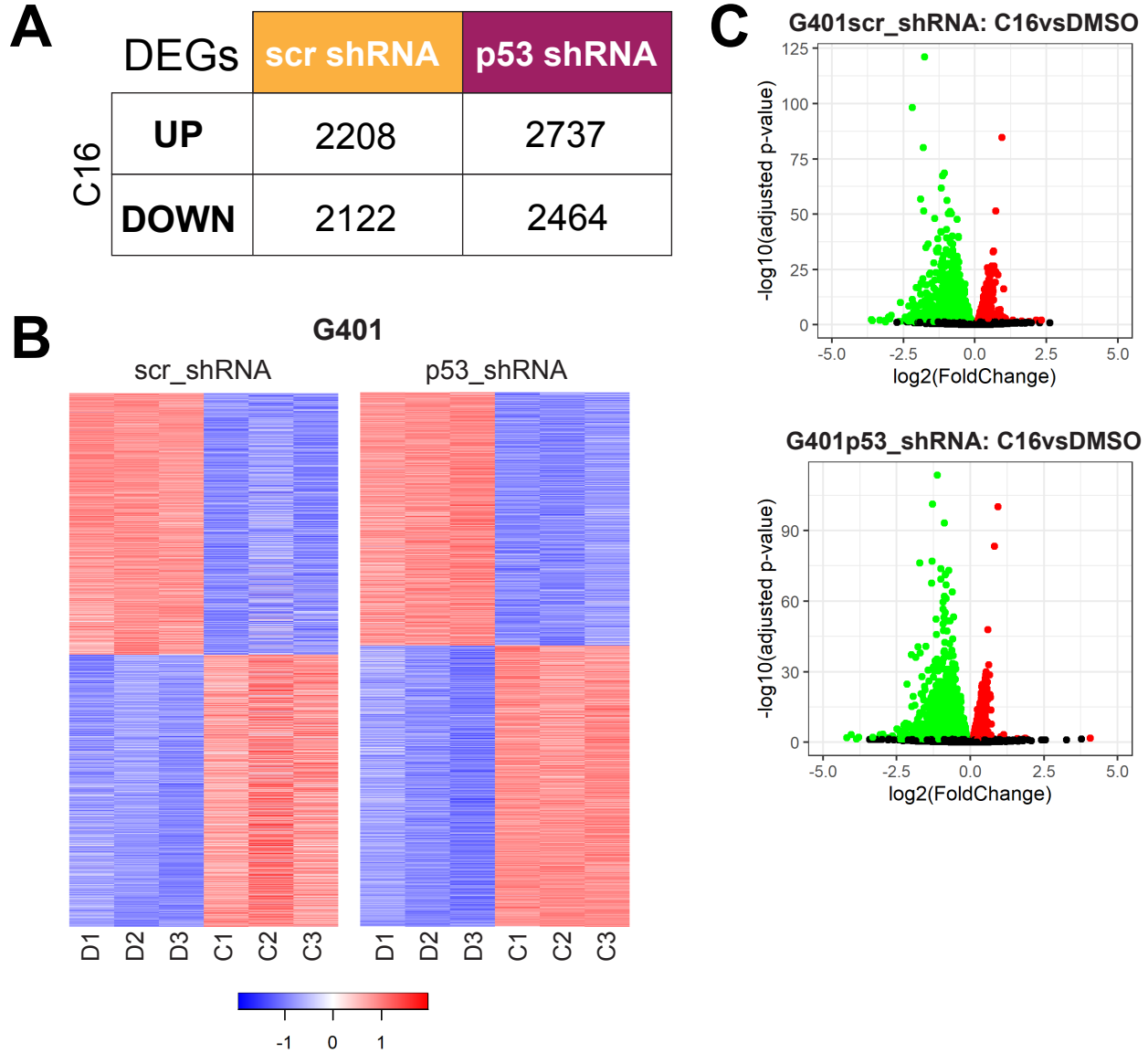
Figure 7.9. Summary of gene expression changes in G401 cells expressing scr or p53 shRNA treated with WIN site inhibitor (**A**) Table showing the number of transcripts significantly altered (FDR < 0.05) altered by three days of treatment of cell lines with 500 nM C16, compared to respective DMSO controls, as determined of RNA-Seq. "DEGs"; differentially expressed genes (n=3). (**B**) Heatmaps displaying consistency amongst replicates of RNA-Seq for the three day C16-treated (500 nM) cell lines (expressing a scrambled or p53 shRNA), by Z-transformation and ranking by fold-change. Transcripts that are significantly (FDR < 0.05) impacted by C16, compared to DMSO, are shown (n=3). (**C**) Volcano plots comparing $\log_2$fold transcript change against log10 adjusted p-values (C16 vs DMSO) for each of the RNA-Seq experiments in the indicated G401 cell lines expressing either scrambled (scr) or p53-directed shRNAs.
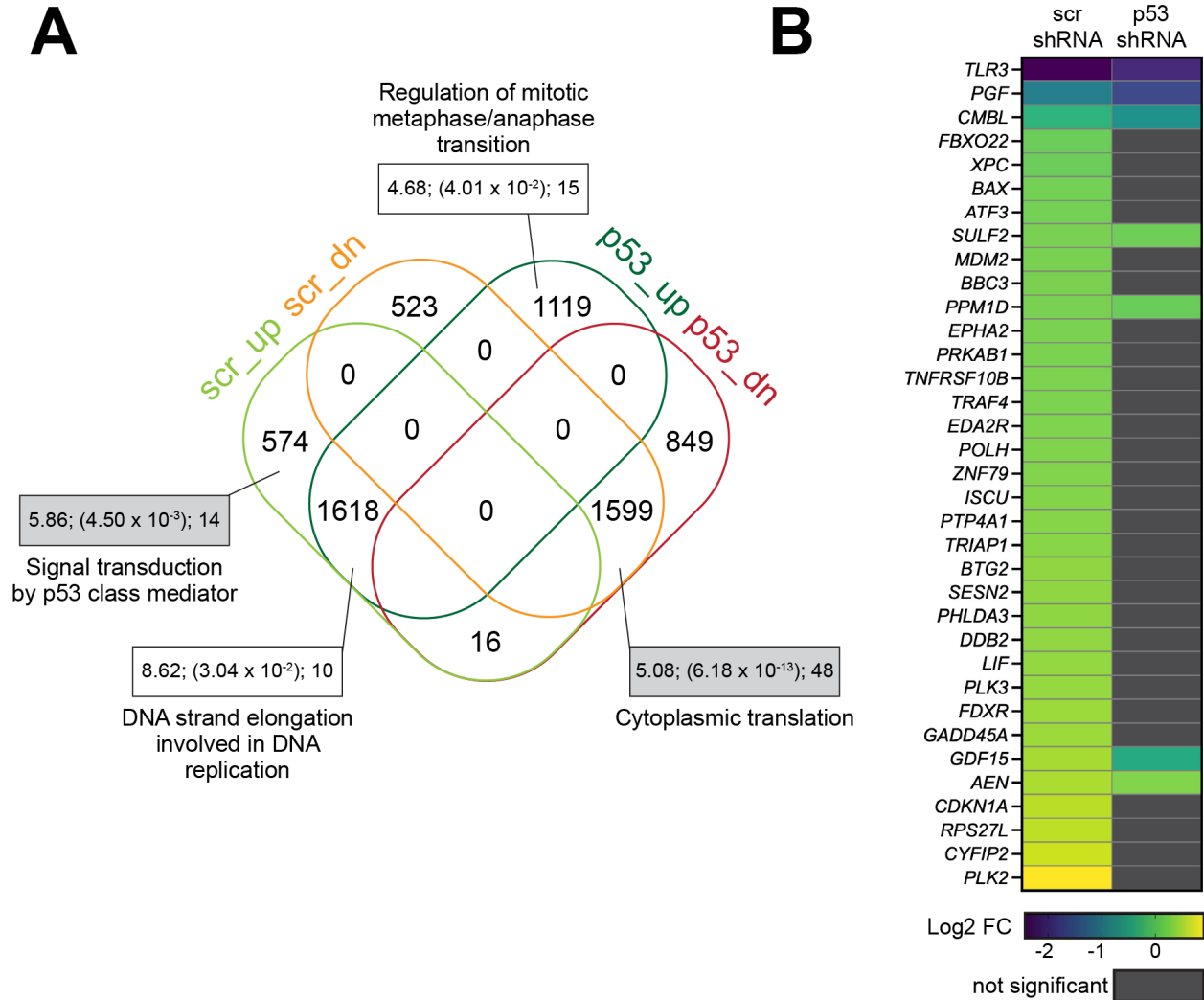
Figure 7.10. Comparison of gene expression changes in G401 cells expressing scr or p53 shRNA treated with WIN site inhibitor (**A**) Venn diagram, comparing genes induced (up) or suppressed (dn) in G401 cells expressing either a scrambled shRNA (scr) or an shRNA against p53 (p53), and treated for three days with 500 nM C16, as determined by RNA-Seq. GO term (Biological Process) enrichment analysis was performed on genes in all segments; only four (shown) generated significant enrichments. The fold enrichment, (FDR), and number of genes for each term are shown in the boxes separated by semicolons. Note that "Signal transduction by p53 class mediator" is only observed in C16-treated scramble control cells, and that the term "Cytoplasmic translation" is observed in both the scrambled- and p53-shRNA cells in response to C16. (**B**) Heatmap, showing the $\log_2$ fold-change (Log2 FC) in consensus p53 target genes induced by C16 treatment in scrambled- and p53-shRNA expressing G401 cells. Note that a majority of these genes are induced by C16 in scrambled cells (FDR < 0.05), but not significantly altered by C16 in the p53-shRNA cells.

119

induced by C16 in both the scrambled- and p53-shRNA cells. WIN site inhibition may be causing DNA damage or may disrupt the cells' ability to repair DNA damage. Further studies are currently underway in our laboratory to determine if WIN site inhibition causes DNA damage. To further confirm that p53 pathway induction is part of the response to WIN site inhibition and that it only occurs if p53 is expressed, we examined a set of consensus p53 target genes [148]. C16 treatment in G401 scrambled shRNA control cells alters the expression of 35 consensus p53 target genes (**Figure 7.10B**). When compared to scr shRNA expressing cells, 33 of the 35 are either not altered, or altered to a lesser extent, by C16 in p53 shRNA knockdown cells (**Figure 7.10B**). Together, these data demonstrate that the p53 shRNA used in this instance is capable of both physically and functionally suppressing p53.

I then used the validated shRNA-mediated p53 knockdown cell lines to test whether decreasing p53 expression alters sensitivity to WIN site inhibitors. Based on previous work, I predicted that knocking down p53 would decrease the sensitivity of RT cells to WIN site inhibitor as it does in MV4:11 cells and CHP-134 NB cells [3, 4]. To test if knocking down p53 decreased the sensitivity of RT cells to WIN site inhibition, I performed five day proliferation assays in cells treated with varying concentrations of C16 compared to a DMSO control. I used MV4:11 cells that express scr or the same p53 shRNA that were developed by Dr. Erin Aho for her work exploring WIN site inhibition in MLLr cells [4]. As expected, shRNA-mediated knockdown of p53 results in a significant rightward shift in the response of MV4:11 cells to C16, increasing the IC_{50} from 40 nM to 750 nM (**Figure 7.11**). When I tested the RT cells expressing the the same shRNA against p53, however, I see little if any impact on the dose-response curves of G401, TTC642, and KYM-1 cells to C16 treatment (**Figure 7.11**). This came as a surprise as previous evidence indicates that an important response to WIN site inhibition is the induction of the p53 pathway and thus, p53 would be required in order to prompt this response [3, 4]. However, the relatively subtle p53 activation observed in response to C16 treatment suggests that activating the p53 pathway is not the primary mechanism by which WIN site inhibitors elicit a cellular response in RT.
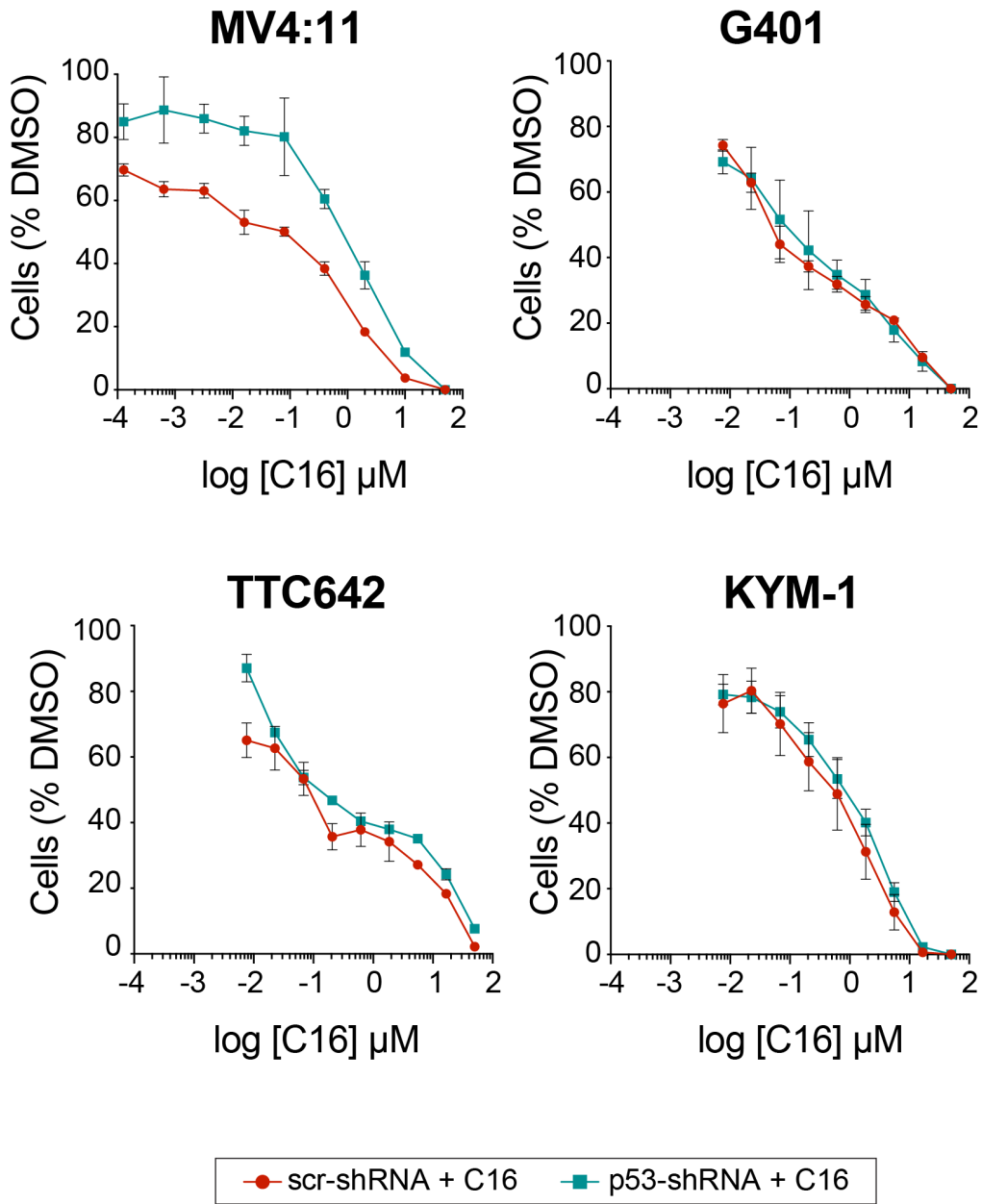
Figure 7.11. Effect of p53 shRNA on C16 response in RT cells Dose response of the indicated cell lines, stably expressing either a scrambled shRNA ("scr-shRNA") or an shRNA against p53 ("p53-shRNA"), to C16. Five day assay. Data are expressed as the percentage of cells remaining at day five, compared to the DMSO control (n=3, mean ± SEM).

To confirm the dispensability of p53 in the RT cell response to WIN site blockade, I independently knocked down p53 expression using an orthologous CRISPRi-based approach [94, 95]. Clustered regularly interspaced short palindromic repeat (CRISPR) is a technique derived from the the adaptive immunity of bacteria and is used to allow precise genomic editing [149]. The traditional CRISPR-Cas9 gene editing system utilizes a short guide RNA (sgRNA) to target the Cas9 endonuclease to a specific location in the genome to mediate double strand DNA breaks. The cell will then use non-homologous end joining (NHEJ) to repair the DNA break, introducing errors in the form of small insertions of deletions which can cause frameshifts and disrupt the expression of the gene. In CRISPR interference (CRISPRi), a catalytically dead Cas9 (dCas9) is used to target the region of interest within the genome without cutting the DNA. The dCas9 is fused to a transcriptional repressor, Kruppel-associated box (KRAB), such that when the sgRNA targets the dCas9-KRAB protein to the gene of interest, it robustly silences expression [150]. To adopt this approach, I first transduced G401 and TTC642 cells with lentiviral particles containing the dCas9-KRAB coding sequence. The lentiviral transfer plasmid also contained a blasticidin resistance gene which was incorporated alongside the dCas9-KRAB sequence. This allowed us to add blasticidin to the culture and kill any cells that did not incorporate the plasmid. Once the cells were stably expressing dCas9-KRAB, I then transduced the cells with a lentivirus encoding an sgRNA targeting p53 or a non-targeting sgRNA as a negative control. The lentiviral genomes also contained a puromycin resistance gene allowing us to add puromycin to the culture and kill any cells that did not incorporate the lentiviral genome. After selection, to confirm that p53 had been silenced, I isolated protein from these cells and probed for p53 and GAPDH as a loading control (**Figure 7.12A**). To see if the CRISPR perturbation of p53 disrupted the cells ability to respond to WIN site inhibition, I treated G401 and TTC642 cells expressing dCas9-KRAB and either the empty or p53 sgRNA with DMSO or 500 nM C16 for three days. I performed a western blot probing for p53 and p21 with GAPDH as a loading control (**Figure 7.12A**). As expected, p53 is expressed in the dCas9-KRAB cell lines with empty sgRNA. In addition, I do see a robust induction of p21 with C16 treatment in the

122
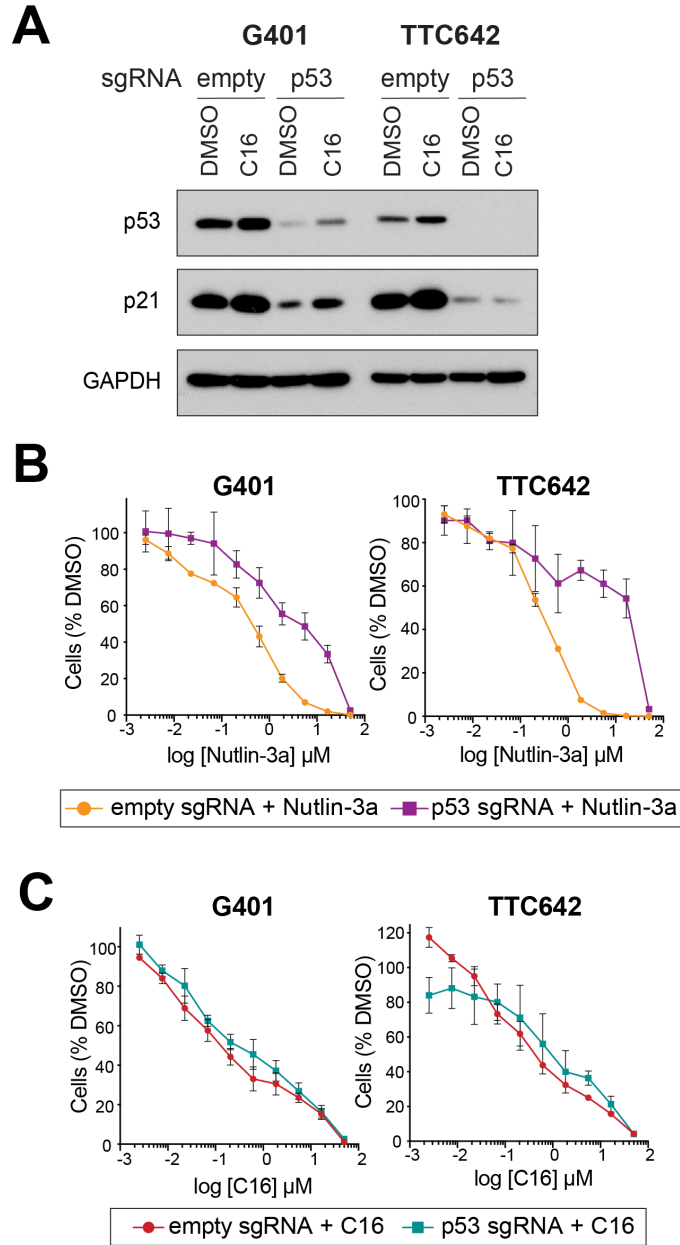
Figure 7.12. Effect of p53 CRISPRi on C16 response in RT cells (A) Western blot performed on lysates from the indicated cell lines that were treated with DMSO or 500 nM C16 for three days. Cells were stably transduced with a vector expression inactive Cas9 fused to KRAB repressor domain, as well as either an "empty" vector or a vector expressing a single guide RNA ("sgRNA") against p53. Blots were probed for the indicated proteins. GAPDH is a loading control. Image is representative of three biological replicates. (**B**) Dose response of the indicated cell lines, stably transduced with a vector expressing inactive Cas9 fused to KRAB repressor domain, as well as either an "empty" sgRNA or a vector expressing a single guide RNA ("sgRNA") against p53 to Nutlin-3a. Five day assay. Data are expressed as the percentage of cells remaining at day five, compared to the DMSO control (n=3, mean ± SEM). (**C**) As in (B) except cells were treated for five days with C16. (n=3, mean ± SEM).

empty sgRNA cell lines indicating that the CRISPR modification did not affect the normal response to WIN site inhibition. In contrast, the p53 sgRNA reduced the expression of p53 compared to the empty negative control in both G401 and TTC642. The gene silencing was more efficient in the TTC642 cells than the G401 cells as the western blot fails to produce p53 signal in the TTC642 p53 sgRNA cell but the G401 cells still have a detectable band. However, the p53 expression is still considerably lower than the cells expressing empty sgRNA. When the p53 sgRNA cells were treated with C16, there is evidence of a slight p53 induction in the G401 cells but not in the TTC642 cells. Similarly, because there is residual p53 expression in the G401 cells, p21 is induced with C16 treatment. In the TTC642 cells, p21 is not induced with C16 treatment validating that the p53 silencing in this cell type was more effective than in G401.

I tested the sensitivity of these CRISPRi cells to Nutlin-3a to validate that the CRISPRi had effectively shut down p53 expression and thus disrupted the cells ability to respond to p53 activation. I performed five day proliferation assays in cells treated with varying concentrations of Nutlin-3a compared to a DMSO control. As expected, I observed a rightward shift in Nutlin-3a sensitivity curves in both the G401 and TTC642 cells (**Figure 7.12B**) indicating that the p53 sgRNA suppressed p53 expression enough to attenuate its ability to respond to HDM2 inhibition. To test if the cells with decreased p53 expression have reduced sensitivity to WIN site inhibition, I performed five day proliferation assays in cells treated with varying concentrations of C16 compared to a DMSO control. I compared the G401 cells expressing dCas9-KRAB and empty sgRNA versus p53 sgRNA, again there is little if any change in the response of these cells to WIN site inhibitor C16 (**Figure 7.12C**). The same is true in the TTC642 dCas9-KRAB cells. Thus, despite a common activation of p53 target genes in RT cell lines, and a strong expectation that the cellular response to C16 is mediated via p53, the growth response of these *SMARCB1*-deficient cell lines respond to WIN site inhibitor is p53-independent.

Discussion

In previous chapters, I have defined that that primary mode of action for WDR5 WIN site inhibitors in RT cells is very similar to what we have previously defined in MLLr leukemia cells and NB cells [3, 4]. An important downstream response is these contexts is the induction of p53. In Chapter VI, I showed that WIN site inhibition activates genes involved in the p53 pathway in five representative RT cell lines. Surprisingly, I determined that WIN site inhibition induces only a subtle induction of p53 protein levels in RT cells. However, I do see the induction of the p53-target gene, p21, in response to C16 treatment which correlates with the upregulation of the p53 pathway that we observe transcriptionally (Chapter VI). Importably, depleting p53 expression in these cells does not change the cellular sensitivity to C16 suggesting that induction of p53 is not the primary mechanism through which WIN site inhibitors elicit the cellular response in RT cells.

In this chapter, I confirmed that RT cells are sensitive to HDM2 inhibition using the small molecule Nutlin-3a, similar to what others have observed [53]. Beyond determining that they were sensitive, I was able to produce RNA-Seq data from RT cells treated with DMSO or Nutlin-3a and overlay it with the transcriptional data we have in RT cells treated with C16 (Chapter VI). I determined that there is a considerable overlap in transcriptional responses between C16 and Nutlin-3a and that the overlap coalesces on the activation of p53. Less than half of the transcriptional alterations were shared between C16 and Nutlin-3a treatment which demonstrates that activation of p53 is part of the response to both inhibitors but that each has its own unique mechanism. Importantly, a mechanism unique to WIN site inhibition is the suppression of WDR5-bound RPGs as alteration of RPG expression was not observed in the cells treated with Nutlin-3a.

I then asked if the expression of functional p53 is required for RT cells to respond to WIN site inhibition which is the case in MV4:11 and CHP-134 cells [3, 4]. Surprisingly, knocking down p53 expression does not change the sensitivity to C16 which suggests that WIN site inhibitors have a mechanism to slow proliferation in RT cell independent of p53. Because induction of p53 is

evidenced only by target gene expression and not at the level of p53 protein, these data support the idea that induction of p53 by WIN site inhibition is relatively subtle. Both of the methods used to decrease p53 expression did not completely delete the protein so it is possible that the residual p53 expression was sufficient to activate the p53 pathway to elicit the cellular response. However, by RNA-Seq, we were able to determine that in G401 cells, the p53 shRNA was sufficient to prevent the induction of p53 target genes with WIN site inhibition.

Understanding how RT cells respond to WIN site inhibition in the absence of p53 and why p53 is not robustly induced by WIN site inhibitor in this context will require further investigation. Regardless of the mechanism, however, my findings here demonstrate that—contrary to my initial postulate [4]—cancer cells can respond to WIN site inhibition in the absence of functional p53. It may thus be possible to identify additional cancer cell types, bereft of p53, that are inhibited by WIN site blockade. If this forecast is correct, WIN site inhibitors could have much broader utility as anti-cancer agents than first imagined. Because WIN site inhibitors only produce a subtle activation of the p53 pathway, I reasoned that activating p53 to a greater extend in RT cells will produce a greater inhibition of proliferation. I hypothesize that co-treating RT cells with an WIN site inhibitor and an HDM2 inhibitor will elicit a greater p53 activation and produce a greater cellular response than either compound alone. This hypothesis will be tested in the next chapter.

VIII. WIN SITE INHIBITORS SYNERGIZE WITH NUTLIN-3A TO INHIBIT PROLIFERATION OF RHABDOID TUMOR CELLS

Introduction

All the work shown thus far has been focused on understanding the mechanism by which WDR5 WIN site inhibitors function in *SMARCB1*-deficient cancer cells. WIN site inhibitors are able to displace WDR5 from chromatin and decrease the expression of WDR5-bound PSGs including specific subset of RPGs. In addition, WIN site inhibition transcriptionally induces the p53 pathway. However, I fail to observe induction of p53 at the protein level with WIN site inhibition in RT cells. Even more interesting, depleting p53 does not affect the response of RT cells to C16 indicating that WIN site inhibitors are able to slow proliferation independent of p53 activation. Drug combinations are commonly used in the clinic to improve outcomes of cancer treatment [151]. Because *SMARCB1*-deficient cells are sensitive to both WDR5 and HDM2 inhibition and both inhibitors induce the p53 pathway, I reasoned that dual treatment with C16 and Nutlin-3a should improve the weak p53 activation and achieve a stronger cellular response.

I explored the response of treating *SMARCB1*-deficient cells with combinations of C16 and Nutlin-3a along with single-agent treatments to determine if the combination is better at disrupting cell growth than either compound alone. Ideally, co-treating cells with C16 and Nutlin-3a will make sensitive cells more sensitive and insensitive cells sensitive. In this chapter, I show that combining C16 and Nutlin-3a is more effective at inhibiting cell proliferation than treatment with either of these inhibitors alone. I also tested the ability of C16 to synergize with a chemically distinct HDM2 inhibitor, HDM201, and validate that HDM2 inhibition in combination WIN site inhibition is an effective combinatorial treatment strategy in RT cells. Finally, I show that the synergy between C16 and Nutlin-3a is dependent on p53 by treating G401 cells expressing scramble or p53 shRNA with C16 and Nutlin-3a. To understand how WIN site inhibitors and HDM2 inhibitors work together to further disrupt cellular proliferation, I examined

the expression of p53 target genes at the mRNA and protein level with C16, Nutlin-3a, or a combination of both compounds. The samples treated with both inhibitors had higher expression of p53 target genes than either of the single-agent treated samples demonstrating that the mechanism by which WIN site inhibitors and HDM2 inhibitors work together is to enhance the activation of the p53 pathway and thus enhance the cellular response.

Results

Evaluation of synergy between WIN site inhibitor and HDM2 inhibitor in RT cells

In order to determine if WIN site inhibitors and HDM2 inhibitors are a suitable dual therapy strategy, I treated *SMARCB1*-deficient cells with combinations of different concentrations of C16 and Nutlin-3a and measured how they affected cell growth. I set up 7x7 matrices with C16 ranging from 50 µM to ~70 nM and Nutlin-3a ranging from 10 µM to ~15 nM. I also treated cells with each compound individually and a DMSO only control. After five days, I quantified the remaining cells using CellTiter-Glo and normalized the number of cells remaining to the DMSO only control. Dr. Caleb Howard used the SynergyFinder software [96] to calculate synergy values using the Highest Single Agent (HSA) method. SynergyFinder is a web-based application that allows users to analyze and visualize drug combinations and quantify synergy using one of four synergy models [96]. We used the HSA model in which a drug combination is considered synergistic if the measured outcome is greater than the highest single agent effect at that dose. This approach is the most straight forward synergy model because it simply looks for an improved efficacy with addition of a second drug [152]. SynergyFinder produces a synergy map in which each drug combination is represented in red if the combination is synergistic or green if the combination is antagonistic. The analysis produces an average δ synergy score which represents the average excess response due to drug interactions at all the doses measured. This is not the most informative measurement because it can vary base on the range of doses that is chosen. SynergyFinder also produces a peak δ synergy score which is the average of the synergy only in the most synergistic 2x2 square on the map. This value is more informative

128

because it identifies the dose of both drugs at which the highest synergy is achieved. According to SynergyFinder, a δ synergy score less than -10 means the interaction between the two drugs is likely to be antagonistic, a δ synergy score from -10 to 10 means the interaction between the two drugs is likely to be additive, and a δ synergy score larger than 10 means the interaction between the two drugs is likely to be synergistic [96]. These values can be applied to both the average and peak δ synergy scores.

I hypothesized that combining a WIN site inhibitor with an HDM2 inhibitor would be more efficacious to inhibit cell growth in sensitive cell lines. In other words, I predicted that adding Nutlin-3a to RT cells that are already sensitive to C16 would result in lower cell numbers compared to C16 or Nutlin-3a treatment alone. I first performed the synergy analysis in the two most sensitive RT cell lines in the panel, G401 and TTC642. In the maps, I observe synergy with C16 and Nutlin-3a in both cell types as monitored by both average and peak synergy δ scores (**Figure 8.1A**). This can also be seen by the downward shift of the C16 dose response curves when Nutlin-3a is added (**Figure 8.1B**). As further evidence, in G401 cells, the percentage of cells remaining with co-treatment with 1.1 µM of Nutlin-3a never got over about 25%, even at the lowest dose of C16. Similarly, in TTC642 cells, the percentage of cells remaining never got over about 6% with Nutlin-3a treatment, even at the lowest dose of C16, indicating that C16 and Nutlin-3a co-treatment significantly disrupts proliferation (**Figure 8.1B** black line). Overall, TTC642 cells have greater synergy with a peak δ synergy score of 55.77 compared to a peak δ synergy score of 19.26 in G401 cells. Both of these peak δ synergy scores are greater than 10 indicating the interactions are likely synergistic rather than simply additive. However, the average δ synergy score in G401 cells is 7.03, a value indicative of an additive interaction rather than synergy. In the TTC642 cells, the average δ synergy score is 21.58, a score indicating that the response at the majority of the combinations tested is synergistic rather than additive. Taken together, these data confirm that combining a WIN site inhibitor with a HDM2 inhibitor can make RT cells even more susceptible to cellular inhibition.

Figure 8.1. Synergy between C16 and Nutlin-3a in sensitive RT cells (**A**) Synergy maps, as well as peak and average HSA δ scores for 49 unique combinations of C16 and Nutlin-3a doses ranging from 14 nM to 10 µM Nutlin-3a and 69 nM to 50 µM C16 in G401 and TTC642 cells. Five day treatment (*n* = 3). HSA synergy score represents average HSA δ score of all dose combinations whereas peak synergy score represents the maximum average δ score for a three-by-three dose matrix within each map (indicated by dashed-line boxes). (**B**) Dose response curves of the G401 or TTC642 to combinations of C16 and Nutlin-3a as in (A). Data are expressed as the percentage of cells remaining at day five, compared to the DMSO control (*n* = 3, mean ± SEM). The top plots display the dose response to C16 in combination with the indicated concentrations of Nutlin-3a. The bottom plots display the dose response to Nutlin-3a in combination with the indicated concentrations of C16.

While improving the response to WIN site inhibitors in sensitive cells is remarkable, what would be even better is if we can improve the response of cells that are insensitive to WIN site inhibition alone. To test this, I performed the synergy analysis in two of the least sensitive RT lines, TTC549 and TM87-16. I was encouraged to see that C16 and Nutlin-3a are synergistic in both cell types as monitored by both average and peak synergy δ scores (**Figure 8.2A**). The peak δ synergy score in TTC549 cells is 20.09 and the peak δ synergy score in TM87-16 cells is 20.29, scores that are very close to the score in G401 cells. As with the sensitive cell lines, the peak δ synergy scores in both of these cell lines are greater than 10 indicating the interaction is likely synergistic rather than simply additive. The average δ synergy score in TTC549 cells is 10.68, a value indicating that the response may be synergistic rather than additive. However, in the TM87-16 cells, the average δ synergy score is 6.56, a score indicating that the response at the majority of the combinations tested is additive rather than synergistic. As further evidence that the co-treatment improves cellular response in insensitive cell lines, some of the C16 dose response curves with the addition of Nutlin-3a in TTC549 and TM87-16 cells (**Figure 8.2B**) resemble the C16 dose response curves of the most sensitive RT cell lines (**Figure 3.1**). As further evidence of improved cellular response, in both TTC549 and TM87-16 cells, the percentage of cells remaining never got over about 50% with co-treatment with 1.1 µM of Nutlin-3a, even at the lowest dose of C16 (**Figure 8.2B** black line). When we compare the synergy maps of the sensitive RT cells (**Figure 8.1A**) and the insensitive cells (**Figure 8.2A**), the regions of peak synergy are at higher concentrations of C16 in the insensitive cell lines than in the sensitive cell lines. This means that while C16 and Nutlin-3a are synergistic in TTC549 and TM87-16 cells, it still requires a higher concentration of C16 to achieve synergy. Taken together, this is encouraging data because it suggests that regardless of cellular sensitivity to the WIN site inhibitors, combination treatment with an HDM2 inhibitor can elicit an improved cellular response.

To confirm that the synergy is due to on-target activity of Nutlin-3a, we performed synergy analyses with C16 and a second, chemically-distinct, HDM2 inhibitor, HDM201 [91]. HDM201

Figure 8.2. Synergy between C16 and Nutlin-3a in insensitive RT cells (**A**) Synergy maps, as well as peak and average HSA δ scores for 49 unique combinations of C16 and Nutlin-3a doses ranging from 14 nM to 10 µM Nutlin-3a and 69 nM to 50 µM C16 in TTC549 and TM87-16 cells. Five day treatment (*n* = 3). HSA synergy score represents average HSA δ score of all dose combinations whereas peak synergy score represents the maximum average δ score for a three-by-three dose matrix within each map (indicated by dashed-line boxes). (**B**) Dose response curves of the TTC549 or TM87-16 to combinations of C16 and Nutlin-3a as in (A). Data are expressed as the percentage of cells remaining at day five, compared to the DMSO control (*n* = 3, mean ± SEM). The top plots display the dose response to C16 in combination with the indicated concentrations of Nutlin-3a. The bottom plots display the dose response to Nutlin-3a in combination with the indicated concentrations of C16.

acts in a similar manner to Nutlin-3a in that it binds to HDM2 to disrupt its interaction with p53, thus stabilizing p53 and activating the p53 pathway [91]. HDM201 is being evaluated in clinical trials for treatment of solid tumors and acute leukemia with WT p53 [153]. We tested synergy between C16 and HDM201 in one sensitive RT cell line, G401, and one insensitive RT cell line, TTC549. We observe synergy between C16 and HDM201 in both cell lines as monitored by both average and peak synergy δ scores (**Figure 8.3A**). The peak δ synergy score in G401 cells is 20.67 and the peak δ synergy score in TTC549 cells is 20.06, both values indicative of a synergistic response rather than additive. Of note, when comparing the synergy maps to those of C16 and Nutlin-3a in the same cell lines, the pattern of synergy is remarkably similar with the region of peak synergy in almost identical locations with both HDM2 inhibitors. As with the synergy between C16 and Nutlin-3a, we see a downward shift in the dose response curves with the addition of the second inhibitor (**Figure 8.3B**). Not only does this confirm that the synergy between WIN site inhibitors and HDM2 inhibitors is via on-target activity, this also lays the groundwork for co-treatment with WIN site inhibitors and a more clinically relevant HDM2 inhibitor.

Another way to determine if the synergy between WIN site inhibitors and the HDM2 inhibitors is via an on target mechanism is by testing whether suppressing p53 expression decreases synergy between C16 and Nutlin-3a. I measured cellular response of co-treatment of C16 and Nutlin-3a in the G401 cells expressing scrambled shRNA or p53 shRNA that we made in Chapter VII. I found that shRNA-mediated knockdown of p53 considerably reduces synergy between these inhibitors (**Figure 8.4A**). More specifically, cells expressing the p53 shRNA require a concentration of Nutlin-3a approximately 81 times higher than in the scr shRNA cells to achieve the same peak synergy. The dose response curves in the G401 cells do not shift downward until co-treatment with higher concentrations of Nutlin-3a (**Figure 8.4B**). We confirmed this phenomenon by testing synergy between C16 and Nutlin-3a in G401 and TTC642 in which we utilized CRISPRi-mediated knockdown of p53 in Chapter VII. Again we observe that knockdown of p53 decreases synergy between C16 and Nutlin-3a, further
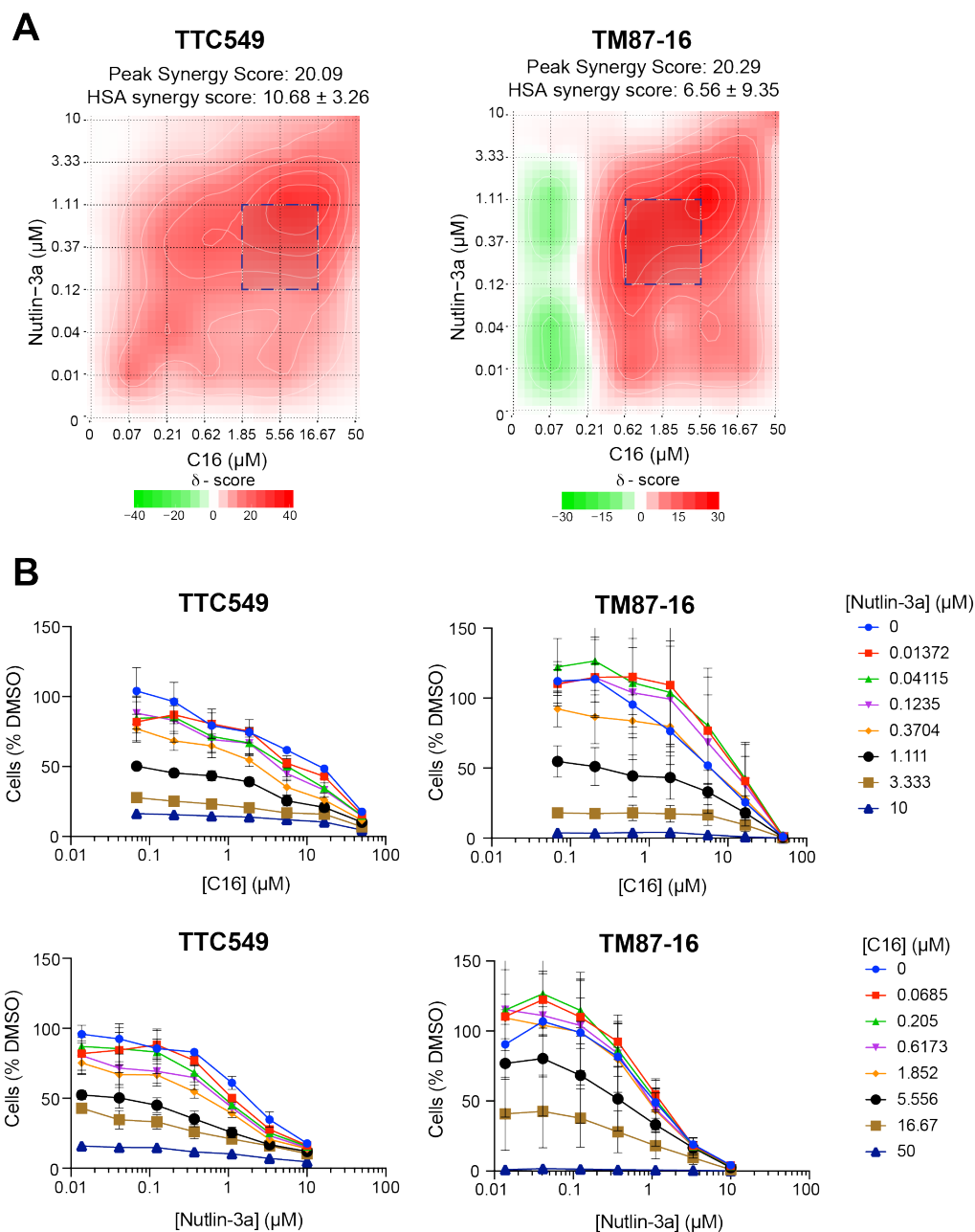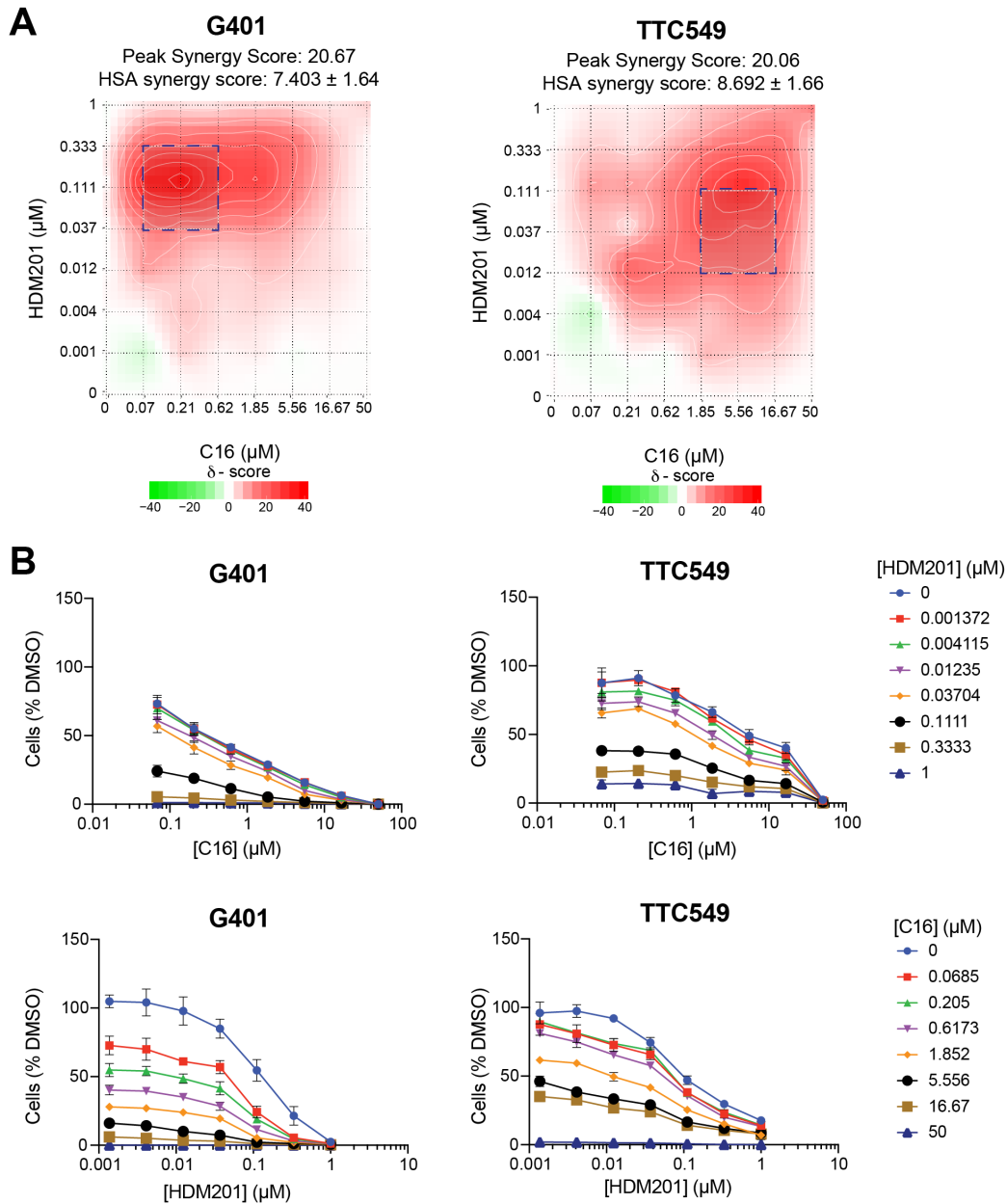
Figure 8.3. Synergy between C16 and HDM201 in RT cells (**A**) Synergy maps, as well as peak and average HSA δ scores for 49 unique combinations of C16 and HDM201 doses ranging from 1.4 nM to 1 µM HDM201 and 69 nM to 50 µM C16 in G401 and TTC549 cells. Five day treatment (*n* = 3). HSA synergy score represents average HSA δ score of all dose combinations whereas peak synergy score represents the maximum average δ score for a three-by-three dose matrix within each map (indicated by dashed-line boxes). (**B**) Dose response curves of the G401 or TTC549 to combinations of C16 and HDM201 as in (A). Data are expressed as the percentage of cells remaining at day five, compared to the DMSO control (*n* = 3, mean ± SEM). The top plots display the dose response to C16 in combination with the indicated concentrations of HDM201. The bottom plots display the dose response to HDM201 in combination with the indicated concentrations of C16.

134

Figure 8.4. Synergy between C16 and Nutlin-3a in G401 cells expressing scramble or p53 shRNA (**A**) Synergy maps, as well as peak and average HSA δ scores for 49 unique combinations of C16 and Nutlin-3a doses ranging from 14 nM to 10 µM Nutlin-3a and 69 nM to 50 µM C16 in G401 cells expressing scramble or p53 shRNA. Five day treatment (*n* = 3). HSA synergy score represents average HSA δ score of all dose combinations whereas peak synergy score represents the maximum average δ score for a three-by-three dose matrix within each map (indicated by dashed-line boxes). (**B**) Dose response curves of the G401 cells expressing scramble or p53 shRNA to combinations of C16 and Nutlin-3a as in (A). Data are expressed as the percentage of cells remaining at day five, compared to the DMSO control (*n* = 3, mean ± SEM). The top plots display the dose response to C16 in combination with the indicated concentrations of Nutlin-3a. The bottom plots display the dose response to Nutlin-3a in combination with the indicated concentrations of C16.

demonstrating that synergy is mediated via an on-target activity of Nutlin-3a against HDM2 (**Figure 8.5A**). Specifically, it requires higher concentrations of Nutlin-3a to achieve similar peak δ synergy scores in the G401 and TTC642 cells expressing p53 sgRNA compared to cells expressing empty sgRNA vector. When we look at the dose response curves, there is only a minor shift in the C16 dose-response curves in the cells expressing p53 sgRNA, even at the highest Nutlin-3a dose (**Figure 8.5B**). Based on these data, we conclude that—independent of the magnitude of response of RT cells to C16 alone—WDR5 WIN site inhibitor C16 and HDM2 antagonist Nutlin-3a act synergistically to inhibit proliferation of *SMARCB1*-deficient cancer cells.

Effect of WIN site inhibitor and HDM2 inhibitor co-treatment on p53 target gene expression

The simplest explanation for the synergy I observe is that the combination of WIN site inhibitor and HDM2 antagonist yields a more pronounced activation of p53—and p53 target genes—than either agent alone. I wanted to test this at the protein level and at the mRNA level. First, I treated RT cells with DMSO, 500 nM C16, 500 nM Nutlin-3a, or a combination of C16 and Nutlin-3a, both at 500 nM. I examined all four cell lines in which I tested for synergy: G401, TTC642, TTC549, and TM87-16. I isolated protein from the cells and probed the lysates with antibodies specific for p53 and p21, a canonical p53 target gene, and histone H3 as a loading control. Indeed, I see a greater induction of p53 in the samples treated with C16 and Nutlin-3a in combination than either of the single-agent treated samples (**Figure 8.6**). In accordance with my hypothesis, co-treatment of RT lines with 500 nM each of C16 and Nutlin-3a results in a stronger induction of p21 then either individual treatment (**Figure 8.6**), indicating that treating with both C16 and Nutlin-3a simultaneously leads to enhanced p53 activation. From this data I can conclude that the mechanism for synergy between C16 and Nutlin-3a is through a greater activation of p53 target genes, specifically p21, at the protein level.

I then wanted to determine how co-treatment of RT cells with a WIN site inhibitor and an HDM2 inhibitor effects the expression of p53 target genes at the mRNA level. I used reverse

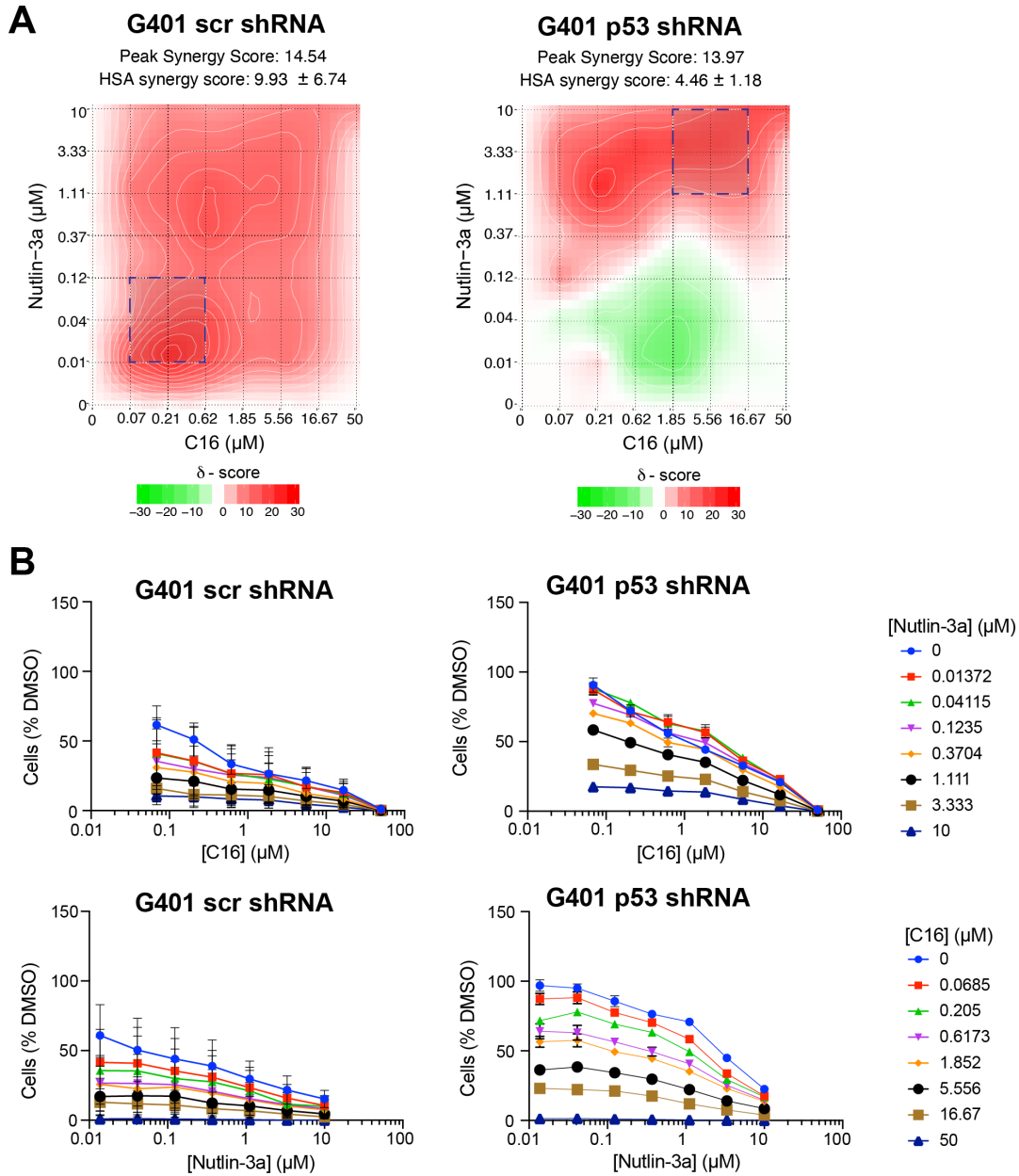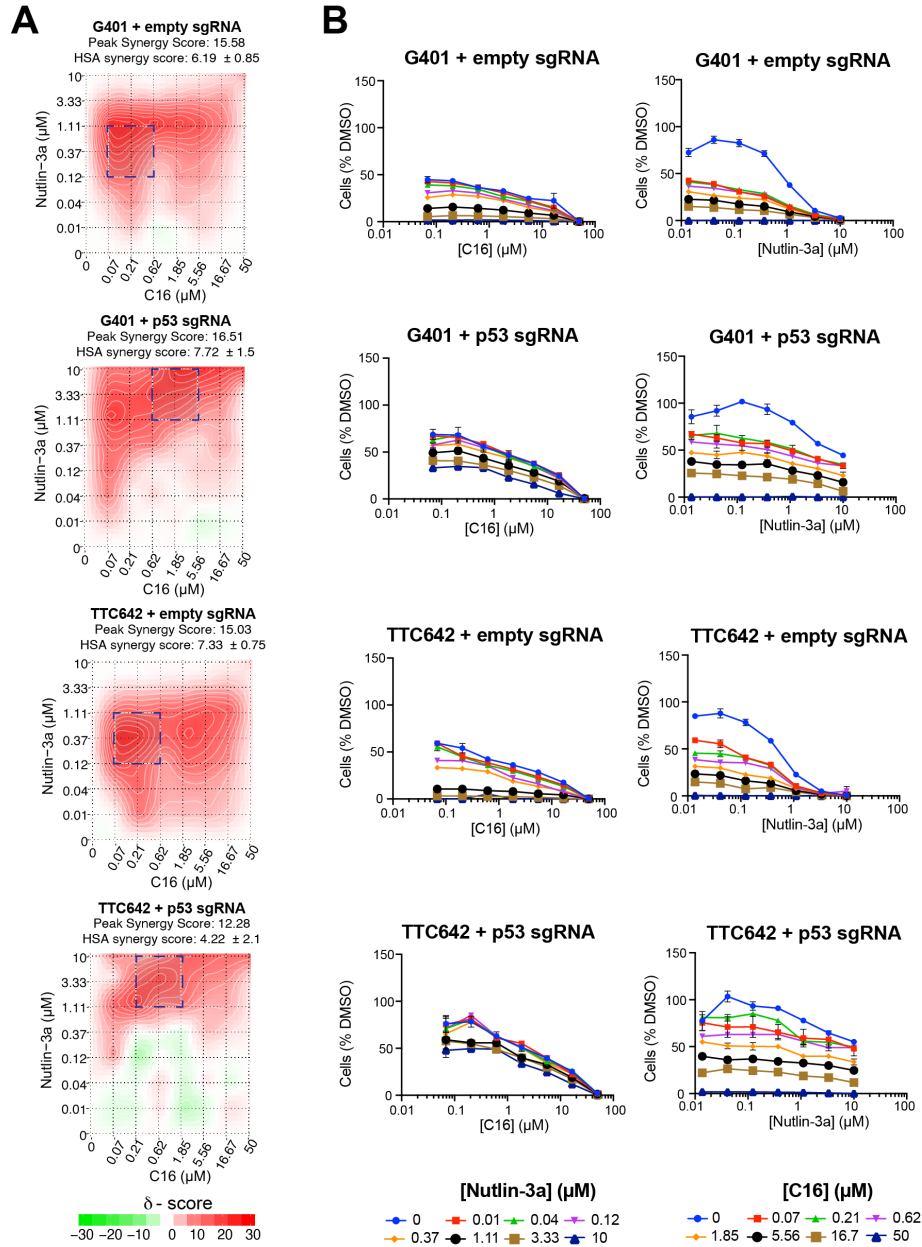**Figure 8.5. Synergy between C16 and Nutlin-3a in G401 and TTC642 cells expressing empty or p53 sgRNA** (**A**) Synergy maps, as well as peak and average HSA δ scores for 49 unique combinations of C16 and Nutlin-3a doses ranging from 14 nM to 10 µM Nutlin-3a and 69 nM to 50 µM C16 in G401 (top) or TTC642 (bottom) cells expressing empty or p53 sgRNA. Five day treatment (*n* = 3). HSA synergy score represents average HSA δ score of all dose combinations whereas peak synergy score represents the maximum average δ score for a three-by-three dose matrix within each map (indicated by dashed-line boxes). (**B**) Dose response curves of the G401 or TTC642 cells expressing empty or p53 sgRNA to combinations of C16 and Nutlin-3a as in (A). Data are expressed as the percentage of cells remaining at day five, compared to the DMSO control (*n* = 3, mean ± SEM). The left plots display the dose response to C16 in combination with the indicated concentrations of Nutlin-3a. The right plots display the dose response to Nutlin-3a in combination with the indicated concentrations of C16.

137
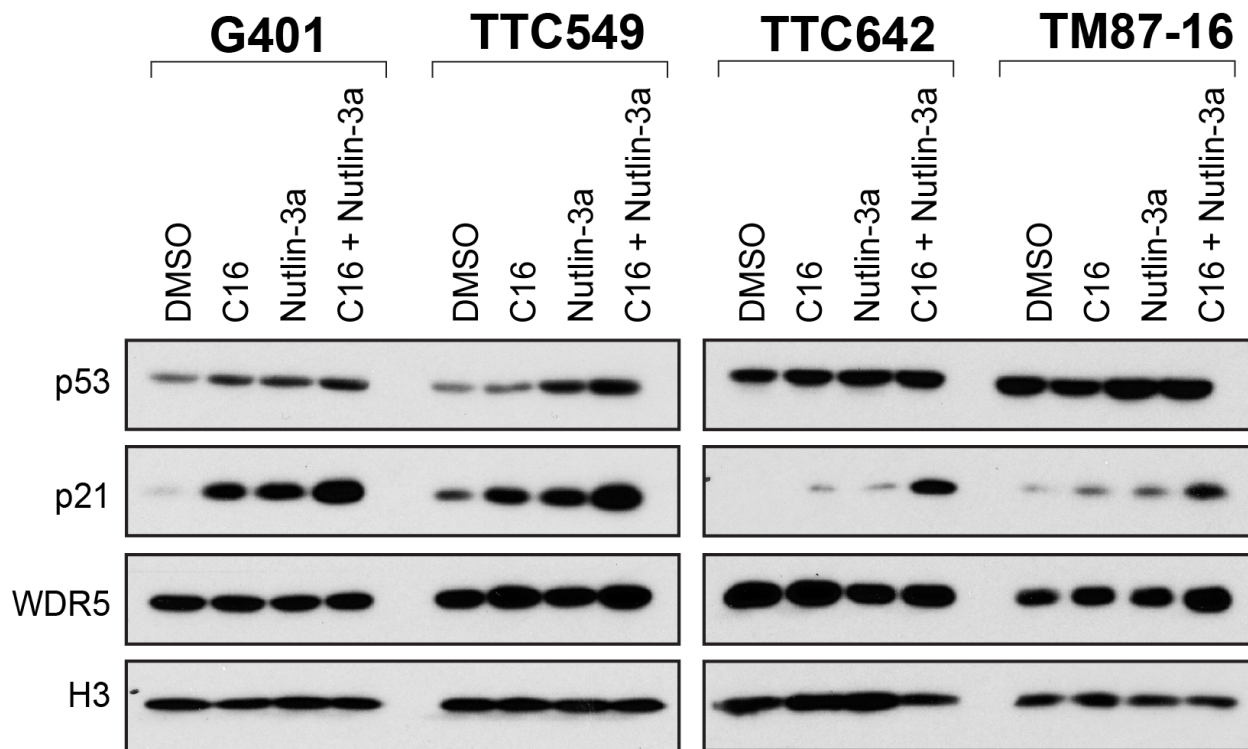
Figure 8.6. C16 and Nutlin-3a synergize to induce p53 and p21 expression Western blot, performed on lysates from cell lines that were treated with DMSO, 500 nM C16, 500 nM Nutlin-3a, or 500 nM C16 and Nutlin-3a for three days. Blots were probed with antibodies against the indicated proteins. Histone H3 is a loading control. Image is representative of three biological replicates.

transcriptase quantitative polymerase chain reaction (RT-qPCR) to quantify the expression of specific genes with and without inhibitor treatment. I treated G401, TTC642, and TTC549 cells with DMSO, 500 nM C16, 500 nM Nutlin-3a, or 500 nM of both C16 and Nutlin-3a for three days. I isolated total RNA using a Zymo Research RNA mini-prep kit with an on-column DNase digestion to remove any contaminating DNA. I then reverse transcribed the RNA to generate cDNA and performed qPCR to quantify four RPGs, *TP53*, and four p53 target genes. I quantified the expression of these genes relative to the housekeeping gene, *GAPDH*. The relative expression was then normalized to the DMSO treated samples.

I first looked at the expression of four RPGs to determine if the combination of WIN site inhibitor and HDM2 inhibitor is affecting the primary mode of WIN site inhibitor action, suppression of WDR5-bound RPGs. *RPL35* and *RPS24* are both bound by WDR5 and *RPL14* and *RPS11* are not bound by WDR5 as determined by the ChIP-Seq presented in Chapter IV. As expected, in all three cell lines, there is a significant decrease in the expression of *RPL35* and *RPS24* in the samples treated with C16 (**Figure 8.7**). There is no change in expression of these genes with Nutlin-3a which is to be expected as Nutlin-3a is not known to affect RPG expression. Thus, suppression of WDR5-bound RPGs was not further enhanced by the addition of Nutlin-3a (**Figure 8.7**). As expected, in RPGs that are non-bound by WDR5, there is neither an increase or decrease in expression with any treatment. The only exceptions are in TTC642 cells were there is a subtle but significant decrease in RPL14 expression the co-treated samples and in the G401 cells were there is a subtle but significant increase in RPS11 expression in the C16 and Nutlin-3a individually treated samples (**Figure 8.7**). The mRNA expression of *TP53* does not change in any of the cell lines with any of the treatment regimens (**Figure 8.7**). This is to be expected as we did not see induction of *TP53* with WIN site inhibit treatment in the RNA-Seq (Chapter VI) and Nutlin-3a functions by preventing p53 protein degradation without affecting the p53 mRNA [91]. I next analyzed four consensus p53 target genes, p21 (*CDKN1A*), *HDM2*, *TP53INP1*, and *BTG2*. As demonstrated by western blot, p21 (*CDKN1A*) is induced by both inhibitors individually but there is a further increase in expression when C16 and Nutlin-3a are
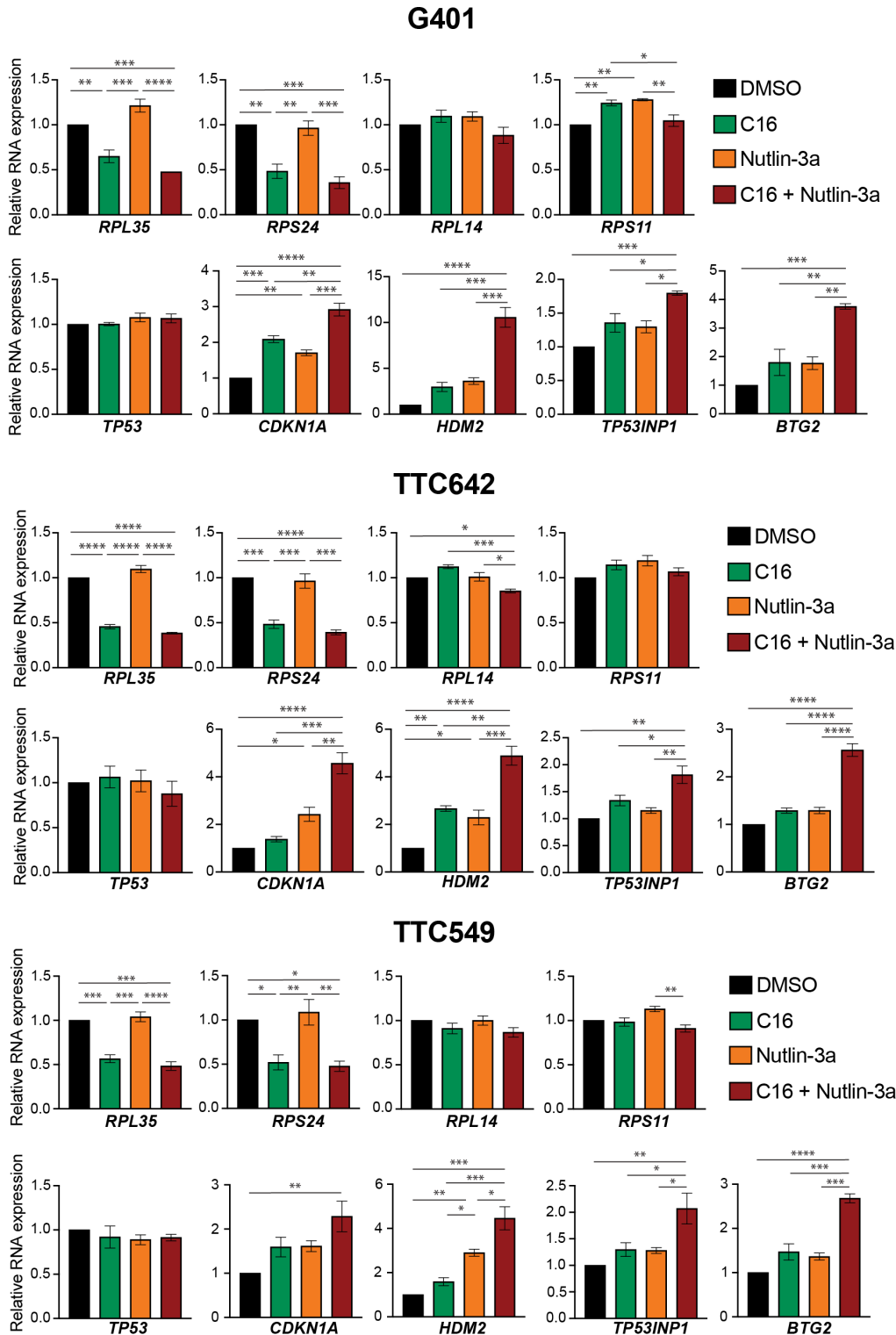
Figure 8.7. C16 and Nutlin-3a synergize to induce p53 target genes RT-qPCR analysis of the indicated mRNA levels in G401, TTC642, and TTC549 cells collected following treatment with DMSO, 500 nM C16, 500 nM Nutlin-3a, or 500 nM C16 and Nutlin-3a for 3 days. RNA expression shown relative to DMSO. *p = <0.05, ** p = <0.01, *** p = <0.001, **** p = <0.0001, as determined by ANOVA (n = 3, mean ± SEM).

treated in combination (**Figure 8.7**). The same pattern exists for the other p53 target genes, *HDM2*, *TP53INP1*, and *BTG2*; each are induced by both C16 and Nutlin-3a individually but there is a significantly greater activation when the inhibitors are applied in combination. From this, I conclude that the mechanism by which the C16 and Nutlin-3a combination enhances cellular inhibition is most likely due to enhanced p53 activation in response to dual inhibitor treatment in this context.

Discussion

Combination therapy has risen to prominence for treating cancer because it has proven to be more effective than traditional monotherapies [151]. One of the main advantages of combination therapy is that treatments can be administered at lower doses than needed for single agent treatment which may reduce toxicity and side effects [151]. Cancers treated with a combination therapy are less likely to acquire resistance to the drugs because they often target multiple pathways so the cancer is less likely to develop alternate pathways. HDM2 inhibitors are a perfect candidate for combination therapy. HDM2 inhibitors have immense promise in the clinic as they activate a tumor suppressor and promote anti-cancer activity [154]. However, HDM2 inhibitors have not yet to succeeded in clinical trials. Current HDM2 inhibitors have to be dosed at extremely high levels which leads to negative side effects [155] or prolonged treatment leads to p53-mutant cells which are resistant to the therapy [156]. These setbacks can be mitigated with a combination therapy that would allow for lower doses and shorter treatment times with HDM2 inhibitor.

I propose that the extent of p53 induction by C16 in RT cells, although detectable by RNA-Seq, is too small to affect a cellular outcome in this context. I further predict that this modest level of p53 induction can be enhanced by HDM2 inhibition, resulting in an enhanced cellular response. Indeed, I find this is the case. C16 and Nutlin-3a are synergistic in all four of the RT cell lines tested as measured by the HSA model. The scores obtained from HSA tend to be overly optimistic because HSA has the lowest threshold for assigning synergy. Perhaps using a more

stringent synergy model such as Bliss, Loewe, or Zero interaction potency (ZIP) would be more informative [96]. However, even minor improvements to therapies for this difficult to treat cancer could have major implications on patient survival and quality of life. It is important to note that synergy occurs not only in our most sensitive RT lines, G401 and TTC642, but also in some of the least sensitive lines, TTC549 and TM87-16, indicating that differences in response to WIN site inhibitor can be overcome when combined with an HDM2 antagonist.

WDR5 WIN site inhibitors and Nutlin-3a have both been shown to activate p53 [4, 91]. I proposed that the mechanism through which C16 and Nutlin-3a elicit synergy is by enhancing activation of p53 target genes and thus improving cellular inhibition. I observe enhanced activation of p53 targets by western blot and by RT-qPCR which translates to more robust cellular inhibition of RT cells. An active area of investigation is understanding the manner in which the combination of WDR5 WIN site inhibitors and HDM2 inhibitors is suppressing cellular growth. We have shown that treatment with C16 alone is not sufficient to push RT cells into apoptosis. Instead, WIN site inhibition appears to slow proliferation in this context. Co-treatment with C16 and Nutlin-3a could be simply slowing proliferation even more or it could be promoting apoptosis. Further studies are needed to determine the mechanism of reduced cell growth with C16 and Nutlin-3a co-treatment.

We also showed that the synergy observed between C16 and Nutlin-3a relies on the expression of WT p53. Reducing expression of p53 in RT cells decreases synergy between the two inhibitors. Because of the unusually simple genetic profile of RT, p53 is nearly universally retained in patients which means that WIN site and HDM2 inhibitor combinations may be viable treatment strategy in the clinic. This synergistic combination approach I demonstrate here with HDM2 and WDR5 inhibitors may also have the potential to overcome limiting factors associated with single agent therapies, especially what has been seen with HDM2 inhibitors. This combination regimen should allow each agent to be used at lower doses than would be required for mono-therapy. This, in combination with the insight we provide here into how WIN site

inhibitors act in RT cells, lays the foundation for future preclinical evaluation of WDR5 and HDM2 inhibitor combinations for treatment of deadly rhabdoid tumors.

IX. DISCUSSION

WDR5 in Rhabdoid Tumor Cells

Discovering strategies to treat rhabdoid tumors is a challenging task. These pediatric cancers are rare and aggressive [1], which make clinical trials particularly difficult due to lack of funding and ethical concerns related to trials in children [157]. In addition, the rarity of these cancers means it is difficult to have enough patients for an informative clinical trial. Genetically, RT is defined by loss of the *SMARCB1* tumor suppressor [7-9] so these tumors lack a clear and present oncogenic target for therapeutic intervention. Current treatment strategies involve a combination of surgery, radiation, and chemotherapy, and even still, the five year survival rate for patients diagnosed with RT is approximately 20% [1]. Even a small improvement in treatment strategy for these cancers will make a huge difference in the quality of life and survival of these patients. As is the case with most current anti-cancers treatment strategies, any practical regimen for RT will involve combinations of agents [151], making it imperative that we identify effective combinational approaches that can inform how existing or future drugs can be used together to ameliorate these cancers.

The goal of my work was to characterize how RT cells respond to a potent inhibitor of the WIN site of WDR5, representative of a novel class of inhibitors currently under development in multiple laboratories [79, 82, 86, 158-160]. WDR5 is a scaffolding protein with a variety of functions at chromatin that control gene expression [2]. In Chapter III, I show that WDR5 is bound to chromatin but that the localization varies between cell lines. Importantly, however, the genes at which WDR5 is bound in all three RT cell lines tested are part of the conserved set of WDR5-target genes connected to protein synthesis [3]. This study strengthens the concept that WDR5 is a conserved regulator of genes connected to biomass accumulation and defines a predictable primary transcriptional response to WIN site inhibition.

My definition of the genomic binding sites of WDR5 in G401, KYM-1, and TTC549 cells in Chapter III reveals a pattern of chromatin association that is similar to what is seen in other contexts [3, 4, 78]; a wide variation in binding site number across cell types, a tendency for WDR5 binding proximal to promoters, and inclusion of a set of ~100 genes that are bound by WDR5 in all cell types examined. These 100 common WDR5-bound genes are connected to protein synthesis and encode roughly half the protein subunits of the ribosome as well as nucleolar RNAs and translation factors. Although we do not yet understand the significance of this specific conserved pattern of WDR5 binding, I will note that a majority of these genes are transcriptionally suppressed by WIN site inhibitor in RT, leukemia [4] and NB [3] cell lines, and by WDR5 degradation in NB cells [3] and Ramos Burkitt lymphoma cells [126], demonstrating that these genes are direct, bona-fide, and universal WDR5 targets. **Figure 9.1** (left) illustrates that in an unperturbed rhabdoid tumor cell, WDR5 binds to chromatin to promote the expression of ribosomal protein genes (RPGs) resulting in rapid proliferation.

How WDR5 is regulating the expression of these RPGs is still an open question. WDR5 is most known for its role in scaffolding the SET1/MLL H3K4 HMT complex which catalyzes a histone mark that defines transcriptionally active genes. However, we have shown that WIN site inhibition does not decrease bulk levels of H3K4me3 [126] suggesting that WDR5 is promoting transcription of RPGs independent of SET1/MLL complexes. I will also note that most of these genes are regulated by MYC in a WDR5-dependent manner in Ramos Burkitt lymphoma cells [78]. MYC is a family of oncogenic transcriptional factors that drive oncogenicity via their ability to bind DNA and to regulate thousands of genes, most notably ones involved in cell growth, cell cycle progression, metabolism, and genome integrity [47]. In fact, overexpression of a MYC family member is observed in over half of all malignancies, and it is estimated that inappropriate MYC expression contributes to one-third of all cancer deaths in the U.S. each year [46]. In 2015, our laboratory reported that recruitment of MYC to chromatin depends on interaction with WDR5 [77]. We showed that WDR5 must bind chromatin in order to recruit MYC at a set of PSGs, encoding subunits of the ribosome, translation factors, and nucleolar RNAs [78], suggesting that
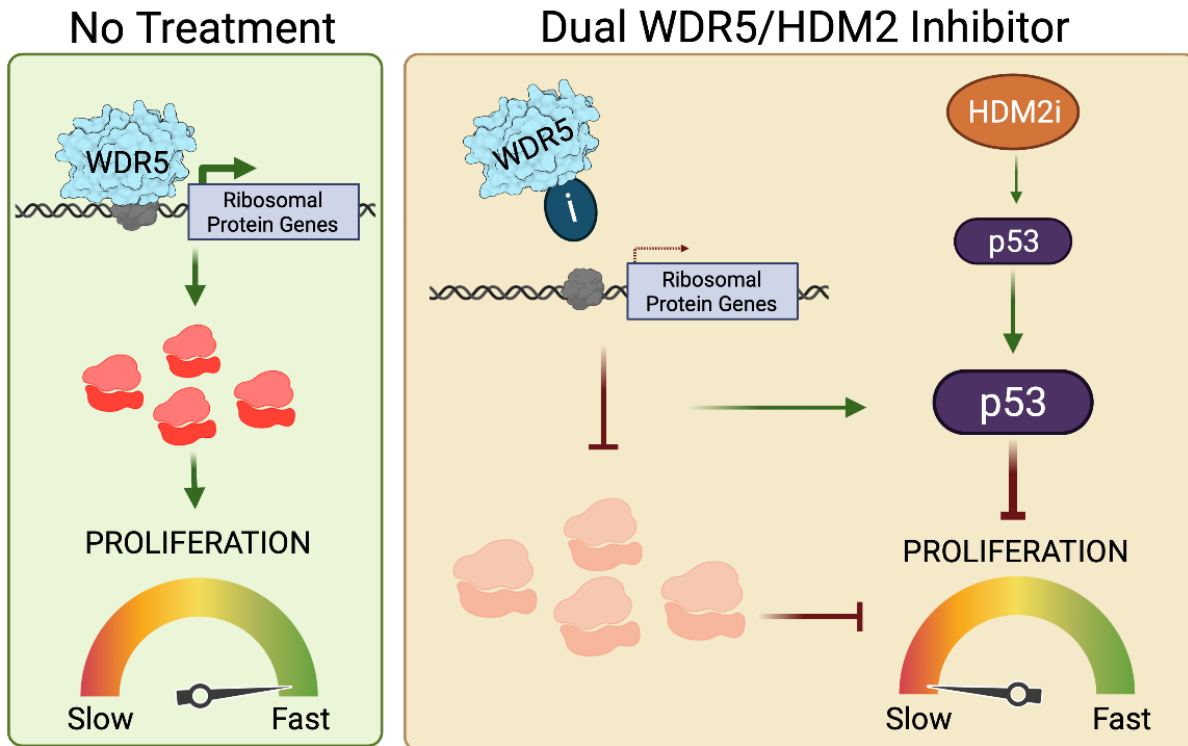
Figure 9.1 Model for WDR5 function and mechanism for dual WDR5 and HDM2 inhibitor treatment in RT cells (Left) Under homeostatic conditions, WDR5 is bound to chromatin at a distinct set of ribosomal protein genes (RPGs). WDR5 engagement at these site promotes RPG transcription and expression which is required fro protein translation and cellular proliferation. (Right) Upon WDR5 WIN site inhibitor treatment, WDR5 is displaced from chromatin, decreasing the expression of WDR5-bound RPGs, inducing p53 and slowing proliferation. HDM2 inhibitor induces p53 but p53 induction is enhanced in combination with the WIN site inhibitor leading to decreased proliferation.

the function of WDR5 at these universal target sites may be dedicated to the actions of MYC. Therefore, I predict that MYC is recruited to these PSGs by WDR5 to promote the expression of these PSGs to promote increased protein synthesis and therefore upregulate growth and proliferation, a hallmark of MYC's tumorigenic abilities.

In RT cells, WIN site inhibitor results in the comprehensive displacement of WDR5 from chromatin, consistent with earlier reports that the integrity of the WIN site is essential for tethering WDR5 to its chromosomal locations [3, 4, 78]. However, the manner at which WDR5 is tethered to chromatin is still relatively opaque. WDR5 has no known DNA binding domain so it is unlikely that WDR5 is binding directly to DNA. Instead, it is more likely that WDR5 is binding to DNA through its interaction with one of its numerous binding partners at the WIN site (Chapter I). In the Future Directions, I will discuss a proteomic approach to define the interactome of WDR5 that will hopefully identify the protein(s) that is responsible for recruiting WDR5 to chromatin.

Another interesting observation is that despite the widespread eviction of WDR5 from chromatin by C16, most genes bound by WDR5 do not respond to WIN site blockade, either early or over the course of days. This phenomenon is most clearly illustrated in KYM-1 cells, in which we track ~700 WDR5 binding sites by ChIP-Seq but observe only 71 genes with altered transcription, as measured by PRO-Seq. The number of WDR5-bound genes that are transcriptionally impacted by WIN site inhibitor does increase by day three, but the vast majority of WDR5-bound genes are unresponsive during extended treatment, and conversely most of the transcriptional changes occur at genes that are not physically linked to WDR5. The disconnect between WDR5 binding and transcriptional response suggests that the function of WDR5 at most of its chromatin-binding sites is not measurable under our conditions. It is possible that these binding sites may serve to bookmark genes for early reactivation after mitosis; a function previously described for WDR5 in human embryonic stem cells [161]. Further investigation of this phenomenon is needed.

Response of *SMARCB1*-deficient cells to WDR5 WIN site inhibitors

A number of important conclusions can be drawn from monitoring the activity of WIN site inhibitor C16 across a panel of *SMARCB1*-deficient cell lines. Despite a common genetic (MRT and AT/RT) or functional (synovial sarcoma) perturbation, these lines differ widely in their sensitivity to WIN site inhibitors. G401 and TTC642 cells, for example, are almost as sensitive to C6 and C16 as MV4:11 leukemia cells, which are often considered the prototype for a WIN site inhibitor-sensitive cell line [4, 86]. TTC549 and TM87-16 cells, in contrast, display IC_{50} values close to those obtained in K562 cells [4, 79], which we and others have classified as insensitive to WIN site inhibition. Previously, it has been challenging to know if a differential response to WIN site inhibitors is due to differences in intracellular compound accumulation or access to WDR5. I used the QuantiGene™ Plex technology to develop a RPG target engagement assay to quantity the primary response of WIN site inhibition by measuring the expression of a set of universal WDR5-target genes in response to C16 treatment. This assay demonstrates that differences in the extent of WDR5 inhibition do not underly the wide differential in cellular response across the panel. Rather, it appears as though WDR5 inhibition, as quantified by RPG transcription, occurs in all cell types regardless of cellular sensitivity. In addition, the precise set of genes that respond early to C16 in our PRO-Seq assays are remarkably similar between cell types. Indeed, given the discrepancy in WDR5 binding events between G401 and KYM-1 cells, and their inherently diverse transcriptomes, it is intriguing to see how similar the primary transcriptional responses to C16 are between the two lines. Again, the majority of these primary target genes are WDR5-bound RPGs, which we know respond rapidly to earlier generation WIN site inhibitors in other cancer cell contexts [3, 4]. The ChIP-Seq, PRO-Seq, and RNA-Seq data collected in these studies along with prior work studying WDR5, has confidently identified a set of RPGs that are ubiquitously bound by WDR5 and altered with WIN site inhibition in diverse cellular settings. Because the pattern of WDR5 binding and the impact of WIN site inhibition is similar across sensitive and insensitive lines, it is not unreasonable to suggest that this response is universal and highly predictable. Whether cells succumb or survive in response to

WIN site inhibition has little to do with differences in how WDR5 and WIN site inhibitors act, but is instead determined by how cells respond to perturbations in the expression of these specific PSGs. This is a major outstanding question of my work, as we do not reach a conclusion for the variation of cellular sensitivities to WIN site inhibition among *SMARCB1*-deficient cell lines.

One determinant of an effective response to WIN site inhibition, based on earlier studies in leukemia [4] and NB [3] cells, is the presence of wild-type p53. In these contexts, the alterations in RPG transcription cause ribosomal stress and induce p53 [4]. It is clear from my transcriptomic analyses that p53 target genes are induced in most RT lines in response to C16 treatment, which is consistent with earlier observations in MLLr and NB cells [3, 4]. What is surprising in RT cells, however, is that p53 is not consistently induced at the bulk protein level by C16. p53 is modestly induced in sensitive cell lines, G401 and TTC642, but not in KYM-1, TTC549, or TM87-16, despite induction of p53 target genes by RNA-Seq in all cell lines. Even more unexpected is that p53 is dispensable for the cellular impact of WIN site inhibitors. *TP53*-independent responses to ribosome perturbation or nucleolar stress have been described [162], although they are mechanistically opaque. Further investigation is required to understand why p53 is not robustly induced by WIN site inhibition and how RT cells are able to respond to WIN site inhibition in the absence of WT p53 expression. However, regardless of the mechanism, my findings demonstrate that cancer cells are able to respond to WIN site inhibition in the absence of functional p53, a mode of action not previously recognized in our initial work with MLLr and NB cells [4]. Given that half of cancers express a mutant form of p53, WIN site blockade may have broader utility as an anti-cancer agent in additional cancer types.

In summary, my work has validated that the primary mechanism by which *SMARCB1*-deficient cells are responding to WIN site inhibition mirrors what we previously observed [3, 4]. WDR5 is bound to a conserved set of PSGs and is displaced with WIN site inhibitor treatment (Chapter IV). This results in the decreased transcription of the WDR5-bound genes (Chapter V) and the suppression of RPG expression (Chapter VI). WIN site inhibition also results in the increased

expression of p53 target genes (Chapter VI) and a subtle increase in p53 bulk protein in the sensitive cells lines (Chapter VII) indicating that WIN site site inhibitors modestly induce the p53 pathway (**Figure 9.1**).

Combination treatment with WDR5 WIN site inhibitor and HDM2 inhibitors

Perhaps the most significant implication of the p53-independence of the response of RT cells to WIN site inhibitor is that it can be exploited to develop a combination inhibitor strategy centered on dual WDR5 and HDM2 inhibition. Combination treatment strategies are becoming more and more common as a way to treat cancer in the clinic as they are more effective and can reduce toxic side effects [151]. Based on my findings, I propose that the extent of p53 induction by C16 in RT cells, although detectable by RNA-Seq, is too small to affect a p53-dependent cellular outcome in this context. I further propose that I can enhance this modest level of p53 induction by co-treating with HDM2 inhibition. This co-treatment does in fact improve cellular inhibition, most likely via the synergistic activation of p53 target genes. While I was encouraged to see that we could improve response in the sensitive cell lines, I was more excited that the improved cellular response was observed in the insensitive cell lines as well, indicating that differences in response to WIN site inhibitor can be overcome when combined with an HDM2 antagonist. HDM2 inhibitors have not yet succeeded in clinical trials, likely due to a combination of acquisition of resistance, toxicities, and inability as a single agent to reliably trigger apoptosis in cancer cells [154]. However, combining an HDM2 inhibitor with an additional synergistic compound has the potential to overcome the limiting factors associated with mono-therapies by allowing lower treatment doses to avoid toxic side effects and by preventing the cancer cells from becoming resistant. The near universal retention of p53 in RT, together with insight we provide here into how WIN site inhibitors act in RT cells, opens the possibility that WDR5 and HDM2 inhibitor combinations could be used to treat these deadly rhabdoid tumors.

Future Directions

While the experiments presented here yielded significant new knowledge about how WDR5 WIN site inhibitors function in *SMARCB1*-deficient cell lines, several topics would benefit from further investigation. Studies in the future should focus on understanding the how WDR5 is bound to RPGs and the furthering the understanding of WIN site inhibitors for the treatment of RT in the clinic.

Previous work in our laboratory has determined that WDR5 is tethered to chromatin via the WIN site, which was confirmed in the work in my theses (Chapter IV). However, the protein(s) responsible for recruiting WDR5 to chromatin are still unknown. A proximity labeling experiment coupled with mass spectrometry-based proteomics would allow the identification and quantification of the WDR5 interactome. Dr. Alissa Guarnaccia, a recent graduate of our laboratory, used quantitative proteomics to characterize how WIN site inhibition alters the WDR5 interactome [163]. For this, Alissa treated lysates from HEK293 cells expressing FLAG-tagged WDR5 with with C6 or C6nc, recovered proteins by FLAG immunoprecipitation (IP), and analyzed samples using mass spectrometry. She identified 17 proteins that decrease their interaction with WDR5 and 8 proteins that increase their interaction with WDR5 with WIN site inhibition [163]. While this work was informative to understand which proteins are more or less associated with WDR5 when the WIN site is inhibited, it only identified proteins with altered WDR5 binding in the presence of WIN site inhibitor and did not discern all the proteins that interact with WDR5. In addition, the WIN site inhibitor treatment was performed in cell lysates rather than live cells and these experiments relied on an immunoprecipitation of tagged WDR5 to pulldown interacting proteins so there are better methods to define the entire interactome of WDR5. A method to do this would be to use the APEX2-proximity labeling. APEX2 is an engineered peroxidase that catalyzes the oxidation of biotin-phenol into a biotin-phenoxyl radical in the presence of hydrogen peroxide which can biotinylate neighboring proteins [164]. The biotinylated proteins can then be pulled down with streptavidin beads and purified and

quantified by mass spectrometry. In these experiments, C16 can be used as a tool compound to compare the proximitome of WDR5 when it is bound to chromatin and after it has been displaced to identify the proteins in close proximity to WDR5 both at and away from chromatin and may identify new proteins in which WDR5 interacts to give insight into how WDR5 is tethered to chromatin.

C6 and C16 are not amenable to *in vivo* assessment in preclinical studies in mouse models. We need to develop more potent WDR5 small molecule inhibitors with more drug-like properties to fully understand the therapeutic potential of this treatment strategy. This will help determine a therapeutic window and if there is any anti-cancer activity *in vivo.* In order to progress WDR5 WIN site inhibitors as an anti-cancer strategy in the clinic, we must first demonstrate efficacy in an animal model. The Fesik laboratory has continued to develop more potent WIN site inhibitors with better pharmacokinetic properties. In fact, they have produced compounds with a high enough potency and drug-like properties to be tested in animal models. Our collaborators at the National Cancer Institute (NCI) and at Pharmaron are actively conducting studies to determine the efficacy of these inhibitors in mouse xenograph models. To fully understand the potential for WIN site inhibition in RT, it would be useful to test these drug-like WIN site inhibitors in a mouse xenograph model with RT cell or in a genetic mouse model of RT [33, 165].

A major takeaway from this work is that we can combine WDR5 WIN site inhibitors with HDM2 inhibitors to improve cellular inhibition. This opens the possibility that WIN site inhibitors could be combined with a number of other therapeutics to improve the anti-cancer activity. An important set of drugs to test for combination treatment are the chemotherapies that are currently in use in the clinic to treat RT. We know that RT at least partially responds to these treatments and pushing current treatment strategies to be more effective is a simple way to improve patient response and outcomes. Current treatment strategies for RT include a combination of many chemotherapies including vincristine, doxorubicin, cyclophosphamide, ifosfamide, carboplatin, and etoposide [13]. Vincristine interferes with microtubule

polymerization to disrupt mitosis [166]. Doxorubicin intercalates within DNA to cause DNA strand breakage and prevents both DNA and RNA synthesis resulting in apoptosis [167]. Cyclophosphamide, ifosfamide, and carboplatin form interstrand and intrastrand DNA crosslinks leading to apoptosis [168-170]. Etoposide inhibits DNA synthesis by forming a complex with topoisomerase II and DNA, inducing double strand breaks, and preventing repair leading to apoptosis [171]. All of these chemotherapies have a mechanism of action that differs from that of WDR5 WIN site inhibitors but all ultimately trigger apoptosis. Perhaps using two different methods to disrupt cellular processes will have a synergistic anti-cancer activity. Chemotherapies have already been very successful in combination therapy strategies [151].

Another interesting opportunity for synergy with WDR5 WIN site inhibitors is with protein translation inhibitors. Translational inhibitors are a promising anti-cancer target because translation is a fundamental cellular processes that typically upregulated in cancer cells, to maintain the enhanced proliferative state of these cells. As such, cancer cells can be susceptible to translation inhibition as it will disrupt the cell's ability to maintain the enhanced proliferative state, WDR5 WIN site inhibitors suppress a small subset of protein synthesis genes including about half of the RPGs that make up the ribosome. Beyond this, WIN site inhibitors decrease the translational capacity of RT cells, albeit only modestly (**Figure 6.11**). I predict that the addition of a translational inhibitor will further decrease the translational capacity of RT cells and thus result in a greater decrease in proliferation. Two inhibitors of particular interest are homoharringtonine (HHT) and CX-5461. Homoharringtonine, as discussed in Chapter I, is a translational inhibitor that binds that active site of the ribosome and prevents the addition of amino acids to the growing polypeptide chain [90]. RT cells have already been shown to be sensitive to HHT [54] and I predict that combining HHT with a WIN site inhibitor will result in a more robust cellular response. CX-5461 is a small molecule that inhibits RNA polymerase I, the polymerase that transcribes rRNA which is an important component of the ribosome [172]. Because WIN site inhibitors only suppress the expression of about half of the RPGs, I reason that combining this will an additional ribosome biogenesis inhibitor will result in further disruption

of ribosome biogenesis and therefore a greater effect of protein translational capacity disrupting proliferation of RT cells. There are countless potential combinatorial approaches to treat RT. I have done work to show that RT cells are sensitive to WIN set inhibitors, but importantly can be combined with an HDM2 inhibitor to improve cellular response. Further exploration of synergistic combinations with WDR5 WIN site inhibitors will provide actionable combinatorial approaches that can be used to enhance the efficacy of WIN site inhibitors in the clinic.

In summary, there are several exciting avenues to expand our understanding of WIN site inhibition for the treatment of a variety of cancers, including rhabdoid tumors. These future directions described above will fill gaps in knowledge concerning the proximitome of WDR5 and the manner in which it is bound to chromatin to hopefully uncover what WDR5 is doing at each of its binding sites. Additionally, continuing to develop more optimized WIN site inhibitors and completing *in vivo* studies will hopefully identify a lead candidate to move into clinical trials. As the anti-cancer treatment strategies improve, many are moving to combination therapy approaches. Identifying other compounds with which WDR5 WIN site inhibitors synergize in RT cells will increase the likelihood that we can improve treatment strategies and the overall outlook of deadly rhabdoid tumors.

REFERENCES

1. Pawel, B.R., SMARCB1-deficient Tumors of Childhood: A Practical Guide. Pediatr Dev Pathol, 2018. **21**(1): p. 6-28.

2. Guarnaccia, A.D. and W.P. Tansey, Moonlighting with WDR5: A Cellular Multitasker. J Clin Med, 2018. **7**(2).

3. Bryan, A.F., et al., WDR5 is a conserved regulator of protein synthesis gene expression. Nucleic Acids Res, 2020.

4. Aho, E.R., et al., Displacement of WDR5 from Chromatin by a WIN Site Inhibitor with Picomolar Affinity. Cell Rep, 2019. **26**(11): p. 2916-2928.e13.

5. Heck, J.E., et al., Epidemiology of rhabdoid tumors of early childhood. Pediatr Blood Cancer, 2013. **60**(1): p. 77-81.

6. Fruhwald, M.C., et al., Atypical teratoid/rhabdoid tumors-current concepts, advances in biology, and potential future therapies. Neuro Oncol, 2016. **18**(6): p. 764-78.

7. Lee, R.S., et al., A remarkably simple genome underlies highly malignant pediatric rhabdoid cancers. J Clin Invest, 2012. **122**(8): p. 2983-8.

8. Hasselblatt, M., et al., High-resolution genomic analysis suggests the absence of recurrent genomic alterations other than SMARCB1 aberrations in atypical teratoid/rhabdoid tumors. Genes Chromosomes Cancer, 2013. **52**(2): p. 185-90.

9. Hoell, J.I., et al., Whole-genome paired-end analysis confirms remarkable genomic stability of atypical teratoid/rhabdoid tumors. Genes Chromosomes Cancer, 2013. **52**(10): p. 983-5.

10. Clapier, C.R. and B.R. Cairns, The biology of chromatin remodeling complexes. Annu Rev Biochem, 2009. **78**: p. 273-304.

11. Wilson, B.G. and C.W. Roberts, SWI/SNF nucleosome remodellers and cancer. Nat Rev Cancer, 2011. **11**(7): p. 481-92.

12. Masliah-Planchon, J., et al., SWI/SNF chromatin remodeling and human malignancies. Annu Rev Pathol, 2015. **10**: p. 145-71.

13. Mittal, P. and C.W.M. Roberts, The SWI/SNF complex in cancer - biology, biomarkers and therapy. Nat Rev Clin Oncol, 2020. **17**(7): p. 435-448.

14. Mashtalir, N., et al., Modular Organization and Assembly of SWI/SNF Family Chromatin Remodeling Complexes. Cell, 2018. **175**(5): p. 1272-1288 e20.

15. Wang, W., et al., Purification and biochemical heterogeneity of the mammalian SWI-SNF complex. EMBO J, 1996. **15**(19): p. 5370-82.

16. Lemon, B., et al., Selectivity of chromatin-remodelling cofactors for ligand-activated transcription. Nature, 2001. **414**(6866): p. 924-8.

17. Raab, J.R., S. Resnick, and T. Magnuson, Genome-Wide Transcriptional Regulation Mediated by Biochemically Distinct SWI/SNF Complexes. PLoS Genet, 2015. **11**(12): p. e1005748.

18. Alpsoy, A. and E.C. Dykhuizen, Glioma tumor suppressor candidate region gene 1 (GLTSCR1) and its paralog GLTSCR1-like form SWI/SNF chromatin remodeling subcomplexes. J Biol Chem, 2018. **293**(11): p. 3892-3903.

19. Brien, G.L., et al., Targeted degradation of BRD9 reverses oncogenic gene expression in synovial sarcoma. Elife, 2018. **7**.

20. Michel, B.C., et al., A non-canonical SWI/SNF complex is a synthetic lethal target in cancers driven by BAF complex perturbation. Nat Cell Biol, 2018. **20**(12): p. 1410-1420.

21. Wang, X., et al., BRD9 defines a SWI/SNF sub-complex and constitutes a specific vulnerability in malignant rhabdoid tumors. Nat Commun, 2019. **10**(1): p. 1881.

22. Versteege, I., et al., Truncating mutations of hSNF5/INI1 in aggressive paediatric cancer. Nature, 1998. **394**(6689): p. 203-6.

23. Kadoch, C., et al., Proteomic and bioinformatic analysis of mammalian SWI/SNF complexes identifies extensive roles in human malignancy. Nat Genet, 2013. **45**(6): p. 592-601.

24. Jones, S., et al., Frequent mutations of chromatin remodeling gene ARID1A in ovarian clear cell carcinoma. Science, 2010. **330**(6001): p. 228-31.

25. Wiegand, K.C., et al., ARID1A mutations in endometriosis-associated ovarian carcinomas. N Engl J Med, 2010. **363**(16): p. 1532-43.

26. Varela, I., et al., Exome sequencing identifies frequent mutation of the SWI/SNF complex gene PBRM1 in renal carcinoma. Nature, 2011. **469**(7331): p. 539-42.

27. Lu, B. and H. Shi, An In-Depth Look at Small Cell Carcinoma of the Ovary, Hypercalcemic Type (SCCOHT): Clinical Implications from Recent Molecular Findings. J Cancer, 2019. **10**(1): p. 223-237.

28. Brennan, B., C. Stiller, and F. Bourdeaut, Extracranial rhabdoid tumours: what we have learned so far and future directions. Lancet Oncol, 2013. **14**(8): p. e329-36.

29. Hasselblatt, M., et al., SMARCA4-mutated atypical teratoid/rhabdoid tumors are associated with inherited germline alterations and poor prognosis. Acta Neuropathol, 2014. **128**(3): p. 453-6.

30. Stacchiotti, S. and B.A. Van Tine, Synovial Sarcoma: Current Concepts and Future Perspectives. J Clin Oncol, 2018. **36**(2): p. 180-187.

31. Kadoch, C. and G.R. Crabtree, Reversible disruption of mSWI/SNF (BAF) complexes by the SS18-SSX oncogenic fusion in synovial sarcoma. Cell, 2013. **153**(1): p. 71-85.

32. Wang, X., et al., SMARCB1-mediated SWI/SNF complex function is essential for enhancer regulation. Nat Genet, 2017. **49**(2): p. 289-295.

33. Roberts, C.W., et al., Haploinsufficiency of Snf5 (integrase interactor 1) predisposes to malignant rhabdoid tumors in mice. Proc Natl Acad Sci U S A, 2000. **97**(25): p. 13796-800.

34. Ae, K., et al., Chromatin remodeling factor encoded by ini1 induces G1 arrest and apoptosis in ini1-deficient cells. Oncogene, 2002. **21**(20): p. 3112-20.

35. Betz, B.L., et al., Re-expression of hSNF5/INI1/BAF47 in pediatric tumor cells leads to G1 arrest associated with induction of p16ink4a and activation of RB. Oncogene, 2002. **21**(34): p. 5193-203.

36. Versteege, I., et al., A key role of the hSNF5/INI1 tumour suppressor in the control of the G1-S transition of the cell cycle. Oncogene, 2002. **21**(42): p. 6403-12.

37. Zhang, Z.K., et al., Cell cycle arrest and repression of cyclin D1 transcription by INI1/hSNF5. Mol Cell Biol, 2002. **22**(16): p. 5975-88.

38. Oruetxebarria, I., et al., P16INK4a is required for hSNF5 chromatin remodeler-induced cellular senescence in malignant rhabdoid tumor cells. J Biol Chem, 2004. **279**(5): p. 3807-16.

39. Nakayama, R.T., et al., SMARCB1 is required for widespread BAF complex-mediated activation of enhancers and bivalent promoters. Nat Genet, 2017. **49**(11): p. 1613-1623.

40. Whyte, W.A., et al., Master transcription factors and mediator establish super-enhancers at key cell identity genes. Cell, 2013. **153**(2): p. 307-19.

41. Bernstein, B.E., et al., A bivalent chromatin structure marks key developmental genes in embryonic stem cells. Cell, 2006. **125**(2): p. 315-26.

42. Carugo, A., et al., p53 Is a Master Regulator of Proteostasis in SMARCB1-Deficient Malignant Rhabdoid Tumors. Cancer Cell, 2019. **35**(2): p. 204-220 e9.

43. Johann, P.D., et al., Atypical Teratoid/Rhabdoid Tumors Are Comprised of Three Epigenetic Subgroups with Distinct Enhancer Landscapes. Cancer Cell, 2016. **29**(3): p. 379-393.

44. Gadd, S., et al., Rhabdoid tumor: gene expression clues to pathogenesis and potential therapeutic targets. Lab Invest, 2010. **90**(5): p. 724-38.

45. Genovese, G., et al., Synthetic vulnerabilities of mesenchymal subpopulations in pancreatic cancer. Nature, 2017. **542**(7641): p. 362-366.

46. Vita, M. and M. Henriksson, The Myc oncoprotein as a therapeutic target for human cancer. Semin Cancer Biol, 2006. **16**(4): p. 318-30.

47. Tansey, W.P., Mammalian MYC Proteins and Cancer. New Journal of Science, 2013. **2014**: p. 1-27.

48. Lourenco, C., et al., MYC protein interactors in gene transcription and cancer. Nat Rev Cancer, 2021. **21**(9): p. 579-591.

49. Weissmiller, A.M., et al., Inhibition of MYC by the SMARCB1 tumor suppressor. Nat Commun, 2019. **10**(1): p. 2014.

50. Cheng, S.W., et al., c-MYC interacts with INI1/hSNF5 and requires the SWI/SNF complex for transactivation function. Nat Genet, 1999. **22**(1): p. 102-5.

51. Wang, X., et al., TCR-dependent transformation of mature memory phenotype T cells in mice. J Clin Invest, 2011. **121**(10): p. 3834-45.

52. Ciavarella, S., et al., Targeted therapies in cancer. BioDrugs, 2010. **24**(2): p. 77-88.

53. Howard, T.P., et al., MDM2 and MDM4 Are Therapeutic Vulnerabilities in Malignant Rhabdoid Tumors. Cancer Res, 2019. **79**(9): p. 2404-2414.

54. Howard, T.P., et al., Rhabdoid Tumors Are Sensitive to the Protein-Translation Inhibitor Homoharringtonine. Clin Cancer Res, 2020. **26**(18): p. 4995-5006.

55. Kadoch, C., R.A. Copeland, and H. Keilhack, PRC2 and SWI/SNF Chromatin Remodeling Complexes in Health and Disease. Biochemistry, 2016. **55**(11): p. 1600-14.

56. Le Loarer, F., et al., Consistent SMARCB1 homozygous deletions in epithelioid sarcoma and in a subset of myoepithelial carcinomas can be reliably detected by FISH in archival material. Genes Chromosomes Cancer, 2014. **53**(6): p. 475-86.

57. Gounder, M., et al., Tazemetostat in advanced epithelioid sarcoma with loss of INI1/SMARCB1: an international, open-label, phase 2 basket study. Lancet Oncol, 2020. **21**(11): p. 1423-1432.

58. Hohmann, A.F., et al., Sensitivity and engineered resistance of myeloid leukemia cells to BRD9 inhibition. Nat Chem Biol, 2016. **12**(9): p. 672-9.

59. Theodoulou, N.H., et al., Discovery of I-BRD9, a Selective Cell Active Chemical Probe for Bromodomain Containing Protein 9 Inhibition. J Med Chem, 2016. **59**(4): p. 1425-39.

60. Schuetz, A., et al., Structural basis for molecular recognition and presentation of histone H3 by WDR5. EMBO J, 2006. **25**(18): p. 4245-52.

61. Jeffery, C.J., *Moonlighting proteins.* Trends Biochem Sci, 1999. **24**(1): p. 8-11.

62. Ernst, P. and C.R. Vakoc, WRAD: enabler of the SET1-family of H3K4 methyltransferases. Brief Funct Genomics, 2012. **11**(3): p. 217-26.

63. Odho, Z., S.M. Southall, and J.R. Wilson, Characterization of a novel WDR5-binding site that recruits RbBP5 through a conserved motif to enhance methylation of histone H3 lysine 4 by mixed lineage leukemia protein-1. J Biol Chem, 2010. **285**(43): p. 32967-32976.

64. Patel, A., V. Dharmarajan, and M.S. Cosgrove, Structure of WDR5 bound to mixed lineage leukemia protein-1 peptide. J Biol Chem, 2008. **283**(47): p. 32158-61.

65. Patel, A., et al., A conserved arginine-containing motif crucial for the assembly and enzymatic activity of the mixed lineage leukemia protein-1 core complex. J Biol Chem, 2008. **283**(47): p. 32162-75.

66. Dharmarajan, V., et al., Structural basis for WDR5 interaction (Win) motif recognition in human SET1 family histone methyltransferases. J Biol Chem, 2012. **287**(33): p. 27275-89.

67. Alicea-Velazquez, N.L., et al., Targeted Disruption of the Interaction between WD-40 Repeat Protein 5 (WDR5) and Mixed Lineage Leukemia (MLL)/SET1 Family Proteins Specifically Inhibits MLL1 and SETd1A Methyltransferase Complexes. J Biol Chem, 2016. **291**(43): p. 22357-22372.

68. Guccione, E., et al., Methylation of histone H3R2 by PRMT6 and H3K4 by an MLL complex are mutually exclusive. Nature, 2007. **449**(7164): p. 933-7.

69. Hyllus, D., et al., PRMT6-mediated methylation of R2 in histone H3 antagonizes H3 K4 trimethylation. Genes Dev, 2007. **21**(24): p. 3369-80.

70. Migliori, V., et al., Symmetric dimethylation of H3R2 is a newly identified histone mark that supports euchromatin maintenance. Nat Struct Mol Biol, 2012. **19**(2): p. 136-44.

158

71. Smith, E.R., et al., A human protein complex homologous to the Drosophila MSL complex is responsible for the majority of histone H4 acetylation at lysine 16. Mol Cell Biol, 2005. **25**(21): p. 9175-88.

72. Dias, J., et al., Structural analysis of the KANSL1/WDR5/KANSL2 complex reveals that WDR5 is required for efficient assembly and chromatin targeting of the NSL complex. Genes Dev, 2014. **28**(9): p. 929-42.

73. Cai, Y., et al., Subunit composition and substrate specificity of a MOF-containing histone acetyltransferase distinct from the male-specific lethal (MSL) complex. J Biol Chem, 2010. **285**(7): p. 4268-72.

74. Basta, J. and M. Rauchman, The nucleosome remodeling and deacetylase complex in development and disease. Transl Res, 2015. **165**(1): p. 36-47.

75. Bode, D., et al., Characterization of Two Distinct Nucleosome Remodeling and Deacetylase (NuRD) Complex Assemblies in Embryonic Stem Cells. Mol Cell Proteomics, 2016. **15**(3): p. 878-91.

76. Ee, L.S., et al., An Embryonic Stem Cell-Specific NuRD Complex Functions through Interaction with WDR5. Stem Cell Reports, 2017. **8**(6): p. 1488-1496.

77. Thomas, L.R., et al., Interaction with WDR5 promotes target gene recognition and tumorigenesis by MYC. Mol Cell, 2015. **58**(3): p. 440-52.

78. Thomas, L.R., et al., Interaction of the oncoprotein transcription factor MYC with its chromatin cofactor WDR5 is essential for tumor maintenance. Proc Natl Acad Sci U S A, 2019. **116**(50): p. 25260-25268.

79. Tian, J., et al., Discovery and Structure-Based Optimization of Potent and Selective WD Repeat Domain 5 (WDR5) Inhibitors Containing a Dihydroisoquinolinone Bicyclic Core. J Med Chem, 2020. **63**(2): p. 656-675.

80. Pelletier, J., G. Thomas, and S. Volarevic, Ribosome biogenesis in cancer: new players and therapeutic avenues. Nat Rev Cancer, 2018. **18**(1): p. 51-63.

81. Nabet, B., et al., The dTAG system for immediate and target-specific protein degradation. Nat Chem Biol, 2018. **14**(5): p. 431-441.

82. Grebien, F., et al., Pharmacological targeting of the Wdr5-MLL interaction in C/EBPalpha N-terminal leukemia. Nat Chem Biol, 2015. **11**(8): p. 571-578.

83. Neilsen, B.K., et al., WDR5 supports colon cancer cells by promoting methylation of H3K4 and suppressing DNA damage. BMC Cancer, 2018. **18**(1): p. 673.

84. Zhang, J., et al., Targeting WD repeat domain 5 enhances chemosensitivity and inhibits proliferation and programmed death-ligand 1 expression in bladder cancer. J Exp Clin Cancer Res, 2021. **40**(1): p. 203.

85. Zhou, Q., et al., WD repeat domain 5 promotes chemoresistance and Programmed Death-Ligand 1 expression in prostate cancer. Theranostics, 2021. **11**(10): p. 4809-4824.

86. Cao, F., et al., Targeting MLL1 H3K4 methyltransferase activity in mixed-lineage leukemia. Mol Cell, 2014. **53**(2): p. 247-61.

87. Wang, F., et al., Discovery of Potent 2-Aryl-6,7-dihydro-5 H-pyrrolo[1,2- a]imidazoles as WDR5-WIN-Site Inhibitors Using Fragment-Based Methods and Structure-Based Design. J Med Chem, 2018. **61**(13): p. 5623-5642.

88. Alimova, I., et al., Inhibition of MYC attenuates tumor cell self-renewal and promotes senescence in SMARCB1-deficient Group 2 atypical teratoid rhabdoid tumors to suppress tumor growth in vivo. Int J Cancer, 2019. **144**(8): p. 1983-1995.

89. Dang, C.V., et al., Drugging the 'undruggable' cancer targets. Nat Rev Cancer, 2017. **17**(8): p. 502-508.

90. Kantarjian, H.M., et al., Homoharringtonine: history, current research, and future direction. Cancer, 2001. **92**(6): p. 1591-605.

91. Furet, P., et al., Discovery of a novel class of highly potent inhibitors of the p53-MDM2 interaction by structure-based design starting from a conformational argument. Bioorg Med Chem Lett, 2016. **26**(19): p. 4837-4841.

92. Kim, J.S., et al., Activation of p53-dependent growth suppression in human cells by mutations in PTEN or PIK3CA. Mol Cell Biol, 2007. **27**(2): p. 662-77.

93. Sarbassov, D.D., et al., Phosphorylation and regulation of Akt/PKB by the rictor-mTOR complex. Science, 2005. **307**(5712): p. 1098-101.

94. Sanson, K.R., et al., Optimized libraries for CRISPR-Cas9 genetic screens with multiple modalities. Nat Commun, 2018. **9**(1): p. 5416.

95. Rosenbluh, J., et al., Complementary information derived from CRISPR Cas9 mediated gene deletion and suppression. Nat Commun, 2017. **8**: p. 15403.

96. Ianevski, A., A.K. Giri, and T. Aittokallio, SynergyFinder 2.0: visual analytics of multi-drug combination synergies. Nucleic Acids Res, 2020. **48**(W1): p. W488-W493.

97. Justin T. Landis, H.A., Aubrey G. Bailey, Dirk P. Dittmer, James S. Marron, *dr4pl: Dose Response Data Analysis using the 4 Parameter Logistic (4pl) Model*. 2019.

98. Langmead, B. and S.L. Salzberg, Fast gapped-read alignment with Bowtie 2. Nat Methods, 2012. **9**(4): p. 357-9.

99. Feng, J., et al., Identifying ChIP-seq enrichment using MACS. Nat Protoc, 2012. **7**(9): p. 1728-40.

100. Stark, R. and G. Brown, DiffBind: differential binding analysis of ChIP-seq peak data. Bioconductor, 2011.

101. Love, M.I., W. Huber, and S. Anders, Moderated estimation of fold change and dispersion for RNA-seq data with DESeq2. Genome Biol, 2014. **15**(12): p. 550.

102. Martin, M., Cutadapt Removes Adapter Sequences From High-Throughput Sequencing Reads. EMBnet.journal, 2011. **17**(May): p. 10-12.

103. Dobin, A., et al., STAR: ultrafast universal RNA-seq aligner. Bioinformatics, 2013. **29**(1): p. 15-21.

104. Liao, Y., G.K. Smyth, and W. Shi, featureCounts: an efficient general purpose program for assigning sequence reads to genomic features. Bioinformatics, 2014. **30**(7): p. 923–930.

105. Wang, J., Y. Zhao, X. Zhou, S.W. Hiebert, Q. Liu, Y. Shyr, Nascent RNA sequencing analysis provides insights into enhancer-mediated gene regulation. BMC Genomics, 2018. **19**: p. 633.

106. Core, L.J., J.J. Waterfall, and J.T. Lis, Nascent RNA sequencing reveals widespread pausing and divergent initiation at human promoters. Science, 2008. **322**(5909): p. 1845-8.

107. Sonobe, H., et al., Establishment and characterization of a new human synovial sarcoma cell line, HS-SY-II. Lab Invest, 1992. **67**(4): p. 498-505.

108. Yanagisawa, S., et al., Identification and metastatic potential of tumor-initiating cells in malignant rhabdoid tumor of the kidney. Clin Cancer Res, 2009. **15**(9): p. 3014-22.

109. Naka, N., et al., Synovial sarcoma is a stem cell malignancy. Stem Cells, 2010. **28**(7): p. 1119-31.

110. Barretina, J., et al., The Cancer Cell Line Encyclopedia enables predictive modelling of anticancer drug sensitivity. Nature, 2012. **483**(7391): p. 603-7.

111. Xu, J., et al., Novel cell lines established from pediatric brain tumors. J Neurooncol, 2012. **107**(2): p. 269-80.

112. Tate, J.G., et al., COSMIC: the Catalogue Of Somatic Mutations In Cancer. Nucleic Acids Res, 2019. **47**(D1): p. D941-D947.

113. Bodnar, A.G., et al., Extension of life-span by introduction of telomerase into normal human cells. Science, 1998. **279**(5349): p. 349-52.

114. Kandoth, C., et al., Mutational landscape and significance across 12 major cancer types. Nature, 2013. **502**(7471): p. 333-339.

115. Crouch, S.P., et al., The use of ATP bioluminescence as a measure of cell proliferation and cytotoxicity. J Immunol Methods, 1993. **160**(1): p. 81-8.

116. Hughes, J.P., et al., Principles of early drug discovery. Br J Pharmacol, 2011. **162**(6): p. 1239-49.

117. Mori, S., et al., Anchorage-independent cell growth signature identifies tumors with metastatic potential. Oncogene, 2009. **28**(31): p. 2796-805.

118. Cifone, M.A. and I.J. Fidler, Correlation of patterns of anchorage-independent growth with in vivo behavior of cells from a murine fibrosarcoma. Proc Natl Acad Sci U S A, 1980. **77**(2): p. 1039-43.

119. Borowicz, S., et al., The soft agar colony formation assay. J Vis Exp, 2014(92): p. e51998.

120. Zhou, F., et al., Toward a new age of cellular pharmacokinetics in drug discovery. Drug Metab Rev, 2011. **43**(3): p. 335-45.

121. Rixe, O. and T. Fojo, Is cell death a critical end point for anticancer therapies or is cytostasis sufficient? Clin Cancer Res, 2007. **13**(24): p. 7280-7.

122. Gaudet, P., et al., Primer on the Gene Ontology. Methods Mol Biol, 2017. **1446**: p. 25-37.

123. Kwak, H., et al., Precise maps of RNA polymerase reveal how promoters direct initiation and pausing. Science, 2013. **339**(6122): p. 950-3.

124. Mahat, D.B., et al., Base-pair-resolution genome-wide mapping of active RNA polymerases using precision nuclear run-on (PRO-seq). Nat Protoc, 2016. **11**(8): p. 1455-76.

125. Subramanian, A., et al., Gene set enrichment analysis: a knowledge-based approach for interpreting genome-wide expression profiles. Proc Natl Acad Sci U S A, 2005. **102**(43): p. 15545-50.

126. Siladi, A.J., et al., WIN site inhibition disrupts a subset of WDR5 function. Sci Rep, 2022. **12**(1): p. 1848.

127. Aubrey, B.J., et al., How does p53 induce apoptosis and how does this relate to p53-mediated tumour suppression? Cell Death Differ, 2018. **25**(1): p. 104-113.

128. Lane, D.P., p53, guardian of the genome. Nature, 1992. **358**(6381): p. 15-6.

129. Lai, P.B., T.Y. Chi, and G.G. Chen, Different levels of p53 induced either apoptosis or cell cycle arrest in a doxycycline-regulated hepatocellular carcinoma cell line in vitro. Apoptosis, 2007. **12**(2): p. 387-93.

130. DeBerardinis, R.J. and N.S. Chandel, *We need to talk about the Warburg effect.* Nat Metab, 2020. **2**(2): p. 127-129.

131. Signer, R.A., et al., Haematopoietic stem cells require a highly regulated protein synthesis rate. Nature, 2014. **509**(7498): p. 49-54.

132. Liu, J., et al., Imaging protein synthesis in cells and tissues with an alkyne analog of puromycin. Proc Natl Acad Sci U S A, 2012. **109**(2): p. 413-8.

133. Jassal, B., et al., The reactome pathway knowledgebase. Nucleic Acids Res, 2020. **48**(D1): p. D498-D503.

134. Fabregat, A., et al., Reactome pathway analysis: a high-performance in-memory approach. BMC Bioinformatics, 2017. **18**(1): p. 142.

135. Liberzon, A., et al., The Molecular Signatures Database (MSigDB) hallmark gene set collection. Cell Syst, 2015. **1**(6): p. 417-425.

136. Bieging-Rolett, K.T., et al., Zmat3 Is a Key Splicing Regulator in the p53 Tumor Suppression Program. Mol Cell, 2020. **80**(3): p. 452-469 e9.

137. Vousden, K.H. and D.P. Lane, *p53 in health and disease.* Nat Rev Mol Cell Biol, 2007. **8**(4): p. 275-83.

138. Kim, T.H., P. Leslie, and Y. Zhang, Ribosomal proteins as unrevealed caretakers for cellular stress and genomic instability. Oncotarget, 2014. **5**(4): p. 860-71.

139. Liu, Y., C. Deisenroth, and Y. Zhang, RP-MDM2-p53 Pathway: Linking Ribosomal Biogenesis and Tumor Surveillance. Trends Cancer, 2016. **2**(4): p. 191-204.

140. Lohrum, M.A., et al., Regulation of HDM2 activity by the ribosomal protein L11. Cancer Cell, 2003. **3**(6): p. 577-87.

141. Zhang, Y., et al., Ribosomal protein L11 negatively regulates oncoprotein MDM2 and mediates a p53-dependent ribosomal-stress checkpoint pathway. Mol Cell Biol, 2003. **23**(23): p. 8902-12.

142. Dai, M.S. and H. Lu, Inhibition of MDM2-mediated p53 ubiquitination and degradation by ribosomal protein L5. J Biol Chem, 2004. **279**(43): p. 44475-82.

143. Xiong, X., et al., Ribosomal protein S27-like and S27 interplay with p53-MDM2 axis as a target, a substrate and a regulator. Oncogene, 2011. **30**(15): p. 1798-811.

144. el-Deiry, W.S., et al., Topological control of p21WAF1/CIP1 expression in normal and neoplastic tissues. Cancer Res, 1995. **55**(13): p. 2910-9.

145. Machado-Silva, A., S. Perrier, and J.C. Bourdon, *p53 family members in cancer diagnosis and treatment.* Semin Cancer Biol, 2010. **20**(1): p. 57-62.

146. Vassilev, L.T., et al., In vivo activation of the p53 pathway by small-molecule antagonists of MDM2. Science, 2004. **303**(5659): p. 844-8.

147. Moore, C.B., et al., Short hairpin RNA (shRNA): design, delivery, and assessment of gene knockdown. Methods Mol Biol, 2010. **629**: p. 141-58.

148. Fischer, M., Census and evaluation of p53 target genes. Oncogene, 2017. **36**(28): p. 3943-3956.

149. Ran, F.A., et al., Genome engineering using the CRISPR-Cas9 system. Nat Protoc, 2013. **8**(11): p. 2281-2308.

150. Alerasool, N., et al., An efficient KRAB domain for CRISPRi applications in human cells. Nat Methods, 2020. **17**(11): p. 1093-1096.

151. Bayat Mokhtari, R., et al., Combination therapy in combating cancer. Oncotarget, 2017. **8**(23): p. 38022-38043.

152. Vlot, A.H.C., et al., Applying synergy metrics to combination screening data: agreements, disagreements and pitfalls. Drug Discov Today, 2019. **24**(12): p. 2286-2298.

153. Stein, E.M., et al., Results from a First-in-Human Phase I Study of Siremadlin (HDM201) in Patients with Advanced Wild-Type TP53 Solid Tumors and Acute Leukemia. Clin Cancer Res, 2021.

154. Mullard, A., *p53 programmes plough on.* Nat Rev Drug Discov, 2020. **19**(8): p. 497-500.

155. Andreeff, M., et al., Results of the Phase I Trial of RG7112, a Small-Molecule MDM2 Antagonist in Leukemia. Clin Cancer Res, 2016. **22**(4): p. 868-76.

156. Skalniak, L., et al., Prolonged Idasanutlin (RG7388) Treatment Leads to the Generation of p53-Mutated Cells. Cancers (Basel), 2018. **10**(11).

157. Joseph, P.D., J.C. Craig, and P.H. Caldwell, *Clinical trials in children.* Br J Clin Pharmacol, 2015. **79**(3): p. 357-69.

158. Li, D.D., et al., Structure-based design and synthesis of small molecular inhibitors disturbing the interaction of MLL1-WDR5. Eur J Med Chem, 2016. **118**: p. 1-8.

159. Karatas, H., et al., Discovery of a Highly Potent, Cell-Permeable Macrocyclic Peptidomimetic (MM-589) Targeting the WD Repeat Domain 5 Protein (WDR5)-Mixed Lineage Leukemia (MLL) Protein-Protein Interaction. J Med Chem, 2017. **60**(12): p. 4818-4839.

160. Zhang, X., et al., Piribedil disrupts the MLL1-WDR5 interaction and sensitizes MLL-rearranged acute myeloid leukemia (AML) to doxorubicin-induced apoptosis. Cancer Lett, 2018. **431**: p. 150-160.

161. Oh, E., et al., Gene expression and cell identity controlled by anaphase-promoting complex. Nature, 2020. **579**(7797): p. 136-140.

162. James, A., et al., Nucleolar stress with and without p53. Nucleus, 2014. **5**(5): p. 402-26.

163. Guarnaccia, A.D., et al., Impact of WIN site inhibitor on the WDR5 interactome. Cell Rep, 2021. **34**(3): p. 108636.

164. Hung, V., et al., Spatially resolved proteomic mapping in living cells with the engineered peroxidase APEX2. Nat Protoc, 2016. **11**(3): p. 456-75.

165. Ng, J.M., et al., Generation of a mouse model of atypical teratoid/rhabdoid tumor of the central nervous system through combined deletion of Snf5 and p53. Cancer Res, 2015. **75**(21): p. 4629-39.

166. Below, J. and M.D. J, *Vincristine*, in *StatPearls*. 2022: Treasure Island (FL).

167. Johnson-Arbor, K. and R. Dubey, *Doxorubicin*, in *StatPearls*. 2022: Treasure Island (FL).

168. Dasari, S. and P.B. Tchounwou, Cisplatin in cancer therapy: molecular mechanisms of action. Eur J Pharmacol, 2014. **740**: p. 364-78.

169. Gangireddy, M. and V. Nookala, *Ifosfamide*, in *StatPearls*. 2022: Treasure Island (FL).

170. Ogino, M.H. and P. Tadi, *Cyclophosphamide*, in *StatPearls*. 2022: Treasure Island (FL).

171. Montecucco, A., F. Zanetta, and G. Biamonti, *Molecular mechanisms of etoposide.* EXCLI J, 2015. **14**: p. 95-108.

172. Drygin, D., et al., Targeting RNA polymerase I with an oral small molecule CX-5461 inhibits ribosomal RNA synthesis and solid tumor growth. Cancer Res, 2011. **71**(4): p. 1418-30.